

# **A Systematic Mix Design Approach for Ultra High Performance Fibre Reinforced Concrete**

## **DISSERTATION**

for obtaining the academic degree  
Doctor of Engineering Sciences  
at Graz University of Technology, Austria

presented by

**Kim Huy Hoang**

M.Sc. in Construction Material Engineering  
from Vietnam

Advisor

**Univ.-Prof. Dr-Ing. habil. Nguyen Viet Tue**

Institute of Structural Concrete  
Graz University of Technology, Austria

Graz, May 2017





Kim Huy Hoang M.Sc., B.Eng

# **Ein Beitrag zur systematischen Rezepturenentwicklung von Ultra-Hochleistungs-Faserbeton**

## **DISSERTATION**

zur Erlangung des akademischen Grades

Doktor der technischen Wissenschaften

eingereicht an der

**Technischen Universität Graz**

Betreuer

Univ.-Prof. Dr.-Ing. habil. Nguyen Viet Tue

Institut für Betonbau



### **Statutory Declaration**

*I declare that I have authored this thesis independently, that I have not used other than the declared sources / resources, and that I have explicitly marked all material which has been quoted either literally or by content from the used sources. The text document uploaded in TUGRAZonline is compatible with the Dissertation.*

Place, Date

Signature

### **Eidesstattliche Erklärung**

*Ich erkläre an Eides statt, dass ich die vorliegende Arbeit selbstständig verfasst, andere als die angegebenen Quellen/Hilfsmittel nicht benutzt, und die den benutzten Quellen wörtlich und inhaltlich entnommene Stellen als solche kenntlich gemacht habe. Das in TUGRAZonline hochgeladene Textdokument ist mit der vorliegenden Dissertation identisch.*

Ort, Datum

Unterschrift



# Abstract

The improvement of packing density of granular composition in combination with highly effective superplasticizer together with fibre reinforcing generates a new class of concretes called Ultra-High Performance Fibre Reinforced Concrete (UHPFRC). The characteristic key properties of UHPFRC are *(i)* its self-flow ability, *(ii)* its ultra-high compressive strength of 150 - 200 MPa, *(iii)* its high ductility and toughness, and *(iv)* its extremely high durability. Due to its outstanding characteristics, many innovative applications of UHPFRC were developed for sustainable and elegant structures.

UHPFRC's mix design using local materials is a challenge due to the high number of the raw materials and their great difference regarding physical and chemical properties. Furthermore, the existing particle packing models for concrete mix design have some limits because of the difference between the assumption of the mathematical models and the real chemical-physical effects. Therefore, the predictions are at variance with the experiments.

The main questions answered in this research project, with regards to the improvement of the packing density and strength are how the proper materials can be selected for UHPFRC production, how the optimum cementitious paste can be determined, how the optimum aggregate can be found out to obtain the optimum concrete considering the combination of the optimum paste and the optimum aggregate, how an effective steel fibre can be established for achieving the best strain-hardening UHPFRC with low fibre content.

This thesis provides a systematic and highly efficient approach that is based on stepwise optimization of particle packing density for UHPFRC mix design using local materials. The proposed approach is an optimization procedure, starting with the materials selection to the optimization of cementitious paste and the whole concrete matrix (UHPC) and finishing by determination of the most effective fibre for improving the ductility and toughness of UHPFRC.

First the advantages and disadvantages of different existing particle packing models and of various existing particle packing density measurement methods were analyzed. Furthermore, the major roles of each raw material in UHPFRC production and the influence of the materials characteristics on UHPFRC performance were summarized. As a result of that, an efficient test method called superplasticizer-water solution demand test, based on mixing energy measurement, was proposed to examine the particle packing density of powder. The reactivities and packing densities of the powders were evaluated, thereby selecting the most suitable materials of cements, superplasticizers, silica fumes, fly ash, ground granulated blast furnace slag, quartz powders, limestone powder for UHPFRC matrix production.

## *Abstract*

Based on the basic idea that the void space between larger grains can be filled by smaller grains in order to improve the packing density of the granular concrete mixture, a method of stepwise optimization of particle packing for granular materials was proposed. Five different optimum binders that include cement, reactive and/or inert powders were developed by applying the test of superplasticizer-water demand and the method of the stepwise optimization of particle packing.

Taking into account the relation between the compressive strength of concrete and the water-cement ratio, the degree of hydration of cement, the gel-space ratio the water-cement ratio of 0.25 was chosen and kept constant for all tests which relate to the rheology behaviour and strength of pastes and concretes. The saturated amount of superplasticizer for each optimum binder was found out by the assessment of the rheological of paste and concrete using a rotational rheometer and spread-flow test.

When an optimum paste having a fixed volume combined with a blended aggregate which was formed by the combination of various aggregates, the best mix proportion of blended aggregates was recognized by showing the highest flowability and the lowest plastic viscosity of concrete mixture as the stepwise optimization of particle packing method was employed for aggregate combinations. Four optimum self-flowing UHPC with different maximum grain sizes of 1 mm, 2 mm, 4 mm and 8 mm were developed, their compressive strength at 28 days age were higher than 190 MPa.

Three existing particle packing models such as the modified Andreasen and Andersen equation-based ideal curve, the Compressible Packing Model (CPM) of de Larrard and the Compaction-Interaction Packing Model (CIPM) of Fennis (which represent the packing together of different monosized classes) were also used to determine the mix proportion of binder and of blended aggregate and the whole concrete matrix. However, the experimental results indicate that these existing models are limited for UHPC mixture proportioning and it is not guaranteed to achieve the highest performance of concrete.

Six different high strength steel fibres were employed to improve the ductility of the developed optimum UHPCs. Four micro steel fibres were two types of smooth straight fibres (F1:  $L_1/D_1 = 13\text{mm}/0.2\text{mm}$ ; F2:  $L_2/D_2 = 20\text{mm}/0.2\text{mm}$ ) and two types of crimped fibres (F3:  $L_3/D_3 = 9\text{mm}/0.12\text{mm}$ ; F4:  $L_4/D_4 = 12\text{mm}/0.18\text{mm}$ ) while two indented macro steel fibres were hooked ends fibre (F5:  $L_5/D_5 = 30\text{mm}/0.55\text{mm}$ ) and straight fibre (F6:  $L_6/D_6 = 25\text{mm}/0.3\text{mm}$ ). Fibre pull-out tests were carried out to determine the fibre-matrix bond strength. The influences of fibre types, contents and matrix composition on the properties of UHPFRC in fresh and hardened states were investigated. The critical fibre volumes for self-flowing properties of UHPFRC without fibres clumping were found out experimentally. The comparative investigations on the mechanical behaviour of the UHPFRCs were then carried out using four points bending test and direct tensile test. The effectiveness of each fibre type in reinforcing UHPCs were analyzed. Self-flowing strain-hardening UHPFRCs with the highest mechanical performance and the lowest fibre content were established.

The developed UHPFRCs were applied successfully to some pilot projects.

# Kurzfassung

Die Verbesserung der Packungsdichte der Kornzusammensetzung in Kombination mit Hochleistungsfließmitteln und Faserbewehrung erzeugt eine Betonsorte namens faserbewehrten Ultra-Hochleistungsbeton (UHPRFC). Die wesentlichen Eigenschaften von UHPRFC sind selbstverdichtende Eigenschaften, Druckfestigkeiten von 150-200 MPa, eine hohe Duktilität und Widerstandsfähigkeit sowie eine extreme Dauerhaftigkeit. Aufgrund dieser außergewöhnlichen Charakteristik wurden viele innovativen Anwendungen mit UHPRFC für nachhaltige und elegante Strukturen entwickelt.

Die Rezepturentwicklung für UHPRFC mit lokalen Materialien ist eine große Herausforderung aufgrund der Vielzahl an Rohstoffen und ihren großen Unterschieden in Bezug auf deren physikalischen und chemischen Eigenschaften. Des Weiteren haben vorhandene Modelle zur Bestimmung der Packungsdichte Grenzen. Dies beruht auf Unterschieden zwischen den Annahmen in mathematischen Modellen und den realen chemischen und physikalischen Effekten. Aus diesem Grund weichen die prognostizierten von den experimentell ermittelten Ergebnissen ab.

Die zentralen Fragen, welche in dieser Forschungsarbeit bezüglich der Verbesserung der Packungsdichte und Festigkeit beantwortet werden, sind wie die geeigneten Materialien für die UHPRFC-Produktion ausgewählt werden können, wie die optimale Leimzusammensetzung bestimmt werden kann, wie die optimale Gesteinskörnung ermittelt werden kann um den optimalen UHPRFC zu erhalten und wie eine wirksame Stahlfaserbewehrung mit möglichst niedrigem Fasergehalt zum Erreichen eines verfestigendem Tragverhaltens unter Zugbeanspruchung ermittelt werden kann.

Diese Arbeit bietet einen systematischen und hocheffizienten Ansatz, der auf einer schrittweisen Optimierung der Packungsdichte zur Rezepturentwicklung von UHPRFC mit lokalen Materialien basiert. Der vorgeschlagene Ansatz ist ein Optimierungsverfahren beginnend mit der Materialauswahl zur Optimierung des Leims und der gesamten UHPRFC-Matrix und endet mit der Bestimmung der wirksamsten Faserbewehrung zur Verbesserung der Duktilität und Widerstandsfähigkeit von UHPRFC.

Die entwickelten UHPRFC-Rezepturen sind bereits erfolgreich in diversen Pilotprojekten eingesetzt worden.



# Acknowledgement

This dissertation would have been impossible without the guidance and help of many persons who in one way or another contributed their valuable time.

First of all, I would like to express my great gratitude to my supervisor Professor Nguyen Viet Tue for giving me the opportunity to join his research group at the Institute of Structural Concrete - TU Graz and to develop my ideas in this challenging research project. He always gives me valuable advice and encourage me to improve my work.

The experiments of this study would not have finished without the help and technical expertise of the laboratory personnel. I would like to express my thanks for their support, especially, Joseph Linder, Uwe Fülöp, Reinhard Holzschuster, Hannes Koitz, Wolfgang Rodler, Robert Weiss, Johann Rath, Philip Andreas Pucher at the Laboratory for Structural Engineering and the Institute of Technology and Testing of Building Materials - TU Graz.

My sincere thanks go to my colleagues and friends Bui Duc Vinh at the Institute of Construction Materials - HCMUT - Vietnam, Nguyen Duc Tung, Katrin Turner, Philipp Hadl, Joachim Juhart, Gheorghe Alexandru David, Elke Krischey at the Institute of Structural Concrete and the Institute of Technology and Testing of Building Materials - TU Graz for many valuable discussion and for all the help. Many thanks to Waltrau Reichl and Matina Ruptlish for their friendship and constant help during my stay in Graz.

Finally, I would to sincerely thank my parents, sister, brother and family for their love, great support and patience during my study.



# Contents

- Abstract** **vii**
- Kurzfassung** **ix**
- Acknowledgement** **xi**
- List of Figures** **xvii**
- List of Tables** **xxi**
- Notations and symbols** **xxiii**
- 
- 1 Introduction** **1**
  - 1.1 UHPFRC research and application . . . . . 1
  - 1.2 Motivation . . . . . 4
  - 1.3 Research Objective . . . . . 6
  - 1.4 Research Strategy and Outline . . . . . 6
- 
- 2 Particle packing model in concrete** **9**
  - 2.1 General definitions . . . . . 9
  - 2.2 Particle packing density measurement . . . . . 9
    - 2.2.1 Agglomeration of fine particles . . . . . 9
    - 2.2.2 Dry packing density of coarse particle . . . . . 12
    - 2.2.3 Wet packing density or water demand of powder . . . . . 12
    - 2.2.4 Assessment of the packing density of concrete including fine powders  
and coarse aggregates . . . . . 16
  - 2.3 Principles of particle packing . . . . . 18
    - 2.3.1 Ideal grading curve-based packing models . . . . . 19
    - 2.3.2 Packing models for a system of discretely sized particles . . . . . 21
  - 2.4 Concluding remarks . . . . . 28
- 
- 3 Influence of the characteristics of constituent materials on UHPFRC's performance** **29**
  - 3.1 Effects of Portland cement composition on setting time and workability of  
concrete . . . . . 29
  - 3.2 Compatibility between superplasticizer and cement . . . . . 30
    - 3.2.1 Dispersion mechanism of cement particles . . . . . 30
    - 3.2.2 Interaction of polycarboxylate-based superplasticizers with cement . 31
  - 3.3 Function of mineral admixtures in UHPC . . . . . 34

3.4	Concluding remarks . . . . .	39
<b>4</b>	<b>Materials selection</b>	<b>41</b>
4.1	Materials . . . . .	41
4.2	Packing density measurement for coarse particles . . . . .	43
4.3	Determination of the water-cement ratio . . . . .	44
4.4	The compatibility of the powders and the superplasticizers . . . . .	47
4.4.1	The influence of the superplasticizers on packing density and strength of the cements . . . . .	47
4.4.2	The influence of the superplasticizer SP1 on packing density of mineral admixtures . . . . .	53
4.5	Concluding remarks . . . . .	55
<b>5</b>	<b>Mix proportioning of UHPC</b>	<b>57</b>
5.1	Experimental methods . . . . .	57
5.1.1	Assessment of the particle packing density of concrete mixture using a rotational rheometer . . . . .	57
5.1.2	Specimen preparation and compression test . . . . .	59
5.2	The rule of granular materials combination . . . . .	60
5.3	Mixture-proportioning of cementitious paste . . . . .	61
5.3.1	The optimum pastes of cement - quartz powder - silica fume binders	61
5.3.2	The optimum paste of binder containing cement and ultra-fine fly ash	70
5.3.3	The optimum paste of binder containing cement - ground granulated blast furnace slag - limestone powder . . . . .	72
5.4	Mixture-proportioning of UHPC . . . . .	74
5.4.1	UHPC with a maximum grain size of 1 mm . . . . .	75
5.4.2	UHPC with a maximum grain size of 2.5 mm . . . . .	82
5.4.3	UHPC with a maximum grain size of 4 mm . . . . .	86
5.4.4	UHPC with a maximum grain size of 8 mm . . . . .	88
5.4.5	UHPC based on the optimum paste containing binary binder of cement and ultra fine fly ash . . . . .	93
5.4.6	UHPC based on the optimum paste containing ternary binder of cement-blast furnace slag-limestone powder . . . . .	96
5.5	Concluding remarks . . . . .	98
<b>6</b>	<b>Steel fibre reinforced UHPC</b>	<b>101</b>
6.1	Introduction . . . . .	101
6.2	Investigation objective and methodology . . . . .	104
6.2.1	Investigation objective . . . . .	104
6.2.2	Testing methods . . . . .	105
6.2.3	Inverse analysis based on four-point bending test for estimation of the tensile constitutive properties of UHPFRC . . . . .	112
6.3	Experimental results . . . . .	113
6.3.1	The effect of fibre types on fibre pullout resistances . . . . .	113
6.3.2	The effect of fibre types, content and matrix compositions on the properties of UHPFRC in fresh and hardened states . . . . .	116

6.3.3	Experimental assessment of the effectiveness of six different fibres in reinforcing UHPC . . . . .	121
6.4	Concluding remarks . . . . .	126
<b>7</b>	<b>Application of the developed UHPFRC</b>	<b>129</b>
7.1	The project Substitution of Steel with UHPFRC . . . . .	129
7.1.1	UHPFRC hollow box girder . . . . .	129
7.1.2	UHPFRC composite column . . . . .	131
7.2	The project Structural Design for The Quickway System . . . . .	133
<b>8</b>	<b>Conclusions and recommendations</b>	<b>137</b>
	<b>Bibliography</b>	<b>150</b>
<b>A</b>	<b>Appendix A: Materials properties</b>	<b>151</b>
<b>B</b>	<b>Appendix B: Experimental data of pastes and concretes</b>	<b>157</b>
	<b>Curriculum Vitea</b>	<b>161</b>



# List of Figures

- 1.1 The arch road bridge WILD in Carinthia-Austria . . . . . 1
- 1.2 Application of UHPFRC as road bridge topping in Austria . . . . . 2
  
- 2.1 Random sections through part of an agglomerate . . . . . 11
- 2.2 Particle-size distribution of silica fume . . . . . 12
- 2.3 Spread flow test using a mini cone (Okamura and Ozawa [1995]). . . . . 14
- 2.4 An example about determination of the packing density of used cement applying Okamura and Ozawa’s water demand test method . . . . . 14
- 2.5 Model of the Superplasticizer Based Approach by Range and Lohaus [2010] for determination of the packing density of granular concrete mixture. . . . . 15
- 2.6 Relationship between viscosity ( $\mu$ ) and normalized solid concentration ( $\Phi/\Phi^*$ ) 16
- 2.7 Packing density determination for granular concrete mixture developed in this research project using the Kwan’s test method of packing density measurement. The maximum solid concentration of the granular concrete mixture was 0.8276. . 18
- 2.8 Relation between void fraction and size ratio of fine to coarse in a binary system of broken solid . . . . . 19
- 2.9 The packing density of binary mixture according to Furnas model . . . . . 23
- 2.10 Loosening effect and Wall effect . . . . . 24
- 2.11 Wedging effect in the dominant cases of coarse (Left) and fine particles (Right) (according to KWAN et al. [2013]). . . . . 27
  
- 3.1 Distribution of electrical potential in the double-layer region . . . . . 30
- 3.2 Illustration of interparticle potentials as a function of the distance from a charge surface . . . . . 31
- 3.3 Chemical structure of PCEs with ether (left) and imide (right) bonds between the backbone and the side chains (Gelardi et al. [2016]). . . . . 32
- 3.4 Chemical composition of the methacrylate ester PCEs and allylether-based PCEs . . . . . 33
- 3.5 Schematic representation to scale of the molecular architecture of the methacrylate ester PCEs and allylether-based PCEs . . . . . 33
- 3.6 The variation in packing density of blended cements by varying the content of fly ash, quartz powder and lime stone powder. . . . . 36
- 3.7 Modelled changes in hydrated Portland cement - silica fume binder . . . . . 37
- 3.8 Modelled changes in hydrated Portland cement - fly ash binder . . . . . 37
- 3.9 Modelled changes in hydrated Portland cement - blast furnace slag . . . . . 38
  
- 4.1 The particle size distribution of cements, reactive fillers and inert fillers in the test program (log-10 scale for the X axis) . . . . . 43

List of Figures

4.2	The particle size distribution of quartz sands and crushed basalt stones for UHPC production (log-10 scale for the X axis) . . . . .	43
4.3	Walz curve . . . . .	45
4.4	The equipment for the superplasticizer-water solution demand test (left), and the development of power consumption during addition of the solution (right) .	48
4.5	The packing density of four cements in the test using SP-Water solutions with the SP-Water ratios of 0 and 10 wt.% . . . . .	49
4.6	The SP-Water solution demands of the cements . . . . .	49
4.7	The influence of SP1 concentration in SP1-water solution on the packing density of Cem1 . . . . .	51
4.8	The influence of three superplastic SP1, SP2, SP3 on the 28 days compressive strength of Cem1, 2, 3 and 4 with W/C = 25 wt.% and SP/C = 2 wt.% . . . .	52
4.9	The influence of superplasticizer SP1 on the packing density of the mineral admixture . . . . .	54
4.10	SP1-water solution demands of the mineral admixtures . . . . .	54
4.11	The influence of types and content of reactive powders on the 28 days compressive strength of Cem1 - reactive powder binders . . . . .	55
5.1	Three standard geometries of rotational rheometers: parallel plates, cone and plate, Couette (Coussot [2005]). . . . .	58
5.2	Viskomat NT and Viskomat XL with paddle . . . . .	59
5.3	The variation in the packing density of QP <sub>i</sub> -Cem1 blends when Cem1 was replaced progressively by QP <sub>i</sub> (i=1,2,3,4) . . . . .	62
5.4	The packing densities of QP1-Cem1-SF2 mixtures . . . . .	64
5.5	The packing densities of QP2-Cem1-SF2 mixtures . . . . .	64
5.6	The packing densities of QP3-Cem1-SF2 mixtures . . . . .	65
5.7	The variations of the efficient water and its thickness corresponding with the improvement of packing densities of QP1-Cem1-SF2 mixtures . . . . .	66
5.8	The variations of the efficient water and its thickness corresponding with the improvement of packing densities of QP2-Cem1-SF2 mixtures . . . . .	67
5.9	The variations of the efficient water and its thickness corresponding with the improvement of packing densities of QP3-Cem1-SF2 mixtures . . . . .	67
5.10	Influence of SP1 on the plastic viscosity of the cementitious pastes . . . . .	68
5.11	Influence of SP1 on the self-flowability of concretes including optimum Binder <sub>1</sub> , QS2 and W/Cem1 ratio of 25 wt.%. . . . .	70
5.12	Packing densities of Cem1-FA blends when FA replaced Cem1 step by step	71
5.13	Influence of SP1 on the self-flowability of concretes including optimum Binder <sub>4</sub> , QS2 and W/Cem1 ratio of 25 wt.%. . . . .	71
5.14	Variations of the packing density of GGBFS-Cem1 blends by increasing of GGBFS content . . . . .	72
5.15	The packing densities of GGBFS-Cem1-limestone powder binders . . . . .	73
5.16	Influence of SP1 on the self-flowability of concretes including optimum Binder 5, QS2 and W/Cem1 ratio of 25 wt.%. . . . .	74
5.17	Determination of the optimum proportion of QS2-QS3 blend using the CPM and CIPM . . . . .	76

5.18	Stepwise optimization for UHPCs-1mm using QS2, QS3 and Paste1 with 720 kg Cem1 . . . . .	77
5.19	Stepwise optimization for UHPCs-1mm using QS2, QS3 and Paste2 with 720 kg Cem1 . . . . .	78
5.20	Stepwise optimization for UHPCs-1mm using QS2, QS3 and Paste3 with 720 kg Cem1 . . . . .	79
5.21	The 28 days compressive strength of concrete formed by ideal grading curve	81
5.22	Stepwise optimization for UHPCs-2.5mm using QS1, QS3 and Paste3 with 720 kg Cem1 . . . . .	83
5.23	Stepwise optimization for UHPCs-2.5mm using QS1, QS2, QS3 and Paste3 with 720 kg Cem1 - STAGE 1 . . . . .	85
5.24	Stepwise optimization for UHPCs-2.5mm using QS1, QS2, QS3 and Paste3 with 720 kg Cem1 - STAGE 2 . . . . .	86
5.25	Stepwise optimization for UHPCs-4mm using CrB2, QS2, QS3 and Paste3 with 720 kg Cem1 - STAGE 1 . . . . .	87
5.26	Stepwise optimization for UHPCs-4mm using CrB2, QS2, QS3 and Paste3 with 720 kg Cem1 - STAGE 2 . . . . .	88
5.27	Stepwise optimization for UHPCs-8mm using CrB1, QS1, QS2, QS3 and Paste3 with 640 kg Cem1 - STAGE 1 . . . . .	89
5.28	Stepwise optimization for UHPCs-8mm using CrB1, QS1, QS2, QS3 and Paste3 with 640 kg Cem1 - STAGE 2 . . . . .	90
5.29	Stepwise optimization for UHPCs-8mm using CrB1, QS1, QS2, QS3 and Paste3 with 640 kg Cem1 - STAGE 2 . . . . .	91
5.30	The packing density of the optimum UHPC-1mm-Paste3, UHPC-2.5mm-Paste3, UHPC-4mm-Paste3 and UHPC-8mm-Paste3 determined applying Kwan's method.	93
5.31	Stepwise optimization for UHPCs-2.5mm using QS1, QS2, QS3 and Paste4 with 720 kg Cem1 - STAGE 1 . . . . .	94
5.32	Stepwise optimization for UHPCs-2.5mm using QS1, QS2, QS3 and Paste4 with 720 kg Cem1 - STAGE 2 . . . . .	95
5.33	Stepwise optimization for UHPCs-2.5mm using QS1, QS2, QS3 and Paste5 with 720 kg Cem1 - STAGE 1 . . . . .	96
5.34	Stepwise optimization for UHPCs-2.5mm using QS1, QS2, QS3 and Paste5 with 720 kg Cem1 - STAGE 2 . . . . .	97
5.35	Strength development of the optimum UHPC-2.5mm-Paste3, UHPC-2.5 Paste4 and UHPC-2.5 Paste5 . . . . .	98
6.1	Stress-strain response in tension of conventional and high performance fibre reinforced concretes . . . . .	102
6.2	The used fibres in the research project . . . . .	106
6.3	Compulsory Mixer for preparation of UHPFRC. . . . .	107
6.4	Specimens preparation for pullout test. . . . .	108
6.5	Configuration of the single fibre pullout test . . . . .	108
6.6	standard test method for flexural performance of FRC according to the ASTM C1609/C1609M . . . . .	109
6.7	Four-point bending test setup for beam . . . . .	109
6.8	Example of end shapes for direct tensile test . . . . .	110

## List of Figures

6.9	Direct tensile test setup developed by Graybeal and Baby [2013]	110
6.10	Specimen preparation and direct tension test setup.	111
6.11	Scheme for the inverse analysis procedure acc. to Lopez et al. [2015].	112
6.12	The pullout resistances of smooth straight fibres F1 and F2	113
6.13	The pullout resistances of crimped fibres F3 and F4 in the matrix of UHPC-1mm.	114
6.14	The pullout resistances of indented hooked ends fibre F5 and indented straight fibre F6 in the matrix of UHPC-1mm.	115
6.15	The slump-flow (top) and T500 time (bottom) of UHPCs with and without fibres F1, F2	117
6.16	Fibre clumps in the UHPCs	118
6.17	The effect of fibres F1 and F2 on the flexural behaviours of UHPFRC-8mm, 4mm, 2mm, 1mm.	119
6.18	Deflection-hardening and Strain-hardening behaviours of UHPFRCs-1mm having 1.75 vol.% F1, experimental and estimated results.	120
6.19	Deflection-hardening and Strain-hardening behaviours of UHPFRCs-1mm having 1 vol.% F1, experimental results and estimated result by Lopez's method.	121
6.20	Influence of fibres F1, F2 on the flexural and tensile behaviours of UHPFRCs-1mm-750kgCem1, experimental results and estimation.	123
6.21	Influence of fibres F3, F4, F5, F6 on the flexural and tensile behaviours of UHPFRCs-1mm-750kgCem1, experimental results and estimation.	124
7.1	Bridge cross section with UHPFRC box girders and a layer of normal strength concrete.	130
7.2	Cross section of the UHPFRC girder including the prestressing strands.	130
7.3	Test setup for pull-out tests with thin plate (left), according to RILEM (right) and cross-section (middle).	131
7.4	Schematic cross section of the UHPC composite column.	132
7.5	Different amount of spiral reinforcement (Types A and C) and test setups for the UHPC columns.	132
7.6	Curved cross section.	134
7.7	Overview of the precast beam elements.	134
7.8	Casting for beam segment of 0.5 m with full scale curved cross section	135
7.9	Evaluation of the structural performance of assembled system for Quickway.	135

# List of Tables

- 1.1 The reference mixtures of the priority program SPP 1182 of German Research Foundation, after Schmidt and Fehling et al. [2014]. . . . . 3
- 1.2 Compressive strength classes for UHPFRC acc. to standards NFP 18-470 [2016b]. 4
- 1.3 Typical composition of Ductal<sup>®</sup> in North America (Russell and Graybeal [2013]). 4
  
- 2.1 Binding mechanisms of agglomeration (Pietsch [2005]). . . . . 10
- 2.2 K values for different packing process (DE LARRARD et al. [1999]). . . . . 25
  
- 4.1 Physical-mechanical properties and chemical component of the used cements. . . 42
- 4.2 Physical-mechanical properties and chemical component of the used reactive fillers. 42
- 4.3 Physical properties and chemical component of the used inert fillers and aggregates. 42
- 4.4 Computing the residual packing densities of monosized classes of polydisperse quartz sand QS1 based on its experimentally actual packing density. . . . . 44
- 4.5 Estimating the degree of hydration of portland cement and the compressive strength of hardened paste. . . . . 47
  
- 5.1 Mix proportion of concrete mixtures computed by the modified Andreasen and Andersen equation-based ideal curve . . . . . 81
- 5.2 Mix proportion and properties of the developed optimum UHPCs based on Paste3 in comparison with the reference mixtures. . . . . 92
  
- 6.1 The experimental results of the maximum concentration of fibres F1 and F2 and the equivalent fibre factors for self-compacting UHPFRCs with maximum grain sizes of 1 mm, 2 mm, 4 mm and 8 mm. . . . . 116
- 6.2 The compressive strength and the average flexural properties of UHPFRCs. . . . 120
- 6.3 Experimental and estimated tensile results of UHPFRC-1mm containing 1.75 vol.% F1 and 1 vol.% F2. . . . . 121
- 6.4 Fibre contents for bending and tension test. . . . . 122
- 6.5 The average flexural properties of UHPFRCs-1mm-750kgCem1 with different fibres types, contents. . . . . 123
- 6.6 Tension test results of UHPFRCs-1mm-750kgCem1 with six different fibre types and contents. . . . . 125
  
- A.1 Passing volume - Particle size distribution of the used cements and reactive fillers. 151
- A.2 Passing volume - Particle size distribution of the used inert fillers. . . . . 152
- A.3 Computing the residual packing densities of monosized classes of polydisperse quartz sand QS1 based on its experimentally actual packing density. . . . . 153
- A.4 Computing the residual packing densities of monosized classes of polydisperse quartz sand QS2 based on its experimentally actual packing density. . . . . 154

*List of Tables*

A.5	Computing the residual packing densities of monosized classes of polydisperse quartz sand QS3 based on its experimentally actual packing density. . . . .	154
A.6	Computing the residual packing densities of monosized classes of polydisperse crushed basalt CrB1 based on its experimentally actual packing density. . . . .	154
A.7	Computing the residual packing densities of monosized classes of polydisperse crushed basalt CrB2 based on its experimentally actual packing density. . . . .	155
A.8	Packing densities, water demand, superplasticizers demand of the used cements . . . . .	155
A.9	The influence of SP1 concentration in SP1-Water solution on the packing density of Cem1. . . . .	155
A.10	The influence of three superplasticizers SP1, SP2, SP3 on the 28 days compressive strength of Cem1, 2, 3 and 4 . . . . .	156
A.11	Packing densities, water demands, SP1 demands of mineral admixtures . . . . .	156
A.12	The influence of types and content of reactive powders on the 28 days compressive strength of binders containing Cem1 and reactive powders . . . . .	156
B.1	The variation in the packing density of QP <sub>i</sub> -Cem1 blends, FA-Cem1 blends and GGBFS-Cem1 blends . . . . .	157
B.2	The variation in the packing density of mixtures containing SF2 and the optimum blends (QP <sub>i</sub> +Cem1) . . . . .	157
B.3	The computed water-powder volume ratios of mixtures containing SF2 and the optimum blends (QP <sub>i</sub> +Cem1) . . . . .	158
B.4	The variations in efficient-water to solid volume ratios and the film thickness of the efficient water in ternary binders containing SF2 and the optimum blends (QP1+Cem1) . . . . .	158
B.5	The variations in efficient-water to solid volume ratios and the film thickness of the efficient water in ternary binders containing SF2 and the optimum blends (QP2+Cem1) . . . . .	159
B.6	The variations in efficient-water to solid volume ratios and the film thickness of the efficient water in ternary binders containing SF2 and the optimum blends (QP3+Cem1) . . . . .	159
B.7	Influence of SP1 on the plastic viscosity of the cementitious pastes . . . . .	159
B.8	The variation in the packing density of mixtures containing LSP and the optimum blends (GGBFS+Cem1) . . . . .	160
B.9	The computed water-powder volume ratios of mixtures containing LSP and the optimum blends (GGBFS+Cem1) . . . . .	160
B.10	Determination of the saturated SP1 based on the influence of SP1 content on the self-flowability of fine grain concretes . . . . .	160
B.11	The 28 days compressive strength of concrete formed by the modified Andreasen and Andersen equation-based ideal curve . . . . .	160

## Notations and symbols

$\alpha(t)$	degree of hydration of portland cement at t(days) age [-]
$\beta$ or $\beta_{\text{mix-actual}}$	real packing density of a granular mixture, measured with a given packing process [-]
$\beta_{\text{mix-virtual}}$	virtual packing density of a granular mixture [-]
$\beta_i$	the residual packing density of the $i^{\text{th}}$ size class in polydisperse aggregate [-]
$\Gamma_P$	relative flow area in a spread-flow test acc. to Okamura [-]
$\varepsilon$	volume ratio of water to granular material corresponding to a null relative flow area in a spread-flow test [-]
$\epsilon_{t,\text{max}}$	the maximum strain [% <sub>0</sub> ]
$\zeta$ -potential	zeta potential
$\rho_{\text{ABC}(i)}$	density of the $i^{\text{th}}$ ABC component of a blended mixture [kg/m <sup>3</sup> ]
$\rho_{\text{bulk}}$	bulk density of a material [kg/m <sup>3</sup> ]
$\rho_{\text{solid}}$	density of a material [kg/m <sup>3</sup> ]
$\varrho$	the solid concentration of a wet mixture measured by Kwan's packing test method [-]
$\sigma_{\text{cc}}, \epsilon_{\text{cc}}$	the first cracking tensile stress [MPa] and the corresponding strain [% <sub>0</sub> ] respectively
$\sigma_{\text{pc}}, \epsilon_{\text{pc}}$	the ultimate tensile stress [MPa] and the corresponding strain [% <sub>0</sub> ] respectively
$\sigma_{\text{mu}}$	the tensile stress of fibre-free matrix [MPa]
$\tau_f$	average fibre-matrix bond strength [MPa]
$\phi$	void fraction of a granular mixture [-]
$\psi_\delta$	Stern potential

## Notations and symbols

C-point	volume ratio of liquid including water and superplasticizer to granular material corresponding to a null relative flow area in a spread-flow test, determined acc. to model of the Superplasticizer Based Approach
$D_f$	fibre diameter [mm]
$D_{\max}, D_{\min}$	the largest and the smallest particle sizes of a granular mixture [mm]
$f_{c,cube}$	compressive strength of concrete cube [MPa]
$f_{c,cyl}$	compressive strength of concrete cylinder [MPa]
h-value	relative plastic viscosity in Bingham model measured by a rotational rheometer [N-mm/rpm]
K-value	the compaction index of a packing process [-]
$L_f$	fibre length [mm]
$M_{ABC(i)}$	mass of the $i^{\text{th}}$ ABC component of a blended mixture [kg]
q-value	the distribution modulus ( $0 < q < 1$ ) in the modified Andreasen and Andersen equation-based packing model [-]
$P_{\text{tar}}(D_i)$	the cumulative finer than $D_i$ computed by the modified Andreasen and Andersen equation-based packing model [vol.%]
SpWD	Superplasticizer-Water demand of a material [wt.%]
Sp*/Pow	Superplasticizer demand of a powder converted from Superplasticizer-Water demand of the powder [wt.%]
$V_{ABC(i)}$	solid volume of the $i^{\text{th}}$ ABC component of a blended mixture [m <sup>3</sup> ]
$t_{\text{efficient-water}}$	the thickness of the efficient water film [nm]
$V_{\text{bulk}}$	bulk volume of a material [m <sup>3</sup> ]
$V_{\text{efficient-water}}$	the efficient water for paste flowing [m <sup>3</sup> ]
$V_{f\text{-critical}}$	the critical volume fraction of fibres to obtain strain-hardening or deflection-hardening behaviour [vol.%]
$V_{\text{Liq}}$	total volume of added liquid until reaching maximum power consumption in Water - Superplasticizer demand test [m <sup>3</sup> ]
$V_{\text{solid}}$	total solid volume of a material [m <sup>3</sup> ]
$V_W/V_{\text{Pow}}$	Volume ratio of Water to Powder

W/C	Weight ratio of Water to Cement
W*/Pow	Water demand of a powder converted from Superplasticizer-Water demand of the powder [wt.%]
WD	Water demand of a material [wt.%]
ACI	American Concrete Institute
AFGC	Association Française de Génie Civil
AFNOR	Association Française de Normalisation
ASTM	American Society for Testing and Materials
CIPM	CompactionInteraction Packing Model
CPM	Compressible Packing Model
DLVO	DLVO theory, developed by Derjaguin, Landau, Verwey, and Overbeek
LVDT	Linear Variable Displacement Transducer
PCEs	Polycarboxylate-based superplasticizers
UHPC	Ultra-High Performance Concrete
UHPFRC	Ultra-High Performance Fiber Reinforced Concrete



# 1. Introduction

## 1.1. UHPFRC research and application

The improvement of packing density of granular composition in combination with highly effective superplasticizer together with fibre reinforcing generates a new class of concretes called Ultra-High Performance Fibre Reinforced Concrete (UHPFRC). Ultra-High Strength Concretes are characterized by brittle failure behaviour. The adding of high volume steel fibres, i.e. higher than 1 vol.%, to the brittle matrix improves the ductility and the toughness considerably. Self-compacting properties of concrete matrix is really essential to ensure a good workability of UHPFRC. The compressive strength of about 150 - 200 MPa, the high ductility and toughness, the extremely good durability properties of UHPFRC make it, more and more, become popular materials for building of new structures with light weight in elegant form as well as for repair and strengthening of existing structures with a longer service life. For instance:

- Figure 1.1 shows an arch road bridge in Austria (Reichel et al. [2011a, 2011b]). Due to the high stiffness of the arch structure a maximum utilization of the high compressive strength of UHPFRC was achieved. The main span of the two parallel arches is about 70 m. The wall thickness of the precast hollow box UHPFRC is 60 mm only.

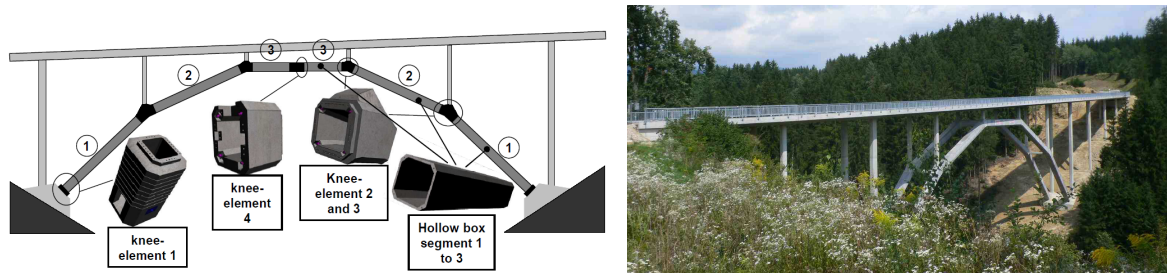


FIGURE 1.1.: The arch road bridge WILD in Carinthia-Austria: assembly of the UHPC precast elements of the arch (left) and the completed bridge in August 2010 (right), after Reichel et al. [2011a, 2011b]

- Figure 1.2 shows the application of UHPFRC in the renovation of an existing reinforced concrete motorway bridge in Austria (Tue et al. [2015]). A thin UHPFRC layer of 7 cm replaced the waterproofing as well as the asphalt pavement and increased the load-carrying capacity.

During the last decades numerous UHPFRC researches all over the world presented and discussed at many prestigious UHPFRC International Symposium (Germany (Fehling

## 1. Introduction



FIGURE 1.2.: Application of UHPFRC as road bridge topping within the adaptation of an existing conventional bridge to an integral abutment bridge - Steinbach bridge S6 motorway in Austria: casting the UHPFRC bridge deck (left) and the finished bridge topping (right), after Tue et al. [2015]

et al. [2004, 2008, 2016] and Schmidt et al. [2012]); France (AFGC/fib [2009, 2013]); USA (Sritharan et al. [2016])) and National Research Program on UHPFRC (France (AFGC [2002, 2013] and AFNOR [2016b, 2016a]); Germany (Schmidt et al. [2014]); USA (FHWA [2015])) have given a broad survey of all aspects of UHPFRC including raw materials, micro- and macro-structures, mechanical behaviour, durability as well as of construction and design specifications appropriate for this material. The detail information about completed UHPC Projects can be found in the books of Resplendino and Toutlemonde [2011] and of Fehling and Schmidt et al. [2013].

**UHPFRC in Germany:** The priority program SPP 1182 of the German Research Foundation with the participation of 26 university and industrial research institutes is a great effort to create the precondition to individually design, produce and purposefully apply UHPFRC from suitable, locally available raw materials (Schmidt and Fehling et al. [2014]). In the program SPP 1182, various standards UHPFRC were developed at the University of Kassel. Holcim sulfo CEM I 52.5 R HS/NA with  $C_3A$  lower than 1.5 wt.% was used for all researches, the quality of the cement clinker phases was monitored very strictly. Table 1.1 describes some typical UHPC compositions developed for the program SPP 1182.

**UHPFRC in France:** Based on the technical consensus expressed in AFGC Recommendations [2002, 2013] two standards for UHPFRC were introduced in France. One standard for UHPFRC as a construction product, referred as NFP 18-470 (AFNOR [2016b]). One standard for the design of UHPFRC structures, referred as NFP 18-710 (AFNOR [2016a]), which stands as a national complement to Eurocode 2. According to NFP 18-470 (AFNOR [2016b]) UHPFRC fulfills the following requirements:

- Maximum size of aggregates is smaller or equal to 10 mm.
- Concrete density is about 2200-2800 kg/m<sup>3</sup>.
- Characteristic value of the elasticity limit under tension at 28 days  $f_{ctk,el} \geq 6$  MPa.
- Water porosity at 90 days  $\leq 9\%$ .
- Coefficient of apparent diffusion of chloride ions at 90 days  $\leq 0.5 \times 10^{-12}$  m<sup>2</sup>/s.
- Apparent gas permeability at 90 days  $\leq 9 \times 10^{-19}$  m<sup>2</sup>.

### 1.1. UHPFRC research and application

Additionally, the 28 days characteristic compressive strength measured on cylinders with 100 mm diameter and 200 mm height is used for the compressive strength classification of UHPFRC, as listed in Table 1.2.

TABLE 1.1.: The reference mixtures of the priority program SPP 1182 of German Research Foundation, after Schmidt and Fehling et al. [2014].

	Unit	M2Q	M2Qb	M3Q	M3BS	B4Q	B5Q
Water	( $kg/m^3$ )	166	166	183	165	158	158
Cement CEMI 52.5R Holcim Sunfo	( $kg/m^3$ )	832	832	775	832	650	650
Silica fume	( $kg/m^3$ )	135	135	164	135	177	177
	Product	Elkem Microsilica Grade 983	Elkem Microsilica Grade 971	Sika Silicoll P undensified	Sika Silicoll P undensified	Elkem Microsilica Grade 983	Sika Silicoll P undensified
Superplasticizer	( $kg/m^3$ )	29.4	29.4	23.5	24.2	30.4	30.3
	Product	FM 1254	Master Glenium 51	Sika Visconcrete 2810	Sika Visconcrete 2810	Master Glenium 51	Sika Visconcrete 20 Gold
Quartz Pow. I - MILLSIL W12	( $kg/m^3$ )	207	207	193	207	325	325
Quartz Pow. II - MILLSIL W3	( $kg/m^3$ )	-	-	-	-	131	131
Quartz sand 0.125-0.5 mm H33 or G33	( $kg/m^3$ )	975	975	946	-	354	354
Basalt 0-2 mm	( $kg/m^3$ )	-	-	-	1104	-	-
Basalt 2-8 mm	( $kg/m^3$ )	-	-	-	-	597	597
Steel fibres STRATEC Weidacon	(%vol.)	2.5	2.5	2.5	2.5	2.5	2.5
W/C ratio		0.22	0.22	0.255	0.22	0.275	0.28
W/B ratio		0.19	0.19	0.21	0.19	0.215	0.22
<b>Compressive strength (MPa)</b>							
Cube 100mm		172.2	-	-	-	-	187.4
Cylinder D16cm/H32cm		154.3	-	-	-	-	168.3

## 1. Introduction

TABLE 1.2.: Compressive strength classes for UHPFRC acc. to standards NFP 18-470 [2016b].

Compressive strength class	Limiting value	
	Minimum $f_{ck-Cylinder}$ (MPa)	Minimum $f_{ck-Cube}$ (MPa)
UHPC 130/140	130	145
UHPC 150/165	150	165
UHPC 175/190	175	190
UHPC 200/215	200	215
UHPC 225/240	225	240
UHPC 250/265	250	265

**UHPFRC in USA:** UHPFRC bridges were developed in USA since 2001 by the Federal Highway Administration as a pioneer in research on the optimal uses of UHPFRC in the highway bridge infrastructure. The products of the developed UHPFRC projects include precast, prestressed girders; precast waffle panels for bridge decks; and jointing material between precast concrete deck panels and girders and between the flanges of adjacent girders. Ductal<sup>®</sup> is a commercial product used in most UHPC researches and applications in North America. Table 1.3 shows a typical composition of this material (Russell and Graybeal [2013]).

TABLE 1.3.: Typical composition of Ductal<sup>®</sup> in North America (Russell and Graybeal [2013]).

Materials	kg/m <sup>3</sup>	wt.% of cement
Portland Cement	712	100
Fine sand	1020	143.3
Silica fume	231	32.4
Ground Quartz	211	29.6
Superplasticizer (SP)	30.7	4.3
Accelerator	30	4.2
Steel fiber	156	21.9
Water	109	15.13 (without water in SP and Accelerator)

## 1.2. Motivation

In order to achieve the highest performance of UHPFRC the basic rules for UHPFRC production have been applied since the first introduction by Bache [1981] and the further development of Reactive Powder Concrete by Richard and Cheyrezy [1995]. These rules are:

- The homogeneity of the concrete is improved by eliminating coarse aggregates because large grains cause stress concentrations that lead to a decrease in strength.
- An optimum packing density for the granular applied materials in concrete is important. As a result of that, the microstructure of concrete is improved significantly by the fine particles of reactive and inert materials.

- Fine steel fibres with a sufficient content have to be added to the brittle matrix to obtain a ductility behaviour.
- Post-set heat treatment of 90 °C should be used to accelerate the cement hydration as well as the pozzolanic reaction that help improve the microstructure and the mechanic properties.

Based on the first three rules most developed UHPFRC mixtures consist of high hydraulic reactivity Portland cement, ultra-fine and high reactive materials like silica fume or fly ash or ground granulated blast furnace slag, fine (or ultra-fine) inert filler materials such as quartz powder or limestone powder, fine sand with grain size of smaller 1 mm, highly effective superplasticizer, water and fine steel fibre with the aspect ratio  $L_f/D_f$  of higher than 65. In addition, it is well-known that UHPFRC has a very low water-binder ratio of about 0.2, cement dosage is from 650 kg/m<sup>3</sup> to 850 kg/m<sup>3</sup>. Silica fume, quartz powder, polycarboxylate ethers based superplasticizer, with respect to the cement, are used in wide ranges of 15-30 wt.%, 30-50 wt.%, 3-4 wt.%, respectively. Fine steel fibres with high aspect ratio are usually used in range of 1-3 vol.%.

Surprisingly, UHPFRC mix design is still one of topics of universal interest with regard to using local materials in order to reduce its production cost but meet fully the highest quality. Generally speaking, mix design is one of the most important tasks of UHPFRC applications. It focuses on optimizing the properties of concrete in fresh and hardened states to satisfy the specific requirements. The particle packing density optimization for the granular composition of the concrete has been accepted as the key concept for UHPFRC mix design (Bache [1981], Richard and Cheyrezy [1995], Schmidt et al. [2005], Fehling et al. [2013]).

However, the available literature about UHPFRC mix design based on particle packing density optimization is not sufficient. In addition, the existing particle packing models for concrete mix design have some limits, leading to a large difference between predictions and experimental results. For instance, in ideal curve models the particle shape, particle packing of input materials are not taken into account. Furthermore, the surface force of fines is not considered in nearly all particle packing models. In reality the modification of the existing UHPFRC mixtures of the available literature by trial and error is very popular for UHPFRC mix design. By this way lots of experiments have to be carried out but the success of the expected concrete is limited due to the different sources of the input materials.

It is a challenging problem to design UHPFRC mixture using local commercial materials. For instance, the local commercial input materials are completely different in comparison to the input materials in the literature, and there are many different products from many materials suppliers for each input material. The questions here are, for example, with regard to the improvement of the packing density and strength, how to select the proper materials for UHPFRC production, how to calculate the optimum powder combination for cementitious materials, how to obtain the best concrete with the highest packing density and an expected performance through the combination of the optimum paste and the optimum blended aggregates which is formed by the mixing of different grain aggregates, what are existing particle packing models suitable for UHPFRC

## 1. Introduction

mix design and how to employ them, how to find out the optimum fibre for reinforcing UHPFRC considering the highest performance and cost efficiency.

### 1.3. Research Objective

The performance requirements for UHPFRCs in this research were the self-compacting properties, the 28 days compressive strength of more than 180 MPa, the high ductility and toughness. Therefore, the answer to the above mentioned questions is very important to obtain the success in production and quality control for UHPFRC.

The objective of this research was the development of a systematic, reliable and efficient method for UHPFRC mix design using local commercial materials.

The research includes two parts:

- In the first part, based on particle packing optimization various optimum mix proportion of UHPC matrices with different maximum grain size from 1 mm to 8 mm were developed.
- In the second part, the influence of the fibre types, volume and the matrices composition on the self-flowing ability and mechanical behaviour of UHPFRCs were investigated.

### 1.4. Research Strategy and Outline

First, the optimum mix proportions of UHPC matrices were developed. This part of the thesis includes chapters 2, 3, 4 and 5.

- In chapter 2 the appropriate test methods for particle packing density measurement were introduced. The principles in particle packing and the existing particle packing models for concrete mix design were also summarized. As a result of that, the idea of modification and application of existing particle packing models for UHPFRC mix design is presented.
- The importance of the compatibility of constituent materials and the role of mineral admixtures in UHPFRC production were emphasized in chapter 3 based on the overview of UHPFRC research focusing in materials.
- Materials selection which is a crucial part in mix design for UHPC was reported in detail in chapter 4. The most suitable materials were selected concerning their highest compatibility for the highest packing density and strength. In this chapter a highly effective method of particle packing density measurement for powder was proposed.
- An optimization process from paste to the whole concrete matrix was carried out and presented in chapter 5. A straightforward and effective method of stepwise optimization was proposed for granular materials combination regarding improvement in packing density as well as rheological behaviour. Some existing packing models were employed for the mix design and their effectiveness were evaluated experimentally.

#### *1.4. Research Strategy and Outline*

The effects of steel fibre on the properties of UHPFRC in fresh and hardened states were investigated and presented in chapter 6. An overview about steel fibre reinforced concrete highlighted the important factors which highly affect the performance of fibre concrete. The influences of fibres and matrix components on the flowability and mechanical behaviour of UHPFRC were investigated in detail.

Chapter 7 describes some pilot projects which have used the developed UHPC.

Chapter 8 is the conclusions of the research project.



## 2. Particle packing model in concrete

### 2.1. General definitions

The packing density of a granular mixture is defined as the ratio of the total solid volume of the granular mixture  $V_{solid}$  to the bulk volume occupied by the particles  $V_{bulk}$ , represented by Equation (2.1).

$$\beta_{mix-actual} = \frac{V_{solid}}{V_{bulk}} = \frac{\frac{M}{\rho_{solid}}}{\frac{M}{\rho_{bulk}}} = \frac{\rho_{bulk}}{\rho_{solid}} \quad (2.1)$$

where:  $M$  is mass of the granular mix (g or kg),  $\rho_{solid}$  and  $\rho_{bulk}$  are the particle density and bulk density of the granular material respectively ( $kg/m^3$  or  $g/cm^3$ ).

The void content within the granular structure is called void fraction which is directly related to the packing density by Equation (2.2).

$$\phi = 1 - \beta_{mix-actual} \quad (2.2)$$

According to Funk and Dinger [1994] the terminology for particles distribution in size classes are as follows:

- Monodispersion refers to particles of one size only, whether spheres or angular particles.
- Discretely sized particles describes the particles within a single, narrow class size such as between two sieves, or a single class in a particle size analyzer. In this context, the opening sizes of a sieves set vary by a factor of  $\sqrt{2}$  or  $\sqrt[4]{2}$ .
- Continuous size distribution concerns the particles cover a range of particle sizes that is continuous from the largest particle size  $D_{max}$  to a smallest particle size  $D_{min}$ .
- Polydispersion applies to a mixture of two or more monodispersions or discrete sizes.

### 2.2. Particle packing density measurement

#### 2.2.1. Agglomeration of fine particles

Agglomeration is the sticking together of particulate solids which is caused by short-range physical or chemical forces between the particles themselves, by chemical or physical modifications of the solids which are triggered by specific process conditions, or by binders,

## 2. Particle packing model in concrete

substances that adhere chemically or physically to the solid surfaces and form a material bridge between the particles. Agglomeration occurs naturally and, especially if a sufficiently large fraction of fine particles is present (particle size is smaller 125 micron). Table 2.1 (Pietsch [2005]) presents the binding mechanisms of agglomeration including five major groups and several subgroups.

TABLE 2.1.: Binding mechanisms of agglomeration (Pietsch [2005]).

<b>I</b>	<b>Solid bridge</b> , caused by:
1	Sintering
2	Partial melting
3	Chemical reaction
4	Hardening binders
5	Recrystallization
6	Drying
	a) Recrystallization (dissolved substances)
	b) Deposition (colloidal particles)
<b>II</b>	<b>Adhesion and cohesion forces</b>
1	Highly viscous binders
2	Adsorption layers (< 3 nm thickness)
<b>III</b>	<b>Surface tension and capillary pressure</b>
1	Liquid bridges
2	Capillary pressure
<b>IV</b>	<b>Attraction forces between solids</b>
1	Molecular forces
	a) van-der-Waals forces
	b) Free chemical bonds (valence forces)
	c) Associations (non-valence); hydrogen bridges
2	Electric forces (electrostatic, electrical double layers, excess charges)
3	Magnetic forces
<b>V</b>	<b>Interlocking bonds</b>

Van der Waals forces, which highly influence the agglomerate of fine particles in both of dry and wet condition, refer to a group of electrodynamic interactions including Keesom, Debye and London dispersion interactions that occur between the atoms in two particles. The dispersion force is a result of Columbic interactions between correlated fluctuating instantaneous dipole moments within the atoms that comprise the two particles. In general the van der Waals interaction is always attractive between two particles with the same materials. The sign and magnitude of the interaction for a particular pair of particles interacting in a given medium is expressed as the numerical value of the Hamaker constant. Oxide minerals in air are strongly attractive and cohesive, they in water are also attractive but less than in air, for example the Hamaker constants of silica-air system and silica-water system are  $6.5 \times 10^{-20}$  J and  $0.7 \cdot 10^{-20}$  J respectively (Franks [2008]). Lomboy et al. [2011] reported that the pull-off forces of quartz powder and calcite powder interacting with  $\text{Si}_3\text{N}_4$  equal  $14.66 \pm 0.57$  nN and  $10.19 \pm 0.55$  nN in air, equal  $2.47 \pm 0.27$  nN and  $1.9 \pm 0.46$  nN in water, respectively, corresponding the effective Hamaker constants of  $1.96 \pm 0.58 \cdot 10^{-20}$  J and  $1.03 \pm 0.34 \cdot 10^{-20}$  J in water. Such results allow to explain the positive effect of limestone powder on the fluidity of concrete in comparison to concrete using

quartz powder.

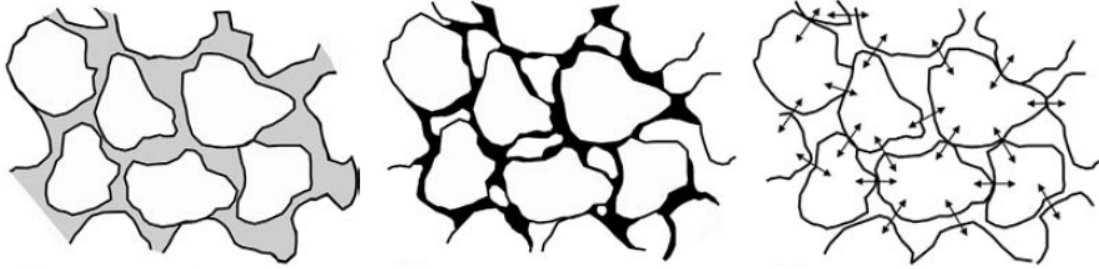


FIGURE 2.1.: Random sections through part of an agglomerate: (left): pore volume filled with a wetting liquid; (middle): liquid bridges at the coordination points; (right): adhesion forces at the coordination points (Pietsch [2005]).

For concrete technology the occurrence of the agglomeration is undesired in dry powders of cement, mineral admixture as well as in concrete mixture.

The agglomerate in dry powders can occur in the production (in grinding of cement, ground granulated blast furnace slag, silica powder, or in burning-cooling-collecting of industrial by-products such as fly ash, silica fume) and in the preservation as well. During grinding bonds between the atoms and molecules of a solid are stressed and ultimately part creating new surfaces. Immediately after separation, unsatisfied valences exist on these newly created surfaces. The recombination of free valence forces at newly created and the van der Waals forces between the particles form strong agglomerates. For example, in the case of silica fume with ultrafine particles van der Waals forces highly arise forming strong adhesion forces in the agglomerates. Besides, the agglomerate can occur in the molten state due to solid bridge mechanism. In preservation most finely divided solids easily attract free atoms or molecules from the surrounding atmosphere. The thin adsorption layers are then formed on particles surfaces, they contact and penetrate each other, leading a bonding forces between the particles.

The wet agglomerate in concrete mixing is formed by liquid bridges at the coordination points between the particles. We can, however, control the wet agglomerate by using polymer admixtures. In most cases, the products of an agglomerate contain a significant void fraction. This problem does not only lead to inaccurate results of materials characterization such as particle size distribution, packing density etc., but also reduces the performance of concrete due to heterogeneous and porous structure.

The agglomerates in silica fume is an interesting example about the disadvantage of agglomerate in concrete technology. Varying the intensity and duration of ultrasonic dispersion gives very different results of particle size distribution for the same silica fume, as presented in Figure 2.2 (ACI 234R-06 [2006]). Diamond et al. [1997, 2004] pointed out the strong agglomerate of silica fume cannot be dispersed in concrete mixing, their size are larger the sizes of cement particles, thus limiting any potential benefits attributed to the filler effect. The agglomerates in silica fume behave as small aggregates, rather than as pozzolans, and react expansively with alkalis in cement. Also, the improvements on

## 2. Particle packing model in concrete

both microstructure and mechanical properties of hardened cement pastes by silica fume addition are not effective due to the agglomeration of silica fume (Yajun et al. [2003]).

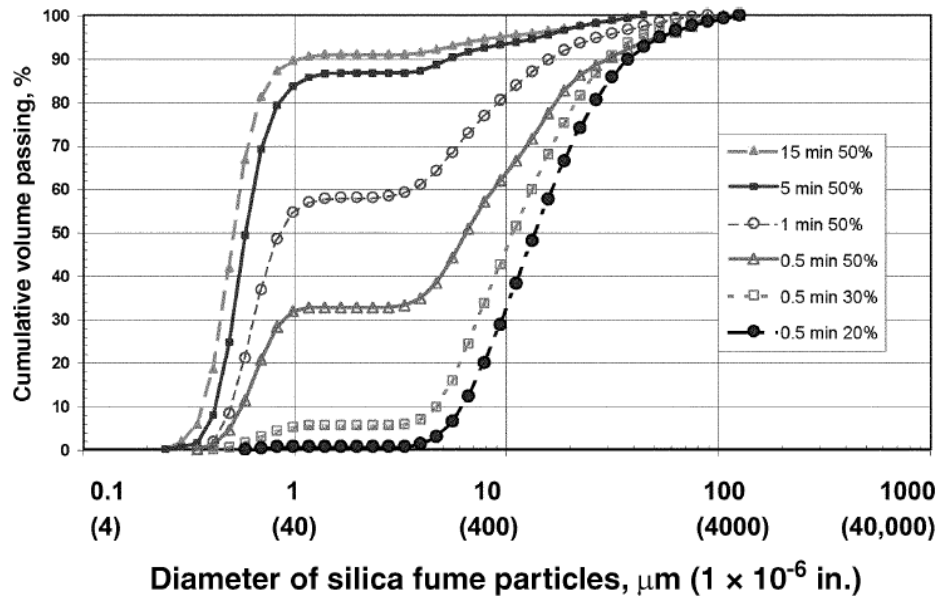


FIGURE 2.2.: Particle-size distribution of silica fume subjected to varying amounts of dispersion. The set of curves shows the importance of the amount of dispersion on the measured distribution. Varying the intensity and duration of ultrasonic dispersion gives very different results for the same silica fume. The values shown are percentages of full stroke in a Microtrac apparatus; higher percentages indicate increased dispersion effort. (Figure courtesy of Elkem ASA Materials.) (ACI 234R-06 [2006]).

### 2.2.2. Dry packing density of coarse particle

For coarse particles (larger than 125 micron) which is not influenced by agglomeration the packing density of granular mixture is determined in dry condition by applying Equation (2.1). Firstly, the bulk density of granular mix ( $\rho_{\text{bulk}}$ ) is determined according to European Standard EN 1097-3 [1998] using a metal cylindrical container of prescribed diameter and depth, depending on the maximum size of the particles. The packing of the particles can be obtained without or with compaction. Thus, the standard EN 1097-3 specified two degrees of bulk density: loose (un-compacted) and compacted. Secondly, the particle density  $\rho_p$  is measured as specified by European Standard EN 1097-6 [2013].

### 2.2.3. Wet packing density or water demand of powder

For fine particle (smaller than 125 micron), which is strongly influenced by interparticle forces forming agglomerates as well as untrue packing density, the principles of packing density measurement are: (i) minimizing the agglomeration in fine particles and (ii) determining liquid or gas filled up the void fraction in the packing. In this context the determined liquid, which is water normally, called water demand of the powder. From

concrete science point of view, the packing density of fine particles should be examined under wet condition which represents the actual working environment in concrete taking the dispersion effect of superplasticizer into account.

Various packing density measurement methods for fine particles under wet condition were proposed in numerous researches (Okamura [1995], Miller [1996], de Larrard [1999], Marquardt [2002], Puntke [2002], Kwan [2008], Rame and Lohaus [2010], etc.). The advantage and disadvantage of these methods were also analyzed experimentally in the researches by Hunger [2010], Fennis [2010], Rame and Lohaus [2010] :

- Hunger and Fennis recommended that water demand measurement by determining mixing energy which proposed by Marquardt [2002] is fast and accurate for obtaining the maximum packing density of a powder.
- Hunger concluded that water demand test introduced by Okamura [1995] is useful to measure the sensitivity on the water need for a specified flowability. Fennis, however, pointed out that this test method is inaccurate method for powder packing density measurement.
- Rame and Lohaus indicated that water demand tests introduced by Okamura [1995] and by Puntke [2002] are only applied for mixture without superplasticizer, these test methods do not include the effect of superplasticizer. Consequently, Rame and Lohaus proposed the superplasticizer based approach to determine packing density of fines or fines and coarse particles mixture according to the principle of the water demand test by Okamura [1995]

The water demand test methods by Okamura [1995], by Marquardt [2002], and by Rame and Lohaus [2010] are described as follows:

- **Water demand test introduced by Okamura and Ozawa [1995]:** In this method, packing density of powder is determined indirectly by the spread flow test using a mini cone (60 mm height, 100 mm base diameter =  $d_0$ , 70 mm cut diameter), as described in Figure 2.3. The spread flow test is performed as follows: after appropriate mixing as a defined mix procedure, the fresh paste is placed on a dry glass plate in the cone. The mould was then lifted straight upwards to allow free flow of the concrete without jolting. Two minutes after the mould lifting, two paste diameters perpendicular to each other,  $d_1$  and  $d_2$ , are determined and used to compute the relative flow area  $\Gamma_P$  by Equation (2.3).

$$\Gamma_P = \frac{d_1 \times d_2 - d_0^2}{d_0^2} = \frac{d_1 \times d_2}{d_0^2} - 1 \quad (2.3)$$

For a given material at least four different volume ratios of water/powder ( $V_W/V_{Pow}$ ) have to be tested, obtaining four corresponding relative flow area  $\Gamma_P$ . The examined data points of  $V_W/V_{Pow}$  and  $\Gamma_P$  are plotted on a 2-D graph with the x-axis of  $\Gamma_P$ . A straight line is then fitted through these points using a linear regression, as presented by Equation (2.4) and illustrated in Figure 2.4. The intersection of the fitting line with the y-axis shows a state of no slump paste in which the water adsorb on the particles surface and fill full the void in the granular mixture. Packing density is

## 2. Particle packing model in concrete

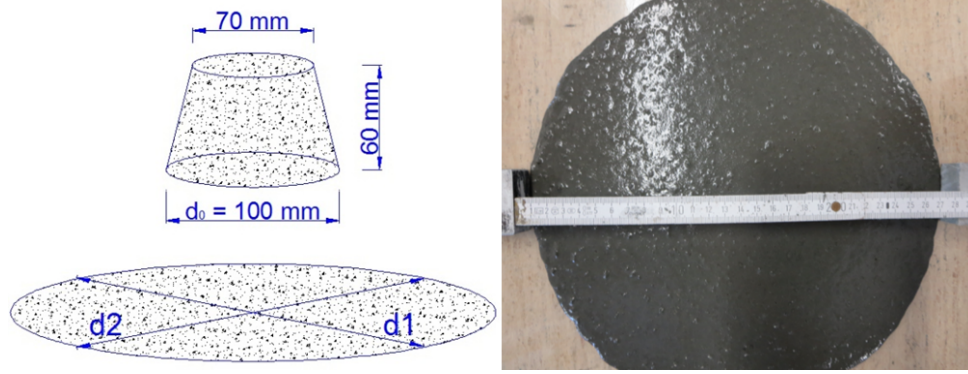


FIGURE 2.3.: Spread flow test using a mini cone (Okamura and Ozawa [1995]).

then calculated by Equation (2.5).

$$\frac{V_W}{V_{Pow}} = E_P \times \Gamma_P + \varepsilon \quad (2.4)$$

$$\beta = \frac{1}{1 + \varepsilon} \quad (2.5)$$

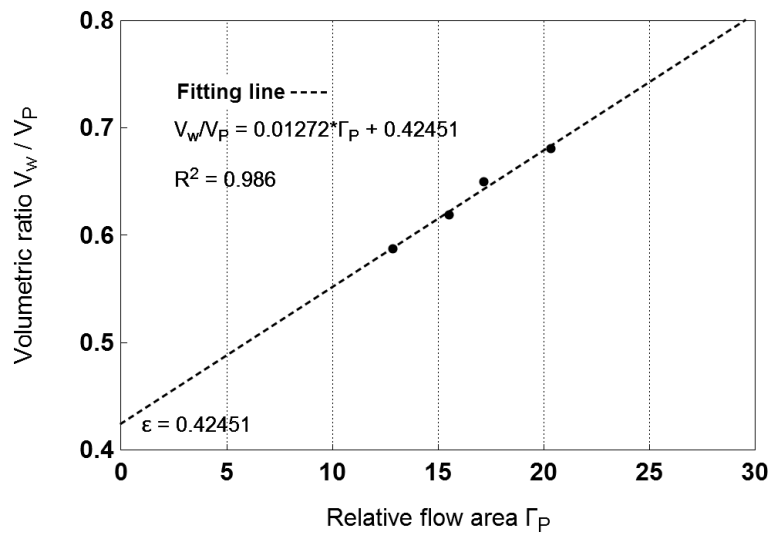


FIGURE 2.4.: An example about determination of the packing density of Cem1 used in this research project, applying Okamura and Ozawa's water demand test method, with Superplasticizer/Cement ratio of 1 wt.%. The result of packing density was 0.702 and much higher than test results of other methods.

- **Water demand proposed by Marquardt [2002]:** The principle of the method is as follows: While powder is mixed in a mixer continuously, water is constantly added to the powder in small quantities. At first the agglomeration of powder and the power consumption of the mixing process increase with the water addition. At

100% saturation, a thin water film surrounds each of the particles, the voids between the particles are filled with the liquid and the liquid pressure is high as the air pressure. With further adding of liquid the power consumption suddenly drops. At reached maximum power consumption, the powder packing density  $\beta$  and the corresponding water demand (WD) of the powder are then calculated by Equations (2.6) and (2.7) respectively. In the work of Marquardt cement amount of about 600 grams was mixed in a mortar mixer with a constant water addition of 1.5 ml/s at a mixing speed of 140 rounds per minute (rpm).

$$\beta = \frac{V_{Pow}}{V_{Liq} + V_{Pow}} = \frac{\sum_{i=1}^n V_{Pow(i)}}{V_{Liq} + \sum_{i=1}^n V_{Pow(i)}} = \frac{\sum_{i=1}^n \frac{M_{Pow(i)}}{\rho_{Pow(i)}}}{V_{Liq} + \sum_{i=1}^n \frac{M_{Pow(i)}}{\rho_{Pow(i)}}} \quad (2.6)$$

$$WD = \frac{M_{Liq}}{M_{Pow}} = \frac{V_{Liq} \times \rho_{Liq}}{\sum_{i=1}^n M_{Pow(i)}} \quad (2.7)$$

where:  $V_{Pow}$  is total solid volume of the blended powder,  $V_{Pow(i)}$ ,  $M_{Pow(i)}$ ,  $\rho_{Pow(i)}$  are solid volume, mass and density of the  $i^{\text{th}}$  component of the blended powder respectively.  $V_{Liq}$  is total volume of added liquid until reaching maximum power consumption,  $\rho_{Liq}$  is density of the liquid,  $\rho_{Liq} = \rho_W = 1 \text{ g/cm}^3$  when the liquid is water.

- **The superplasticizer based approach presented by Ramge and Lohaus [2010]:** This method can be employed for powder or mixture of powder and fine aggregate to examine packing density of granular mixture taking into account the effect of superplasticize. The conception of the model is illustrated in Figure 2.5.

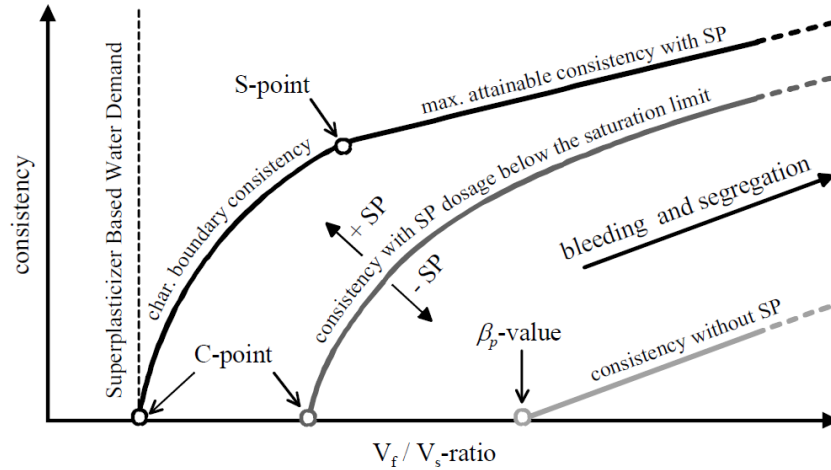


FIGURE 2.5.: Model of the Superplasticizer Based Approach by Ramge and Lohaus [2010] for determination of the packing density of granular concrete mixture.

The spread flow tests according to Okamura and Ozawa [1995] are performed. For each granular mixture a certain consolidation point (C-point) exists when just enough

## 2. Particle packing model in concrete

liquid is present to fill all the voids but no additional liquid to enable flowing of the paste or mortar. In case of mixture without superplasticizer, the  $C\text{-point}_{\text{water}}$  corresponds to  $\beta_p$  ( $= \varepsilon$  in Equation (2.5)) according to Okamura and Ozawa. The  $C\text{-point}_{\text{water-SP}}$  of mixture including superplasticizer is much lower than the  $C\text{-point}_{\text{water}}$ . For each  $V_{\text{fluid}}/V_{\text{solid}}$  ( $V_f/V_s$ ) the consistency can be increased to a maximum value by increasing of the superplasticizer content. Following the characteristic boundary consistency curve, the minimum  $C\text{-point}_{\text{water-SP}} = \varepsilon_{\text{min}}$  and the segregation point (S-point) are recognized. Then, the real packing density of mixture at the saturated superplasticizer content is calculated with Equation (2.5). However, this approach requires a great number of tests to determine packing density for each mixture, it is a time-consuming process.

### 2.2.4. Assessment of the packing density of concrete including fine powders and coarse aggregates

#### 2.2.4.1. Particle packing and concrete rheological behaviour

Ferraris and de Larrard [1998] investigated the relationship between plastic viscosity and the normalized solid concentration which is defined as the ratio of the solid volume in a unit volume of concrete to the packing density of granular mixture including the aggregates and the cement. The result pointed out that the plastic viscosity of concrete appears to be controlled essentially by the normalized solid concentration, as illustrated in Figure 2.6.

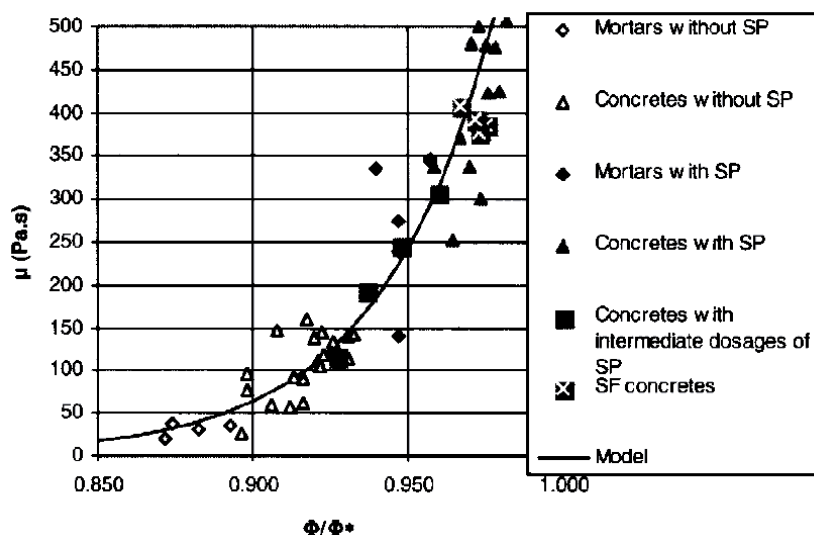


FIGURE 2.6.: Relationship between plastic viscosity ( $\mu$ ) and normalized solid concentration ( $\Phi/\Phi^*$ ),  $\Phi$  = solid volume,  $\Phi^*$  = packing density of granular mixture (Ferraris and de Larrard [1998]).

In this context, when the proportion of cementitious mixture, the water-cement ratio, the superplasticizer-cement ratio and the paste volume are constant, the modification of

the aggregate characteristics (size and size distribution, packing density, shape, surface texture) by the combination of different aggregates will change the particle packing density of the whole concrete, leading to the change of plastic viscosity. Then, the highest packing density of the granular concrete mixture can be recognized by the lowest plastic viscosity or by the highest spread-flow of concrete mixture. This idea is highly effective to evaluate the packing density of different concretes containing the same paste (volume, mix proportion).

#### 2.2.4.2. Packing density measurement for concrete granular mixture using Kwan's test method

The water demand test method proposed by Kwan (Wong and Kwan [2008], Kwan et al. [2012]) can be employed for packing density measurement of mortar and concrete granular mixture including powders and coarse particles. In this test, the packing density of granular mixture is defined as the maximum solid concentration when the volume ratios of Water/Solid are varied. The method is described as follows:

- For a given granular concrete mixture, N values of weight ratio of Water/Cement (W/C) are chosen for N tests. The first value of W/C should be chosen to achieve a flow concrete, the next values of W/C are reduced gradually. The last value of W/C corresponds with a clear decrease of the solid concentration. The weight and volume of granular materials including cement ( $M_C$ ,  $V_C$ ), fillers ( $M_{Fil(i)}$ ,  $V_{Fil(i)}$  with  $i=1\div h$ ), aggregates ( $M_{Agg(j)}$ ,  $V_{Agg(j)}$  with  $j=1\div k$ ) are determined as the given proportion and kept constant for N tests. The weight of superplasticizer ( $M_{SP}$ ) is determined by the weight ratio of Superplasticizer/Cement (its volume is  $V_{SP}$ ). Water amount (denoted by  $M_W$ ,  $V_W$  for weight and volume) is then weighed according to the W/C ratio.
- Concrete is mixed.
- The concrete mixture is placed in a cylindrical mould in several layers to excess, diameter of the mould is at least five times larger than  $D_{max}$  of the aggregates. The compaction is applied for each layer. For self flowing concrete the compaction is just the dropping of the mould on a strong ground. In other case tamping with a rod is used. The same condition of compacting for each layer as well as for different test is required. The excess concrete is then removed with a straight edge and weigh the amount of concrete in the mould.
- Let the weight and bulk volume of concrete in the mould are  $M$  and  $V$ , respectively. The solid volume of the granular mixture  $V_{granular-mix}$  is computed by Equation (2.8). The solid concentration  $\varrho$  is determined by Equation (2.9). The air ratio (denoted by  $u_{air}$ ) is defined as the ratio of the volume of air to the solid volume of the granular mixture, and expressed by Equation (2.10).

$$V_{granular-mix} = \frac{M}{M_W + M_{SP} + M_C + \sum_{i=1}^h M_{Fil(i)} + \sum_{j=1}^k M_{Agg(j)}} \quad (2.8)$$

$$V_C + \sum_{i=1}^h V_{Fil(i)} + \sum_{j=1}^k V_{Agg(j)}$$

$$\varrho = \frac{V_{granular-mix}}{V} \quad (2.9)$$

## 2. Particle packing model in concrete

$$u_{air} = \frac{V - V_{granular-mix} - \frac{V_W + V_{SP}}{V_C + \sum_{i=1}^h V_{Fil(i)} + \sum_{j=1}^k V_{Agg(i)}} V_{granular-mix}}{V_{granular-mix}} \quad (2.10)$$

Figure 2.7 illustrates a process to determine packing density of the granular concrete mixture using the Kwan's method. The mixture includes 43.4 vol.% of binder and 56.6 vol.% of aggregate, the proportion of cementitious powder is Cem1/SF2/QP16900 = 100/12/30 in mass, the proportion of blended aggregate is QS1/QS2/QS3 = 54/36/10 in volume. The weight ratio of SP/Cem1 is 3/100. The detail explanation about the mix proportion of this mixture are shown in chapters 4 and 5. The maximum solid concentration or the packing density of the granular concrete mixture was 0.8276.

This method allows to determine the value of the packing density of granular concrete mixture considering the dispersing effect of a fixed superplasticizer amount on cementitious powder. However, this procedure is time-consuming when various Water/Solid volume ratios have to be investigated to point out the maximum solid concentration.

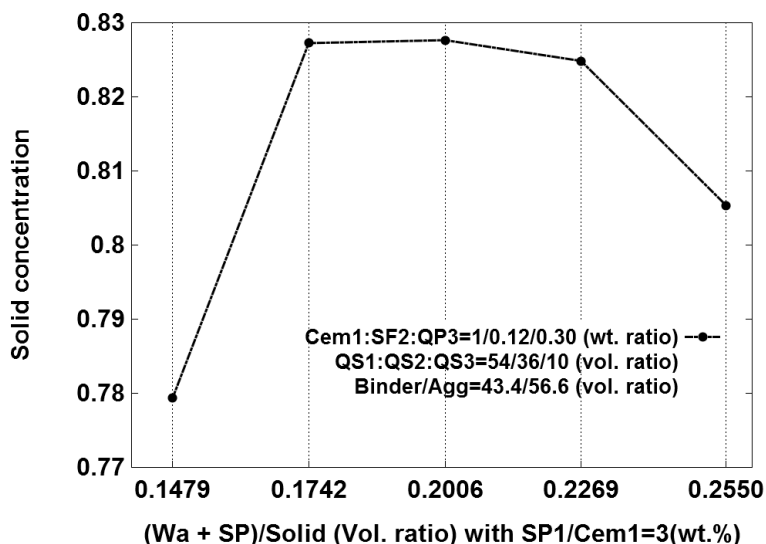


FIGURE 2.7.: Packing density determination for granular concrete mixture developed in this research project using the Kwan's test method of packing density measurement. The maximum solid concentration of the granular concrete mixture was 0.8276.

### 2.3. Principles of particle packing

Particle packing refers to the arrangement of particle in a finite volume. Particle packing optimization is an important topic in many different technologies such as concrete, ceramic, chemical engineering, geology, foundation, pharmaceuticals, foods etc. In concrete, the improvement of particle packing density, which is used to evaluate the void space in granular system, leads to the increase of concrete performance in fresh and hardened states as well as the benefit of materials saving.

The early works by Furnas [1929, 1931] and by Westman [1930] in particle packing based on different classes of monosized particles presented that: (i) If the space in between coarse particle can be filled up by adding of fine particles the packing density of the granular mixture will be increased; (ii) The effectiveness of the filling of fine particles in packing density improvement is affected significantly by the size ratio of components, as illustrated in Figure 2.8; (iii) The increase of the number of size class results in a higher packing density for granular mixture.

In addition, White and Walton [1936] demonstrated that the packing of monosized spheres system is not depended on particle size. There are five different ways of geometrical packing for monosized spheres system, such as: cubic, cubical-tetraheral, tetragonal-sphenoidal, pyramidal and tetrahedral. Theoretically, the cubical structure is the loosest packing density of 0.5236, the pyramidal and tetrahedral structures are the densest packing density of 0.7405.

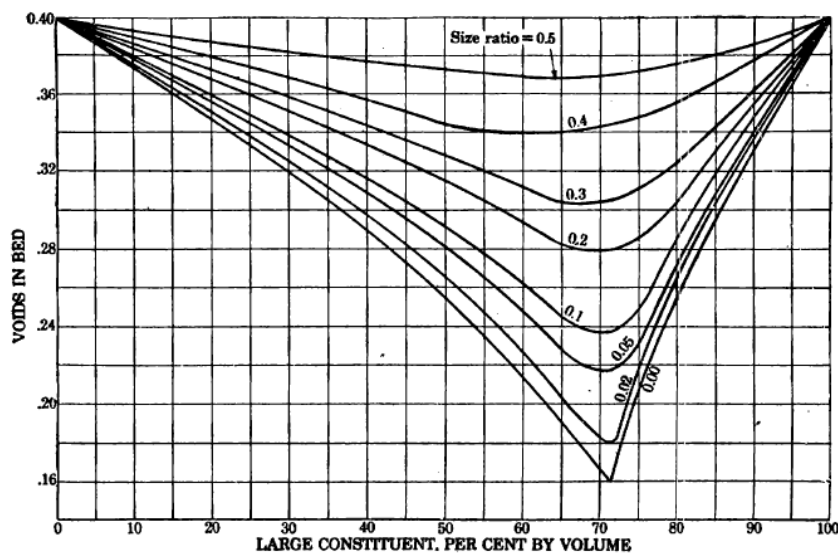


FIGURE 2.8.: Relation between void fraction and size ratio of fine to coarse in a binary system of broken solid when void fractions of single components = 0.4, according to Furnas [1929]

In practice most of granular materials have a continuous size distribution, whereas monosized particles are rare. However, two kinds of packing models for a polydisperse systems have been developed (Funk and Dinger [1994]):

- The packing together of different discretely sized particles.
- Ideal grading curve-based packing models.

### 2.3.1. Ideal grading curve-based packing models

The study by Fuller and Thompson [1907] showed that an optimum aggregate grading with a continuous size distribution according to Equation (2.11) increases concrete

## 2. Particle packing model in concrete

performance in fresh and hardened states.

$$P(D_i) = \left( \frac{D_i}{D_{max}} \right)^{1/2} \quad (2.11)$$

where:  $P(D_i)$ , the cumulative finer than  $D_i$  (in volume);  $D_i$ , sieve opening of the  $i^{\text{th}}$  sieve;  $D_{max}$ , maximum size particle. This curve is called Fuller curve and still used today for concrete mix design.

Furnas [1931] proposed a model for a mixture of continuous grading of sizes, considered both of the smallest  $D_{min}$  and largest  $D_{max}$  size particles of granular mixture, as described by Equation (2.12), which was based on his previous work (Furnas [1929]) about packing model for a system of discretely sized particles.

$$P(D_i) = \frac{r^{\log D_i} - r^{\log D_{min}}}{r^{\log D_{max}} - r^{\log D_{min}}} \quad (2.12)$$

The value of  $r$  is ratio of the quantity of particles on one sieve to the quantity of particles on the next smaller sieve. The relation between  $r$  and void fraction ( $\phi$ ) of granular mixture is represented by Equation (2.13).

$$r = \frac{1}{\phi^{\frac{n}{m}}} \quad (2.13)$$

with  $n$  is one less than the number of component sizes for maximum density in intermittent grading,  $m$  is number of screen size intervals of ratio  $\sqrt{2}$  included between  $D_{max}$  and  $D_{min}$ .

Stating from the continuous distributions for packing model of continuously graded particles Andreasen and Andersen [1930] concluded that optimum packing can be achieved when the cumulative finer than  $D_i$  obeys Equation (2.14).

$$P(D_i) = \left( \frac{D_i}{D_{max}} \right)^q \quad (2.14)$$

The  $q$ -value is distribution modulus ( $0 < q < 1$ ). They suggest the  $q$ -value in range of 0.33-0.5. Obviously, the packing model of Fuller and Thompson (Eq.2.11) represents a special case of Andreasen and Andersen packing model.

According to the works by Furnas [1931] (Eq. (2.12)) and by Andreasen and Andersen [1930] (Eq. (2.14)) Funk and Dinger [1994] recognized that the Andreasen and Andersen model prescribes a grading down to a particle diameter of zero (corresponding to  $P(0) = 0$ ) but a minimum diameter of a real granular mixture is non-zero (corresponding to  $P(D_{min}) \neq 0$ ). Thus, Funk and Dinger modified the model of Andreasen and Andersen concerning influence of the largest and smallest particles on the size distribution. The modified Andreasen and Andersen equation by Funk and Dinger is described by Equation (2.15) with  $0 < q < 1$ .

$$P(D_i) = \frac{D_i^q - D_{min}^q}{D_{max}^q - D_{min}^q} \quad (2.15)$$

The modified Andreasen and Andersen equation (Eq.2.15) (it is also called Funk-Dinger model) is used widely for concrete mix design during recent years. Brouwers and Radix [2005] used the model with the q-value of 0.25 for mix design of self compacting concrete. Brouwers [2006] demonstrated that the q-value for an optimal packing is in range of 0-0.28 theoretically. Hunger [2010] investigated self compacting mortar (coarse grains up to 4 mm) using the model with q-value of 0.22, 0.23, 0.25, 0.35 and used q-value of 0.22, 0.25 for self compacting concrete (coarse grains up to 16 mm). Hüsken and Brouwers [2008, 2010] suggested the q-values in range of 0.35-0.40 for earth-moist concrete with a maximum particle size of 16mm and a minimum particle size of 0.5  $\mu\text{m}$ . Vogt [2010] designed high strength and ultra-high strength concrete containing ultra-fine particles based on applying the model with various q-value, recommending q-value of 0.3 for conventionally vibrated concrete and q-value of 0.2-0.25 for self compacting concrete. Yu et al. [2014, 2015] employed the model and fixed the q-value of 0.23 for mix design of ultra high performance concrete with maximum sand grains of 2 mm and minimum grains of nano-silica of smaller than 0.1  $\mu\text{m}$ . Ha et al. [2015] used the model with q-value of 0.25 to determine the aggregate grading having  $D_{\text{max}} = 16 \text{ mm}$  and  $D_{\text{min}} = 0.63 \text{ mm}$  for self compacting concrete. The q-values in these research works were adjusted and selected to satisfy the required workability. The decreasing of q-value increases volume of fine particles and vice versa.

Actually, the application of Equation (2.15) for concrete mix design is not unproblematic. In this model the particles are assumed as spheres and the particle shape, surface texture, particle packing of raw materials, surface force of fines are not taken into account. When this model is applied for concrete mix design, a suitable process would be as the followings: First, the particle size distribution of each material in the input materials set have to be known (including fillers, cements, aggregates). Normally, N values of q have to be selected (at least three values) in an interval [a;b] ( $0 \leq a \leq q \leq b \leq 1$ ) for investigation, depending on type of concrete and designer experience. For each q-value a target grading of granular mixture is formed. The proportion of the input granular materials is computed in such away that the particle size distribution of the real granular mixture is closest to the target curve. This means that N calculated granular mixtures have to be verified experimentally to find out the optimum value of q corresponding the highest performance of packing density or/and workability or/and mechanical strength. This process is complicated. It should be noted that there is only one optimum q-value in the interval [a;b] for a given set of granular materials with regard to the highest packing density. Thus, ones have to determine the optimum q-value by themselves if the input materials are changed. A random selection of only one q-value for mix design is not convincing to insure the best quality of the obtained mixture.

#### 2.3.2. Packing models for a system of discretely sized particles

##### 2.3.2.1. The Furnas model

The study by Furnas [1929] is one of the earliest works about the packing of discretely sized particles. For the packing of discretely sized particles the Furnas's idea was that the best packing of binary mixture of discretely sized particles occurs when finer particles exactly fill the void space within the larger particles. It is assumed that there is no interaction between the particles when diameter of fine particles ( $d_2$ ) is much smaller than

## 2. Particle packing model in concrete

diameter of coarse particle  $d_1$  ( $d_1 \gg d_2$ ). In case of ternary mixture, the medium size particles must exactly fill the void space within the coarse particles and the finest must exactly fill the void space within the medium (and coarse) particles. This can similarly be applied to system of  $N$  discretized size classes.

The Furnas packing model for a binary of monosized classes can be explained in detail as follows: The packing density for each class on its own must be known, they are called residual packing density, denoted by  $\beta_1$  and  $\beta_2$  for coarse and fine grains respectively. The relative volume of each size class in mixture is expressed as its volume fraction  $y_1$  and  $y_2$  as Equation (2.16). The volumes occupied by coarse and fine classes in a unit bulk volume of the binary mixture are denoted by  $\varphi_1$  and  $\varphi_2$  (partial volume). The relations between  $y_i$  and  $\varphi_i$  ( $i=1,2$ ) are described by Equation (2.17). The packing density of the binary mixture,  $\beta_{mix}$  is calculated by Equation (2.18).

$$y_1 + y_2 = 1 \quad (2.16)$$

$$y_i = \frac{\varphi_i}{\varphi_1 + \varphi_2} \quad (2.17)$$

$$\beta_{mix} = \varphi_1 + \varphi_2 \quad (2.18)$$

Two cases of dominant coarse grains or dominant fine grains can be distinguished when the volume fractions of the coarse and the fine grains vary, resulting in the change of the packing density of the binary mixture.

- Case 1: dominant coarse grains, occurred when the volume fraction of the coarse particles is much larger than the volume fraction of the fine particles ( $y_1 \gg y_2$ ). First, the container is filled fully by the coarse grains, at that time  $\varphi_1 = \beta_1$ . The voids between the coarse particles are then filled up by adding the fine particles. Thus the total occupied volume and the packing density increase. The packing density of mixture is calculated as Equation (2.19).

$$\begin{aligned} \beta_{mix} &= \varphi_1 + \varphi_2 = \beta_1 + \varphi_2 = \beta_1 + (\varphi_1 + \varphi_2) \times y_2 = \beta_1 + \beta_{mix}y_2 \\ \Rightarrow \beta_{mix} &= \frac{\beta_1}{1 - y_2} \end{aligned} \quad (2.19)$$

- Case 2: dominant fine grains, arisen when the volume fraction of the coarse particles is much smaller than the volume fraction of the fine particles ( $y_1 \ll y_2$ ). Some coarse particles is added into a matrix of small particles in a container. Coarse particles contribute to the packing density of mixture an amount of their partial volume  $\varphi_1$ . The small particles then fill up the rest of the unit volume ( $1-\varphi_1$ ). The packing density of mixture is calculated as Equation (2.20).

$$\begin{aligned} \beta_{mix} &= \varphi_1 + \varphi_2 = \varphi_1 + (1 - \varphi_1) \times \beta_2 = (1 - \beta_2)\varphi_1 + \beta_2 \\ &= (1 - \beta_2)\beta_{mix}y_1 + \beta_2 \\ \Rightarrow \beta_{mix} &= \frac{\beta_2}{1 - (1 - \beta_2)y_1} \end{aligned} \quad (2.20)$$

The maximum packing density of binary mixture ( $\beta_{\text{mix-Max}}$ ) and the corresponding volume fractions of coarse particles ( $y_{1\text{-optimum}}$ ) and fine particles ( $y_{2\text{-optimum}}$ ) are then calculated by Equation (2.21), (2.22) and (2.23).

$$\beta_{\text{mix-Max}} = \beta_1 + \beta_2 - \beta_1\beta_2 \quad (2.21)$$

$$y_{1\text{-optimum}} = \frac{\beta_1}{\beta_1 + \beta_2 - \beta_1\beta_2} \quad (2.22)$$

$$y_{2\text{-optimum}} = \frac{\beta_2 - \beta_1\beta_2}{\beta_1 + \beta_2 - \beta_1\beta_2} \quad (2.23)$$

For instance, Figure 2.9 shows the packing density of binary mixture of monosized classes, having  $d_1 = 1122.67 \mu\text{m}$  and  $d_2 = 11.19 \mu\text{m}$ . Packing density of coarse and fine particle are  $\beta_1 = 0.675$  and  $\beta_2 = 0.637$  respectively.

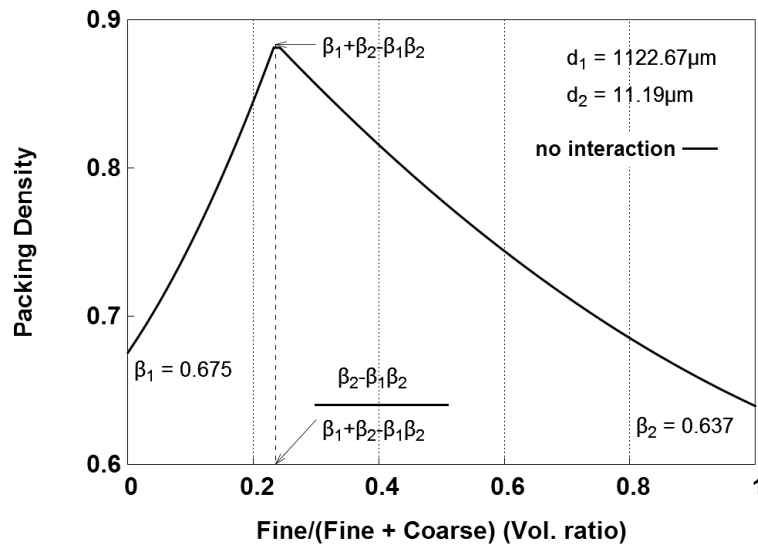


FIGURE 2.9.: The packing density of binary mixture according to Furnas model. First, the fine volume fraction ( $y_2$ ) increases gradually and the void between coarse particles is filled up, leading the increase in packing density. For higher value of  $y_{2\text{-optimum}}$ , coarse grains are replaced by an equivalent bulk volume of fine particle, decreasing the overall solid volume.

### 2.3.2.2. The Linear Packing Density Model

The Linear Packing Density Model was proposed by Stovall et al. [1986]. The model can predict the packing density for system of several mono-size classes taking into account the wall effect and the loosening effect between grain groups, which are geometrical interactions leading decrease of the packing density of particle system.

## 2. Particle packing model in concrete

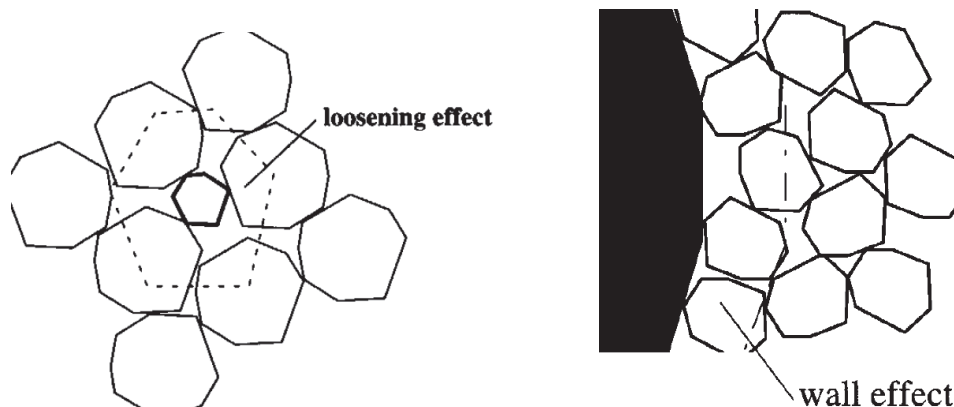


FIGURE 2.10.: (Left) Loosening effect exerted by a fine grain in a coarse grain packing. (Right) Wall effect exerted by a coarse grain on a fine grain packing. (from de Larrard [1999]).

- Loosening effect: A physical effect describes a local decrease of volume of class 1 coarse grains when the void between them is not able to fit by inserting of a fine grain of class, see Figure 2.10.
- Wall effect: A physical effect depict a remaining void because fine particles close to a coarse particle (or the wall of a container) cannot be packed as dense as the maximum bulk packing density of the fine particles, see Figure 2.10.

Considering a granular mixture of  $n$  classes of monosized particles with  $d_i \geq d_{i+1}$  ( $i=1:1:(n-1)$ ), class  $i$  grains are dominant if

$$\varphi_i = \beta_i(1 - \varphi_1 - \varphi_2 - \dots - \varphi_{i-1}) \quad (2.24)$$

Stovall demonstrated that there is always at least one dominant class. In general case, the packing density of the granular mixture is then computed by Linear Packing Density Model using Equation (2.25).

$$\beta_{mix} = \min_{1 \leq i \leq n} \left\{ \frac{\beta_i}{1 - (1 - \beta_i) \sum_{j=1}^{i-1} g(j, i)y_j - \sum_{j=i+1}^n f(i, j)y_j} \right\} \quad (2.25)$$

where: the functions  $g(j, i)$  and  $f(i, j)$  express the wall effect and loosening effect.

### 2.3.2.3. The Compressible Packing Model

The further improvement of Linear Packing Density Model by de Larrard [1999] resulted in the Compressible Packing Model (CPM). The CPM considers the influence of the applied compaction energy on the real packing density of a granular mixture including  $n$  classes of monosized particles, expressed by Equation (2.26).

$$K = \sum_{i=1}^n \frac{\frac{y_i}{\beta_i}}{\frac{1}{\beta_{mix-actual}} - \frac{1}{\beta_{mix-i}}} \quad (2.26)$$

with  $K$  is a characteristic of the packing process, called compaction index,  $K$ -values are shown in Table 2.2. The  $\beta_{\text{mix-actual}}$  is the real packing density of granular mixture. The  $\beta_{\text{mix-}i}$  is determined by Equation (2.27).

$$\beta_{\text{mix-}i} = \frac{\beta_i}{1 - \sum_{j=1}^{i-1} \left( 1 - \beta_i + b_{ij}\beta_i \left[ 1 - \frac{1}{\beta_j} \right] \right) y_j - \sum_{j=i+1}^n \left( 1 - \frac{a_{ij}\beta_i}{\beta_j} \right) y_j} \quad (2.27)$$

where: the wall effect coefficient  $b_{ij}$  and the loosening effect coefficient  $a_{ij}$  are computed by Equations (2.28) and (2.29) respectively.

$$b_{ij} = 1 - (1 - d_i/d_j)^{1.50} \quad (2.28)$$

$$a_{ij} = \sqrt{1 - (1 - d_j/d_i)^{1.02}} \quad (2.29)$$

If the compaction index ( $K$ -value) tends to infinity, the real packing density tends to the virtual packing  $\beta_{\text{mix-virtual}}$  which determined by Equations (2.30).

$$\beta_{\text{mix-virtual}} = \min_{1 \leq i \leq n} (\beta_{\text{mix-}i}) \quad (2.30)$$

TABLE 2.2.:  $K$  values for different packing process (DE LARRARD et al. [1999]).

Packing process		K value
<b>dry</b>	pouring	4.1
	sticking with a rod	4.5
	vibration	4.75
	vibration + compression 10 kPa	9
<b>wet</b>	smooth thick paste	6.7
<b>virtual</b>		$\infty$

In the CPM  $\beta_i$  is the residual packing density of the size class  $i$ . It is deduced from the actual packing density, which is measured with a given packing process. De Larrard suggested a way to calculate  $\beta_i$  of the size class  $i$  in polydisperse aggregate as follows:

- A mass  $M_{\text{mix}}$  of dry aggregate is put in a cylinder having a diameter  $D_{\text{cyl}}$ , which is more than five times the maximum size of aggregate. A piston is introduced in the cylinder, applying a pressure of 10 kPa on the surface of the specimen. Then the cylinder is fixed on a vibrating table, and submitted to vibration for 2 min. The actual packing density is calculated from the final height,  $h$ , of the sample by Equation (2.31). In this case the compaction index  $K$  equal to 9.

$$\beta_{\text{mix-actual}} = \frac{4M_{\text{mix}}}{\pi D_{\text{cyl}}^2 h \rho_P} \quad (2.31)$$

## 2. Particle packing model in concrete

- It is generally assumed that  $\beta$  is uniform among the aggregate grading span. By applying Eq. (2.26) and Eq. (2.27) the value of  $\beta$  is determined. The residual packing density of the size class  $i$  is then calculated by Equation (2.32).

$$\beta_i = \{1 - (1 - k_w)[1 - (1 - d_i/D_{cyl})^2(1 - d_i/h)]\}\beta \quad (2.32)$$

where: wall effect coefficient  $k_w$  are 0.88 and 0.73 for rounded grains and crushed grains respectively.

For example, Tables A.3 in appendix represents how the used quartz sand QS1 in this research project was divided to several monosized classes and how the residual packing densities of the monosized classes were computed according to the experimentally actual packing density of the origin material.

It is noted that the interaction of fine particles due to the surface force is not taken into account in the Compressible Packing Model.

### 2.3.2.4. The Compaction - Interaction Packing Model

Fennis [2010] developed the Compaction - Interaction Packing Model (CIPM) based on Compressible Packing Model. In the CIPM the loosening effect coefficient  $a_{ij}$  and the wall effect coefficient  $b_{ij}$  were reprogrammed. Taking into account the effect of surface force of fines, the interaction between fines and coarses, the effect of compacting process on different size classes the CIPM is expressed by Equations 2.33, 2.34, 2.35, 2.36.

$$K_t = \sum_{i=1}^n K_i = \sum_{i=1}^n \frac{\varphi_i/\varphi_i^*}{1 - \varphi_i/\varphi_i^*} \quad (2.33)$$

$$\frac{\varphi}{\varphi^*} = \frac{y_i \beta_{mix-actual}}{\beta_i \left( 1 - \sum_{j=1}^{i-1} \left( 1 - b_{ij,c} \left[ 1 - \frac{1}{\beta_j} \right] \right) y_j \beta_{mix-actual} - \sum_{j=i+1}^n \frac{a_{ij,c}}{\beta_j} y_j \beta_{mix-actual} \right)} \quad (2.34)$$

$$a_{ij,c} = \begin{cases} 1 - \frac{\log(d_i/d_j)}{w_{0,a}} & \text{if } \log(d_i/d_j) < w_{0,a} \\ 0 & \text{if } \log(d_i/d_j) \geq w_{0,a} \end{cases} \quad w_{0,a} = \begin{cases} w_a * C_a & \text{if } d_j < 25\mu\text{m} \\ w_a & \text{if } d_j \geq 25\mu\text{m} \end{cases} \quad (2.35)$$

$$b_{ij,c} = \begin{cases} 1 - \frac{\log(d_j/d_i)}{w_{0,b}} & \text{if } \log(d_j/d_i) < w_{0,b} \\ 0 & \text{if } \log(d_j/d_i) \geq w_{0,b} \end{cases} \quad w_{0,b} = \begin{cases} w_b * C_b & \text{if } d_i < 25\mu\text{m} \\ w_b & \text{if } d_i \geq 25\mu\text{m} \end{cases} \quad (2.36)$$

The modification of the interaction coefficient  $a_{ij,c}$  and  $b_{ij,c}$  by the implementation of  $w_{0,a}$  and  $w_{0,b}$  as functions gives the model some advantages to control the interaction between particles with regard to size ratio and particle size.

### 2.3.2.5. The 3-parameter particle packing model incorporating the wedging effect

Kwan et al. [2013] proposed a particle packing model incorporating the wedging effect, called 3-parameter particle packing model (loosening, wall and wedging effects). The wedging effect is caused by entrapment of isolated fine particles at the gaps between coarse particles, illustrated in Figure 2.11.

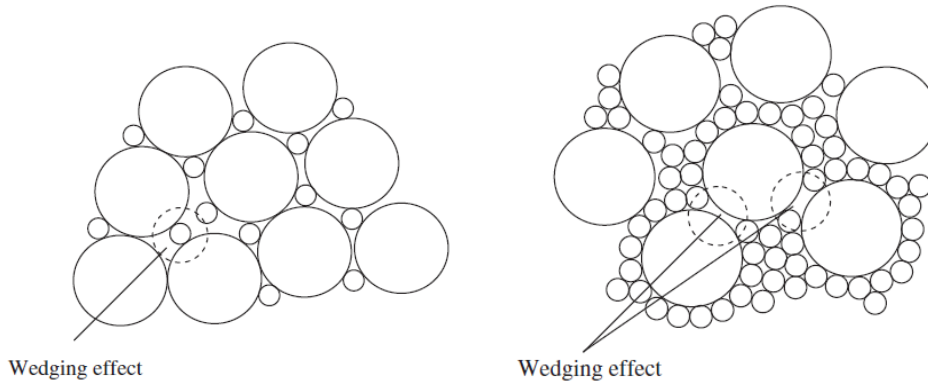


FIGURE 2.11.: Wedging effect in the dominant cases of coarse (Left) and fine particles (Right) (according to KWAN et al. [2013]).

The model for a binary mixture ( $d_1 > d_2$ ) is expressed by Equation (2.37) when the coarse particles are dominant, and by Equation (2.38) when the fine particles are dominant. Equations (2.39), (2.40), (2.41) are used to determine the loosening, wall and wedging effect coefficients respectively, which are depended on size ratio  $s = d_2/d_1$ .

$$\frac{1}{\beta_{mix-1}} = \left( \frac{y_1}{\beta_1} + \frac{y_2}{\beta_2} \right) - (1-a) \frac{y_2}{\beta_2} \left[ 1 - c \left( \frac{y_2}{y_2^*} \right)^2 \right] \quad (2.37)$$

$$\frac{1}{\beta_{mix-2}} = \left( \frac{y_1}{\beta_1} + \frac{y_2}{\beta_2} \right) - (1-b)(1-\beta_1) \frac{y_1}{\beta_1} \left[ 1 - c \left( \frac{y_1}{y_1^*} \right)^2 \right] \quad (2.38)$$

$$a = 1 - (1-s)^{3.3} - 2.6s(1-s)^{3.6} \quad (2.39)$$

$$b = 1 - (1-s)^{1.9} - 2s(1-s)^6 \quad (2.40)$$

$$c = 0.322 \tanh(11.9s) \quad (2.41)$$

where:  $y_1^*$  and  $y_2^*$  are volume fractions of coarse and fine particles at the theoretical optimum packing density of the binary mix determined by Eq. (2.21), Eq. (2.22), Eq. (2.23).

Nevertheless, the interaction of fine particles due to the surface force is not taken into account in this model. Besides, a general solution based on this model for a mixture of more than two components having any type of size distribution have not developed yet.

## 2.4. Concluding remarks

Experimental methods of packing density measurement are important for concrete mix design based on particle packing optimization. Packing of coarse particles with grain size larger than  $125\ \mu\text{m}$  is influenced by gravitational forces and compaction energy. Packing density of coarse particles is determined in dry condition with or without compaction by existing standard methods. The strong effect of the surface forces of fines form agglomerates in powder. Thus, a suitable method of packing density measurement in wet condition is needed for powder. The method of water demand measurement by determining mixing energy, developed by Marquardt, is an accepted method to determine packing density of powder materials and blended binder. In this research project, this method is modified to a highly effective test method, called superplasticizer-water solution demand test, to measure packing density of powder and to assess the compatibility of powder and superplasticizer. The water demand test of Okamura is not suitable for packing density measurement but the spread-flow test is useful to evaluate the rheological behaviour of concrete. The superplasticizer based approach of Range and Lohaus take a lot of time for testing, it is not efficient for this research project due to high number of raw materials. Due to low time efficiency, the Kwan's method of packing density measurement is only employed to test for the established optimum mixture in this research project. The plastic viscosity of concrete is controlled essentially by the normalized solid concentration. This implies that when paste in concrete mixture is constant (i.e. volume, mix proportion) the modification of the aggregate characteristics (size and size distribution, packing density, shape, surface texture) by the combination of different aggregates will change the particle packing density of the whole concrete, the highest packing density of the granular concrete mixture can be recognized by the lowest plastic viscosity or by the highest spread-flow of concrete mixture.

The interaction of fine particles due to the influence of surface forces have a strong effect on the difference between experimental result and prediction of packing models. The Compressible Packing Model (CPM) of de Larrard work well for coarse granular mixture but the interaction of fine particles due to surface forces is not taken into account. Although the Compaction Interaction Packing Model was developed by Fennis to make good CPM's shortcomings, the interaction of fine particles due to surface forces is very complex, the CIPM should be verified for different blended powder. In ideal curve models, the particles are assumed as spheres and the particle shape, surface texture, particle packing of raw materials, surface force of fines are not taken into account. In addition, a random selection of distribution modulus, q-value, is not convincing to insure the best quality of the obtained mixture. Ideal curve models are still used in concrete mix design because of its simplicity. In this research project, the effectiveness of the ideal curve based on the modified Andreasen and Andersen equation, the Compressible Packing Model of de Larrard and the Compaction - Interaction Packing Model of Fennis in concrete mix proportioning are experimentally evaluated. The 3-parameter particle packing model of Kwan is not used due to its disadvantage for mixture of more than two components.

The simple idea of stepwise optimization of particle packing by Furnas is mentioned, the idea plays an important role for the further development.

### 3. Influence of the characteristics of constituent materials on UHPFRC's performance

#### 3.1. Effects of Portland cement composition on setting time and workability of concrete

In clinker production alkalis ( $\text{Na}_2\text{O}$  and  $\text{K}_2\text{O}$ ), which are from raw materials and fuel, are volatilized in the clinkering zone and combine with  $\text{SO}_3$  to form  $\text{Na}_2\text{SO}_4$  or  $\text{K}_2\text{SO}_4$  or  $(\text{K}, \text{Na})_2\text{SO}_4$ , and they are more or less trapped in the  $\text{C}_3\text{A}$ . According to Regourd's study [1978] the orthorhombic structure of  $\text{C}_3\text{A}$  can be formed from its cubic structure if the trapped  $\text{Na}_2\text{O}$  in  $\text{C}_3\text{A}$  is higher than 2.4% up to 3.8%. The other morphologies of  $\text{C}_3\text{A}$  in commercial available cements have not yet found (Aïtcin [2004]). Jawed et al. [1978] indicated that early hydration of Portland cement is generally accelerated by the presence of alkalis, thus a higher optimum gypsum is required when alkali content increases. Furthermore, Odler et al. [1983] found that the hydration of  $\text{C}_3\text{A}$  is retarded by  $\text{Na}_2\text{O}$  but the presence of  $\text{K}_2\text{O}$  accelerate the hydration of  $\text{C}_3\text{A}$ , leading to a longer setting time in high- $\text{Na}_2\text{O}$  content cement and a shorter setting time in high- $\text{K}_2\text{O}$  content cement. In fact, Portland cement with a high content of  $\text{C}_3\text{A}$  or a high reactivity  $\text{C}_3\text{A}$  has a negative effect on initial rheology of concrete, especially concrete having low water-cement ratio, the concrete slump is deteriorated quickly. For the production of UHPFRC with a very low water-cement ratio, Portland cements CEM I of strength classes 42.5 R and 52.5 R according to DIN EN 196 are generally used, in which the  $\text{C}_3\text{A}$  content and alkalis content of clinker should be as lowest as possible (Fehling et al. [2013], Aïtcin [2016]).

It is well-known that gypsum (or calcium sulfate dihydrate  $\text{CaSO}_4 \cdot 2\text{H}_2\text{O}$ ) is added to the clinker grinding in order to retard the intense initial hydration reactions of  $\text{C}_3\text{A}$ . Therefore, the setting time of Portland cement is controlled. In fact, gypsum is dehydrated partially by the increase of the temperature in the grinding mill, forming calcium sulfate hemihydrate ( $\text{CaSO}_4 \cdot 1/2\text{H}_2\text{O}$ ) or soluble anhydrite ( $\text{CaSO}_4$ ). In addition, natural mineral  $\text{CaSO}_4$  or synthetic calcium sulfate  $\text{CaSO}_4$  can be used to replace gypsum partially. These calcium sulfates have different solubility rate. Taylor [1997a] emphasized that if the calcium sulfates content is too low or solubility rate of calcium sulfates is not sufficient, the early reaction of  $\text{C}_3\text{A}$  increase quickly, leading to a rapid set, called "flash set", with much evolution of heat, strength development of concrete is poor. Further, a "false set" with a premature stiffening of concrete can be occurred if calcium sulfate hemihydrate content in cement is too high. It is very important to avoid the "flash set" and "false set" in the production of UHPC.

## 3.2. Compatibility between superplasticizer and cement

### 3.2.1. Dispersion mechanism of cement particles

Most solid surfaces in contact with a liquid having a high dielectric constant (such as water) are charged (negative or positive surface charge). An electrically charged surface in contact with water generates an electrical field which attracts oppositely charged ions. These ions are called counterions. Due to the thermal motion, these counterions form a diffuse layer of charge outside the charged surface. The diffuse layer of charge and the surface charge form a so-called electrical double-layer (Wall [2002]), as shown in Figure 3.1, in which the Debye length is the thickness of the diffuse layer, the interaction between charged particles is governed by the overlap of their diffuse layers. The Stern potential ( $\psi_\delta$ ) cannot be measured directly, however, zeta potential ( $\zeta$ -potential), which is the potential at the shear plane close to the Stern plane can be experimentally measured and is often used as a measure of the surface potential (Somasundaran et al. [2009]). The higher absolute value of zeta potential the particles have, the more stable the particles are in suspension. The stability of colloidal suspension is explained successfully using the DLVO theory, developed by Derjaguin, Landau, Verwey, and Overbeek, in which the interaction of two adjacent colloidal particles is described by the sum of van der Waals attraction and electrostatic repulsion (Yang et al. [1997]), as described by the blue solid curve called total interparticle potential energy in Figure 3.2 (Gelardi and Flatt [2016]). The dispersibility is increased when the energy barrier is increased. It should be noted that the thickness of the diffuse layer represents the distance between surfaces within which the repulsive potential is significant.

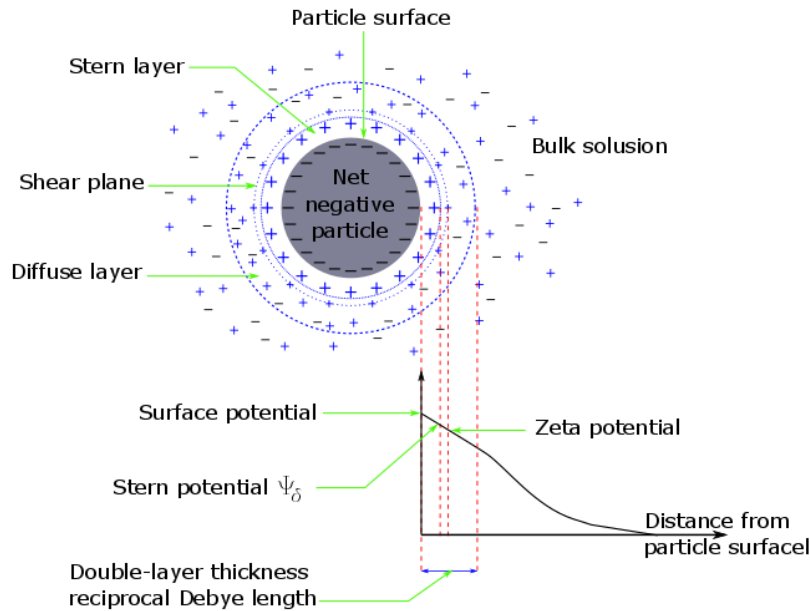


FIGURE 3.1.: Distribution of electrical potential in the double-layer region surrounding a charged particle showing the zeta potential and the reciprocal Debye length (Somasundaran et al. [2009]).

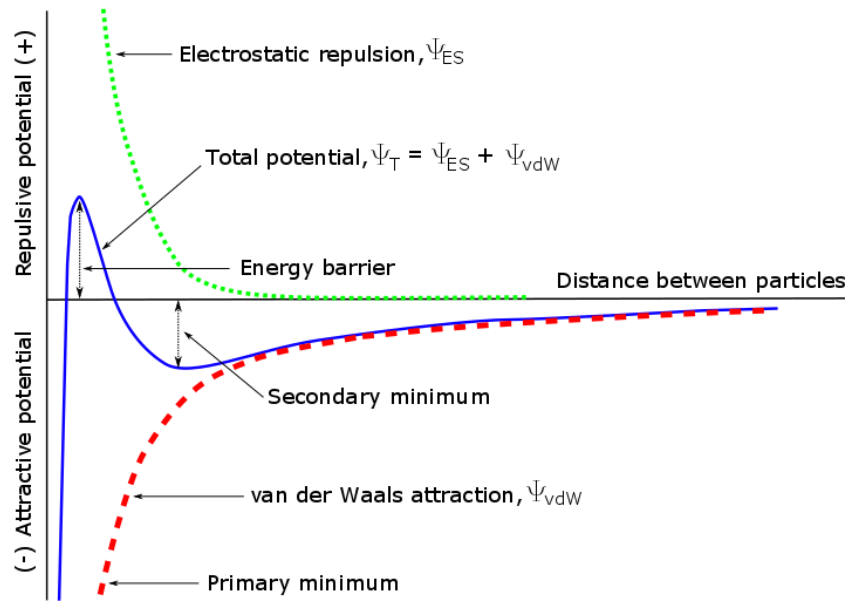


FIGURE 3.2.: Illustration of interparticle potentials as a function of the distance from a charge surface. The positive potential corresponds to electrostatic repulsion, and the negative one to van der Waals attraction (Gelardi and Flatt [2016]).

### 3.2.2. Interaction of polycarboxylate-based superplasticizers with cement

Polycarboxylate-based superplasticizers (PCEs) are comb-shaped copolymers, they are the most effective superplasticizers for producing self-compacting concrete as also high strength concrete mixtures (Sakai et al. [2003]). These PCEs, therefore, are currently used as major superplasticizers for UHPC.

A typical PCE consists of a polyanionic backbone (or main chain) and neutral side chain. The backbone of PCE contains carboxylic groups which dissociate in water and cause the negative charge for the backbone. The side chains of PCEs are made of poly(ethylene glycol) (PEG) which are also called as poly(ethylene oxide) (PEO). Figure 3.3 represents the bond between the backbone and the side chain of PCEs (Gelardi et al. [2016]).

Due to the negatively charge of the backbone PCEs only adsorb on particles having a positive surface charge (or a positive  $\zeta$ -potential in suspension). Many studies clarified the surface charge of clinker phases and cement hydration phases, and pointed out the adsorption of superplasticizer on these phases. The work by Yoshioka et al. [2002] showed that without superplasticizer, tricalcium silicate ( $3\text{CaO}\cdot\text{SiO}_2$  or  $\text{C}_3\text{S}$ ) and dicalcium silicate ( $2\text{CaO}\cdot\text{SiO}_2$  or  $\text{C}_2\text{S}$ ) have negative  $\zeta$ -potential while tricalcium aluminate ( $3\text{CaO}\cdot\text{Al}_2\text{O}_3$  or  $\text{C}_3\text{A}$ ) and tetracalcium ferroaluminate ( $4\text{CaO}\cdot\text{Al}_2\text{O}_3\cdot\text{Fe}_2\text{O}_3$  or  $\text{C}_4\text{AF}$ ) have positive  $\zeta$ -potential; therefore, a larger amount of superplasticizer is adsorbed on  $\text{C}_3\text{A}$  and  $\text{C}_4\text{AF}$  than  $\text{C}_3\text{S}$  and  $\text{C}_2\text{S}$ . Nachbaur et al. [1998] reported that the initial  $\zeta$ -potentials of calcium silicate hydrate phases (C-S-H) is negative at low  $\text{Ca}^{2+}$  concentration, but can be positive as the  $\text{Ca}^{2+}$  concentration in the cement pore solution increases and adsorption of  $\text{Ca}^{2+}$  on the C-S-H phases occurs; this can explain for the adsorption of superplasticizer C-S-H phases. Another study by Plank et al. [2007] also indicated that among early cement

### 3. Influence of the characteristics of constituent materials on UHPFRC's performance

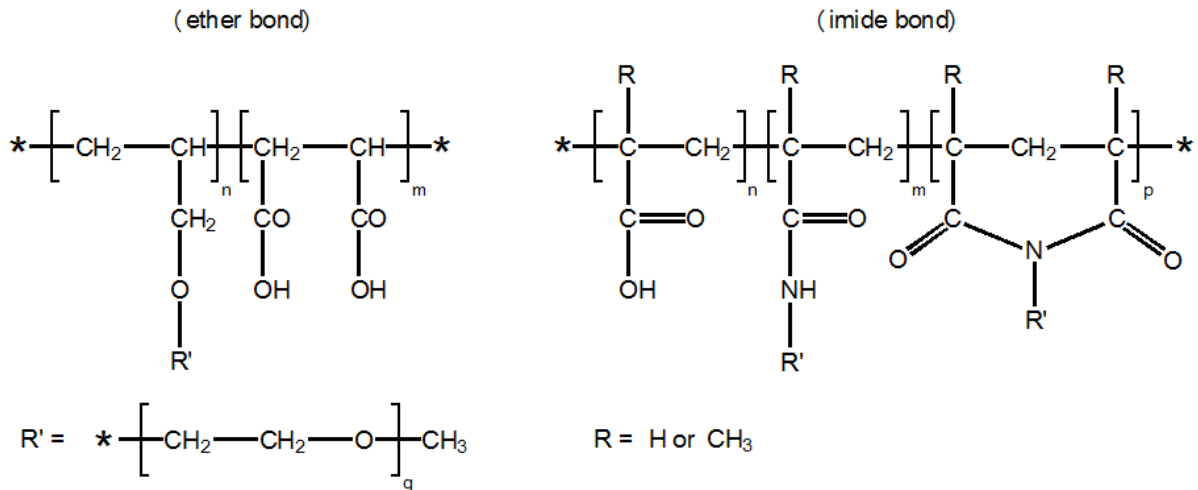


FIGURE 3.3.: Chemical structure of PCEs with ether (left) and imide (right) bonds between the backbone and the side chains (Gelardi et al. [2016]).

hydration phases, the positive  $\zeta$ -potentials of ettringite and monosulfate are the highest, in which ettringite have the highest potential to adsorb negatively charged superplasticizers via electrostatic attraction. However, syngenite, portlandite and gypsum have zero or negative  $\zeta$ -potentials and do not adsorb superplasticizers. Due to high adsorption capability of superplasticizer on aluminate phases it is clear to explain that is why cement with high  $C_3A$  requires higher PCE concentrations in order to reach saturation (Zingg et al. [2009]). Flatt and Houst [2001] propose three categories to describe the interactions and state of the superplasticizers with the cement suspension, thereby recommending that a stepwise or delayed addition of superplasticizer give a better fluidity of concrete in comparison to direct addition method. The stepwise adding of superplasticizer is also significant for UHPC concerning improvement of the fluidity (Ma et al. [2008]).

The studies by Uchikawa et al. [1997] and by Yoshioka et al. [1997] demonstrated that the addition of comb-shaped superplasticizers to cement suspension improves cement particles dispersing as also paste fluidity significantly due to a strong increasing of electrostatic and steric repulsive force, in which the steric hindrance effect dominates the dispersion behavior of superplasticizers. The performance of PCEs is strongly depended on its chemical structure. The studies by Yamada et al. [2000] and by Winnefeld et al. [2007] pointed out: (i) PCEs with higher molecular weight adsorb stronger compared to PCEs with lower molecular weight and same molecular architecture, (ii) at the same molecular weight, PCE molecules with short PEO side chain and low side chain densities have high anionic charge density, leading to higher amount adsorbed PCEs on the positive surface of the hydrating cement particles. The increase of the PEO side chain length result in large decrease in the fluidity with time and increase in yield stress, plastic viscosity as well. However, Plank et al. [2009] indicate that PCE main chain is not only surrounded by a cloud of cations but also bound with calcium ions in cement pore solution, these effects may result in very low anionic charge densities and reduce adsorption capability. Ushiro et al. [2013] reported that the fluidity of cementitious paste with low water/powder ( $W/P=0.16$ ) improved by both adsorbed PCE on the surface of particles and PCE present

### 3.2. Compatibility between superplasticizer and cement

in pore solution due to the effect of the delay adsorption of PCE, concluding that PCE present in pore solution play important role in improvement of fluidity at low W/C; this implies that determination of the saturated amount of PCE in cementitious suspension with low water/powder is essential, especially UHPC.

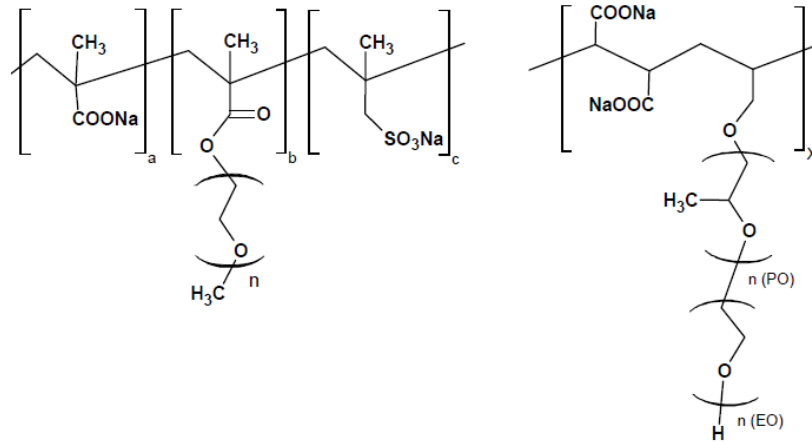


FIGURE 3.4.: Chemical composition of the methacrylate ester PCEs 11 to 13 (left) (monomer ratio a/b/c = 12/1.0/3.0, 12/1.0/1.4, 12/1.2/0.48 respectively) and of the allylether-based PCEs 21 to 23 (right) (Plank et al. [2009]).

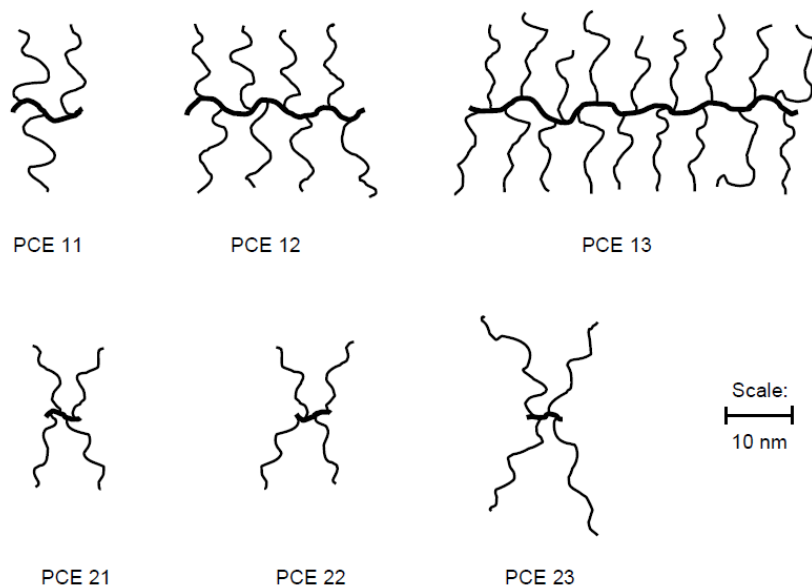


FIGURE 3.5.: Schematic representation to scale of the molecular architecture of the methacrylate ester PCEs 11 to 13 (trunk chain length of 13, 27, 48 nm and side chain  $n_{EO}$  of 45 and anionic charge density of 2800, 2500, 2400  $\mu\text{eq/g}$  respectively) and of allylether-based PCEs 21 to 23 (trunk chain length of 2.3, 2.2, 2.2 nm, side chain  $[n_{EO}+n_{PO}]$  of 34, 34, 52 and anionic charge density of 65, 90, 60  $\mu\text{eq/g}$  respectively) (Plank et al. [2009]).

Plank et al. [2009] and Schöffl et al. [2012] used methacrylate ester and allylether

### 3. Influence of the characteristics of constituent materials on UHPFRC's performance

based polycarboxylates (PCEs), as illustrated in Figure 3.4 and Figure 3.5, to investigate the compatibility of PCEs and cement as well as of PCEs and silica fume in UHPC having a water/cement ratio of 0.22. It was concluded that for silica fume slurry, the higher negative surface charge silica fume need a higher PCE content to achieve a given flowability. In cement pore solution the surface charge of silica fume turns from negative to positive due to surface adsorption of  $\text{Ca}^{2+}$  which formed by cement hydration. Thus, silica fume with high negative surface charge have a higher saturated adsorption for  $\text{Ca}^{2+}$ , requires a higher PCE dosage and is more difficult to disperse in comparison a with low negative surface charge silica fume. In addition, due to the very high surface area of silica fume, an effective dispersion of silica fume is necessary to obtain highly flowable UHPC paste.

### 3.3. Function of mineral admixtures in UHPC

Mineral admixtures (or additions) with grain size of smaller than 125 microns are used in concrete to improve the performance of concrete in fresh and hardened state (Aïtcin [2004], Mindess et al. [2003a], Mehta and Monteiro [2006]). According to the European Standard EN 206-1 [2000] mineral admixtures are classified as follows:

- Chemically inert additions (type I), such as quartz powder, limestone powder.
- Pozzolanic and latent hydraulic additions (type II), which are called supplementary cementitious materials or reactive materials, for example, natural pozzolans, silica fume, fly ash, metakaolin, rice husk ash, ground granulated blast furnace slag. In this research project three main reactive materials were considered as follows:
  - **Silica fume**, also known as microsilica, mostly composed of sub-micron spherical particle of amorphous silicon dioxide  $\text{SiO}_2$ , is a by-product of the production of silicon metals and ferrosilicon alloys. Owing to its ultra-fine size (about of  $0.1 \mu\text{m}$ ), spherical shape, high amorphous  $\text{SiO}_2$  content (higher 90 wt.%), large total surface area (about of  $20000 \text{ m}^2/\text{g}$ ), silica fume is the most highly reactive powder working as an effective filler to improve concrete engineering properties and microstructure, especially UHPFRC (Fehling et al. [2013]).
  - **Fly ash**, also called pulverized fuel ash, is a by-product of burning coal or lignite in an electrical generating station. The fused particles are quenched when they leave the flame, and they solidify in the shape of vitreous spheres, then collected in the dust collectors. For use in concrete fly ash is classified to Class F - low-calcium fly ash and Class C - high-calcium fly ash by ASTM C618 [2008] based on the total content of  $\text{SiO}_2$ ,  $\text{Al}_2\text{O}_3$  and  $\text{Fe}_2\text{O}_3$ . Low-calcium fly ash (class F) has a higher 70 wt.% of  $(\text{SiO}_2 + \text{Al}_2\text{O}_3 + \text{Fe}_2\text{O}_3)$  and a lower 10 wt.% of CaO content. In contrast, the sum of  $(\text{SiO}_2 + \text{Al}_2\text{O}_3 + \text{Fe}_2\text{O}_3)$  is smaller than 70 wt.% and CaO content is higher than 10 wt.% for high-calcium fly ash (class C). The carbon content of a fly ash is requested to be lower 5 wt.% in accordance with European Standard EN 450-1 [2005b], because carbon particles can adsorb preferentially admixtures, increasing water and superplasticizer demand. Actually, these fly ashes are suitable only for normal strength and regular high performance concrete. For use in UHPFRC the fineness of fly ash must be increased to improve the pozzolanic and filler effects. Recently, ultra-fine fly ash with very low carbon content and mean diameter of about 3

$\mu\text{m}$  was used to produce UHPFRC having high flowability and 150 MPa 28 days compressive strength (Heinz et al. [2014]).

- **Ground granulated blast furnace slag**, which exhibits latent hydraulic properties, is an industrial by-products of producing pig iron in a blast furnace. The liquefied slag must be quenched quickly when it is tapped from the furnace to form a hydraulically active calcium aluminosilicate glass. The slag granules are then ground to cement fineness or finer, called ground granulated blast furnace slag (GGBFS). The finer the GGBFS is, the higher its reactivity is. GGBFS displays hydraulic properties when it is activated by lime, calcium sulphate and alkalis. That is why Portland cement is a good catalyst for slag activation. When slag particles are in the presence of a saturated solution of  $\text{Ca}^{2+}$  ions, slag hydration accelerates, and well-crystallized hydration products are formed within the slag particle. Thus, partial cement can be replaced by GGBFS to reduce the high Portland cement clinker. However, the early strength of GGBFS - Portland cement concrete is usually lower than that of Portland cement, especially at low curing temperature. Heinz et al. [2014] reported that UHPC (fibre-free) with cement replacement by 73 wt.% fine GGBFS can obtain strength of more than 165 MPa immediately after 24 hours heat treatment at  $90^\circ\text{C}$ .

Filler effect is a physical nature of mineral admixture. It results in a better packing of the granular mixture of concrete when the fine additions with grains of smaller cement grains fill up the voids between the larger ones (cement-cement particles or cement-aggregate particles). As discussed in Chapter 2, from physical point of view, the addition has a better filler effect as its fineness is increased. However, for packing of fines in wet condition, the characteristic of fines (the wettability and adhesion, the particle shape), the liquid characteristics have a strong influence on the packing of fines. Indeed, Figure 3.6 shows the variation in packing density of blended cements when the cement was replaced step by step by fly ash (FA) or quartz powder (QP) or limestone powder (LSP) in this research project, the detail information of the used materials is described in Chapter 4. Obviously, these mineral addition have the relatively similar size distribution but their effectiveness in improvement of packing density are different.

The hydration of the calcium silicate compounds,  $\text{C}_3\text{S}$  (or alite) and  $\text{C}_2\text{S}$  (or belite) in portland cement produces calcium silicate hydrate (C-S-H) and calcium hydroxide ( $\text{Ca}(\text{OH})_2$  or CH) as represented by Equations (3.1) and (3.2) (according to Mindess et al. [2003b]). C-S-H is a principal strength-giving compound in the hardened concrete whereas calcium hydroxide is considered as a weak link in the concrete structure. Addition of pozzolanic powders to Portland cement increases the quantity of the C-S-H phase due to the pozzolanic reaction between the calcium hydroxide and the glassy silica ( $\text{SiO}_2$  or S) of the pozzolanic powders as described by Equation (3.3). The reactive alumina in pozzolanic powders also react with the calcium hydroxide to form calcium aluminate hydrate C-A-H. The chemical effect of reactive powders lead to long term benefits, including increase in compressive strength and decrease in transport coefficients.



### 3. Influence of the characteristics of constituent materials on UHPFRC's performance



Typically, the Ca/Si ratio ( $x/y$  in Eq. (3.3)) of the C-S-H that forms from pozzolanic reaction will be lower than the Ca/Si ratio measured for C-S-H in hydrated portland cement without pozzolan, and the difference will vary depending on the age, type, and amount of pozzolan (Taylor [1997b]). Lothenbach et al. [2011] used thermodynamic modelling to predict the phase change in hydrated portland cement - reactive mineral powder system in which the reactive addition is silica fume or fly ash or ground granulated blast furnace slag, as illustrated by Figures 3.7, 3.8, 3.9. The modelling agrees with published experimental investigations, the results indicate that the pore structure of portland cement - reactive addition paste is refined, resulting to more fine pores and less coarse capillary pores than PC pastes. In addition, the high Ca/Si ratio jennite like C-S-H gradually converts to lower Ca/Si ratio tobermorite like C-S-H when the content of reactive addition increases.

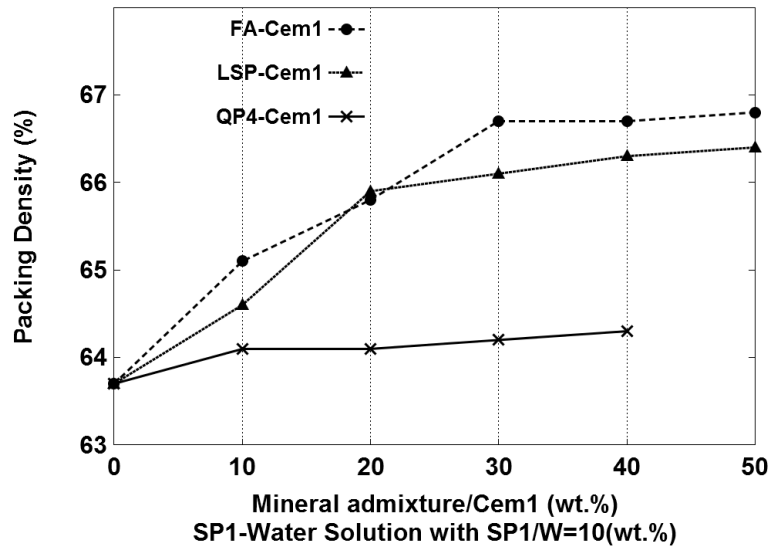


FIGURE 3.6.: The variation in packing density of blended cements by varying the content of fly ash, quartz powder and lime stone powder.

Furthermore, it has been realized for a long time that fine and ultra-fine additions act as nucleation sites for the hydration products of the clinker phases, resulting in an acceleration of the cement hydration (Soroka et al. [1977], Gutteridge et al. [1990b] [1990a]).

### 3.3. Function of mineral admixtures in UHPC

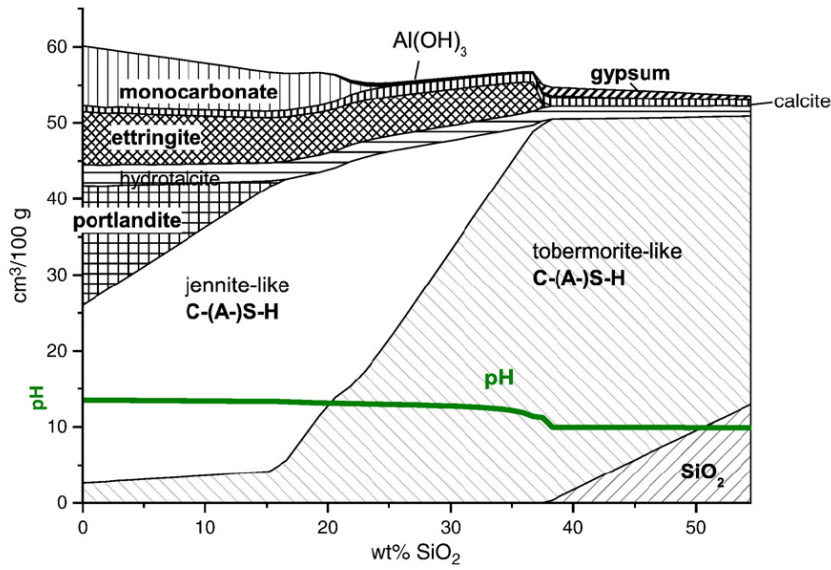


FIGURE 3.7.: Modelled changes in hydrated Portland cement - silica fume binder, assuming complete reaction of the Portland cement (CaO 60, SiO<sub>2</sub> 22, Al<sub>2</sub>O<sub>3</sub> 4.6, Fe<sub>2</sub>O<sub>3</sub> 2.7, MgO 1.9, Na<sub>2</sub>O 0.3, K<sub>2</sub>O 1.0, SO<sub>3</sub> 3.2, CO<sub>2</sub> 2 wt.%) and silica fume (100% SiO<sub>2</sub>) (Lothenbach et al. [2011]).

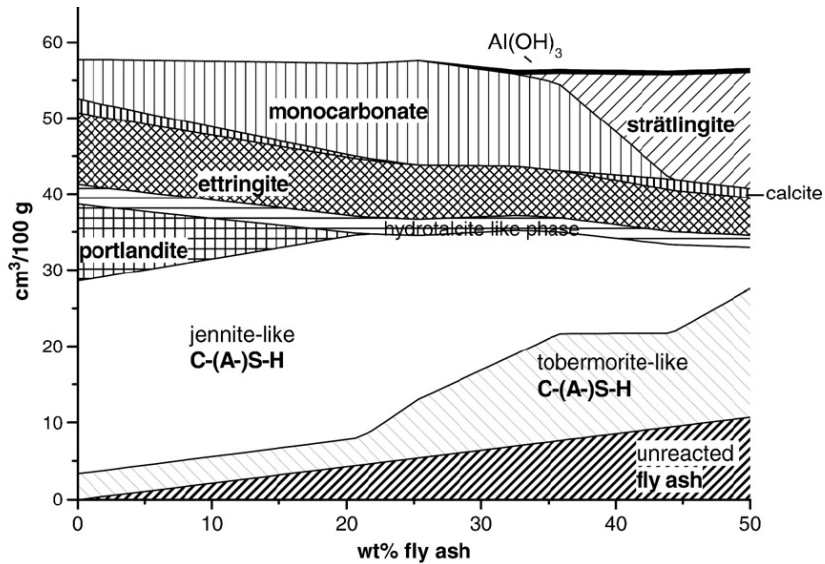


FIGURE 3.8.: Modelled changes in hydrated Portland cement - fly ash binder, assuming complete reaction of the Portland cement (CaO 60, SiO<sub>2</sub> 22, Al<sub>2</sub>O<sub>3</sub> 4.6, Fe<sub>2</sub>O<sub>3</sub> 2.7, MgO 1.9, Na<sub>2</sub>O 0.3, K<sub>2</sub>O 1.0, SO<sub>3</sub> 3.2, and CO<sub>2</sub> 3 wt.%) and 50% reaction of a low Ca fly ash (CaO 4.4, SiO<sub>2</sub> 54, Al<sub>2</sub>O<sub>3</sub> 31, Fe<sub>2</sub>O<sub>3</sub> 4.6, MgO 0.8, Na<sub>2</sub>O 0.6, K<sub>2</sub>O 0.8, and SO<sub>3</sub> 0.4 wt.%). (Lothenbach et al. [2011]).

### 3. Influence of the characteristics of constituent materials on UHPFRC's performance

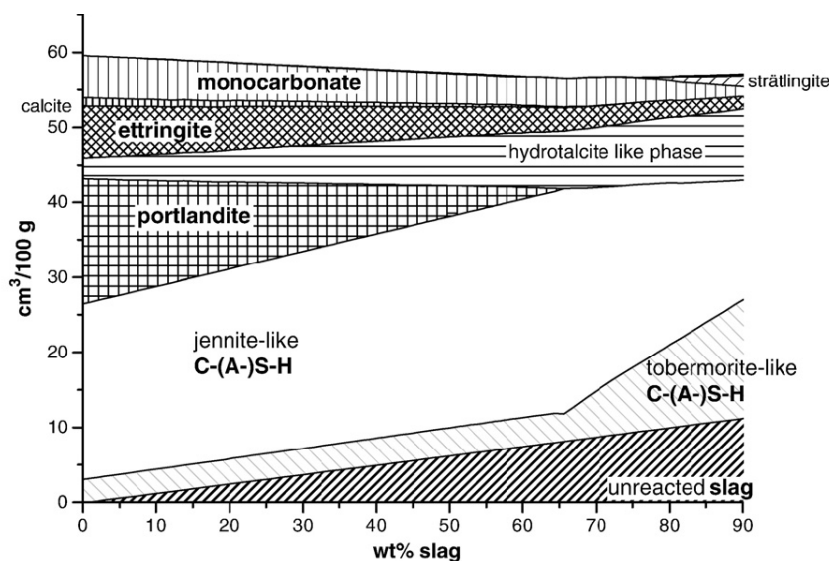


FIGURE 3.9.: Modelled changes in hydrated Portland cement - blast furnace slag, assuming complete reaction of the Portland cement (CaO 60, SiO<sub>2</sub> 22, Al<sub>2</sub>O<sub>3</sub> 4.6, Fe<sub>2</sub>O<sub>3</sub> 2.7, MgO 1.9, Na<sub>2</sub>O 0.3, K<sub>2</sub>O 1.0, SO<sub>3</sub> 3.2, and CO<sub>2</sub> 3 wt.%) and 75% reaction of a blast furnace slag (CaO 39, SiO<sub>2</sub> 38, Al<sub>2</sub>O<sub>3</sub> 11, Fe<sub>2</sub>O<sub>3</sub> 1, MgO 10, K<sub>2</sub>O 0.3, and S 1 wt.%). Al/Si in C-S-H=0.1 (Lothenbach et al. [2011]).

Generally speaking, fine and ultra-fine highly reactive powders possess both filler and pozzolanic effects, they are thus indispensable for improving the microstructure of the bulk cement paste and the interfacial transition zone in the production of high/ultra-high performance concrete.

Talking about the influence of the granulometry and water content of fine particles on the rheology and strength of pastes in fresh and hardened states Teichmann [2008] and Geisenhanslüke [2009] indicated that: (i) Within the range in which the filler increase the packing density, the water demand and plastic viscosity decrease in despite of the increase of total surface area of filler. However, surface area of filler significantly affect to packing density, water demand, plastic viscosity when filler content increases over the optimum dosage. (ii) At W/C ratio of higher 0.35 wt.% the influence of the packing density increasing on compressive strength is not clear, but at lower W/C ratio of 0.35, especially W/C ratio of 0.25, the improvement of packing density leads to a high increase in compressive strength of binder stone.

Papadakis [1999b, 1999a, 2000] proposed a theoretical approach to estimate the maximum silica fume or fly ash content that can react with all lime produced during cement hydration at high W/C ratio of 50 wt.% or higher. As a result, the maximum contents of silica fume, low-calcium fly ash and high-calcium fly ash were determined of 18.3 wt.%, 24 wt.% and 50 wt.% of cement respectively. Silica fume or fly ash addition exceeding these optimum values is inert and play a role of filler only. These results are meaningful for the employing of reactive powders in UHPC having very low W/C ratio. It implies that the extra amount of reactive powder which only play a role of filler can be replaced by an effective filler to reduce material cost.

### 3.4. Concluding remarks

The composition of cement clinker has a great influence on the processing characteristic of UHPC having a very low Water/Cement ratio. A high content of  $C_3A$  or a high reactivity  $C_3A$  give a negative effect on initial rheology of UHPC. Furthermore, the early hydration of cement is accelerated by the presence of alkalies. Thus, the  $C_3A$  content and alkalis content of cement clinker should be as lowest as possible. Gypsum and other kinds of calcium sulfate in Portland cement have to control to avoid the “flash set” and “false set” in the production of UHPC.

The compatibility of cement and superplasticizer strongly govern the fluidity of UHPC. This is depended on the composition of cement clinker and the chemical structure of superplasticizer. The compatibility of cement and superplasticizer is experimentally evaluation by complex process, the development of a fast and simple method is needed. Selection of cements and superplasticizers concerning their compatibility is crucial to achieve the best performance for UHPC.

Ultra-fine highly reactive powder is indispensable for improving the microstructure of the bulk cement paste and the interfacial transition zone in the production of UHPC. The extra amount of reactive powder which only play a role of filler can be replaced by an effective inert filler to reduce material cost.



## 4. Materials selection

### 4.1. Materials

At the beginning of this research project, the collection of raw materials includes 21 materials of five different groups. Tables 4.1, 4.2, 4.3 summarize the basic properties of the used materials. In order to determine the particle size distribution of the materials, the laser diffraction technique with HELOS-RODOS instrument, Sympatec GmbH was used for the powders, while the image analysis technique with QICPIC-RODOS instrument, Sympatec GmbH was applied for the quartz sands. However, the particle size distribution of silica fumes were analyzed by the LS 13 320 equipment of Beckman Coulter. Other tests for material characterization were carried out partly in the own lab, while in some cases the data was available from materials producers. Figure 4.1 and Figure 4.2 display the particle size distribution of powders and aggregates respectively, the detail data of the particle size analysis are shown in Tables A.1 to A.7 in Appendix A.

**Cement:** Four different cements were investigated, they were produced in Austria. As discussed in the previous chapter, these cements are sulphate resistant,  $C_3A$  free, high early strength portland cements according to EN 197-1 (CEM I 52.5 N, CEM I 42.5 R). Two cements (Cem1, Cem2) were supplied by Cement Lafarge. The third one (Cem3) was from W&P Cement. The last one (Cem4) was from Kirchdorfer Cement.

**Reactive fillers:** Four different reactive powders were used. The undensified silica fumes Elkem 971U (SF1) and RW Füller Q1 (SF2) were supplied by Elkem - Norway and by RW silicium GmbH - Germany respectively. The ultra-fine and low-calcium fly ash Microsit H10 (FA) ( $0.45\text{-}15\mu\text{m}$ ) is a commercial product delivered by BauMineral GmbH - Germany. Ground Granulated Blast Furnace Slag (GGBFS) ( $0.45\text{-}180\mu\text{m}$ ) is produced and supplied by Bernegger GmbH - Austria. The activity indices of the reactive fillers was determined according to European Standard EN 13263-1 [2005a] for silicafume, EN 450-1 [2005b] for fly ash, EN 15167-1 [2006] for ground granulated blast furnace slag.

**Inert fillers:** Four quartz powders QP110 ( $0.45\text{-}21.5\mu\text{m}$ ), QP16900 ( $0.45\text{-}87.5\mu\text{m}$ ), QP10000 ( $0.45\text{-}150\mu\text{m}$ ), QP2500 ( $0.45\text{-}215\mu\text{m}$ ) produced by Gebrüder Dorfner GmbH - Germany and the ultra-fine limestone powder Betoflow-D (LSP) ( $0.45\text{-}12.5\mu\text{m}$ ) from Omya International AG were used as inert fillers.

**Aggregates:** Three different crushed quartz sands QS1 ( $803\text{-}2580\mu\text{m}$ ), QS2 ( $369\text{-}1185\mu\text{m}$ ), QS3 ( $64\text{-}304\mu\text{m}$ ) produced by Gebrüder Dorfner GmbH - Germany were used as fine aggregates. The coarse aggregates include two crushed basalt rocks CrB1 ( $2000\text{-}9000\mu\text{m}$ ), CrB2 ( $800\text{-}5600\mu\text{m}$ ) from Steirischer Basalt und Hartgesteinwerke Appel Steinbruch GmbH - Austria.

#### 4. Materials selection

TABLE 4.1.: Physical-mechanical properties and chemical component of the used cements.

	<b>Cem1</b>	<b>Cem2</b>	<b>Cem3</b>	<b>Cem4</b>
Type	CEM I 52.5N	CEM I 42.5N	CEM I 42.5R	CEM I 52.5N
C <sub>3</sub> A (wt.%)	< 2.5	< 2.5	< 2.5	< 2.5
D <sub>50</sub> (μm)	7.70	12.32	10.00	9.52
Vol. Mean Diameter (μm)	11.19	16.64	14.94	12.75
Density (g/cm <sup>3</sup> )	3.10	3.05	3.05	3.10
28 days Comp.Strength (MPa)	61	56	57	61
SiO <sub>2</sub> (wt.%)	20.25	20.48	20.60	21.59
CaO (wt.%)	66.07	60.81	60.48	64.86
Al <sub>2</sub> O <sub>3</sub> (wt.%)	2.76	4.33	4.5	–
Fe <sub>2</sub> O <sub>3</sub> (wt.%)	4.91	5.91	5.65	–
Na <sub>2</sub> O (wt.%)	0.21	0.33	0.21	0.23
K <sub>2</sub> O (wt.%)	0.49	0.68	0.69	0.76
Na <sub>2</sub> O equivalent (wt.%)	0.53	0.77	0.66	0.73
SO <sub>3</sub> (wt.%)	2.61	2.36	2.75	2.35

TABLE 4.2.: Physical-mechanical properties and chemical component of the used reactive fillers.

	<b>SF1</b>	<b>SF2</b>	<b>FA</b>	<b>GGBFS</b>
D <sub>50</sub> (μm)	0.327	0.342	2.850	9.200
Vol. Mean Diameter (μm)	1.839	4.864	3.650	17.280
Density (g/cm <sup>3</sup> )	2.20	2.20	2.51	2.82
Activity Index (28 days)(%)	112.4	114.5	105.1	100.0
SiO <sub>2</sub> (wt.%)	98.4	97.0	54.0	–
Al <sub>2</sub> O <sub>3</sub> (wt.%)	0.20	0.15	25.00	–
Fe <sub>2</sub> O <sub>3</sub> (wt.%)	0.10	0.03	6.00	–
CaO (wt.%)	0.30	0.25	4.00	–
Na <sub>2</sub> O (wt.%)	0.20	0.05	–	–
K <sub>2</sub> O (wt.%)	0.30	0.45	–	–
Loss on Ignition (wt.%)	0.5	0.8	2.7	–
pH-value	6.8	7.5	–	–

TABLE 4.3.: Physical properties and chemical component of the used inert fillers and aggregates.

	SiO <sub>2</sub> (wt.%)	Density (g/cm <sup>3</sup> )	D <sub>50</sub> (μm)	Vol. Mean Diameter (μm)
<b>QP110</b>	99	2.63	3.40	4.68
<b>QP16900</b>	99	2.63	13.13	18.28
<b>QP10000</b>	99	2.63	22.85	31.29
<b>QP2500</b>	99	2.63	33.78	47.43
<b>LSP</b>	–	2.70	2.17	2.95
<b>QS1</b>	99	2.63	1696.20	1715.43
<b>QS2</b>	99	2.63	515.80	693.88
<b>QS3</b>	99	2.63	103.30	152.63
<b>CrB1</b>	–	2.95	–	5872.80
<b>CrB2</b>	–	2.95	–	2812.40

**Superplasticizers:** Three polycarboxylate ether based superplasticizers in liquid

#### 4.2. Packing density measurement for coarse particles

form (solid content of 30 wt.%, densities of 1.05 g/cm<sup>3</sup>) were used, namely Premment H500 (SP1) from BT3 Betontechnik GmbH, Sika<sup>®</sup> ViscoCrete<sup>®</sup>-20 Gold (SP2) from Sika Austria and Glenium<sup>®</sup> ACE430 (SP3) from BASF Construction Polymers GmbH.

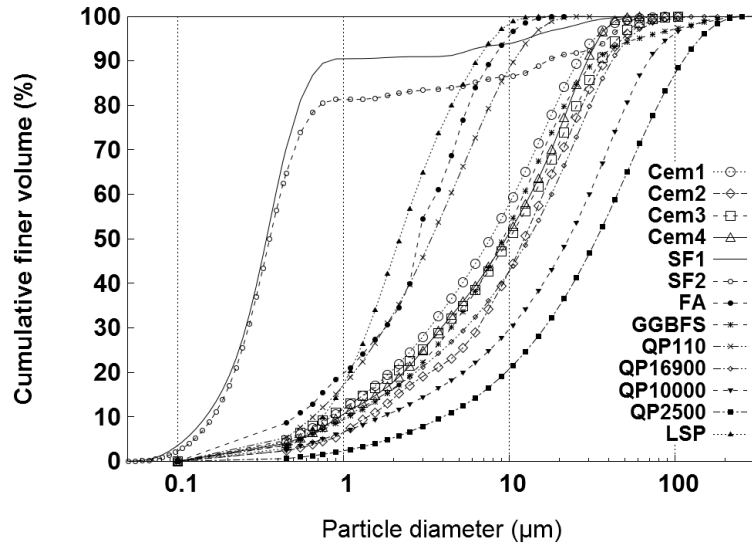


FIGURE 4.1.: The particle size distribution of cements, reactive fillers and inert fillers in the test program (log-10 scale for the X axis)

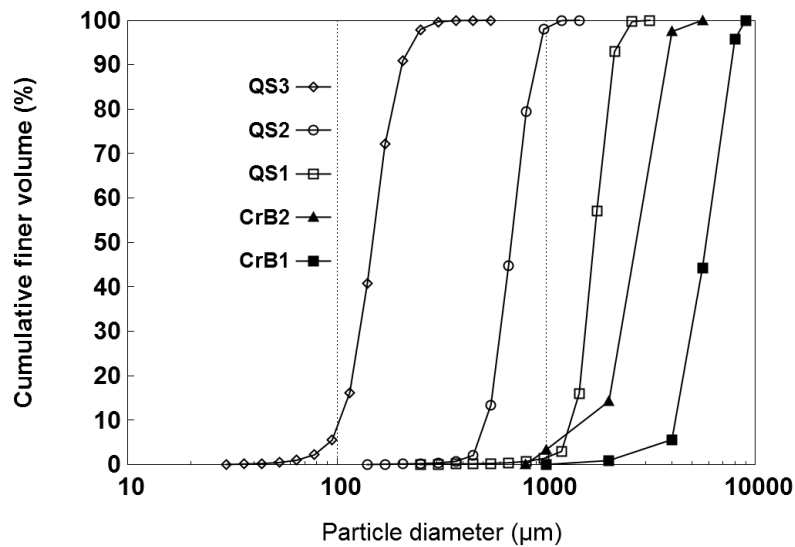


FIGURE 4.2.: The particle size distribution of quartz sands and crushed basalt stones for UHPC production (log-10 scale for the X axis)

#### 4.2. Packing density measurement for coarse particles

The actual packing densities of quartz sands (QS1, QS2, QS3) and crushed basalt (CrB1, CrB2) were examined according to the method recommended by de Larrard as the

#### 4. Materials selection

description in section 2.3.2.3 (compaction index  $K = 9$  and wall effect coefficient  $k_w = 0.73$ ). A cylindrical mould of 150 mm diameter and 300 mm height was used for testing. The residual packing densities of monosized classes of each material were then computed. Table 4.4 (or Table A.3) shows the results for quartz sand QS1. The results of the other aggregates are reported in Tables A.4, A.5, A.6, A.7 in Appendix A.

TABLE 4.4.: Computing the residual packing densities of monosized classes of polydisperse quartz sand QS1 based on its experimentally actual packing density.

Quartz sand QS1		K-value	$\beta_{\text{exp}}$	monosized classes			$\beta$	$\beta_i$
Size ( $\mu\text{m}$ )	Passing (vol.%)			Class i	Size ( $\mu\text{m}$ )	$y_i$ (vol.%)		
2580.23	100	9	0.6360	1	2341.24	7.08	0.6744	0.66633
2124.39	92.92			2	1927.62	35.84		0.66774
1749.08	57.08			3	1587.07	41.07		0.66891
1440.07	16.01			4	1306.68	13.06		0.66987
1185.65	2.95			5	1075.83	1.59		0.67067
976.19	1.36			6	885.77	0.65		0.67133
803.73	0.71			7	729.28	0.30		0.67187
661.73	0.41			8	600.44	0.16		0.67232
544.83	0.25			9	494.36	0.08		0.67269
448.57	0.17			10	407.02	0.04		0.67299
369.32	0.13			11	335.11	0.13		0.67324
304.08	0							

### 4.3. Determination of the water-cement ratio

The varying of water-cement weight ratio (W/C) influence on the compressive strength of cement, cementitious material and concrete, leading to an impractical amount of design variables to be investigated. Therefore various W/C ratios were computed and only one value of W/C ratio was selected to use for all investigations relate to compressive strength. For normal and high strength concrete having compressive strength up to 130 Mpa the relation between compressive strength and W/C ratio was already built and shown as Figure 4.3 in some textbooks (BetonKalender [2010]; Betontechnische Daten [2014]). However, these data can not applied for ultra high strength concrete in range of 165 MPa to 200 MPa.

Actually, the research by Powers and Brownyard [1947] and the deeper explanation about Powers work by Hansen [1986] allow to estimated the the physical structure and strength of room temperature cured Portland cement paste from information on W/C ratio and degree of hydration of the cement. This approach was accepted as a general method for determining the influence of W/C ratio on hardened paste compressive strength, and it was introduced in some textbooks (Neville [1996]; Mindess et al. [2003a]; the International Federation for Structural Concrete (*fib* [2009])).

### 4.3. Determination of the water-cement ratio

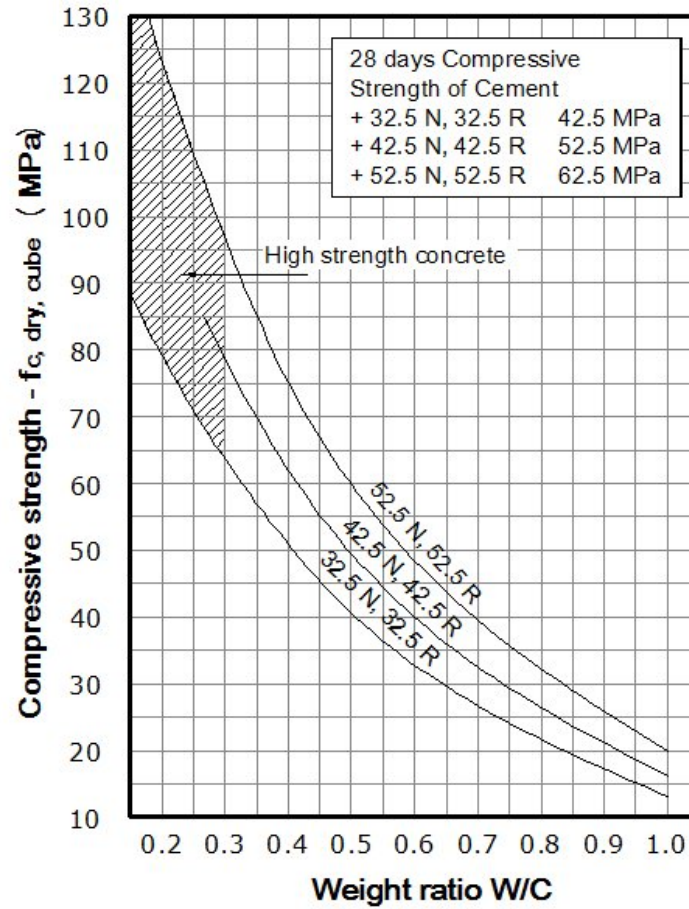


FIGURE 4.3.: Walz curve

In the Powers-Brownnyard model, hardened Portland cement paste is assumed to comprise three volumetric components: (i) unreacted cement, (ii) hydration product and (iii) capillary pores. The relationship between the compressive strength of the hardened paste,  $f_{c(hp)}$ , and the capillary porosity,  $V_{cp}/V_0$ , is described by Equations (4.1) and (4.2) (*fib* [2009]).

$$f_{c(hp)} = f_{c,0} \left( 1 - a \frac{V_{cp}}{V_0} \right)^n \quad (4.1)$$

$$a = \frac{\frac{W}{C} + 0.32}{\frac{W}{C} + 0.32\alpha} \quad (4.2)$$

where:  $f_{c,0}$  is the compressive strength of a hydrated cement paste gel free of capillary pores. The values of  $f_{c,0}$  and  $n$  depend on the type of cement and other technological parameters, they were determined as 240 MPa and 3 respectively in Powers work.  $V_0$  is the initial volume of cement and mixing water.  $V_{cp}$  is the volume of capillary pores. The  $\alpha$  value is the degree of hydration, defined as the mass fraction of the cement which has

#### 4. Materials selection

hydrated at a given point in time. Powers and Brownyard [1947] demonstrated that at complete hydration, 1 gram of cement binds approximately 0.23 gram water chemically (non-evaporable water) and 0.19 gram gel water. Complete and unimpeded hydration is only possible at W/C ratios above 0.42 ( $= 0.23 + 0.19$ ). Therefore, the maximum degree of hydration,  $\alpha_{\max}$  for a paste with W/C of lower than 0.42 is limited by the value of (W/C)/0.42. The relation between capillary porosity  $V_{cp}/V_0$ , W/C ratio and degree of hydration  $\alpha$  is be described Equation (4.3) (*fib* [2009]).

$$\frac{V_{cp}}{V_0} = \frac{\frac{W}{C} - 0.36\alpha}{\frac{W}{C} + 0.32} \quad (4.3)$$

Thus, the compressive strength of a hardened paste can be estimated by applying Equation (4.4).

$$f_{c(hp)} = 240 \left( 1 - \frac{\frac{W}{C} + 0.32}{\frac{W}{C} + 0.32\alpha} \frac{\frac{W}{C} - 0.36\alpha}{\frac{W}{C} + 0.32} \right)^3 = 240 \left( \frac{0.68\alpha}{\frac{W}{C} + 0.32\alpha} \right)^3 \quad (4.4)$$

the value

$$v = \frac{0.68\alpha}{\frac{W}{C} + 0.32\alpha}$$

is call gel/space ratio.

Mills [1966] presented an empirical model to estimate the final degree of hydration of portland cement depending on W/C ratio, expressed by Equation (4.5).

$$\alpha(\infty) = \frac{1.031 \frac{W}{C}}{0.194 + \frac{W}{C}} \quad (4.5)$$

Lam et al. [2000] examined the degree of hydration of the cement in Portland cement paste by determining the non-evaporable water (W<sub>n</sub>) content that was the method used in Powers work. Thereby, a model to predict the degree of hydration of the cement in Portland cement paste at 7 and 28 days was proposed, as shown by Equations (4.6) and (4.7). Furthermore, it was proved experimentally that the gel/space ratio of the blended cement paste in the presence of pozzolans increase in comparison with plain cement paste, leading to a higher compressive strength.

$$\alpha(7d) = 0.8529 \exp(-0.1172 / (\frac{W}{C})) \quad (4.6)$$

$$\alpha(28d) = 0.9658 \exp(-0.1345 / (\frac{W}{C})) \quad (4.7)$$

#### 4.4. The compatibility of the powders and the superplasticizers

Using Eqs. (4.4), (4.6) and (4.7) the compressive strengths of hardened pastes with various W/C ratios at 7, 28 days were estimated. Eqs. (4.4) and (4.5) were used to compute the final compressive strength of hardened pastes. The calculated results are presented in Table 4.5

TABLE 4.5.: Estimating the degree of hydration of portland cement and the compressive strength of hardened paste.

	W/C ratio (wt.%)						
	0.28	0.27	0.26	0.25	0.24	0.23	0.22
	7 days						
$\alpha_{,7d}$	0.5612	0.5526	0.5434	0.5337	0.5234	0.5124	0.5007
$f_{c(hp),7d}$	137.4	142.7	148.2	154.0	159.9	166.0	172.3
	28 days						
$\alpha_{,28d}$	0.5974	0.5869	0.5757	0.5639	0.5514	0.5382	0.5241
$f_{c(hp),28d}$	153.8	159.0	164.3	169.7	175.2	180.8	186.4
	$\infty$						
$\alpha_{,\infty}$	0.6090	0.5999	0.5904	0.5805	0.5701	0.5593	0.5479
$f_{c(hp),\infty}$	159.2	165.3	171.7	178.4	185.5	193.0	200.9

Based on this calculation the W/C ratio of 0.25 was chosen and kept constant for all tests that relate to the rheology behaviour and strength of pastes and concretes. This was done because this W/C ratio is not only low enough for an expected concrete strength of 180 MPa due to the strength improvement by pozzolanic reaction, but also high enough to ensure a good workability of concrete.

#### 4.4. The compatibility of the powders and the superplasticizers

##### 4.4.1. The influence of the superplasticizers on packing density and strength of the cements

The method of mixing energy measurement introduced by Marquardt (see section 2.2.3) was employed to examine the packing density (as well as the water demand) of the cements. An Eirich intensive mixer, type R01, was used for the experiment, as shown in Figure 4.4 (left). The mixer has a driven, rotating mixing pan and a mixing tool which rotates eccentrically, in addition the fixed wall scraper cleans the wall of the mixing pan. The mixer can be operated via PC-controller for multi-stage, freely definable mixing instructions and recording of all operating parameters. The cement amount was 5000 grams for each test. First, packing densities of the four cements were determined using water only. By using a flow velocity adjusting tool the water velocity was kept constant of 1.68 ml/s during test process.

The test procedure was as follows:

- The mixing pan and mixing tool were controlled to rotate in reverse order.

#### 4. Materials selection

- The mixing pan speed was 84 rpm.
- The dry cement was mixed for 60 seconds at a mixing tool speed of 84 rpm.
- Water was then added to the powder at a mixing tool speed of 150 rpm for 120 seconds.
- The speed of the mixing tool was then increased up to 450 rpm, while water was still added to the cement until a clear decrease of the power consumption was recognized.
- The duration of water adding ( $t_{\text{water-add}}$ ) from the beginning to the maximum power consumption was determined.
- Tests on each powder were performed twice. The mean value was reported.

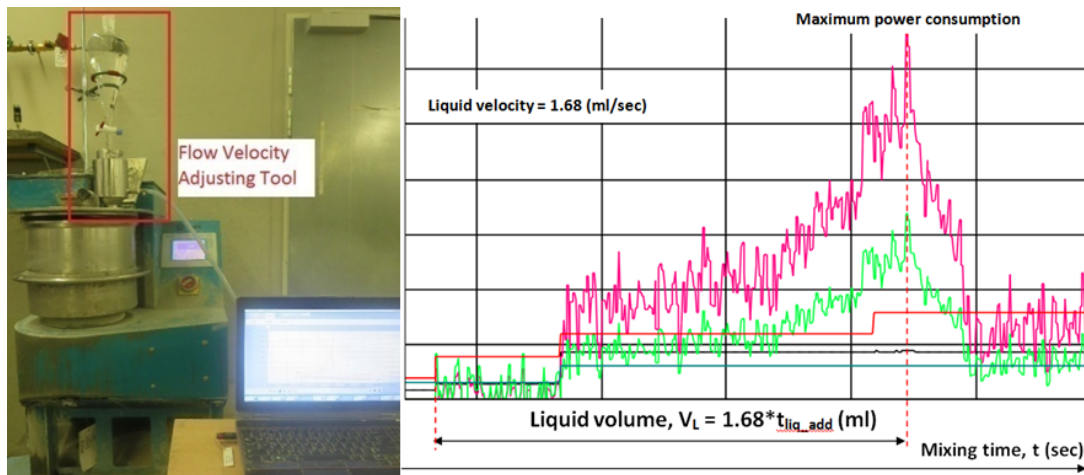


FIGURE 4.4.: The equipment for the superplasticizer-water solution demand test (left), and the development of power consumption during addition of the solution (right)

The packing densities and the corresponding water demands of the cements were then calculated by Equations (2.6) and (2.7) respectively, in which the value  $V_{\text{Liq}}$  was  $1.68 \times t_{\text{water-add}}$  ml, as illustrated in Figure 4.4 (right).

The test results, as described by the first bar of each group in Figure 4.5 and Figure 4.6, did not show a significant difference between the cements. The dispersion of all cements was low, their packing densities were similar (55.8% - 56.5%) and corresponded to the water demands of 25.3 wt.% - 25.66 wt.%. Obviously, strong agglomerates were formed as water came into powder. The fine particles in the agglomerates could not disperse well when water was used only. According to these results there was no persuasive reason for concluding about cements quality. The detail data of the tests are shown in Table A.8 in Appendix A.

For a better packing of cement grains due to a high dispersibility in cement-liquid system the use of superplasticizer is essential to reduce the interparticle forces between cement particles. The description in section 3.2 emphasizes that molecular structure of superplasticizer and cement composition influence on cement dispersion considerably. This implies that the best compatibility of cements and superplasticizers can be recognized by a precondition of the highest packing density of cement in superplasticizer-water-cement system.

#### 4.4. The compatibility of the powders and the superplasticizers

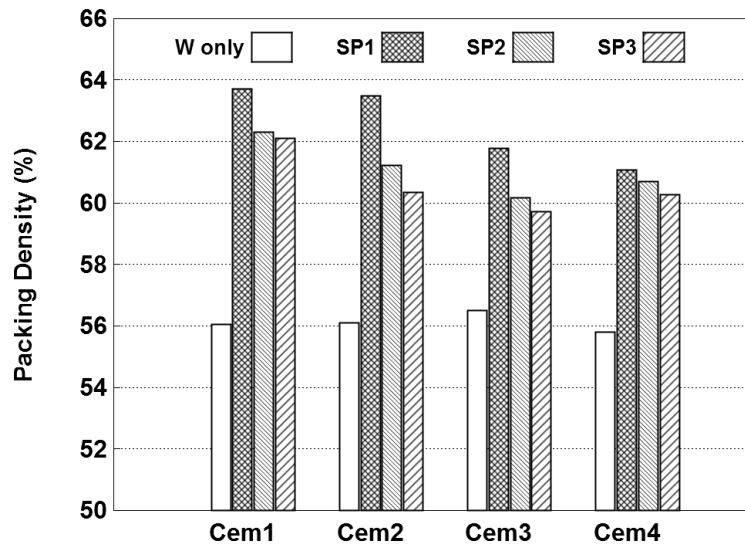


FIGURE 4.5.: The packing density of four cements in the test using SP-Water solutions with the SP-Water ratios of 0 and 10 wt.%

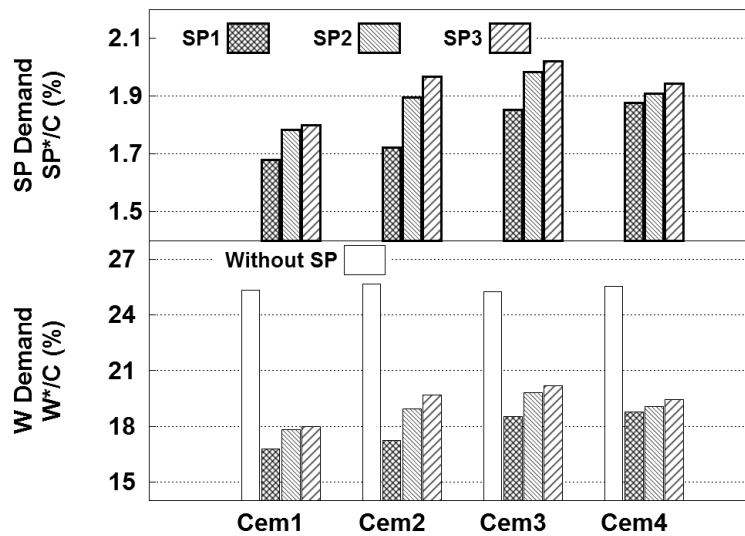


FIGURE 4.6.: The SP-Water solution demands of the cements are described by water demand ( $W^*/C$ ) and superplasticizer demand ( $SP^*/C$ ) in the test using SP-Water solutions with the SP-Water ratios of 0 and 10 wt.%

The questions are here: (i) what are the superplasticizer dosages for cement packing density examination and (ii) how can the superplasticizer be introduced to cement.

- De Larrard [1999] suggested that water demand measurement should be performed with the same proportion of superplasticizer in the concrete (with respect to the cement). This leads to a relatively high amount of superplasticizer for cement packing

#### 4. Materials selection

measurement because the superplasticizer-cement ratio is used in range 3-4 wt.% for UHPFRC (Schmidt and Fehling et al [2014]).

- In the research of Fennis [2010] PCE Glenium 51 was used for powder packing density measurement as a constant amount of 1.2 wt.% of powders to ensure stable mixtures and avoid overdosage. The effectiveness of different superplasticizers in combination with powders was not investigated. First, 1500 grams of cement and 264 grams of water and the superplasticizer were mixed in a three liters Hobart mixer for one minute. After one minute of mixing and two minutes of resting and scraping, mixing was continued and further water was added in drops until maximum power consumption was reached. Clearly, the further water adding reduces the concentration of superplasticizer. This means the dispersion effect of new solution is lower than that of the initial solution, leading to a lower packing density of powder compared to packing density of powder with a constant superplasticizer concentration like the initial solution.

From the above analysis it was recommended to use a superplasticizer-water solution for cement packing density measurement in this research project. After trial tests, the superplasticizer concentration in solution was determined by superplasticizer/water ratio of 10 wt.%. The powder amount, the velocity of liquid, the test procedure were not changed in comparison to the test using water only. The powder packing density ( $\beta$ ) was still calculated using Eq. (2.6). The corresponding superplasticizer-water solution demand (denoted SpWD) of the cement was calculated using Equation (4.8) which is based on Eq. (2.7). This SpWD value can be described by the Water\*-Powder ratio (denoted W\*/Pow) and the Superplasticizer\*-Powder ratio (denoted SP\*/Pow) (weight ratio) as Equation (4.9) and Equation (4.10) respectively).

$$SpWD = \frac{M_{Liq}}{M_{Pow}} = \frac{V_{Liq} \times \frac{1 + \frac{M_{SP}}{M_W}}{M_{SP}}}{\frac{1}{\rho_W} + \frac{M_W}{\rho_{SP}}} \quad (4.8)$$

$$W^*/Pow = \frac{SpWD}{1 + \frac{M_{SP}}{M_W}} \quad (4.9)$$

$$SP^*/Pow = \frac{SpWD}{1 + \frac{1}{\frac{M_{SP}}{M_W}}} \quad (4.10)$$

where:  $\rho_{SP}$  and  $\rho_W$  are the densities of the superplasticizer and water.  $M_{SP}/M_W$  is the weight ratio of superplasticizer to water of the superplasticizer-water solution, for instance,  $M_{SP}/M_W=0.1$  was determined experimentally as a constant parameter in this research project.

#### 4.4. The compatibility of the powders and the superplasticizers

The above Figures 4.5 and 4.6 also represent the packing densities of the four cements measured by using superplasticizer-water solutions with SP/W = 10wt.% and three different SP1, SP2, SP3. The packing density of the cements were increased significantly. The results showed that superplasticizer SP1 had the highest dispersing effect on the four cements in comparison to SP2 and SP3. The highest dispersibility was found in the cement-water-SP1 system. When SP1 was used, Cem1 had the highest packing density of 63.7% and the lowest corresponding SP1-Water solution demand with  $W^*/C$  of 16.784 wt.% and  $SP^*/C$  of 1.678 wt.%. These phenomena could be explained successfully based on the compatibility of superplasticizer and cement. The detail data of the tests are shown in Table A.8 in Appendix A.

The influence of superplasticizer SP1 concentration in the solution on Cem1 packing density was investigated by varying SP1/W ratios of 10 wt.%, 12.5 wt.%, 15.0 wt.%, 17.5 wt.%. The real and highest packing density of 64.86% of Cem1 was determined corresponding to the SP1/W of 15 wt.%, as described in Figure 4.7. However, it was clear to recognize that when SP1/W ratio increased from 10 wt.% to 17.5% the packing density of Cem1 was increased negligibly of less than 2%,  $W^*/Cem1$  ratio was also reduced slightly, while  $SP^*/Cem1$  increased quickly from 1.678 wt.% to 2.628 wt.%. This means SP1/water of 10 wt.% allows to achieve SP1-Water solution with a sufficient dispersing effect for determining the real and highest packing density of Cem1. When SP1/W is higher than 10 wt.%, the excess amount of SP1 plays a role of water replacing liquid rather than a dispersing agent. The detail test data are shown in Table A.9 in Appendix A.

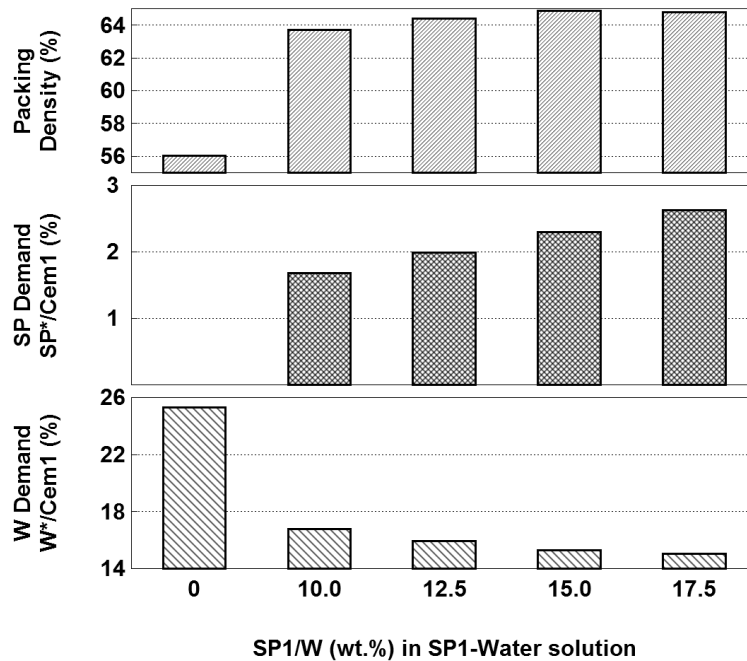


FIGURE 4.7.: The influence of SP1 concentration in SP1-water solution on the packing density of Cem1

Based on the above experimental analysis SP1/W ratio of 10 wt.% in SP1-Water

#### 4. Materials selection

solution was used as a constant parameter in this research project.

The results in the above Figures 4.5 and 4.6 indicated that Cem1 and Cem2 had the advantage over Cem3 and Cem4 in term of packing density. Nevertheless, the influence of the superplasticizers on 28 days compressive strength of the cements was investigated to achieve a convincing selection of cements. The experiments were carried out using W/C ratio of 25 wt.% and SP/C of 2 wt.%. The value SP/C of 2 wt.% was selected because the results of SP-water solution demand test for the cements, shown in Figure 4.6, pointed out that Cem3 had the highest SP3 demand of 2.02 wt.%. Quartz sand QS2 (369-1185  $\mu\text{m}$ ) was used as aggregate. The volume ratio of paste to aggregate was 1. To provide a general idea about the comparative performance of cements-superplasticizers, the compressive strength all tests were normalized by the compressive strength of Cem1-SP1, since the strength of Cem1-SP1 was the highest. The results are showed in Figure 4.8 and in Table A.10 in Appendix A. Obviously, the compatibility of cement and superplasticizer is also very important considering strength development of cement, especially concrete with a very low W/C ratio.

Cement is the major component of cementitious powder, a large amount of cement is used in cementitious powder. Besides, the compatibility of superplasticize (SP) and cement have a strong influence on the performance (the dispersion and strength) of cement. Cement with a low water demand and SP demand insures to achieve lower water demand and SP demand in combination with an effective filler. Therefore, the best cement and SP regarding the highest packing density (the lowest water demand and SP demand) and the highest strength must be chosen.

The above results about the influence of the superplasticizers on the packing density and the strength development of the cements are the compelling evidences to select Cem1 and SP1 for further investigation.

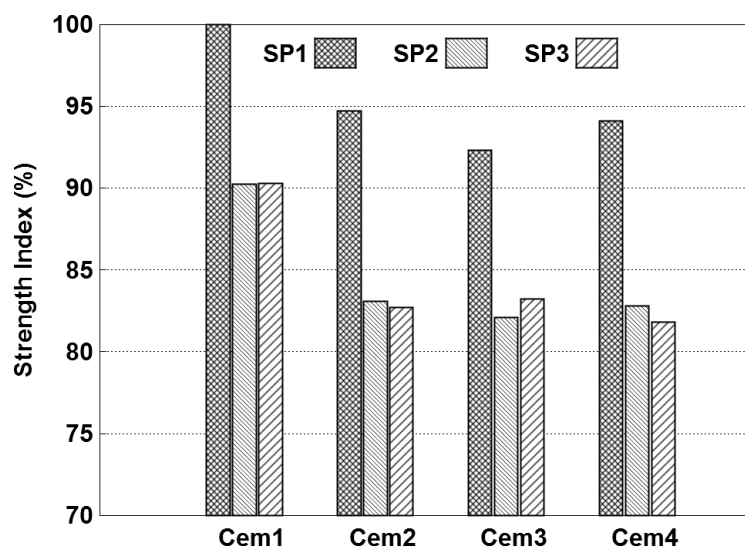


FIGURE 4.8.: The influence of three superplastic SP1, SP2, SP3 on the 28 days compressive strength of Cem1, 2, 3 and 4 with W/C = 25 wt.% and SP/C = 2 wt.%

#### 4.4.2. The influence of the superplasticizer SP1 on packing density of mineral admixtures

The SP-water solution demand test using SP1/W ratio of 10 wt.% was employed to measure the packing density of silica fumes (SF1, SF2), fly ash (FA), ground granulated blast furnace slag (GGBFS or BFS), quartz powders (QP1, QP2, QP3, QP4) and lime stone powder (LSP). The results in Figures 4.9 and 4.10 show that the packing densities of FA, GGBFS, QP1, QP2, QP3, QP4, LSP were increased by the positive dispersing effect of SP1 in comparison with the tests using water only (the detail data are shown in Table A.11 in Appendix A). However, SP1 had a negative effect on the dispersion of both silica fumes SF1 and SF2, in which the SP1-water solution demand of SF1 was increase considerably.

According to the study by Plank et al. [2009] and by Schöfl et al. [2012] this effect was attributed to the negatively charged surface of both silica fumes, in which the surface of SF1 is more negative and the total surface area of SF1 is much larger than that SF2. Thus, it could be predicted that concrete with SF1 needs higher SP content than concrete with the same SF2 content at a given flowability. This prediction is also supported by the results from the study by Glotzback et al. [2014]. The zeta potentials of four silica fume Elkem 971, Elkem 983, Silicoll P, Elkem 940 US were measured in the Glotzback's study, the negatively charged surface of the silica fumes were in descending order and correspond to the increase of the flowability of mortars with Elkem 971, Elkem 983, Silicoll P respectively, using the same superplasticizer and water content.

The activity of the reactive powders in Cem1 - reactive admixtures binders were investigated using W/Cem1 ratio of 25 wt.% and SP1/Cem1 of 2 wt.%. The aggregate was quartz sand QS2 (369-1185  $\mu\text{m}$ ). The volume ratio of paste to aggregate was 1. Figure 4.11 shows the normalized compressive strength of all Cem1 - reactive admixture binders with respect to the compressive strength of Cem1, since the strength of Cem1 was the lowest. The detail data are presented in Table A.12 in Appendix A.

Adequate reason was thus given to select SF2 for further investigations. The 28 days age compressive strength of the binder with SF2-Cem1 ratio of 10 wt.% was 14.5% higher than that of the binder with only Cem1. This can be attributed to the dual effect of silica fume SF2 that acts as both a pozzolanic material and a filler. The additional improvement of compressive strength was not remarkable, however, when SF2 increased corresponding to SF2/Cem1 ratio from higher than 10 to 20 wt.%.

It was interesting to recognize that the SP1-water solution demands of the limestone powder (LSP) and fly ash (FA) were much lower than that of the quartz powders (QP1, QP2, QP3, QP4) and ground granulated blast furnace slag (GGBFS), although the total surface area of the LSP and of FA were very high in comparison to the QPs and GGBFS because of the higher fineness. Furthermore, a strong dispersing effect of SP1 on the FA was observed clearly whereas its influence on the dispersion of the QPs, GGBFS, LSP powder was weak. This could be attributed to the adsorption of superplasticizer on  $\text{Ca}^{2+}$  of high CaO content in the FA. Further comparison within the quartz powders showed that the finer the quartz powder was, the higher the SP1-water solution demand was, as

#### 4. Materials selection

shown in Figure 4.9, but their effect on the compressive strength of concrete could not be determined clearly based on their packing densities. Therefore, the fly ash, ground granulated blast furnace slag, all quartz powders and the limestone powder were considered in further investigations.

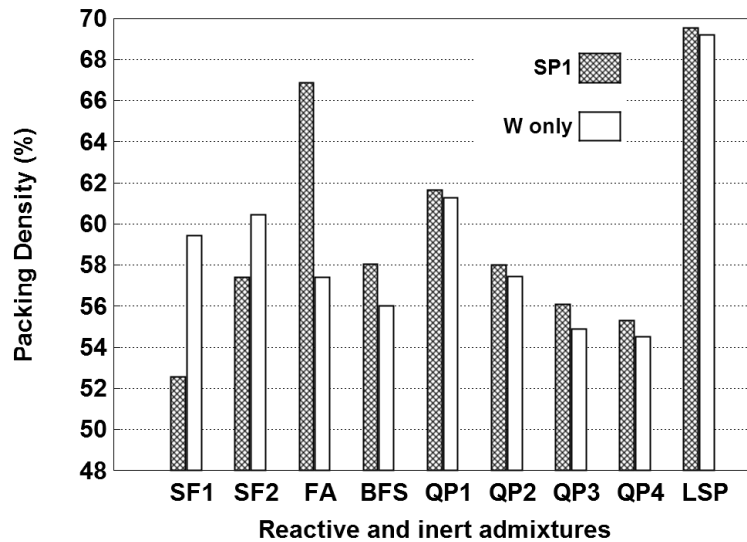


FIGURE 4.9.: The influence of superplasticizer SP1 on the packing density of the mineral admixture, measured by SP1-water solution demand test with SP1/W ratios of 0 and 10 wt.%

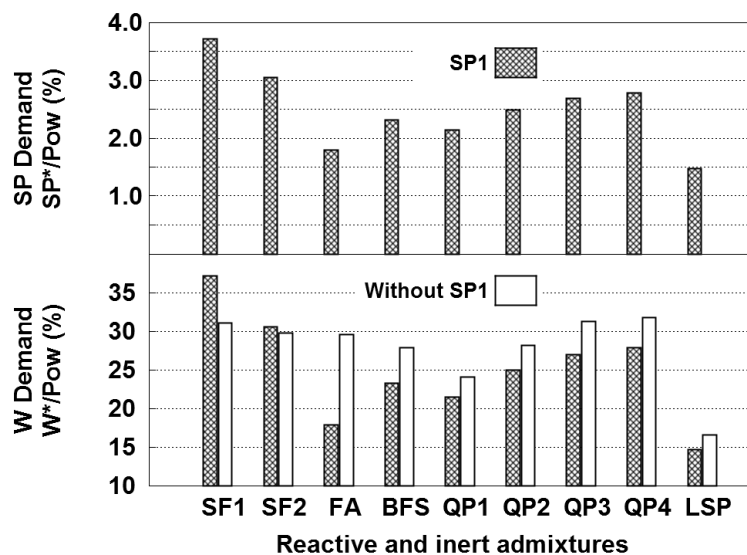


FIGURE 4.10.: SP1-water solution demands of the mineral admixtures are illustrated by water demand ( $W^*/Pow$ ) and superplasticizer demand ( $SP^*/Pow$ ) in the test using SP1-Water solutions with SP1/W ratios of 0 and 10wt.%

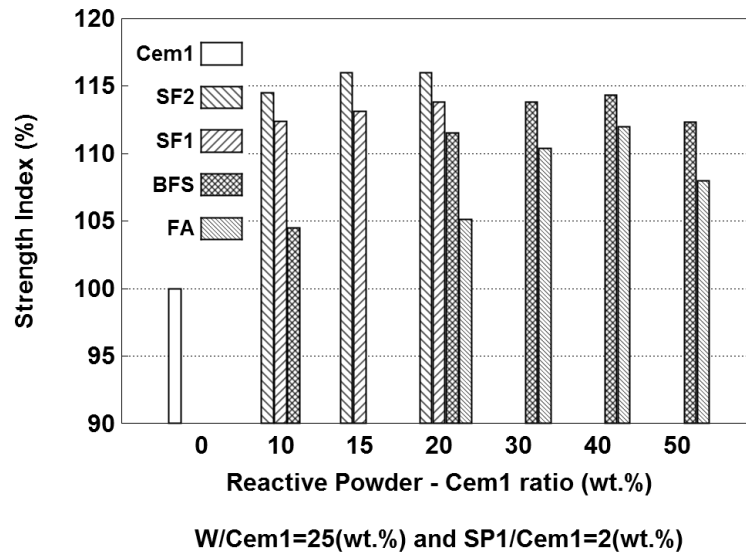


FIGURE 4.11.: The influence of types and content of reactive powders on the 28 days compressive strength of Cem1 - reactive powder binders using W/Cem1 ratio of 25 wt.% and SP1/Cem1 of 2 wt.%

## 4.5. Concluding remarks

Commercially available materials were used in this study. It was observed that superplasticizer has a great effect on the cement dispersion, subsequently cement packing density. Therefore, the method of water demand measurement by determining mixing energy, developed by Marquardt, was modified to a highly effective test method called superplasticizer-water solution demand test. The compatibilities between superplasticizers and cements as well as other kinds of fillers were recognized clearly by applying the superplasticizer-water solution demand test. The influences of superplasticizers on the compressive strength of cements were carried out. Based on the obtained results the most suitable Cem1 and the most effective superplasticizer SP1 were convincingly chosen. The activities of reactive fillers and Cem1 were examined considering the effect of SP1. The appropriate reactive fillers including ultra-fine silica fume SF2, ultra-fine fly ash FA, ground granulated blast furnace slag GGBFS were then selected for further investigation. The packing densities of the inert fillers could not give an adequate reason for the selection taking their influence on the strength of concrete into account. Therefore, all investigated inert fillers were considered in further investigations.

The negative effect of superplasticizer SP1 on silica fumes SF1 and SF2, recognized by SP1-water solution demand test for silica fumes in this research project, was also described elsewhere (Plank et al. [2009], Schöfl et al. [2012], Glotzback et al. [2014]). It implies that the stronger negative compatibility the silica fume - superplasticizer - water system have, the higher superplasticizer content the concrete needs.

The investigation into the influence of superplasticizer SP1 concentration in SP1-water solution on Cem1 packing density indicated that SP1/W ratio of 10 wt.% was an acceptable

#### *4. Materials selection*

SP1 concentration in SP1-water solution for applying of the superplasticizer-water solution demand test in further investigation.

The advantage of the superplasticizer-water solution demand test in packing density measurement for powder as well as in cement-superplasticizer compatibility assessment was convincingly demonstrated by the highest reproducibility and time efficiency.

Taking into account the relation of the water-cement ratio, the degree of hydration of cement, the gel-space ratio and the compressive strength of mortar, W/C ratio of 0.25 was chosen and kept constant for all tests that relate to the rheology behaviour and strength of pastes and concretes in further investigation because this W/C ratio is not only low enough for an expected concrete strength of 180 MPa due to the strength improvement by pozzolanic reaction, but also high enough to ensure a good workability of concrete.

## 5. Mix proportioning of UHPC

### 5.1. Experimental methods

The absolute volume method is employed to calculate the content of materials in a unit volume of mixture.

In order to examine the particle packing density of blended binder the superplasticizer-water solution demand test with SP1/W ratio of 10 wt.%, described in detail in section 4.4, was applied.

The packing density test method developed by Kwan et al. (Wong and Kwan [2008], Kwan et al. [2012]), expressed in detail in section 2.2.4.2 was employed to measure the particle packing densities of the established optimum concretes in this research project.

For assessment of the self-flowability of a small concrete batch the spread flow test, explained in section 2.2.3, was used. The slump flow test in accordance with DIN EN 12350-8 [2010] was only applied for the established optimum mixtures, the T500-time was also recorded in the test.

#### 5.1.1. Assessment of the particle packing density of concrete mixture using a rotational rheometer

As introduced and explained in section 2.2.4.1 that when the proportion of cementitious mixture, the water-cement ratio, the superplasticizer-cement ratio and the paste volume are constant, the modification of the aggregate characteristics (size and size distribution, packing density, shape, surface texture) by the combination of different aggregates will change the particle packing density of the whole concrete, leading to the change of plastic viscosity. Thus, the highest packing density of the granular concrete mixture can be recognized by showing: (i) the lowest plastic viscosity or (ii) the highest self-flowability.

Viskomat NT and Viskomat XL which are commercial available rotational rheometer of Schleibinger Gerte Teubert u. Greim GmbH (Germany) were used to measure the plastic viscosity of paste and concrete. Basically, rotational rheometers have three standard geometries: parallel plates, cone and plate, Couette (two coaxial cylinders), as illustrated in Figure 5.1 (Coussot [2005]).

## 5. Mix proportioning of UHPC

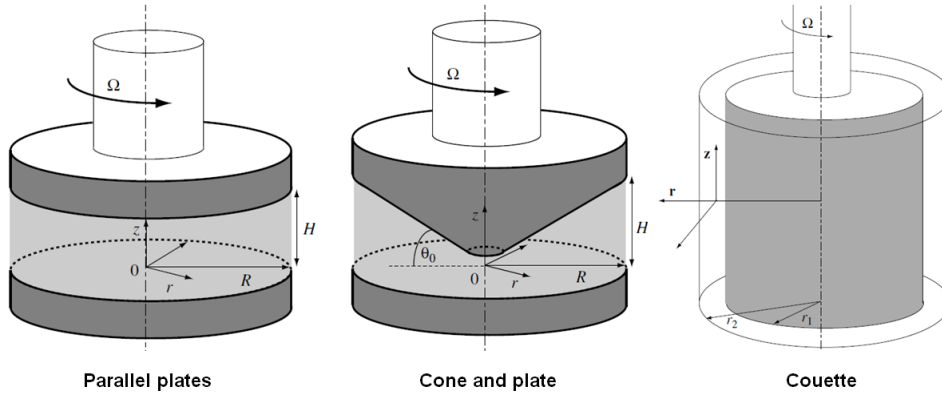


FIGURE 5.1.: Three standard geometries of rotational rheometers: parallel plates, cone and plate, Couette (Coussot [2005]).

However, Viskomat NT and Viskomat XL used in this research have a paddle fixed to a torque cell. Furthermore, Viskomat NT has rotating vessels of about 500 ml, and the rotating vessel of Viskomat XL is 3500 ml, see Figure 5.2. The material was stirred at a rotation speed  $N$ , generating shear resistance of torque  $T$ . A series of data points of  $T$  and  $N$  were recorded by a computer. Exactly, during operation, the rotational speed was imposed and controlled while the torque was measured. In the test for cementitious paste, the Viskomat NT accelerated the rotational speed from 0 to 80 rpm within 150 seconds. For the tests of concrete with aggregate smaller than 5 mm the rotational speed increases from 0 to 15 rpm within 150 seconds. The Viskomat XL was used for the tests of concrete with maximum grains of 8 mm, it accelerated the rotational speed from 0 to 10 rpm within 150 seconds. Using Bingham model the relation between the torque  $T$  (N.mm) and the rotational speed  $N$  (rpm) was described with Equation (5.1) and Figure 5.2, in which  $g$ -coefficient is relative yield stress  $g$  (N-mm) and  $h$ -coefficient is relative plastic viscosity (N-mm/rpm). Because the geometries of Viskomat NT and Viskomat XL are complex and not complied with the standard geometries, the rotation speed was not converted into a shear rate and torque was not converted into a shear stress due to the complexity of convert process using a calibration liquid. That is why the  $h$ -coefficient in Equation (5.1) (relative plastic viscosity (N-mm/rpm)) is not a plastic viscosity in Pa.s unit. Nevertheless, if test setup of Viskomat NT (or Viskomat XL) is kept constant for all mixtures, the plastic viscosities of these mixtures can be compared together by assessment of  $h$ -coefficients.

$$T = g + h.N \quad (5.1)$$

For the spread-flow test and the plastic viscosity measurement, a small Hobart mixer with a 5 liters mixing bowl and a three speed transmission (speed I/II/III equal to 136/281/580 for the agitator and 60/124/255 for the paddle) was used to prepare one liter of cementitious paste (or concrete with aggregates of smaller than 5 mm ). For the production of three liters of concrete with maximum grains of 8 mm, a larger Hobart mixer with a 12 liters mixing bowl and a three speed transmission (speed I/II/III equal to 107/198/365 for the agitator and 61/113/207 for the paddle) was used. The mixing

procedure was as follow: (i) dry cementitious mixture including cement, quartz powder and silica fume (and other powders if any) was put into the mixer and then mixed for 30 seconds at the speed I; (ii) 80 wt.% water was added firstly for 60 seconds at the speed I, the premixed remaining water with superplasticizer was then added for 30 seconds; (iii) the paste was mixed at speed II for 120 seconds; (iv) the paste was homogenized for 120 seconds at speed III; (vi) the aggregate, if any, was added to the paste and the concrete mixture was mixed at speed I for 300 seconds. All tests were only carried out five minutes after the completion of the mixing process, this waiting time was sufficient for the de-aeration of mixture.

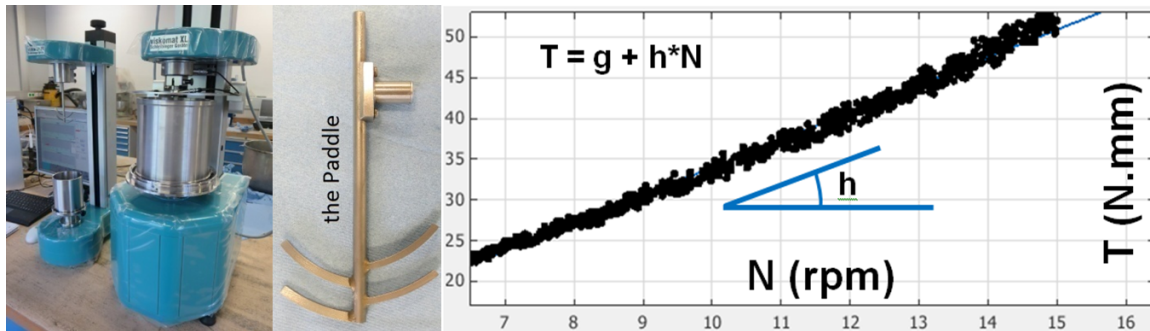


FIGURE 5.2.: Viskomat NT and Viskomat XL with paddle (two left pictures). A linear relation between the torque  $T$  (N.mm) and the rotational speed  $N$  (rpm) is expressed by Bingham model (right).

### 5.1.2. Specimen preparation and compression test

For each concrete mixture six cube specimens of  $100 \times 100 \times 100 \text{ mm}^3$  were produced to determine the 28 days compressive strength ( $28d-f_c$ ). For each established optimum concrete mixture, an additional eighteen cubes 100 mm and three cylinders with 100 mm diameter and 200 mm height were tested for the 28 days compressive strength (6 cubes) and modulus of elasticity (3 cylinders), and for the compressive strength of concrete at 90 days (6 cubes) and 180 days (6 cubes).

The homogeneous UHPFRCs were produced by using Eirich intensive mixers. The mixers have a driven, rotating mixing pan, a mixing tool which rotates eccentrically and a fixed wall scraper cleans the wall of the mixing pan. The mixing procedure was as follows: (i) dry cementitious mixture including cement, quartz powder, silica fume (and other powders if any) were added to the mixer, then mixed for 30 seconds at the speed of 150 rpm of mixing tool and lowest speed of mixing pan; (ii) 80 wt.% water was added firstly for 60 seconds at the mixing tool speed of 150 rpm, the premixed remaining water with superplasticizer was then added for 30 seconds; (iii) the paste was homogenized for 240 seconds at the mixing tool speed of 450 rpm; (iv) the aggregate was added to the paste at the mixing tool speed of 150 rpm for 240 seconds; (vi) the speed of the mixing tool was decreased down to 84 rpm, the UHPCs without fibres were mixed for a further 60 seconds; in case of fibres addition, the further mixing time at this stage was 180 seconds. It is noted that the speed of the mixing pan was constant during mixing.

## 5. Mix proportioning of UHPC

All specimens were cast without compaction. After casting, the specimens were covered with plastic sheets and stored at room temperature for 24 hours. The specimens were then de-moulded and cured in water at 20°C for 6 days. Subsequently they were stored at ambient laboratory conditions until testing. The compression test was carried out according to DIN EN 12390-3 [2009]. Before compression test, both loading faces of all specimens were ground by a grinding machine, this ensured a uniform load being applied on the brittle specimen to obtain a high test results consistency. The loading rate for compression test was 0.6 MPa/s. The mean values were reported.

### 5.2. The rule of granular materials combination

As introduced in Chapter 2, the earlier studies by Furnas [1929, 1931] highlighted that the void space between larger grains can be filled by smaller grains leading to improvement of the packing density of the granular concrete mixture. In this research project, with supporting of some efficient test methods for packing density measurement, this simple idea was employed for the combination of granular materials of concrete considering improvement of particle packing density.

The rule of granular materials combination is expressed as follows:

- At the beginning of concrete mix design, a collection of  $n$  different polydisperse grain groups are available. The group  $(i+1)$  is finer than the group  $(i)$ . Furthermore, it is assumed that the maximum grain size of the expected mixture is the same as the maximum grain size of the group  $(i)$ .
- **Stage 1:** group  $(i)$  is replaced progressively by the next finer group, group  $(i+1)$ . The packing density of the formed mixture in each step is measured. If the compatibility of the groups  $(i)$  and  $(i+1)$  is sufficient, the smaller particles will fill up the void between larger particles and this leads to an increase in packing density of the new grain groups. At showing of highest packing density, the optimum combination of group  $(i)$  and group  $(i+1)$  is established, corresponding to the optimum proportion of the group  $(i+1)$  to the group  $(i)$ . If not, this means the combination of the group  $(i)$  and group  $(i+1)$  is meaningless, the groups  $(i)$  and  $(i+2)$  will be combined and so on. As a result, the optimum proportion of the group  $(i+k)$  to the group  $(i)$  is determined commensurate with the new group  $(i+k)$ . Then Stage 2 can start.
- **Stage 2:** group  $(i+k)$  is gradually replaced by the next finer group, group  $(i+k+1)$ , and the process like in Stage 1 is repeated.
- The combination process is completed when the group with the smallest grain size, group  $(n)$ , is used.
- The wettability and adhesion of powders and aggregates are considerably different. That is why this rule is applied at first for the powders system to establish the optimum cementitious paste. The rule is then used for the aggregates system to determine the optimum blended aggregate corresponding to the optimum of the whole UHPC with a fixed volume of the optimum paste

### 5.3. Mixture-proportioning of cementitious paste

In the previous chapters, it is clear that the cementitious powder of UHPFRC should include at least 2 components of cement and ultra-fine reactive powder, in which the ultra-fine reactive powder also play a role of filler. If the cost of ultra-fine reactive powder is insignificant, a binder of two components should be developed regarding the simple procedures for materials preservation and control. If the cost of ultra-fine reactive powder is high, an effective inert filler can be used to replace the ultra-fine reactive powder for reducing materials cost. Therefore, a binder including three components of cement, inert filler, ultra-fine reactive powder can be developed for UHPFRC. If reactive powder is coarse, leading to a low filler effect, an ultra-fine inert filler should be used to improve packing density of the three components system. Two reactive powders should not be used simultaneously in the same system because there is not any additional benefit due to the limitation of chemical reaction. In this context, based on the materials characteristics and the rule of granular materials combination, three kinds of blended binders were developed as follows:

- Binder of cement, quartz powder and silica fume.
- Binder of cement and ultra-fine fly ash.
- Binder of cement, GGBFS and ultra-fine limestone powder.

#### 5.3.1. The optimum pastes of cement - quartz powder - silica fume binders

##### 5.3.1.1. Experimental determination of the optimum binary mixtures including Cem1 and quartz powders based on packing density assessment

Experimental investigations into the packing densities of binary mixtures consisting of Cem1 and the four quartz powders were carried out. Each quartz powder and Cem1 were combined. The packing densities of  $QP_i$ -Cem1 blends were measured by applying the method of SP1-Water solution demand test with SP1/W of 10 wt.%. Figure 5.3 shows the packing densities of  $QP_i$ -Cem1 blends when Cem1 was replaced gradually by  $QP_i$ . The highest packing densities of QP1-Cem1 blends, QP2-Cem1 blends and QP3-Cem1 blends were 67.4%, 66.7% and 66.7% respectively, corresponding to QP1/Cem1 of 40 wt.%, QP2/Cem1 of 35 wt.% and QP3/Cem1 of 30 wt.%. Surprisingly, there was no improvement of the packing density in the combination of QP4 and Cem1, although QP4 is much finer than Cem1, concluding their compatibility was poor. Thus, QP4 was not used for further investigation. The detail test data are shown in Table B.1 in Appendix B.

##### 5.3.1.2. Determination of the optimum ternary mixtures of the optimum $QP_i$ -Cem1 blends and silica fume SF2

Each optimum blend of  $QP_i$  and Cem1 ( $i=1,2,3$ ) was combined with silica fume SF2 by the stepwise replacement of  $QP_i$  - Cem1 blend by SF2. The method of SP1-Water solution demand test with SP1/W of 10 wt.% was also employed for packing density measurement. The test results, described by the solid curves in Figures 5.4, 5.5 and 5.6,

## 5. Mix proportioning of UHPC

show that the packing density of the cementitious mixtures increased significantly as SF2 content increased up to 22.5 (wt.%) of the optimum QP<sub>i</sub>-Cem1 blends. The detail test data are shown in Table B.2 in Appendix B.

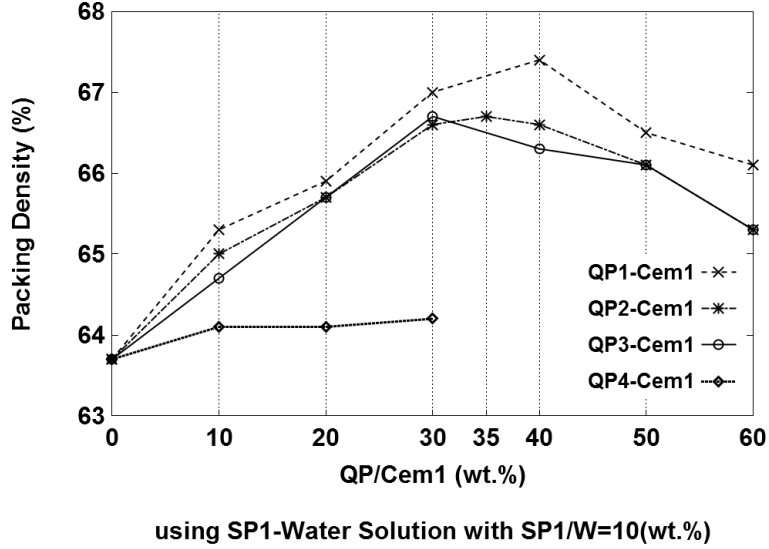


FIGURE 5.3.: The variation in the packing density of QP<sub>i</sub>-Cem1 blends when Cem1 was replaced progressively by QP<sub>i</sub> (i=1,2,3,4). The optimum QP<sub>i</sub>/Cem1 ratios was determined by showing the highest packing density.

The flowability of cementitious pastes at each combination step was determined, in which W/Cem1 of 25 wt.% and SP1/Cem1 of 2 wt.% were kept constant. It was observed that the higher SF2 content the pastes had, the lower flowability the pastes showed. This can be explained by the fact that the increasing of SF2 content in the cementitious paste reduced the thickness of water film, which surrounds the cementitious particles and governs the consistence of the cementitious paste due to the increasing of the number and the total surface area of the particles. This was represented by the reducing of the volume ratio of water to powder, as computed and shown by the dashed curves in Figures 5.4, 5.5 and 5.6. The detail computed data are shown in Table B.3 in Appendix B.

Let us make a theoretical calculation about the efficient water that lubricate the particles. It is assumed that the water in the void between particles ( $V_{\text{void-water}}$ ) does not contribute to the fluidity of the paste, this water can be described by Equation 5.2.

$$\frac{V_{\text{void-water}}}{V_{\text{solid}}} = \frac{1 - \beta_{\text{mix-actual}}}{\beta_{\text{mix-actual}}} \quad (5.2)$$

where:  $V_{\text{solid}}$  is the total solid volume of mixture,  $\beta_{\text{mix-actual}}$  is the actual packing density of mixture. Then, the efficient water for paste flowing ( $V_{\text{efficient-water}}$ ) can be expressed by Equation 5.3.

$$\frac{V_{\text{efficient-water}}}{V_{\text{solid}}} = \frac{V_{\text{mixing-water}}}{V_{\text{solid}}} - \frac{V_{\text{void-water}}}{V_{\text{solid}}} \quad (5.3)$$

### 5.3. Mixture-proportioning of cementitious paste

This efficient water spreads out all particles surface, corresponding to the thickness of the efficient water film ( $t_{\text{efficient-water}}$ ) as Equation 5.4.

$$\begin{aligned}
 t_{\text{efficient-water}} &= \frac{\left(\frac{V_{\text{mixing-water}}}{V_{\text{solid}}} - \frac{V_{\text{void-water}}}{V_{\text{solid}}}\right)V_{\text{solid}}}{S_{\text{particles}}} \\
 &= \frac{\left(\frac{V_{\text{mixing-water}}}{V_{\text{Cem1}} + V_{\text{QP}} + V_{\text{SF2}}} - \frac{V_{\text{void-water}}}{V_{\text{solid}}}\right)V_{\text{solid}}}{S_{\text{particles(Cem1)}} + S_{\text{particles(QP)}} + S_{\text{particles(SF2)}}} \\
 &= \frac{\left(\frac{\frac{W}{\text{Cem1}} \frac{1}{\rho_W}}{\frac{1}{\rho_{\text{Cem1}}} + \frac{\text{QP/Cem1}}{\rho_{\text{QP}}} + \frac{\text{SF2/Cem1}}{\rho_{\text{SF2}}}} - \frac{V_{\text{void-water}}}{V_{\text{solid}}}\right)V_{\text{solid}}}{S_{\text{particles(Cem1)}} + S_{\text{particles(QP)}} + S_{\text{particles(SF2)}}} \\
 &= \frac{\left(\frac{\frac{W}{\text{Cem1}} \frac{1}{\rho_W}}{\frac{1}{\rho_{\text{Cem1}}} + \frac{\text{QP/Cem1}}{\rho_{\text{QP}}} + \frac{\text{SF2/Cem1}}{\rho_{\text{SF2}}}} - \frac{V_{\text{void-water}}}{V_{\text{solid}}}\right)V_{\text{solid}}}{V_{\text{Cem1}} \sum_{i=1}^{N1-1} \frac{6 * \text{Retained}_{i,i+1}}{\sqrt{d_i d_{i+1}}} + V_{\text{QP}} \sum_{j=1}^{N2-1} \frac{6 * \text{Retained}_{j,j+1}}{\sqrt{d_j d_{j+1}}} + V_{\text{SF2}} \sum_{k=1}^{N3-1} \frac{6 * \text{Retained}_{k,k+1}}{\sqrt{d_k d_{k+1}}}} \\
 &= \frac{\left(\frac{\frac{W}{\text{Cem1}} \frac{1}{\rho_W}}{\frac{1}{\rho_{\text{Cem1}}} + \frac{\text{QP/Cem1}}{\rho_{\text{QP}}} + \frac{\text{SF2/Cem1}}{\rho_{\text{SF2}}}} - \frac{1 - \beta_{\text{mix-actual}}}{\beta_{\text{mix-actual}}}\right)}{\frac{V_{\text{Cem1}}}{V_{\text{solid}}} \sum_{i=1}^{N1-1} \frac{6 * \text{Retained}_{i,i+1}}{\sqrt{d_i d_{i+1}}} + \frac{V_{\text{QP}}}{V_{\text{solid}}} \sum_{j=1}^{N2-1} \frac{6 * \text{Retained}_{j,j+1}}{\sqrt{d_j d_{j+1}}} + \frac{V_{\text{SF2}}}{V_{\text{solid}}} \sum_{k=1}^{N3-1} \frac{6 * \text{Retained}_{k,k+1}}{\sqrt{d_k d_{k+1}}}} \quad (5.4)
 \end{aligned}$$

where:  $W/\text{Cem1}$ ,  $\text{QP}/\text{Cem1}$ ,  $\text{SF2}/\text{Cem1}$  are weight ratios of Water, QP, SF2 to Cem1 respectively;  $\rho_{\text{materials}}$  are the densities of the materials;  $V_{\text{Cem1}}/V_{\text{solid}}$ ,  $V_{\text{QP}}/V_{\text{solid}}$ ,  $V_{\text{SF2}}/V_{\text{solid}}$  are volume fraction of Cem1, QP and SF2 in mixture respectively;  $S_{\text{particles}}$  is the total surface area of particles in mixture;  $N1$ ,  $N2$ ,  $N3$  are the number of sieves in particle size distribution analysis for Cem1, QP, SF2 respectively; the value of  $\text{Retained}_{i,i+1}$  of Cem1 is the volume fraction of particles passed sieve  $d_i$  and retained in sieve  $d_{i+1}$  in measurement of Cem1 size distribution, these particles have a mean diameter of  $\sqrt{d_i d_{i+1}}$ ; they are noted similarly for  $\text{Retained}_{j,j+1}$ ,  $\sqrt{d_j d_{j+1}}$  of QP and  $\text{Retained}_{k,k+1}$ ,  $\sqrt{d_k d_{k+1}}$  of SF2.

## 5. Mix proportioning of UHPC

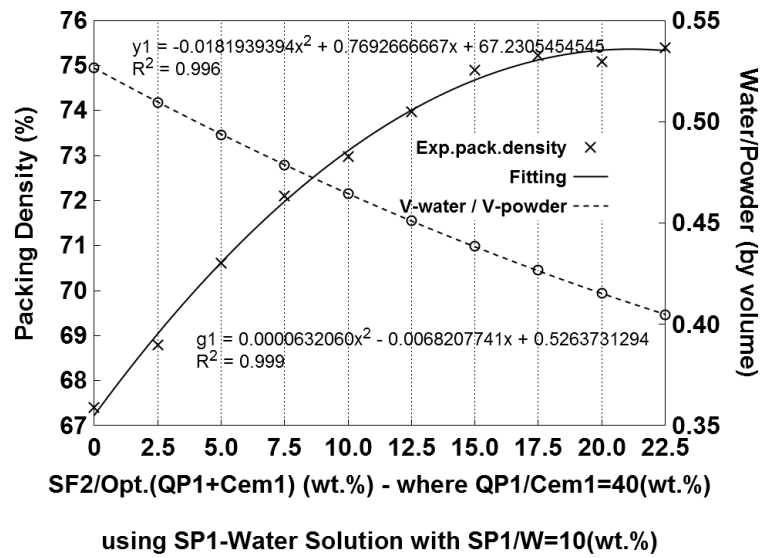


FIGURE 5.4.: The solid curve shows the increase of the packing densities of QP1-Cem1-SF2 mixtures, in which QP1/Cem1 = 40 wt.%, when SF2 increased steadily by SF2/(QP1+Cem1) ratios from 0 to 22.5 wt.% (corresponding SF2/Cem1 ratios from 0 to 31.5 wt.%); whereas the dashed curve represents the decrease of Water/Solid volume ratios in the pastes having W/C ratio of 25 wt.%.

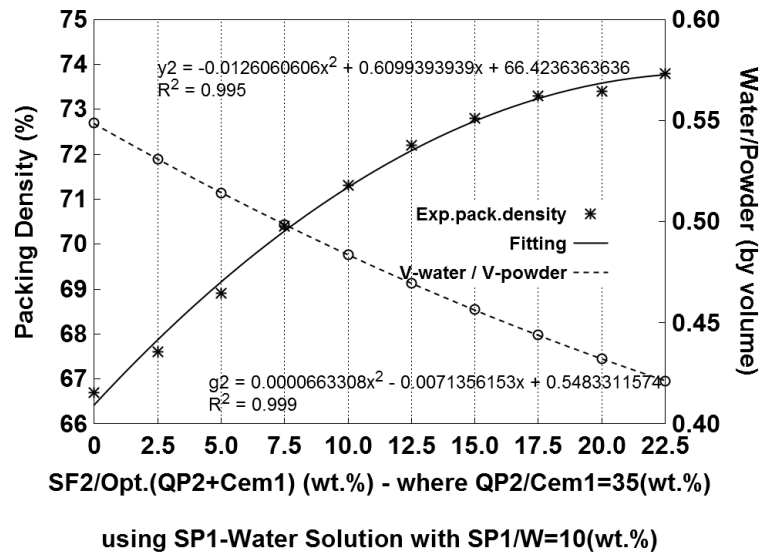


FIGURE 5.5.: The solid curve shows the increase of the packing densities of QP2-Cem1-SF2 mixtures, in which QP2/Cem1 = 35 wt.%, when SF2 increased steadily by SF2/(QP2+Cem1) ratios from 0 to 22.5 wt.% (corresponding SF2/Cem1 ratios from 0 to 30.375 wt.%); whereas the dashed curve represents the decrease of Water/Solid volume ratios in the pastes having W/C ratio of 25 wt.%.

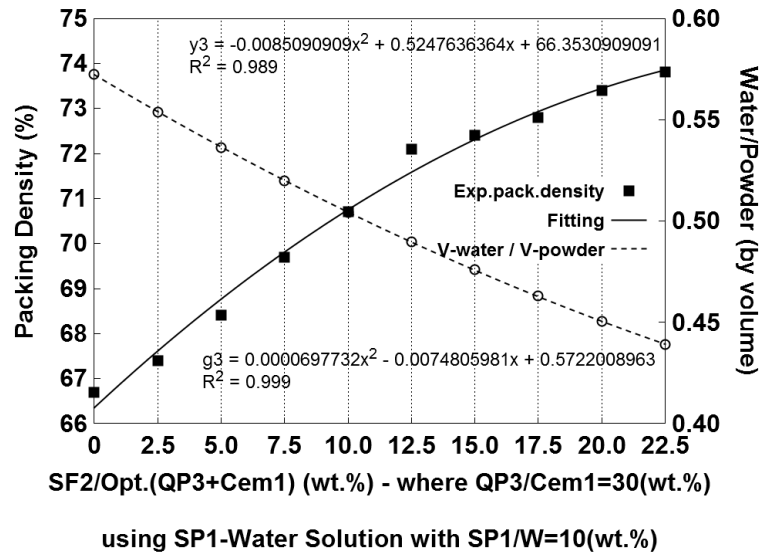


FIGURE 5.6.: The solid curve shows the increase of the packing densities of QP3-Cem1-SF2 mixtures, in which QP3/Cem1 = 30 wt.%, when SF2 increased steadily by SF2/(QP3+Cem1) ratios from 0 to 22.5 wt.% (corresponding SF2/Cem1 ratios from 0 to 29.25 wt.%); whereas the dashed curve represents the decrease of Water/Solid volume ratios in the pastes having W/C ratio of 25 wt.%.

Figures 5.7, 5.8, 5.9 illustrate the variations of the efficient water and of the efficient water film thickness in QP-Cem1-SF2 system when SF2 content increases. The detail computed data are shown in Tables B.4, B.5, B.6 in Appendix B. The variation of the efficient water is in good agreement with the packing theory which assumes that adding fine particles to a particle structure helps filling up the voids in the particle structure, leading to minimum space for water as well as maximum efficient water for particles lubrication. However, the decrease of the efficient water film thickness in conformity with the water layer theory which claims that adding small particles increases surface area, reduce the water film thickness and consequently the flowability. The observed results in Figures 5.7, 5.8, 5.9 indicate that the thickness of the efficient water film are depended pronouncedly on the size distribution and the content of constituents which influence directly total surface area of particles. In the cases of QP1-Cem1-SF2 and QP2-Cem1-SF2 mixtures, in which QP1 and QP2 are coarser than QP3, the increase of packing density of mixtures by SF2 content increasing lead to increase of efficient water film thickness firstly. Then, total surface area of particles in mixtures enlarge quickly and result to lowering of the efficient water film thickness while the volume of efficient water is still increased due to the improvement of packing density. However, the thickness of the efficient water film of QP3-Cem1-SF2 mixtures reduce continuously regardless of the increase of the volume of efficient water.

In order to solve this problem, the method of multi-objective optimization was applied to determine the SF2 content in QPi-Cem1-SF2 cementitious mixtures in such a manner that blended binders achieve a high packing density and a high volume ratio of W/Powder. For this purpose, the NIMBUS program which has been developed at the University of

## 5. Mix proportioning of UHPC

Jyväskylä Finland, Department of Mathematical Information Technology by Miettinen and Mäkelä [2000, 2006] was used. For QP1-Cem1-SF2 blends Functions 5.5 and 5.6 was requested to achieve the highest values simultaneously when SF2/(QP1+Cem1) ratios vary in range of 0-22.5 wt.%. The similar requirements were applied for QP2-Cem1-SF2 blends with Functions 5.7 and 5.8 and QP3-Cem1-SF2 blends with Functions 5.9 and 5.10.

$$y_1 = -0.0001819394X_1^2 + 0.0076926667X_1 + 0.6723054545 \quad (5.5)$$

$$g_1 = 0.0000632060X_1^2 - 0.0068207741X_1 + 0.5263731294 \quad (5.6)$$

$$y_2 = -0.0001260606X_2^2 + 0.0060993939X_2 + 0.6642363636 \quad (5.7)$$

$$g_2 = 0.0000663308X_2^2 - 0.0071356153X_2 + 0.54833115740 \quad (5.8)$$

$$y_3 = -0.0000850909X_3^2 + 0.0052476364X_3 + 0.6635309090 \quad (5.9)$$

$$g_3 = 0.0000697732X_3^2 - 0.0074805981X_3 + 0.5722008963 \quad (5.10)$$

where:  $X_1 = \text{SF2}/(\text{QP1}+\text{Cem1})$ ,  $X_2 = \text{SF2}/(\text{QP2}+\text{Cem1})$ ,  $X_3 = \text{SF2}/(\text{QP3}+\text{Cem1})$  wt.%,  $0 \leq X_1, X_2, X_3 \leq 22.5$  wt.% and  $\text{QP1}/\text{Cem1} = 40$ ,  $\text{QP2}/\text{Cem1} = 35$ ,  $\text{QP3}/\text{Cem1} = 30$  wt.%.

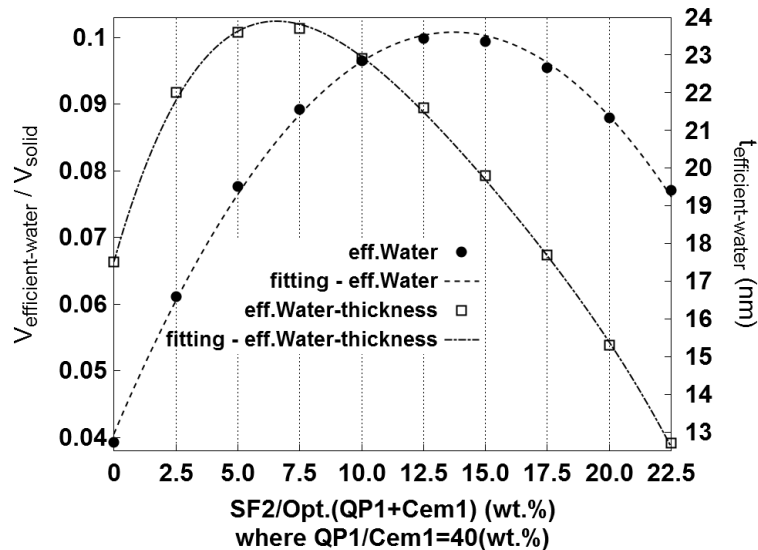


FIGURE 5.7.: The variations of the efficient water and its thickness corresponding with the improvement of packing densities of QP1-Cem1-SF2 mixtures when QP1/Cem1 ratio is 40 wt.%, W/C ratio is 25 wt.% and SF2 content increased steadily by SF2/(QP1+Cem1) ratios of 0-22.5 wt.%.

### 5.3. Mixture-proportioning of cementitious paste

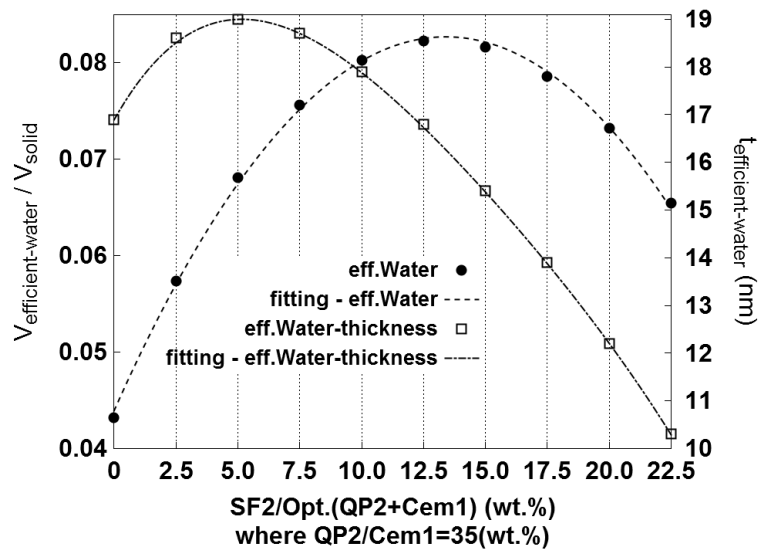


FIGURE 5.8.: The variations of the efficient water and its thickness corresponding with the improvement of packing densities of QP2-Cem1-SF2 mixtures when QP2/Cem1 ratio is 35 wt.%, W/C ratio is 25 wt.% and SF2 content increased steadily by SF2/(QP2+Cem1) ratios of 0-22.5 wt.%.

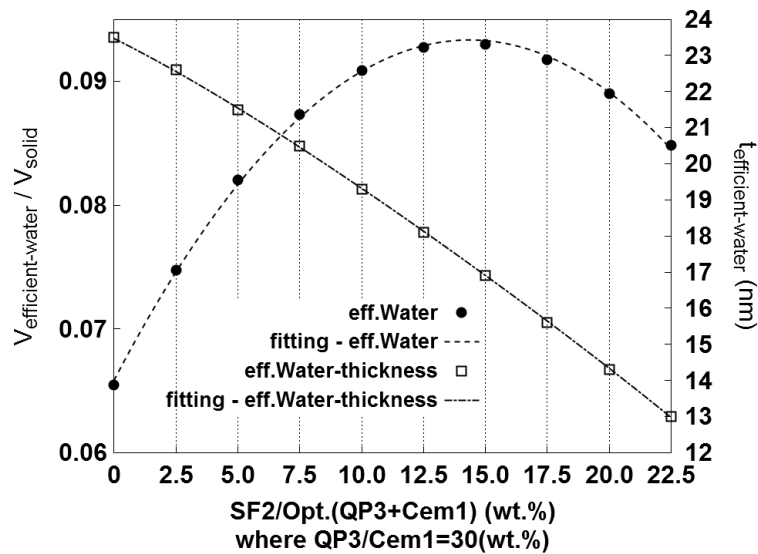


FIGURE 5.9.: The variations of the efficient water and its thickness corresponding with the improvement of packing densities of QP3-Cem1-SF2 mixtures when QP3/Cem1 ratio is 30 wt.%, W/C ratio is 25 wt.% and SF2 content increased steadily by SF2/(QP3+Cem1) ratios of 0-22.5 wt.%.

As a results, three optimum binders were determined as the followings:

- **Binder 1:** SF2/(QP1+Cem1) = 7.84735 wt.%, where QP1/Cem1 = 40 wt.%  $\Rightarrow$  QP1/Cem1/SF2 = 40/100/11 wt.%, packing density is 72.1%.

## 5. Mix proportioning of UHPC

- **Binder 2:**  $SF2/(QP2+Cem1) = 8.50566$  wt.%, where  $QP2/Cem1 = 35$  wt.%  $\Rightarrow$   $QP2/Cem1/SF2 = 35/100/11.5$  wt.%, packing density is 70.7%.
- **Binder 3:**  $SF2/(QP3+Cem1) = 9.20616$  wt.%, where  $QP3/Cem1 = 30$  wt.%  $\Rightarrow$   $QP3/Cem1/SF2 = 30/100/12$  wt.%), packing density is 70.5%.

The SF2 content of each optimum blended binder is sufficient regarding strength development due to pozzolanic reaction because the strength of Cem1-SF2 binders with SF2/Cem1 ratio from higher 10 wt.% to 20 wt.% was not considerably higher than that of Cem1-SF2 binder having SF2/Cem1 ratio of 10 wt.% as shown in Figure 4.11.

### 5.3.1.3. Determination of the saturated SP1 content for the pastes and concretes containing the optimum Binders 1, 2, 3

In order to determine the saturated content of SP1 for Pastes 1, 2, 3 corresponding to the optimum Binders 1, 2, 3 and constant W/Cem1 ratio of 25 wt.%, the influences of SP1 content on the rheological behaviour of Pastes 1, 2, 3 were investigated. Viskomat NT was used to measure plastic viscosity of paste.

The results in Figure 5.10 indicate that the plastic viscosities of Pastes 1, 2, 3 decreased with the increasing of SP1 dosage, and they then gradually increased as SP1 dosage exceeded the saturated concentration of adsorbed polymer, which corresponded with the lowest points of the three curves at the SP1/Cem1 ratios of 3.30, 2.88, 2.75 wt.% respectively. The detail test data are shown in Table B.7 in Appendix B. This phenomenon is observed in suspension with low Water/Powder ratio as reported in the studies by Ushiro et al. [2013], and Sakai et al. [2003].

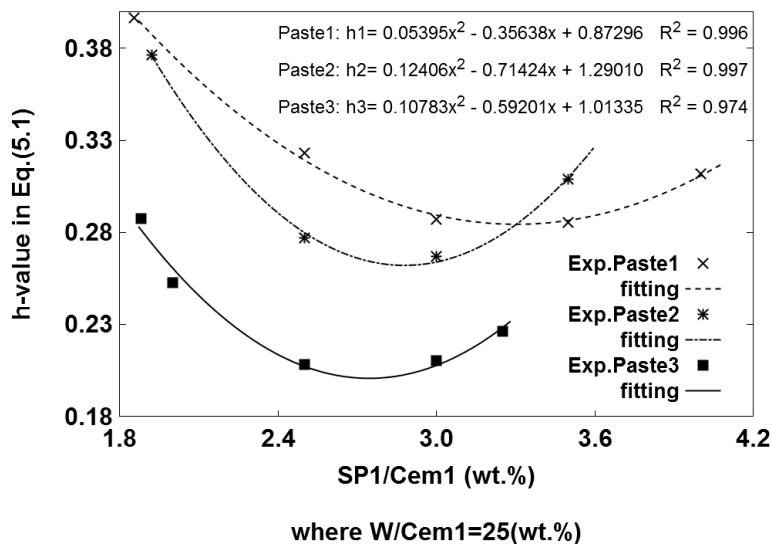


FIGURE 5.10.: Influence of SP1 on the plastic viscosity of the cementitious pastes having constant W/Cem1 of 25 wt.%. The optimum Binders 1, 2, 3 are the cementitious powders of Pastes1, 2, 3 respectively.

### 5.3. Mixture-proportioning of cementitious paste

The segregation was not observed in the experiments. The reason for the phenomena may be attributed to the increase of polymer concentration in the liquid phase of the pastes. In these tests, W/Cem1 weight ratio is constant, the change of solid volume is negligible when SP1/Cem1 increase, but the polymer concentration in liquid phase increase quickly leading to the saturation of the adsorbed SP1 on the surface of particles and SP1 present in pore solution. The SP1 exceeding the saturation amount is unnecessary and result to a thick polymer layer in pore solution. It implies that an amount of efficient water contributing to fluidity of paste is replaced by unnecessary SP1. Thus, the plastic viscosity of paste increase.

It should be noted that superplasticizer does not disperse aggregate for improving the fluidity of concrete. Therefore, the superplasticizer in the liquid film around aggregate particles is an useless consumption. It means SP1 content will be not sufficient to achieve the highest dispersing of Pastes 1, 2, 3 for maximum fluidity of concretes if the saturated SP1 contents as the above estimation are used. For that reason the investigation into the influence of SP1 content on the flowability of concretes with Pastes 1, 2, 3 was carried out. Quartz sand QS2 (0.3-0.8mm) was used as a standard sand for the experiments. Based on the estimated saturated SP1 contents of 3.30, 2.88, 2.75 wt.% Cem1 for Pastes 1, 2, 3, it was predicted that the saturated SP1 contents for concretes of Paste1-QS2, Paste2-QS2, Paste3-QS2 could be 3.5, 3 and 3 wt.% Cem1 respectively. In order to insure the self-compacting properties of concrete with the predicted saturated SP1 contents and constant W/Cem1 ratio of 25 wt.%, preliminary tests with different cement contents were conducted to select a sufficient amount of cement with that self-compacting concrete has a spread flow of about 24 cm. As a result, Cem1 amount of 720 kg was decided.

Figure 5.11 shows the self-flowability at different SP1 contents of concretes including optimum Binders 1, 2, 3 and QS2 using a constant W/Cem1 ratio of 25 wt.%. The detail test data are shown in Table B.10 in Appendix B. The results indicate that within each kind of Binder the tendencies of the influences of SP1 content on the viscosity of Paste and on the flow of concrete are similar. The experimental results about the saturated amounts of SP1 for pastes and for concretes allow to fix the SP1/Cem1 ratios of 3.5, 3, 3 wt.% as saturated SP1 content for the concretes having W/Cem1 ratio of 25 wt.% and cementitious component of Binders 1, 2, 3 respectively.

In summary, for further investigation the optimum proportion of pastes including QP, Cem1, SF2, SP1, W were determined as follows:

- **Paste 1:** QP1/Cem1/SF2/SP1/W = 40/100/11/3.5/25 wt.%.
- **Paste 2:** QP2/Cem1/SF2/SP1/W = 35/100/11.5/3/25 wt.%.
- **Paste 3:** QP3/Cem1/SF2/SP1/W = 30/100/12/3/25 wt.%.

Besides, Cem1 amount of 720 kg/m<sup>3</sup> was the criterion by which the self-flowing properties of concrete with a maximum grain size of 1 mm was guaranteed. The cement amount could be adjusted based on the critical amount of 720 kg/m<sup>3</sup> depending on the requirement of the flow properties and the maximum grain size of aggregate.

## 5. Mix proportioning of UHPC

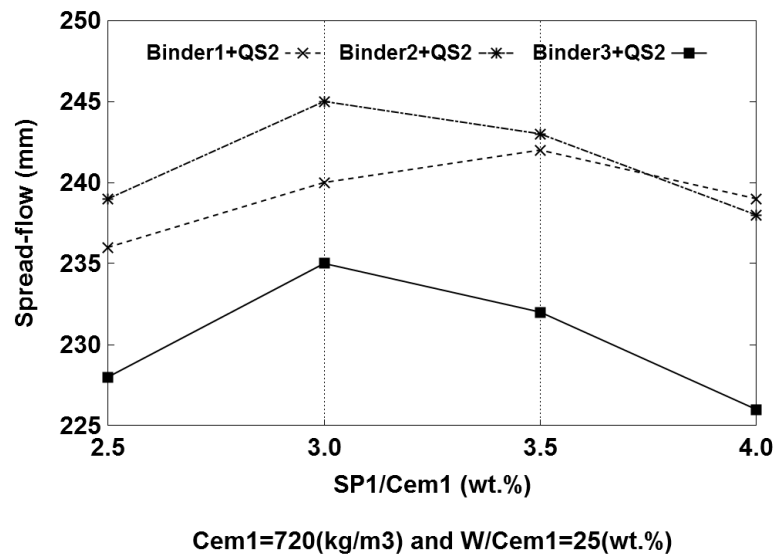


FIGURE 5.11.: Influence of SP1 on the self-flowability of concretes including optimum Binder<sub>i</sub>, QS2 and W/Cem1 ratio of 25 wt.%.

### 5.3.2. The optimum paste of binder containing cement and ultra-fine fly ash

#### 5.3.2.1. Determination of the optimum binary mixture of Cem1 and ultra-fine fly ash

The packing densities of Cem1-FA blends were examined using the superplasticizer-water solution demand test method with SP1/W ratio of 10 wt.%. The optimum proportion of Cem1-FA blends corresponded to the highest packing density of 67.3% as FA/Cem1 ratio was 40 wt.%. The experimental results are shown in Figure 5.12 and Table B.1 of Appendix B.

Due to the low cost of FA in comparison to silica fume, it is possible to use ultra-fine FA up to 40 wt.% of Cem1 as an effective reactive filler in Cem1-FA binder without any more filler materials. In addition, the experimental results in Figure 4.11 indicated that the strength of Cem1-FA binder increase considerably due to filler and pozzolanic effects of FA when FA increases up to 40wt.% of Cem1, over this FA content the strength decreases. Consequently, the optimum Cem1-FA binder was determined as Binder 4 with FA/Cem1 ratio of 40 wt.%.

#### 5.3.2.2. Experimental determination of the saturated SP1 content for the paste of Binder 4

The experience from the experiment in 5.3.1.3 exhibits that the saturated SP1 content for concrete having W/Cem1 ratio of 25 wt.% and Binder 4 can be established quickly by investigation into the influence of SP1 content on the flowability of concretes. The tests were done using Cem1 content of 720 kg and aggregate QS2. SP1 content of 3 wt.% of

### 5.3. Mixture-proportioning of cementitious paste

Cem1 was optimum for highest self-flowability as shown in Figure 5.13. The detail test data are shown in Table B.10 in Appendix B.

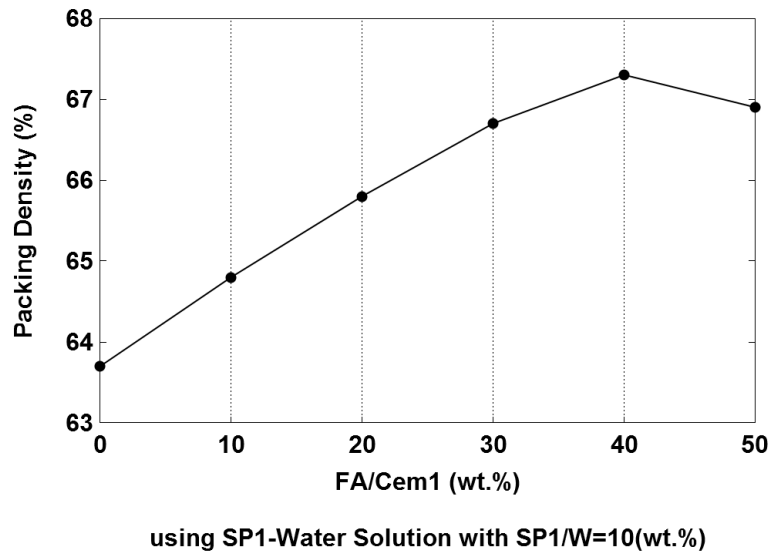


FIGURE 5.12.: Packing densities of Cem1-FA blends when FA replaced Cem1 step by step. The FA/Cem1 ratio of 40 wt.% was the optimum proportion of Cem1-FA blend regarding highest packing density.

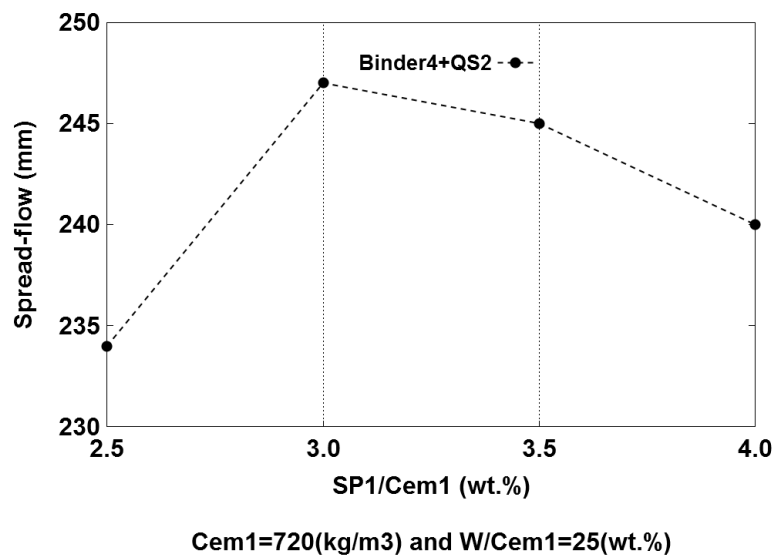


FIGURE 5.13.: Influence of SP1 on the self-flowability of concretes including optimum Binder4, QS2 and W/Cem1 ratio of 25 wt.%.

For further investigation the optimum proportion of Paste 4 including ultra-fine FA, Cem1, SP1 and W was determined by FA/Cem1/SP1/W ratios of 40/100/3/25 wt.%

## 5. Mix proportioning of UHPC

### 5.3.3. The optimum paste of binder containing cement - ground granulated blast furnace slag - limestone powder

#### 5.3.3.1. Determination of the optimum binary mixture of Cem1 and GGBFS

GGBFS replaced Cem1 gradually. SP1-water solution demand test using SP1/W ratio of 10 wt.% was employed to measure packing density of GGBFS-Cem1 blends. The packing densities of the mixtures increased slightly and decreased when GGBFS/Cem1 ratio was higher than 30 wt.% as depicted in Figure 5.14. The detail test data are shown in Table B.1 in Appendix B. With regard to packing density improvement, the GGBFS - Cem1 blend having GGBFS content of 30 wt.% of Cem1 was the optimum. However, its packing density is low. An effective inert filler was needed to improve packing density of the whole binder. Ultra-fine limestone powder could be a good solution.

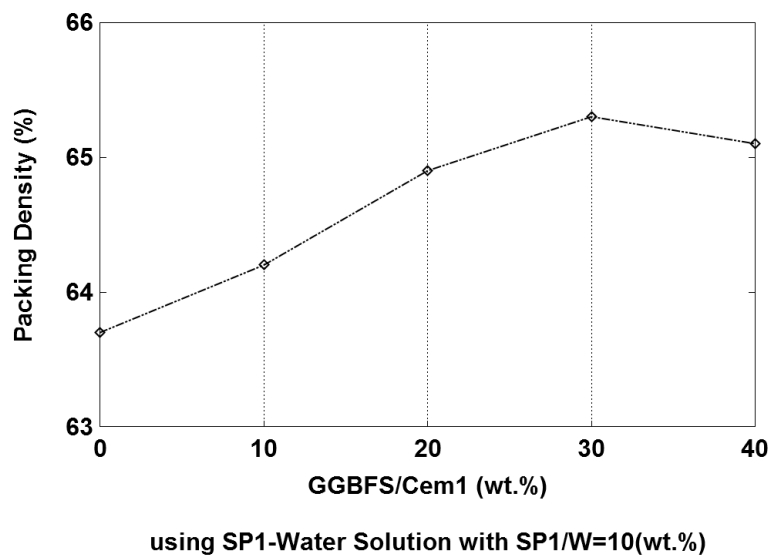


FIGURE 5.14.: Variations of the packing density of GGBFS-Cem1 blends by increasing of GGBFS content. The optimum GGBFS-Cem1 blend with highest packing density corresponded to GGBFS/Cem1 ratio of 30 wt.%.

#### 5.3.3.2. Determination of the optimum ternary mixture of the optimum GGBFS-Cem1 blend and limestone powder

Based on the rule of granular materials combination the ultra-fine limestone powder (LSP) was combined with the optimum GGBFS-Cem1 blend. The packing densities of GGBFS-Cem1-LSP mixtures were examined by SP1-water solution demand test with SP1/W ratio of 10 wt.%. The experiments showed a significant improvement in packing density of GGBFS-Cem1-LSP mixtures when LSP content increased, see the solid curve in Figure 5.15. The detail test and computed data are shown in Tables B.8, B.9 in Appendix B.

Due to the low strength of limestone particle in comparison with silica particle, limestone powder content should be limited (Fehling and Schmidt et al. [2013]). Furthermore,

as described and explained in section 5.3.1.2, with a constant W/Cem1 ratio of 0.25 for paste, the increase of LSP content leads to thinner efficient water film around particles and affects the flowability. Therefore, the NIMBUS program (Miettinen and Mäkelä [2000, 2006]) was used again to solve the multi-objective optimization problem for obtaining a high packing density and a high W/Powder volume ratio of Cem1-GGBFS-LSP mixture. Exactly, it requested to achieve the maximum for Functions 5.11 and 5.12 simultaneously when LSP/(GGBFS+Cem1) ratios vary in range of 0-30 wt.%.

$$y_4 = -0.0000214286X_4^2 + +0.0019500000X_4 + 0.6522857143 \quad (5.11)$$

$$g_4 = 0.0000470749X_4^2 - 0.0062831778X_4 + 0.5824447017 \quad (5.12)$$

where:  $X_4 = \text{LSP}/(\text{GGBFS}+\text{Cem1})$  wt.%,  $0 \leq X_4 \leq 30$  wt.% and  $\text{GGBFS1}/\text{Cem1} = 30$  wt.%.

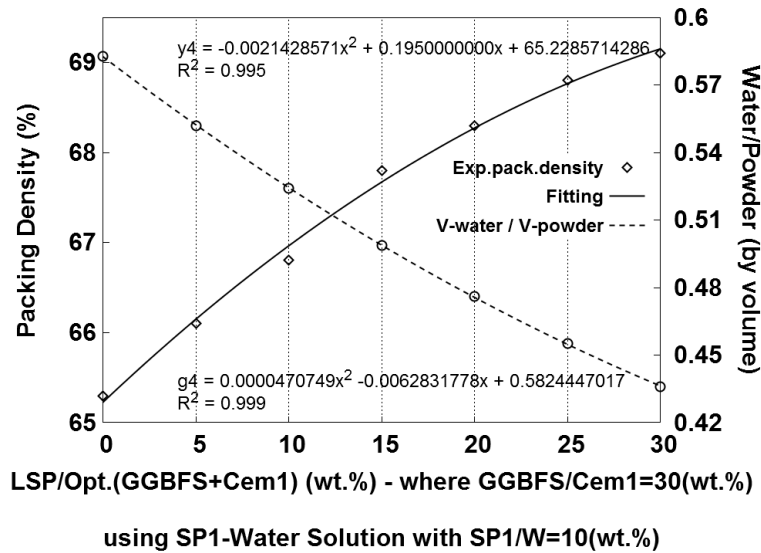


FIGURE 5.15.: The solid curve shows the increase of the packing densities of GGBFS-Cem1-LSP mixtures, in which GGBFS/Cem1 = 30 wt.%, when LSP increased steadily by LSP/(GGBFS+Cem1) ratios from 0 to 30 wt.% (corresponding LSP/Cem1 ratios of 0-39 wt.%); whereas the dashed curve represents the decrease of Water/Solid volume ratio in the pastes having W/C ratio of 25 wt.%.

As a result, the optimum binder of Cem1-GGBFS-LSP was established as **Binder 5**: LSP/(GGBFS+Cem1) = 12.3407 wt.%, where GGBFS/Cem1 = 30 wt.%  $\Rightarrow$  GG-BFS/Cem1/LSP = 30/100/16 wt.%, packing density was 67.3%.

### 5.3.3.3. Determination of the saturated SP1 content for the paste of the optimum Binder 5

The investigation into the influence of SP1 content on the flowability of concretes with Paste 5 was carried out using Cem1 amount of 720 kg and aggregate QS2. The detail

## 5. Mix proportioning of UHPC

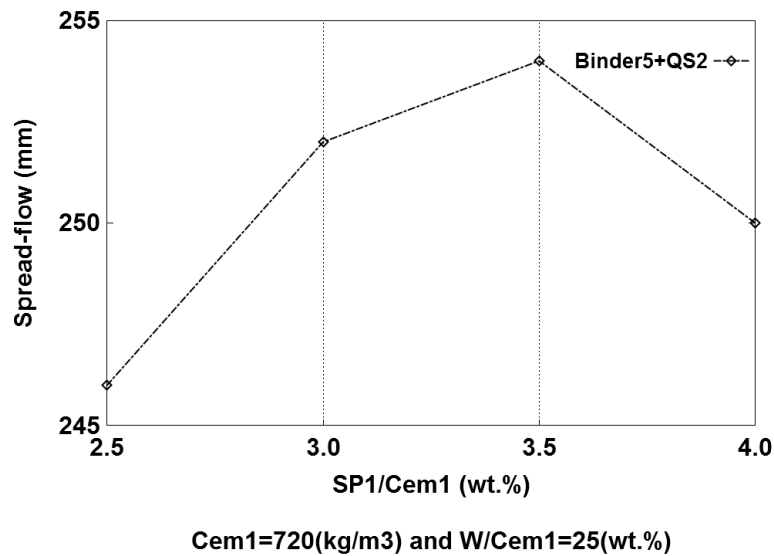


FIGURE 5.16.: Influence of SP1 on the self-flowability of concretes including optimum Binder 5, QS2 and W/Cem1 ratio of 25 wt.%.

test data are shown in Table B.10 in Appendix B. The results in Figure 5.16 indicated that SP1 content of 3.5 wt.% of Cem1 was optimum.

The optimum **Paste 5** having GGBFS/Cem1/LsP/SP1/W ratios of 30/100/16/3.5/25 wt.% was determined and used for further investigation.

### 5.4. Mixture-proportioning of UHPC

In the previous work five different optimum pastes were developed. The optimum Paste 1, Paste 2, Paste 3 were based on ternary binders of Cem1-QPs-SF2. The optimum Paste 4 and Paste 5 were based on binary binder of Cem1-FA and ternary binders of Cem1-GGBFS-LSP respectively. The mix proportions of these optimum paste are summarized as follows:

- Paste 1: QP1/Cem1/SF2/SP1/W = 40/100/11/3.5/25 wt.%.
- Paste 2: QP2/Cem1/SF2/SP1/W = 35/100/11.5/3/25 wt.%.
- Paste 3: QP3/Cem1/SF2/SP1/W = 30/100/12/3/25 wt.%.
- Paste 4: FA/Cem1/SP1/W = 40/100/3/25 wt.%.
- Paste 5: GGBFS/Cem1/LSP/SP1/W = 30/100/16/3.5/25 wt.%.

Cem1 amount of 720 kg/m<sup>3</sup> was selected as a critical amount of Cem1, thereby assuring the self-flowing properties of concrete with a maximum grain size of 1 mm (or higher than 1 mm) .

For the development of the whole concrete (without fibre) the following questions have to be answered:

- Can the highest performance concrete be obtained by the combination of the optimum paste and the highest packing density aggregate which can be formed by blending of different raw aggregates?
- How can the existing particle packing models is applied for mix proportioning of the whole concrete?
- Are the influences of Paste 1, Paste 2, Paste 3 on the performance of concrete similar? If their effects are different, which is the best paste for achieving the highest concrete quality?
- How different are the performance among concretes made of the developed optimum binders?

### 5.4.1. UHPC with a maximum grain size of 1 mm

#### 5.4.1.1. Mix proportioning based on the packing together of different discretely sized particles

The experiment in section 5.3.1, i.e. the results in Figure 5.11 shows that self-flowing concretes with maximum grains of 1mm can be produced when Paste 1, 2, 3 including Cem1 amount of 720 kg/m<sup>3</sup> combine with QS2 (304-1185 $\mu$ m). The question is here, if the paste fractions in concrete and paste components are kept constant, can concrete performance (rheological behaviour and strength) be improved by the combination of QS2 (304-1185 $\mu$ m) and the finer quartz sand QS3 (64-304 $\mu$ m), regarding the modification of the aggregate characteristics as well as of the whole granular concrete mixture (size and size distribution, packing density, shape, surface texture)?

Basically, it is presumed that the higher packing density the aggregate is, the lower paste the concrete needs for a given workability or the better workability the concrete having a given paste is . This presumption seems reasonable for concrete having high volume of aggregate because the improvement of the workability can be attributed to the increase of paste thickness when packing density of aggregate increase in accordance with particle packing theory. For UHPC with high volume of binder, to obtain an optimum concrete mixture with a known volume of optimum paste, is it a simple combination of the paste and the highest packing density aggregate mixture?

The Compressible Packing Model (CPM) developed by de Larrard [1999], described in detail in section 2.3.2.3, and the Compaction - Interaction Packing Model (CIPM) developed by Fennis [2010], introduced in section 2.3.2.4, were employed to determined the optimum proportion of QS2-QS3 blend for obtaining the highest packing density aggregate. Figure 5.17 shows the variation of the calculated actual packing density of QS2-QS3 blend when QS3/(QS2+QS3) ratio varies in range of 0-100 vol.%. The highest actual packing density of QS2-QS3 blend corresponded to QS3/(QS2+QS3) ratios of 38 vol.% and of 30 vol.%, computed by the CPM and CIPM (K-value = 9) respectively.

A simple experimental process was proposed to answer the above two questions and to determine the right proportion of blended aggregate. The rule of granular materials combination was applied. The procedure was as follows: Cem1 content of 720 kg/m<sup>3</sup> was kept constant for Paste 1, 2, 3 in all concrete mixtures, corresponding 564.1, 551.2, 539.1

## 5. Mix proportioning of UHPC

liters/m<sup>3</sup> of Paste 1, 2, 3 respectively. Thus, the volume of aggregate was determined exactly by the absolute volume method with Equation (5.13).

$$V_{Paste} + V_{Aggregate} + V_{Air} = 1m^3 \quad (5.13)$$

In this study, it was assumed that the air content of concrete ( $V_{air}$ ) was small and ignored ( $V_{air} = 0$  vol.%). The blended aggregates were formed by the combination of QS2 and QS3. Concrete corresponding to each blended aggregate was examined for plastic viscosity, self-flowability, 28 days compressive strength. First, the aggregate consisted of QS2 only. Then, QS2 was replaced gradually by the finer QS3.

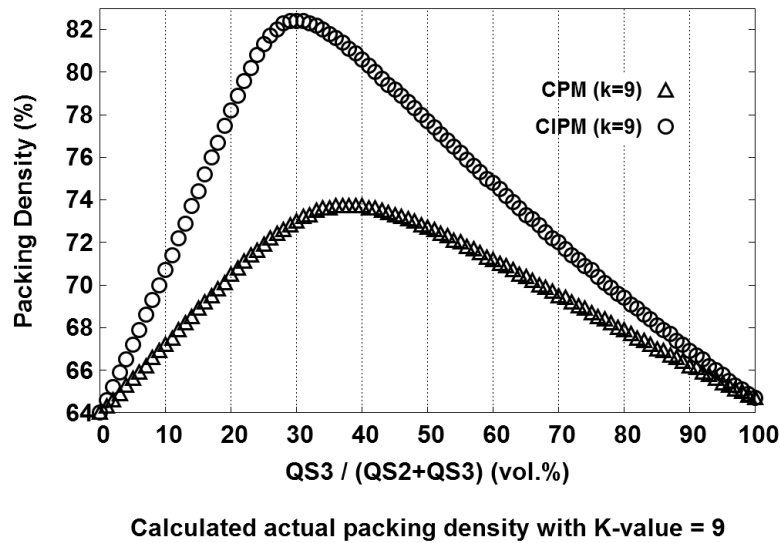


FIGURE 5.17.: Determination of the optimum proportion of QS2-QS3 blend for obtaining the highest packing density aggregate based on calculation of the actual packing density using the Compressible Packing Model (CPM) and the Compaction - Interaction Packing Model (CIPM)

Figures 5.18, 5.19, 5.20 present the experimental results of the rheological behaviour and compressive strength of concrete mixtures in accordance with the proposed experiment model. The experimental results show a good correlation between plastic viscosity and flowability of the UHPCs. Regarding the highest self-flowability and the lowest plastic viscosity of concretes, the best volume ratios of QS3/(QS2+QS3) were 10 vol.% for UHPCs with Paste1 and UHPCs with Paste2 (notated UHPC-1mm-Paste1-90QS2-10QS3, UHPC-1mm-Paste2-90QS2-10QS3), and for UHPCs with Paste3 the ratio was 20 vol.% (notated UHPC-1mm-Paste3-80QS2-20QS3). In general, for each kind of paste, the compressive strength of concretes tend to increase as the packing density increased. However, it is not sure to conclude that the concrete with the highest packing density, showing by the highest self-flowability and the lowest viscosity, can be obtained the highest strength. Indeed, as shown in Figure 5.18 and Figure 5.19, the highest compressive strengths are not in agreement with the highest packing densities, in contrast to the result shown in Figure 5.20. It can be recognized that Paste 1 and Paste 2 include particles with larger diameter

in comparison to Paste 3, such coarse particles seem play a role of fine aggregate, leading to less fine quartz sand QS3 in blended aggregate.

As can be seen in Figure 5.18 for Paste1 and Figure 5.19 for Paste2, the self-flowability of concrete with the highest packing density QS2-QS3 aggregate ( $QS3/(QS2+QS3) = 40$  vol.%) computed by CPM, were lower than that of concretes consisting of QS2 only. The same phenomenon was observed in Figure 5.18 for concrete with Paste1 using the highest packing density QS2-QS3 aggregate ( $QS3/(QS2+QS3) = 30$  vol.%) computed by CIPM. The results imply that the use of the highest packing density aggregate can not insure to achieve the highest packing density UHPC having a given and high paste volume. The interaction between fine particles of the given paste and coarse particles of aggregate have to be taken into account in the particle packing calculation of the whole concrete mixture.

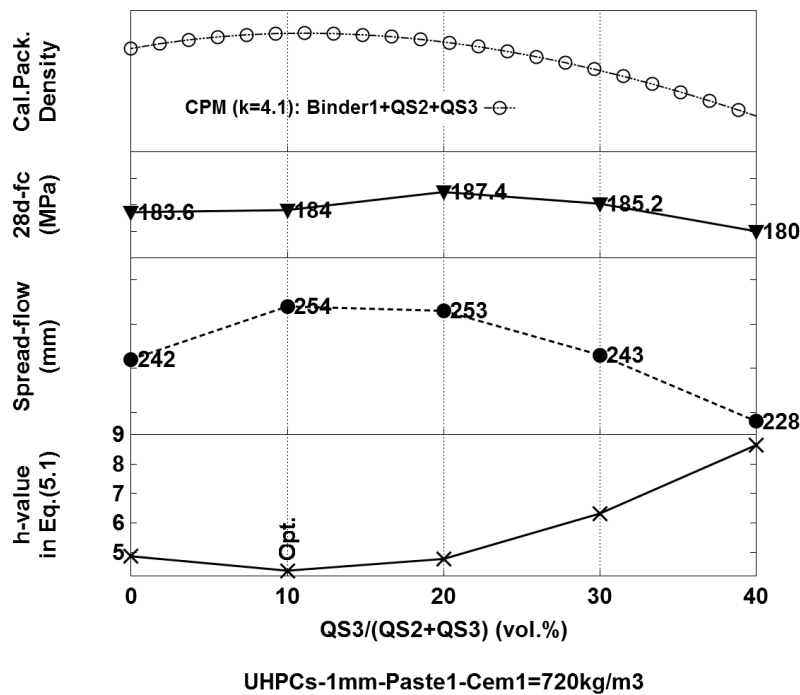


FIGURE 5.18.: Three diagrams from bottom: the experimental results of the viscosity, spread-flow, 28 days compressive strength of concretes with Paste1 containing 720 kg Cem1 when QS3 replaces QS2 step by step. The top diagram: estimation of the packing density of Binder1-QS2-QS3 mixtures, in which the volume mean diameter of Binder1 is  $20.664 \mu\text{m}$  and  $\text{Binder1}/(\text{Binder1}+\text{QS2}+\text{QS3})$  ratio is 46.4 vol.%, using Compressible Packing Model with K-value of 4.1.

Considering the interaction between aggregate particles and fine particles of Binder 1, Binder 2, Binder 3, the Compressible Packing Model (CPM) and the Compaction - Interaction Packing Model (CIPM) were used again to estimate the packing density of granular concrete mixture. Thus, the computed optimum proportions of QS2-QS3 aggregates in UHPCs-Paste1, UHPCs-Paste2 and UHPCs-Paste3 could be determined and compared to the experimental results of the proposed experiment model.

## 5. Mix proportioning of UHPC

The following two case were inspected:

- **In case of using the Compaction - Interaction Packing Model:** the binder was divided into ten size classes. The compaction index, K-values, of 12.2 was applied.
- **In case of using the Compressible Packing Model:** because the interaction between fine particles within the binders related to surface force is not taken into account in the model, the computing of mix proportion and packing density was not accurate if the binder was divided into many size classes. This effect was eliminated in the model by assuming that binder has only one size of volume mean diameter which is computed according to ISO 9276-2 [2014]. The volume mean diameter of Binders 1, 2, 3 were 20.664, 15.343, 11.635  $\mu\text{m}$  respectively. Based on the known proportion and volume of Paste1, Paste2, Paste3 the volume ratios of Binder1/(Binder1+Aggregate), Binder2/(Binder2+Aggregate), Binder3/(Binder3+Aggregate) were 0.464, 0.449, 0.434 respectively. The compaction indexes, K-values, of 4.1, 6.7, 9 were employed.

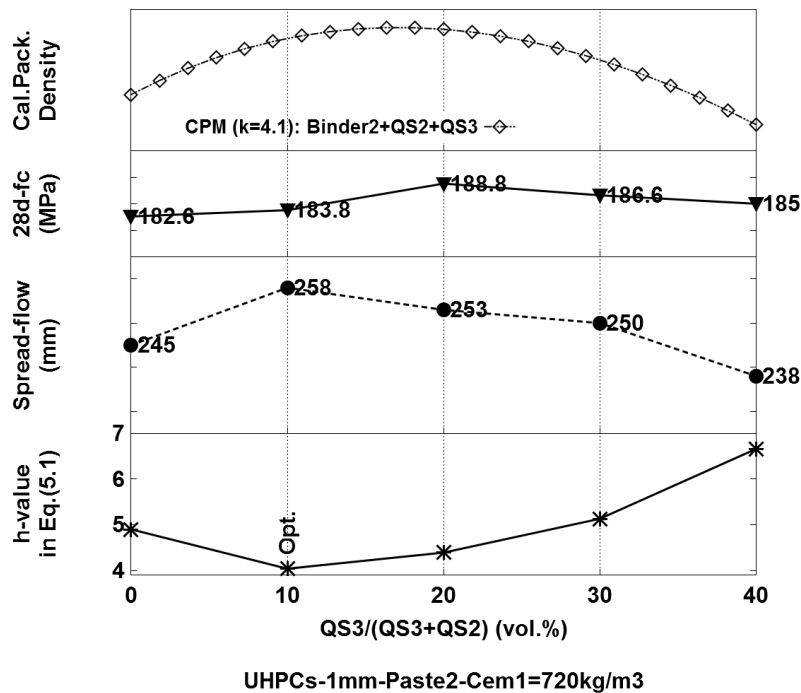


FIGURE 5.19.: Three diagrams from bottom: the experimental results of the viscosity, spread-flow, 28 days compressive strength of concretes with Paste2 containing 720 kg Cem1 when QS3 replaces QS2 step by step. The top diagram: estimation of the packing density of Binder2-QS2-QS3 mixtures, in which the volume mean diameter of Binder2 is 15.343  $\mu\text{m}$  and Binder2/(Binder2+QS2+QS3) ratio is 44.9 vol.%, using Compressible Packing Model with K-value of 4.1.

In the calculation using the Compaction - Interaction Packing Model, the combination of QS2 and QS3 was not influenced by increasing binder volume and coarse particles in binder, QS3/(QS2+QS3) ratios in all case of Pastes1, 2, 3 converge to the value of 20 vol.%, the trend was more clear when the compaction index increase to infinite.

Only the Compressible Packing Model with K-value of 4.1 exhibits the best agreement between the estimation and the experiment, as illustrated in Figures 5.18, 5.19, 5.20. The estimation showed that the highest packing densities of UHPCs-Paste1, UHPCs-Paste2, UHPCs-Paste3 corresponded to QS3/(QS2+QS3) ratios of 10.4, 16.5, 24 vol.% respectively. However, it should be noted that the computed packing densities are much lower than the experimental results.

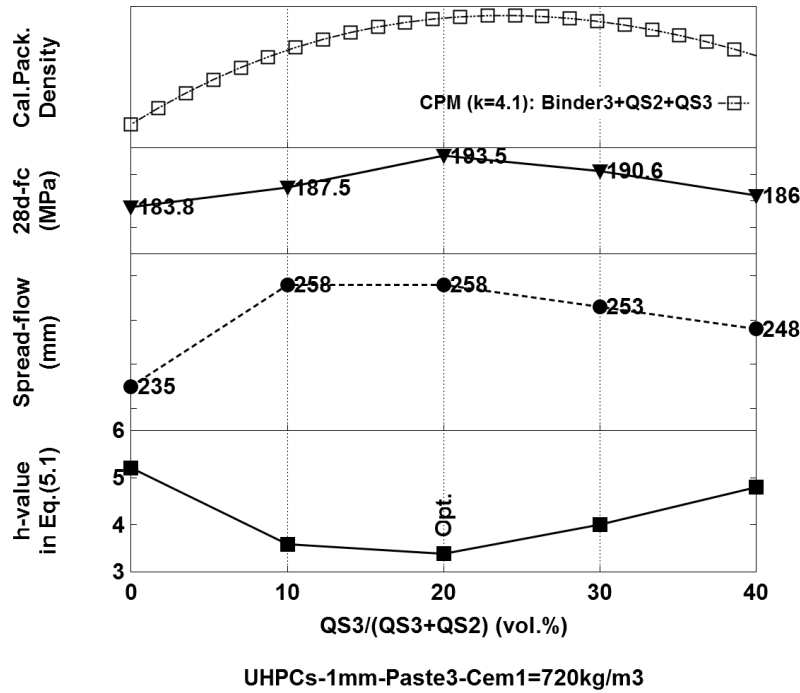


FIGURE 5.20.: Three diagrams from bottom: the experimental results of the viscosity, spread-flow, 28 days compressive strength of concretes with Paste3 containing 720 kg Cem1 when QS3 replaces QS2 step by step. The top diagram: estimation of the packing density of Binder3-QS2-QS3 mixtures, in which the volume mean diameter of Binder3 is  $11.635 \mu\text{m}$  and Binder3/(Binder3+QS2+QS3) ratio is 43.4 vol.%, using Compressible Packing Model with K-value of 4.1.

Comparing the three experimentally optimum UHPC-1mm mixtures, i.e. UHPC-1mm-Paste1-90QS2-10QS3, UHPC-1mm-Paste2-90QS2-10QS3 and UHPC-1mm-Paste3-80QS2-20QS3), indicates that the UHPC-1mm with Paste3 and volume ratios of QS3/(QS2+QS3) of 20% (UHPC-1mm-Paste3-80QS2-20QS3) was the best mixture with the lowest viscosity, the highest spread-flow of 258 mm and the highest 28days compressive strength of 193.5 MPa, although the volume of Paste3 is lower than volume of Paste1 and Paste2. This is probably due to the low viscosity of Paste3 and the good filling effect of QP3, which is finer than QP1 and QP2, leading to better de-aeration and denser microstructure for concrete. **For this reason, only Paste3 was selected for further investigations.**

## 5. Mix proportioning of UHPC

### 5.4.1.2. Mix proportioning using the modified Andreasen and Andersen equation-based ideal curve

The modified Andreasen and Andersen equation-based ideal curve can be employed easily for concrete mix proportioning considering the entire grading of all solid ingredients. The modified Andreasen and Andersen equation (Eq.2.15) is used to build the target grading curve, described by:

$$P_{tar}(D_i) = \frac{D_i^q - D_{min}^q}{D_{max}^q - D_{min}^q}$$

in which,  $D_{max}$  and  $D_{min}$  are the maximum and minimum grain size of the real blended granular mixture including all solid ingredients of concrete; the  $q$ -values for self-compacting concrete involving UHPC vary in range of 0.20-0.25 (as introduced in section 2.3.1);  $D_i$  is equal to the opening size of the  $i^{th}$  sieve of the sieve set containing all sieves for powder size distribution analysis from  $D_{min}$  up to 125  $\mu\text{m}$  and all sieves for coarse particle size distribution analysis from 125  $\mu\text{m}$  up to  $D_{max}$  according to the real particle size distribution analysis. The volume fractions of solid ingredients in the real blended granular mixture are varied in such a way that the actual particle size distribution of the mixture, described by  $P_{mix}(D_i)$ , is closest to the target grading curve, described by  $P_{tar}(D_i)$ , resulting in a curve fitting problem. The least squares technique solves this fitting problem by finding the minimum of the sum of squared residuals (SSR) as expressed mathematically in Equation (5.14).

$$SSR = \sum_{i=1}^n \left( P_{mix}(D_i) - P_{tar}(D_i) \right)^2 \rightarrow Min \quad (5.14)$$

Further information on the algorithm of the modified Andreasen and Andersen equation-based ideal curve for concrete mix proportioning can be found in Hüsken and Brouwers [2008, 2010].

In this research project, the modified Andreasen and Andersen equation based ideal curve was used to calculate the proportion of the granular concrete system containing Cem1, quartz powder QP3, silica fume SF2, quartz sands QS2 and QS3, in which  $D_{max}$  was 1185.65  $\mu\text{m}$  and  $D_{min}$  was 0.042  $\mu\text{m}$ . The distribution moduli,  $q$ -values, of 0.2 and 0.23 were selected according to the recommendation of literature introduced in section 2.3.1. Table 5.1 shows the mix proportion of concrete mixtures computed by the modified Andreasen and Andersen equation-based ideal curve, the experimental results of concrete flowability are also presented. As seen in Table 5.1,  $q$ -value of 0.2 was applied for Mix 1 to Mix 5. Mix 1, 2 and 3 had the same W/Cem1 ratio of 25 wt.% and SP1/Cem1 ratio of 3 wt.%, and the cement contents were 720, 680, 640  $\text{kg}/\text{m}^3$  respectively. Obviously, the water content (or total liquid), W/Cem1 ratio and W/Powder ratio were reduced when cement content decreased, leading to decrease of the spread-flow of Mix 2 and Mix 3 in comparison to Mix 1. Therefore, Mix 4 and Mix 5 were design using cement contents of 680 and 640  $\text{kg}/\text{m}^3$  and SP1/Cem1 ratio of 3 wt.% respectively, but water amount was calculated in such away that total liquid was equal to total liquid of Mix 1. The  $q$ -value of 0.23 was applied for Mix 6 to Mix 10, the principle of the calculation for Mix 1 to Mix

5 was employed once again. The variations of q-values, cement contents, water contents insured that the investigation was adequate.

TABLE 5.1.: Mix proportion of concrete mixtures computed by the modified Andreasen and Andersen equation based ideal curve. Granular system of Cem1, QP3, SF2, QS2 and QS3;  $D_{\max} = 1185.65 \mu\text{m}$  and  $D_{\min} = 0.042 \mu\text{m}$ .

Mix	q	Cem1 [kg]	$\frac{QP3}{Cem1}$	$\frac{SF2}{Cem1}$	$\frac{SP1}{Cem1}$	$\frac{W}{Cem1}$	$\frac{W}{Pow.}$	W+SP1 [lit]	Paste [lit]	$\frac{QS2}{Agg.}$	$\frac{QS3}{Agg.}$	Spread flow [mm]
			[by weight]							[by volume]		
Mix1	0.20	720	0.2306	0.2924	0.030	0.2500	0.1641	185.4	576.5	0.4953	0.5047	241
Mix2	0.20	680	0.3031	0.3202	0.030	0.2500	0.1540	175.1	571.8	0.4961	0.5039	224
Mix3	0.20	640	0.4033	0.3445	0.030	0.2500	0.1430	164.8	569.6	0.4997	0.5003	191
Mix4	0.20	680	0.2914	0.3163	0.030	0.2650	0.1555	185.4	577.8	0.4969	0.5031	238
Mix5	0.20	640	0.3682	0.3360	0.030	0.2821	0.1467	185.4	579.2	0.4985	0.5015	233
Mix6	0.23	720	0.2008	0.2302	0.030	0.2500	0.1747	185.4	548.0	0.5046	0.4954	236
Mix7	0.23	680	0.2791	0.2468	0.030	0.2500	0.1638	175.1	543.0	0.5053	0.4947	219
Mix8	0.23	640	0.3603	0.2727	0.030	0.2500	0.1531	164.8	538.3	0.5065	0.4935	187
Mix9	0.23	680	0.2678	0.2438	0.030	0.2651	0.1653	185.4	549.3	0.5061	0.4939	232
Mix10	0.23	640	0.3347	0.2660	0.030	0.2821	0.1561	185.4	550.7	0.5076	0.4924	230

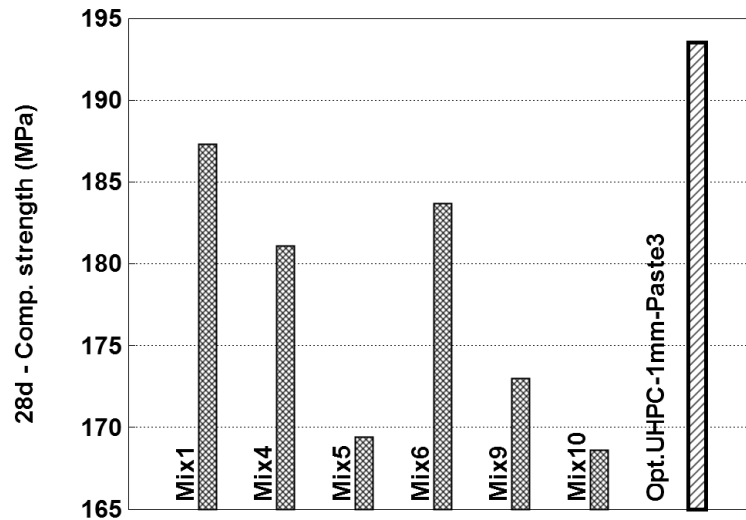


FIGURE 5.21.: The 28 days compressive strength of concrete formed by the modified Andreasen and Andersen equation based ideal curve, in comparison to Optimum UHPC-1mm-Paste3-80QS2-20QS3.

The calculated results in Table 5.1 indicated that the volume ratio of  $QS3/(QS3 + QS2)$  was stable around 0.5 for all mixtures. The variations of q-value and cement content led to a large change of the fractions of QP3 and SF2 for binder. Exactly, the calculation showed that the grading curves of mixtures had a better fitting with the target curve when cement content and liquid content decreased, corresponding to Mixes 2, 3, 7, 8. However,

## 5. Mix proportioning of UHPC

the spread-flow values of Mixes 2, 3, 7, 8 were lower than the standard value of 240 mm for the self-flow properties of concrete, these mixtures could not be used. Compression test was carried out for Mixes 1, 4, 5, 6, 9, 10, the test results were present in Figure 5.21. The detail test data are shown in Table B.11 in Appendix B. Within these mixtures, Mix 1 was the best regarding the highest self-flowability and highest strength, Mix 4 could be a right option due to its low cement content, high flowability and medium strength in comparison to other mixtures. It is noted that the proportion of binder of Mix4 has a very high packing density as seen in Figure 5.6.

It should be emphasized that the performance in terms of self-flowability and strength of the optimum UHPC-1mm-Paste3-80QS2-20QS3 developed by using the method of stepwise optimization of packing density is much better than that of all mixtures designed by the modified Andreasen and Andersen equation-based ideal curve, although Mix 1 to Mix 10 as shown in Table 5.1 have higher paste content and use a very high silica fume amount. This implies that the use of the modified Andreasen and Andersen equation-based ideal curve is unreliable to achieve an optimum UHPC.

### 5.4.2. UHPC with a maximum grain size of 2.5 mm

The investigation in section 5.4.1 presents how the experimental method of stepwise combination of granular materials and how the Compressible Packing Model can be applied for determination of the optimum proportion of a blended aggregate in UHPC regarding to the highest flowability and the lowest viscosity of concrete.

The effectiveness of such ideas were verified once again in the development of UHPC with a maximum grain size of 2.5 mm. Two kinds of blended aggregate, i.e binary aggregate and ternary aggregate, were investigated. Paste3 was used in this investigation, its volume was kept constant, corresponding to 539.1 liters/m<sup>3</sup>, by a fixed amount of 720 kg/m<sup>3</sup> Cem1.

#### 5.4.2.1. UHPC with a binary aggregate having maximum grains of 2.5 mm

The binary aggregates were formed by the combination of QS1 (1-2.5mm) and QS3 (0.064-0.3mm). Figure 5.22 shows the estimated packing density and the experimental results of the rheological and mechanical behaviour of concretes when the volume replacement of QS1 by QS3 increased. The estimation of packing density was good agreement with the experiment of plastic viscosity and spread-flow. The experimental optimum proportion of blended aggregate corresponded to QS3/(QS1+QS3) ratio of 20 vol.%, resulting to the optimum packing density UHPC with the lowest plastic viscosity, the highest spread-flow of 276 mm and the 28 days compressive strength of 193.8 MPa (notated UHPC-2.5mm-Paste3-80QS1-20QS3). The calculated packing density was highest as QS3/(QS1+QS3) ratio was 24 vol.%.

In comparison to UHPC-1mm-Paste3-80QS2-20QS3, the increase of grain size of QS1 in UHPC-2.5mm-Paste3-80QS1-20QS3 led to a better plastic viscosity and a higher self-flowability due to the increase of paste layer thickness which surrounds and lubricates

each aggregate particle.

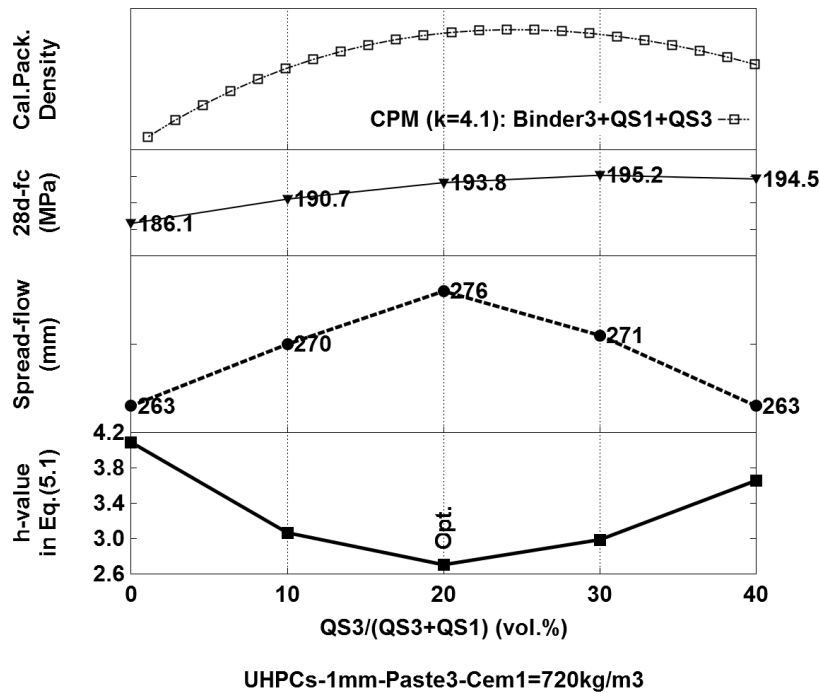


FIGURE 5.22.: Three diagrams from bottom: the experimental results of the viscosity, spread-flow, 28 days compressive strength of concretes with Paste3 containing 720 kg Cem1 when QS3 replaces QS1 step by step. The top diagram: estimation of the packing density of Binder3-QS1-QS3 mixtures, in which the volume mean diameter of Binder3 is  $11.635 \mu\text{m}$  and  $\text{Binder3}/(\text{Binder3}+\text{QS1}+\text{QS3})$  ratio is 43.4 vol.%, using Compressible Packing Model with K-value of 4.1.

#### 5.4.2.2. UHPC with a ternary aggregate having maximum grains of 2.5 mm

This investigation was an extension of case study of UHPC with a maximum grain size of 2.5 mm using a continuous aggregate grading generated by the combination of QS1 (1-2.5 mm), QS2 (0.3-1 mm), QS3 (0.064-0.3 mm). The stepwise combination of aggregates included into two stages for both experiment and estimation. The procedure and results are expressed as the following description:

- Experiment:** First, QS1 was gradually replaced by QS2. This process resulted in the increase of the self-flowability and the compressive strength of concretes, as well as the decrease of the plastic viscosity of concretes. The first experimental optimum packing density corresponded to  $\text{QS2}/(\text{QS2}+\text{QS1})$  ratio of 40 vol.%, shown in Figure 5.23. In the second stage, the first optimum blended aggregate including 40 vol.% QS2 and 60 vol.% QS1 was replaced by QS3 step by step. An additional improvement of concrete performance was observed, the optimum packing density UHPC with the lowest plastic viscosity, the highest spread-flow of 283 mm and the 28 days compressive strength of 196.5 MPa was determined when the volume ratios of  $\text{QS3}/(\text{QS3} + \text{blend of 40 vol.\% QS2 and 60 vol.\% QS2})$  was 10 vol.% (i.e.

## 5. Mix proportioning of UHPC

QS1/QS2/QS3 = 54/36/10 vol.%), (notated UHPC-2.5mm-Paste3-54QS1-36QS2-10QS3), presented in Figure 5.24.

- **Estimation using CPM:** The procedure was similar to the experimental process. The first computed highest packing density mixture of Binder3-QS1-QS2 corresponded to QS2/(QS2+QS1) ratio of 41.7 vol.%, illustrated in Figure 5.23. In the second stage, the first optimum blended aggregate including 41.7 vol.% QS2 and 58.3 vol.% QS1 was replaced by QS3 gradually. The packing density of mixture of Binder3-QS1-QS2-QS3 increased when the volume ratios of QS3/(QS3 + blend of 41.7 vol.% QS2 and 58.3 vol.% QS1) increased up to 12.1 vol.% (i.e. QS1/QS2/QS3 of 51.2/36.7/12.1 vol.%), then the packing density of mixture decreased, as depicted in Figure 5.24. The estimation of packing density was in good agreement with the experiment of plastic viscosity and spread-flow.

Furthermore, a direct estimation without stepwise combination was also performed. The calculation showed that the highest packing density of Binder3-QS1-QS2-QS3 mixture, in which Binder3/Aggregate ratio is 43.4 vol.%, was achieved when QS1/QS2/QS3 ratios were 56.5/28.3/15.2 vol.%. Concrete with this proportion of aggregate possessed a spread-flow of 280 mm and a 28 days compressive strength of 196.1 MPa. Obviously, this direct estimated mix proportion can be only verified by a comparison with the experiment results of the stepwise optimization method. This implies that the experiment using the stepwise optimization method is crucial regardless of support of particle packing model, especially aggregate of more than two components.

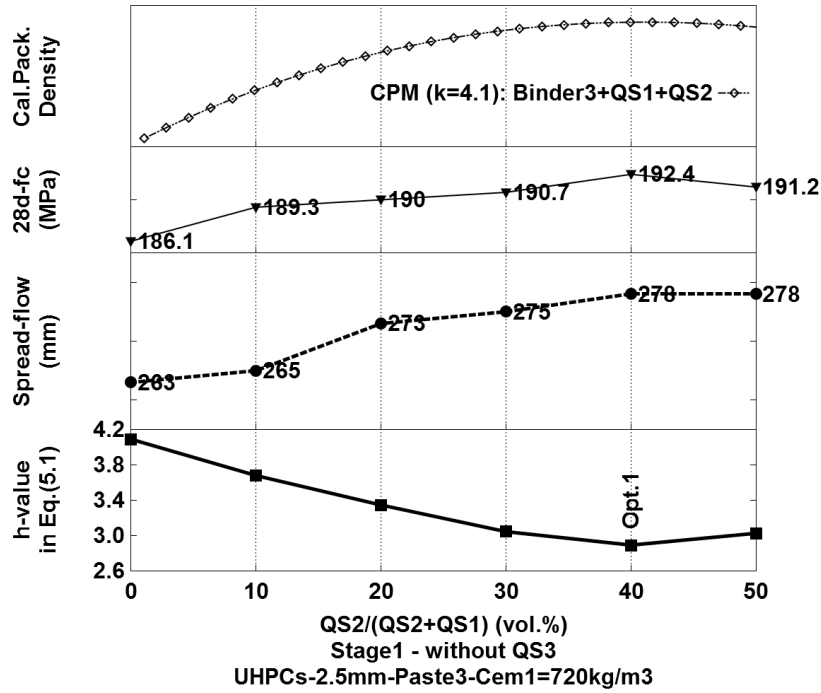


FIGURE 5.23.: STAGE1 - Stepwise optimization for UHPCs-2.5mm using Paste3 and QS1-QS2-QS3 aggregate. Three diagrams from bottom: the experimental results of the viscosity, spread-flow, 28 days compressive strength of concretes with Paste3 consisting of 720 kg Cem1 when QS2 replaces QS1 step by step. The top diagram: estimation of the packing density of Binder3-QS1-QS3 mixtures, in which the volume mean diameter of Binder3 is  $11.635 \mu\text{m}$  and  $\text{Binder3}/(\text{Binder3}+\text{QS1}+\text{QS3})$  ratio is 43.4 vol.%, using Compressible Packing Model with K-value of 4.1.

## 5. Mix proportioning of UHPC

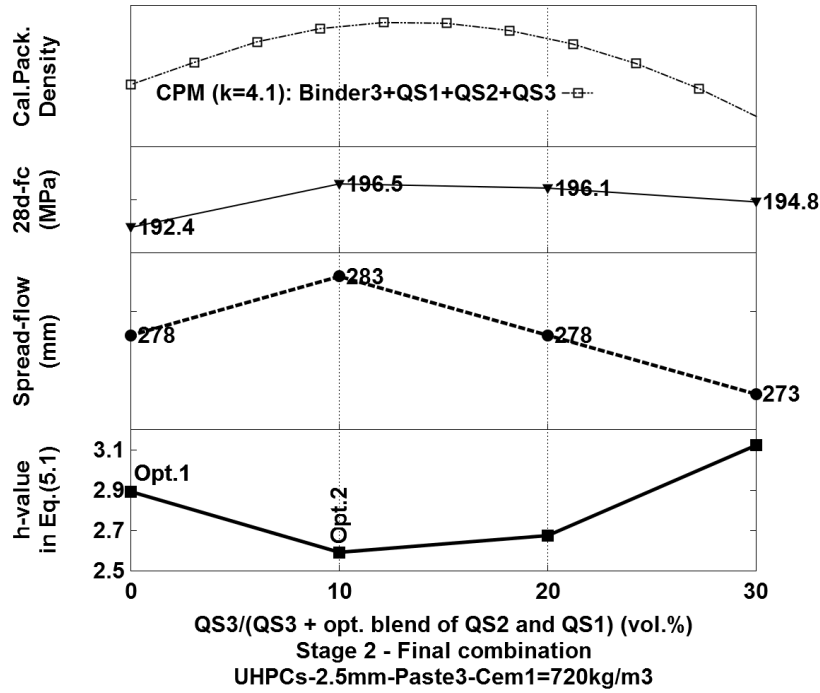


FIGURE 5.24.: STAGE2 - Stepwise optimization for UHPCs-2.5mm using Paste3 and QS1-QS2-QS3 aggregate. Three diagrams from bottom: the experimental results of the viscosity, spread-flow, 28 days compressive strength of concretes with Paste3 consisting of 720 kg Cem1 when QS3 replaces the blend of 60 vol.%QS1 and 40 vol.%QS2 gradually. The optimum UHPC-2.5mm was determined at QS1/QS2/QS3 = 54/36/10 vol.%. The top diagram: estimation of the packing density of Binder3-QS1-QS3 mixtures, in which the volume mean diameter of Binder3 is  $11.635 \mu\text{m}$ , Binder3/(Binder3+QS1+QS2+QS3) ratio is 43.4 vol.% and QS2/QS1 ratio is 41.7/58.3 vol.%, using Compressible Packing Model with K-value of 4.1.

The total surface area of aggregate of UHPC-2.5mm-Paste3-54QS1-36QS2-10QS3 is higher than that of UHPC-2.5mm-Paste3-80QS1-20QS3 but UHPC-2.5mm-Paste3-54QS1-36QS2-10QS3 has a better plastic viscosity, self-flowability and compressive strength using the same Paste3 volume. This mean the stepwise combination of aggregates modifies the packing structure of the whole concrete and leads to a higher liquid layer for lubrication of particle.

### 5.4.3. UHPC with a maximum grain size of 4 mm

In this investigation, a three components aggregate system including CrB2 (2-4 mm), QS2 (0.3-1 mm) and QS3 (0.064-0.3 mm) was used. The crushed basalt particles CrB2 are very angular (with sharp edges and corners) and have a rough surface texture unlike quartz sand having a relatively round shape. Paste3 with  $720 \text{ kg/m}^3$  Cem1 was used. For aggregate of three components, the stepwise combination of aggregates including two stages was carried out. First, CrB2 was progressively replaced by QS2. The particle packing density of concrete mixture was improved significantly when a high amount up to 70 vol.%

of CrB2 was replaced, as shown in Figure 5.25. This phenomenon may be attributed to the strong effect of the high angular CrB2 particles on the interaction of particles in mixture. In the second stage, as presented in Figure 5.26, the blended aggregate including 70 vol.% QS2 and 30 vol.% CrB2 was then replaced with QS3 gradually. This process created the optimum packing density UHPC-4mm showing the lowest plastic viscosity, the highest spread-flow of 283 mm and the highest compressive strength of 197.4 MPa at the volume ratio of QS3/(QS3 + blend of 30 vol.% CrB2 and 70 vol.% QS2) of 20 vol.% (i.e. CrB2/QS2/QS3 = 24/56/20 vol.%) (notated UHPC-4mm-Paste3-24CrB2-56QS2-20QS3).

In a way similar to section 5.4.2.2, the Compressible Packing Model was used to compute packing densities of Binder3-CrB2-QS2-QS3 blends with Binder3/(Binder3 + CrB2 + QS2 + QS3) ratio of 43.4 vol.% for finding optimum proportion of CrB2-QS2-QS3 aggregate. However, the estimation of packing density variation was completely different to the experiment of rheological behaviour. This mean the loosening effect and wall effect coefficients of the model should be modified in case of UHPC including high angular and round aggregates.

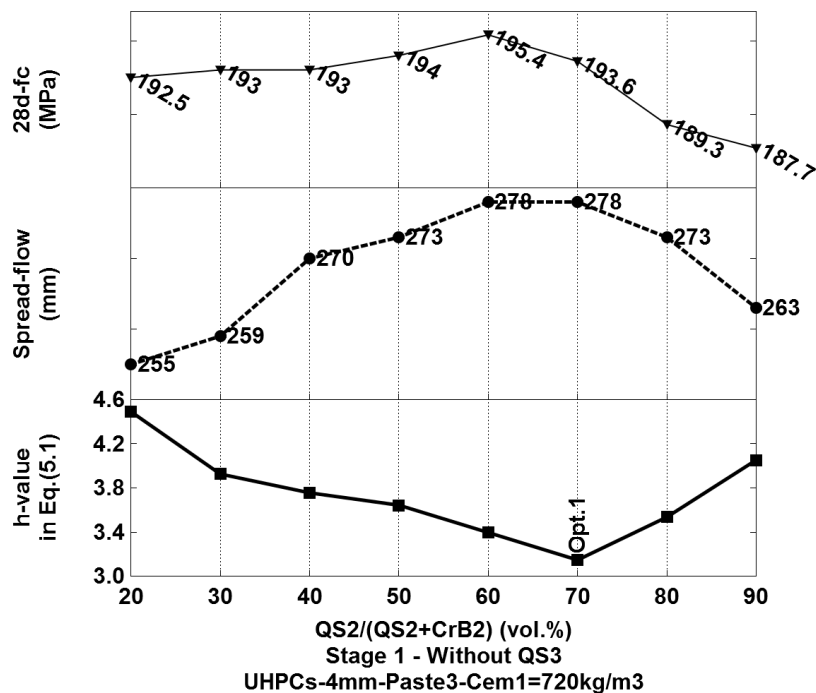


FIGURE 5.25.: STAGE1 - Stepwise optimization for UHPCs-4mm using Paste3 and CrB2-QS2-QS3 aggregate. The experimental results of the viscosity, spread-flow, 28 days compressive strength of concretes with Paste3 consisting of 720 kg Cem1 when QS2 replaces CrB2 step by step. The first optimum packing density was achieved at QS2/(QS2+CrB2) ratio of 70 vol.%.

## 5. Mix proportioning of UHPC

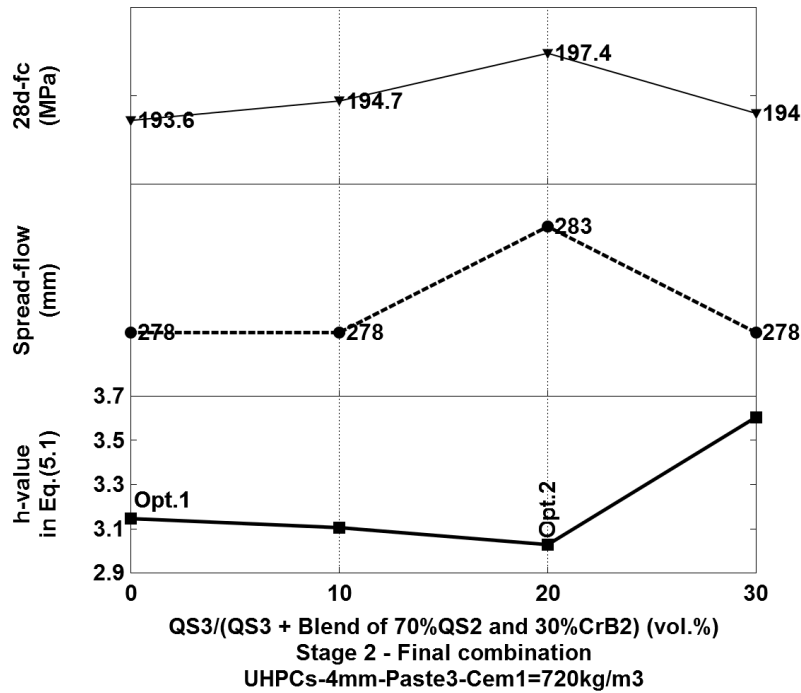


FIGURE 5.26.: STAGE2 - Stepwise optimization for UHPCs-4mm using Paste3 and CrB2-QS2-QS3 aggregate. The experimental results of the viscosity, spread-flow, 28 days compressive strength of concretes with Paste3 consisting of 720 kg Cem1 when the blend of 70 vol.% QS2 and 30 vol.% CrB2 was gradually replaced by QS3. The optimum UHPC-4mm was determined at CrB2/QS2/QS3 = 24/56/20 vol.%.

### 5.4.4. UHPC with a maximum grain size of 8 mm

The successfully developed UHPCs using binary and ternary aggregates demonstrates the advantage of the stepwise optimization method. The method was applied once again to develop UHPC with maximum grains of 8 mm using a four components aggregate system of CrB1 (4-8 mm), QS1 (1-2.5 mm), QS2 (0.3-1 mm) and QS3 (0.064-0.3 mm). The cement content for the UHPCs-8mm was 640 kg/m<sup>3</sup> (corresponding to 479.2 liters of Paste3), because the significant increasing of the grain sizes of aggregate permitted the retaining of good self-compacting properties with less paste. The optimization process includes three stages for blended aggregate of four components. With the same experimental process used in the previous case studies from section 5.4.1 to section 5.4.3, the gradual replacements of larger aggregate particles by smaller aggregate particles in each stage was achieved, as described in Figures 5.27, 5.28, 5.29. The final result was the optimum packing density UHPC-8mm with the lowest plastic viscosity, the highest spread-flow of 278 mm and the highest compressive strength of 191.2 MPa at the ratios of CrB1/QS1/QS2/QS3 of 25.2/37.8/27/10 (notated UHPC-8mm-Paste3-25.2CrB1-37.8QS1-27QS2-10QS3). It was clear to perceive that the paste layer thickness was reduced corresponding to the increasing of the number and the total surface area of the smaller aggregate particles. However, the plastic viscosity, the self-flowability and the compressive strength of the concretes were improved significantly.

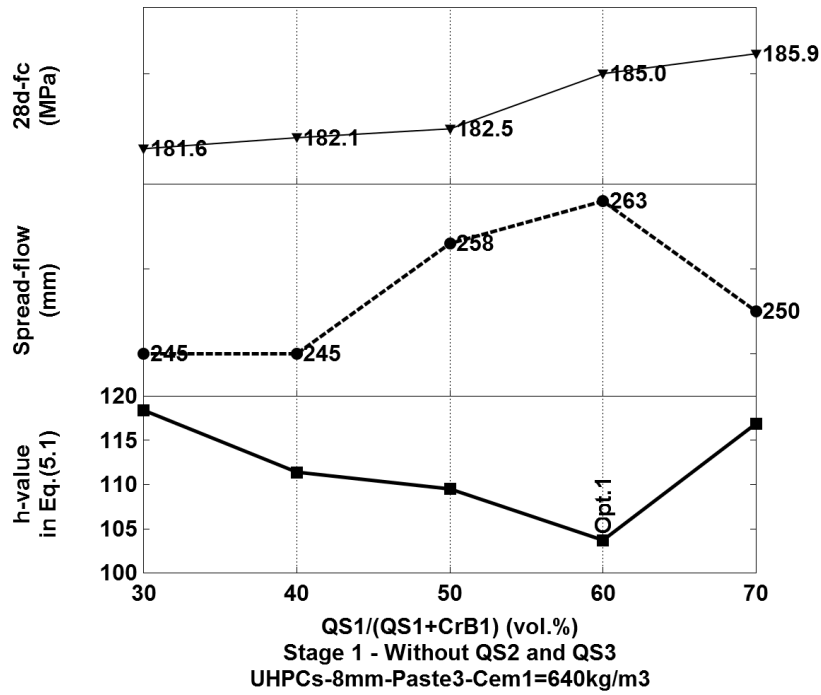


FIGURE 5.27.: STAGE1 - Stepwise optimization for UHPCs-8mm using Paste3 and CrB2-QS1-QS2-QS3 aggregate. The experimental results of the viscosity, spread-flow, 28 days compressive strength of concretes with Paste3 consisting of 640 kg Cem1 when QS2 replaces CrB1 step by step. The first optimum packing density was achieved at QS1/(QS1+CrB1) ratio of 60 vol.%.

## 5. Mix proportioning of UHPC

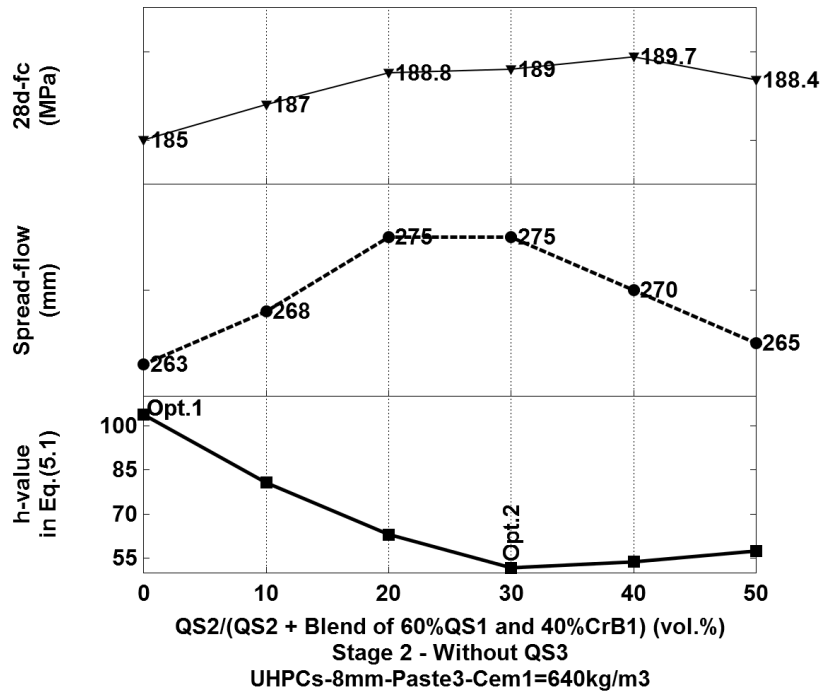


FIGURE 5.28.: STAGE2 - Stepwise optimization for UHPCs-8mm using Paste3 and CrB2-QS1-QS2-QS3 aggregate. The experimental results of the viscosity, spread-flow, 28 days compressive strength of concretes with Paste3 consisting of 640 kg Cem1 when when the blended of 60 vol.% QS1 and 40 vol.% CrB1 was gradually replaced by QS2. The second optimum packing density was achieved at CrB1/QS1/QS2 ratios of 28/42/30 vol.%.

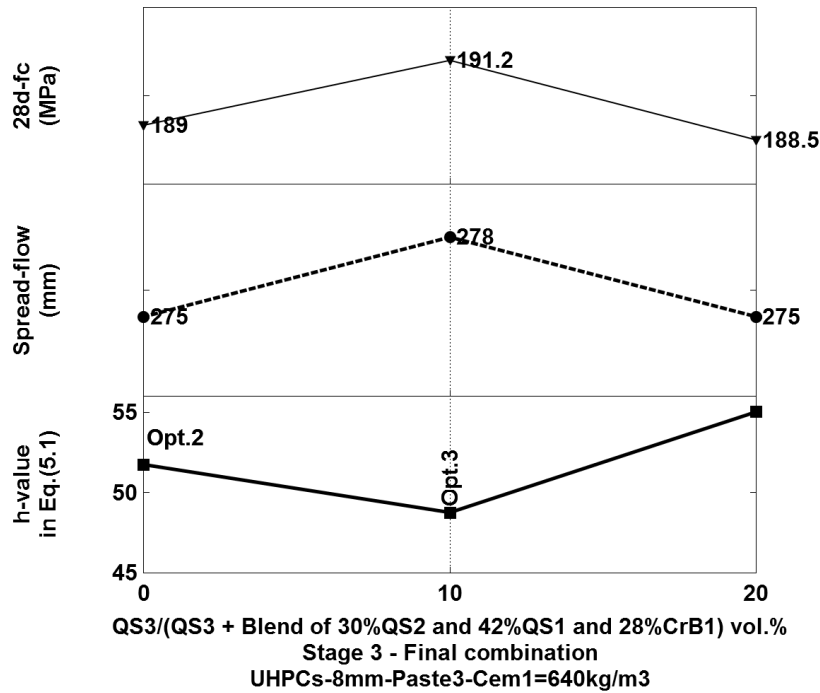


FIGURE 5.29.: STAGE3 - Stepwise optimization for UHPCs-8mm using Paste3 and CrB2-QS1-QS2-QS3 aggregate: The experimental results of the viscosity, spread-flow, 28 days compressive strength of concretes with Paste3 consisting of 640 kg Cem1 when when the blended of 30 vol.% QS2 and 42 vol.% QS1 and 28 vol.% CrB1 was progressively replaced by QS3. The optimum UHPC-8mm was determined at CrB1/QS1/QS2/QS3 ratios of 25.2/37.8/27/10 vol.%.

#### 5.4.4.1. A summary for the developed optimum UHPCs using Paste 3

Based on the three optimum Paste 1, 2 and 3, UHPCs containing maximum grains of 1 mm using QS2 and QS3 were developed firstly. Therefore, it was recognized that Paste 3 was better than Paste 1 and Paste 2 considering the improvement of flowability and strength of concrete. Paste 3 was then used for the further development of UHPC with maximum grain size from 2.5 mm to 8 mm.

The developed optimum UHPCs were compared to reference mixtures. The reference mixtures include two groups. The mixtures of the first reference group were produced in the own lab using unselected materials of the initial materials collection of this research project and applying recipes of the existing mixtures from literature (Fehling and Schmidt et al. [2013], Schmidt and Fehling et al. [2014], Yu et al. [2014]). The second reference group consists of data of recent researches from literature (Yu et al. [2014], Fröhlich and Schimdt [2014], Wille et al. [2012]). The mix-proportion, the self-flowing and the 28 days compressive strength of the developed optimum UHPCs-Paste3 in this research project and the reference mixtures are summarized in Table 5.2.

It is clearly apparent that the developed optimum UHPCs were much more effective than the reference mixture in terms of materials saving and performance improving. For

## 5. Mix proportioning of UHPC

instance, in comparison to the mixture M2Q, published by Fröhlich and Schimdt [2014], the optimum UHPC-1mm-Paste3-80QS2-20QS3 has 13.4 wt.% lower cement, 35 wt.% lower silica fume, 25.8 wt.% lower superplasticizer, 12 wt.% higher comp. strength. In another case of using unsuitable materials the flowability and the compressive strength of the control mixture 1 are much lower than that of the optimum UHPC-1mm-Paste3-80QS2-20QS3.

TABLE 5.2.: Mix proportion and properties of the developed optimum UHPCs based on Paste3 in comparison with the reference mixtures.

Mix-proportion		Spread flow	Slump flow	28d- f <sub>c,cube</sub>	28d- f <sub>c,cyl.</sub>	28d- E
[wt. ratio for paste and vol. ratio for aggregate]		[mm]	[mm]	[MPa]	[MPa]	[GPa]
<b>The developed optimum UHPCs based on Paste3</b>						
Paste3	QP3/Cem1/SF2/W/SP1 = 0.3/1/0.12/0.25/0.030					
UHPC-1mm	Paste3 with 720 kg Cem1 QS2/QS3 = 80/20	258	800	193.5	183.3	53.4
UHPC-2.5mm	Paste3 with 720 kg Cem1 QS1/QS2/QS3 = 54/36/10	283	875	196.5	189.8	54.9
UHPC-4mm	Paste3 with 720 kg Cem1 CrB2/QS2/QS3 = 24/56/20	283	840	197.4	188.1	53.8
UHPC-8mm	Paste3 with 640 kg Cem1 CrB1/QS1/QS2/QS3 = 25.2/37.8/27/10	278	805	191.2	185.6	57.0
<b>Reference mixtures - 1<sup>st</sup> Group</b>						
Control1	640 kg Cem4; QS2 = 100% QP3/Cem4/SF2/W/SP3 = 0.3/1/0.12/0.25/0.040	210	–	137.5	–	–
Control2	800 kg Cem2; QS2/QS3 = 80/20 QP3/Cem2/SF2/W/SP3 = 0.4/1/0.18/0.25/0.040	268	–	158.3	–	–
<b>Reference mixtures - 2<sup>nd</sup> Group</b>						
Yu [2014]	875 kg Cem and 2.5 vol.% StF 13mm/0.2mm QP/Cem/SF/W/SP=0.25/1/0.05/0.23/0.052	–	–	156.0	–	–
UHPC1	QS 0-2 mm = 100%; sample 40x40x160 mm					
Wille [2012]	775 kg Cem; sample 50x50x100 mm QP/Cem/SF/W/SP = 0.25/1/0.25/0.22/0.014 and QS 0.2-0.8 mm / QS 0-0.2 mm = 80/20	–	910	192.0	–	–
UHPC						
Fröhlich [2014]	832 kg Cem and 2.5 vol.% StF 9mm/0.15mm QP/Cem/SF/W/SP=0.25/1/0.16/0.22/0.035	–	–	172.2	–	–
M2Q	QS 0.125-0.5mm = 100%					
Fröhlich [2014]	650 kg Cem and 2.5 vol.% StF 9mm/0.15mm QP/Cem/SF/W/SP = 0.7/1/0.27/0.24/0.046	–	800	187.4	–	–
B5Q	QS 0.125-0.5mm / Basalt 2-8mm = 40/60					

The packing density of these optimum UHPCs were determined by Kwan's method and depicted in Figure 5.30. It is interesting to compare the packing density and the flowability of the three optimum concretes UHPC-1mm-Paste3, UHPC-2.5mm-Paste3 and UHPC-4mm-Paste3 containing the same paste (content and proportion). UHPC-1mm-

Paste3 has the lowest spread flow of 258 mm, the lowest slump flow of 800 mm and also has the lowest packing density of 81.77%. UHPC-2.5mm-Paste3 has the highest spread flow of 258 mm, the highest slump flow of 875 mm and also has the highest packing density of 82.76%. Due to the replacement of Binder3 with a angular shape aggregate, UHPC-8mm-Paste3 has the highest packing density of 84.26% but its spread flow of 278 mm and slump flow of 805 mm are lowest in comparison to the other mixtures.

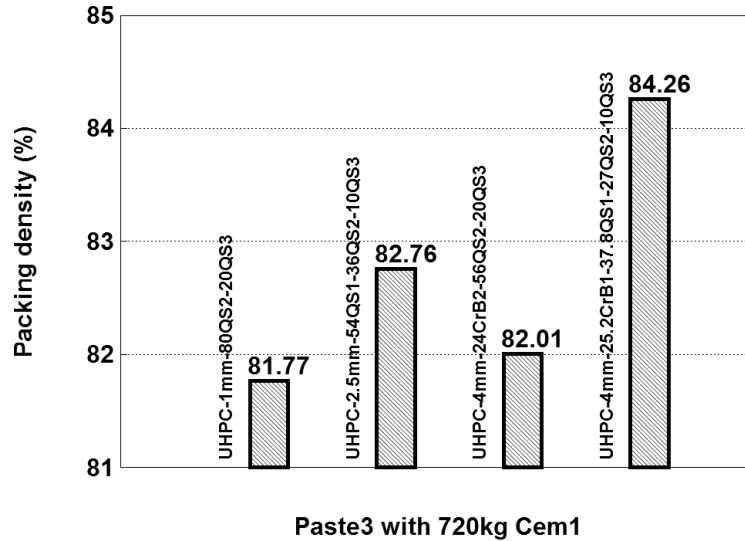


FIGURE 5.30.: The packing density of the optimum UHPC-1mm-Paste3, UHPC-2.5mm-Paste3, UHPC-4mm-Paste3 and UHPC-8mm-Paste3 determined applying Kwan's method.

The strength development of the optimum UHPC-2.5mm-Paste3 was examined at 28, 90, 180 days age to compare with the strength development of the optimum UHPCs-2.5mm using Paste 4 and Paste 5. The experimental results is shown in Figure 5.35.

#### 5.4.5. UHPC based on the optimum paste containing binary binder of cement and ultra fine fly ash

In the previous work, the optimum paste containing binary binder of cement and ultra fine fly ash was established, i.e Paste 4 with FA/Cem1/SP1/W ratios of 40/100/3/25 wt.%. In this investigation, Paste 4 containing 720 kg/m<sup>3</sup> Cem1 (corresponding to 532.5 liters/m<sup>3</sup>) and blended aggregates of QS1 (1-2.5 mm), QS2 (0.3-1 mm) and QS3 (0.064-0.3 mm) were used to produce UHPCs with maximum grains of 2.5 mm. This aggregate system was chosen because it allows to create high flowable concrete and the Compressible Packing Model (CPM) can be applied for computing the optimum aggregate proportion without any effect of angular particles on results, as reported in the previous investigation in section 5.4.1.1. The use of Cem1 content of 720 kg/m<sup>3</sup> allows an appropriate comparison between UHPCs-Paste4 and the previously developed UHPCs-Paste3. A procedure including two stages of stepwise optimization as described in section 5.4.2.2 was carried out. The comprehensive investigation in section 5.4.1.1 demonstrated a very good agreement between

## 5. Mix proportioning of UHPC

the spread-flow and plastic viscosity of concrete. Thus, measurement of plastic viscosity was not performed in this investigation to simplify the test procedure. First, QS1 was replaced by QS2 step by step. The experiment showed the first highest flowability of concrete at QS2/(QS2+QS3) ratio of 40 vol.%. In the estimation using the CPM, the volume mean diameter of Binder 4 is  $8.7 \mu\text{m}$ , the first highest packing density of Binder4-QS2-QS3 blend was achieved when QS2/(QS2+QS3) ratio was 42.5 vol.%. Figure 5.31 shows the experimental results and the variation of the computed packing density of Binder4-QS1-QS2 mixtures. In the second stage, the optimum blended aggregate of QS1 and QS2 determined in the first stage was progressively replaced by QS3. Figure 5.32 shows that the computed highest packing density of Binder4-QS1-QS2-QS3 corresponded to QS3/(QS3 + Blend of 42.5% QS2 and 57.5% QS1) ratio of 18.2 vol.% (i.e. QS1/QS2/QS3 = 47.035/34.765/18.2 vol.%), while the experimental highest spread-flow of concrete was obtained at QS3/(QS3 + Blend of 40% QS2 and 60% QS1) ratio of 15 vol.% (i.e. QS1/QS2/QS3 = 51/34/15 vol.%) (notated UHPC-2.5mm-Paste4-51QS1-34QS2-15QS3). Actually, the experimental optimum aggregate was determined after the estimated optimum aggregate proportion was compared to the experimental results of spread-flow at QS3/(QS3 + Blend of 40% QS2 and 60% QS1) ratios of 10 and 20 vol.%.

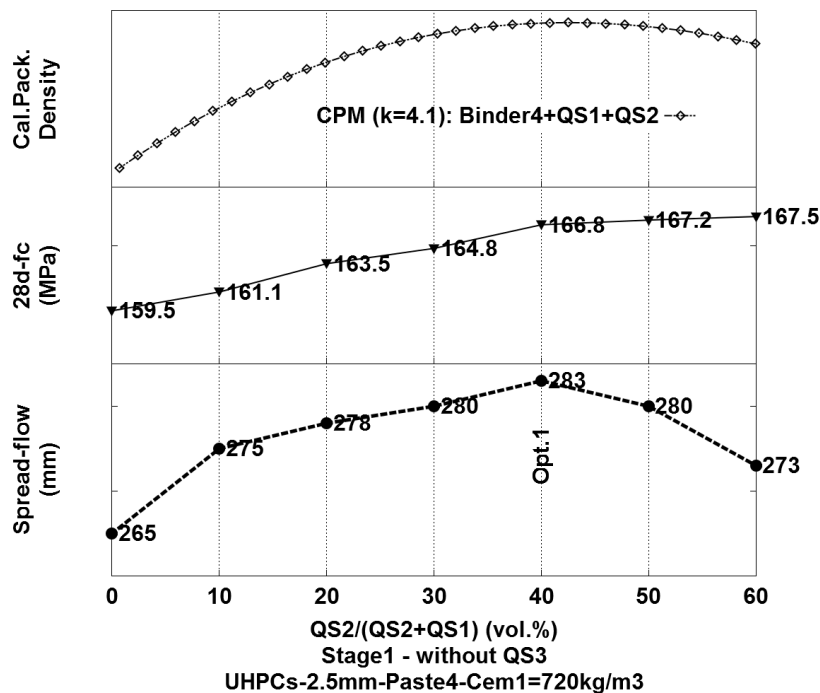


FIGURE 5.31.: STAGE1 - Stepwise optimization for UHPCs-2.5mm using Paste4 and QS1-QS2-QS3 aggregate. Two diagrams from bottom: the experimental results of the spread-flow and 28 days compressive strength of concretes with Paste4 containing 720 kg Cem1 when QS2 replaces QS1 step by step. The top diagram: Estimation of the packing density of Binder4-QS1-QS3 mixtures, in which the volume mean diameter of Binder4 is  $8.7 \mu\text{m}$  and Binder4/(Binder4+QS1+QS3) ratio is 42.6 vol.%, using Compressible Packing Model with K-value of 4.1.

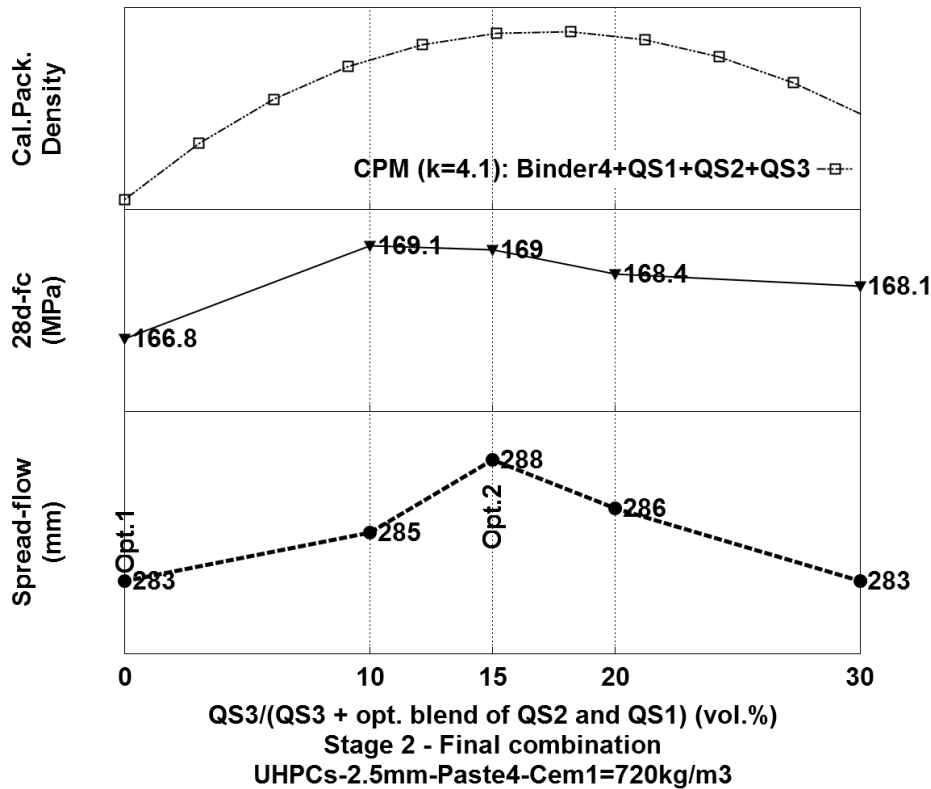


FIGURE 5.32.: STAGE2 - Stepwise optimization for UHPCs-2.5mm using Paste4 and QS1-QS2-QS3 aggregate. Two diagrams from bottom: the experimental results of the spread-flow and 28 days compressive strength of concretes with Paste4 containing 720 kg Cem1 when QS3 replaces the blend of 60 vol.%QS1 and 40 vol.%QS2 gradually. The optimum UHPC-2.5mm was determined at QS1/QS2/QS3 = 51/34/15 vol.%. The top diagram: Estimation of the packing density of Binder4-QS1-QS3 mixtures, in which the volume mean diameter of Binder4 is  $8.7 \mu\text{m}$ , Binder4/(Binder4+QS1+QS2+QS3) ratio is 42.6 vol.% and QS2/QS1 ratio is 42.5/57.5 vol.%, using Compressible Packing Model with K-value of 4.1.

In comparison to the optimum UHPC-2.5mm-Paste3-54QS1-36QS2-10QS3 the self-flowability of UHPC-2.5mm-Paste4-51QS1-34QS2-15QS3 was higher, although the packing density of Binder 4 was lower than that of Binder 3, the volume of Paste 4 was lower and the total surface area of aggregate were higher than that of UHPC-2.5mm-Paste4-51QS1-34QS2-15QS3. This can be attributed to (i) the positive effect of the spherical shape of ultra-fine fly ash on the fluidity, and (ii) the very positive effect of superplasticizer SP1 on the fly ash in comparison with silica fume (see Figure 4.9 in section 4.4.2. However, the 28 days compressive strength of UHPC-2.5mm-Paste4-51QS1-34QS2-15QS3 was much lower than that of UHPC-2.5mm-Paste3-54QS1-36QS2-10QS3 due to low activity and low rate of pozzolanic reaction of fly ash compared to silica fume.

UHPC-2.5mm-Paste4-51QS1-34QS2-15QS3 was not used for further investigation into steel fibre reinforced UHPC. However, its strength development was still examined and shown in Figure 5.35

## 5. Mix proportioning of UHPC

### 5.4.6. UHPC based on the optimum paste containing ternary binder of cement-blast furnace slag-limestone powder

The optimum Paste 5 containing binder of cement-blast furnace slag-limestone powder was found out and expressed by GGBFS/Cem1/LSP/SP1/W ratios of 30/100/16/3.5/25 wt.% in the previous work. UHPCs having maximum grains of 2.5 mm were developed using Paste 5 and blended aggregates of QS1 (1-2.5 mm), QS2 (0.3-1 mm) and QS3 (0.064-0.3 mm). The Cem1 content of 720 kg/m<sup>3</sup> was fixed (corresponding to 537.9 liters/m<sup>3</sup>). In comparison with UHPCs-2.5mm using Paste3 and blended aggregate of QS1, QS2 and QS3 developed in section 5.4.2.2, UHPCs-2.5mm in this investigation have the same paste volume, Binder 5 and Binder 3 have the same volume mean diameter (11.514  $\mu$ m for Binder 5 and 11.635  $\mu$ m for Binder 3). Therefore, it was predicted that the optimum proportion of aggregate for UHPC-2.5mm-Paste5 could be similar to UHPC-2.5mm-Paste3-54QS1-36QS2-10QS3. Surprisingly, the experimental results and calculation demonstrated that the prediction is exact. Figures 5.33 and 5.34 show two stages of the stepwise optimization for experiment and calculation of the optimum aggregate proportion.

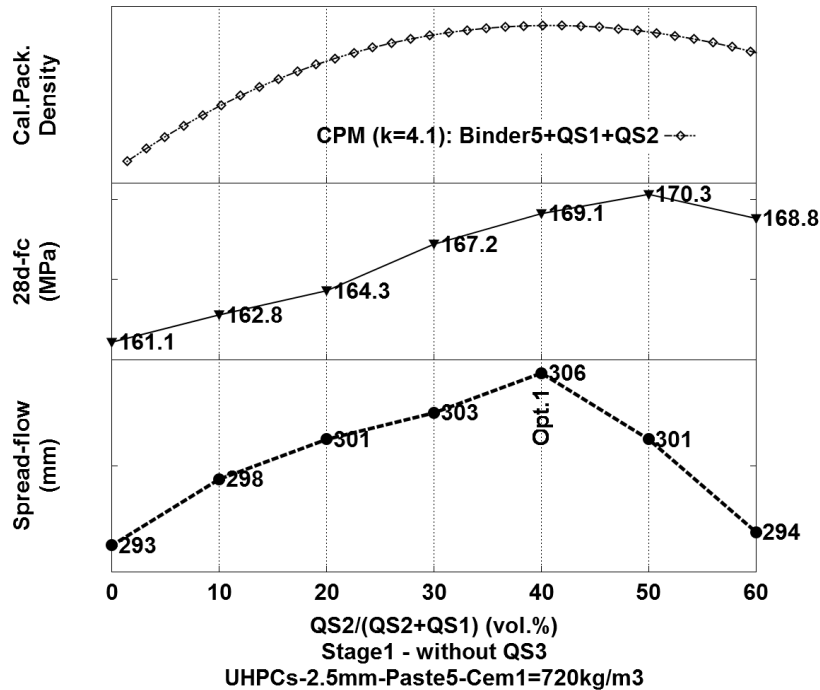


FIGURE 5.33.: STAGE1 - Stepwise optimization for UHPCs-2.5mm using Paste5 and QS1-QS2-QS3 aggregate. Two diagrams from bottom: the experimental results of the spread-flow and 28 days compressive strength of concretes with Paste5 containing 720 kg Cem1 when QS2 replaces QS1 step by step. The top diagram: estimation of the packing density of Binder5-QS1-QS3 mixtures, in which the volume mean diameter of Binder5 is 11.514  $\mu$ m and Binder5/(Binder5+QS1+QS3) ratio is 43.2 vol.%, using Compressible Packing Model with K-value of 4.1.

The first experimentally highest flowability of concrete was obtained at QS2/(QS1+QS3) ratio of 40 vol.%, and the first calculated highest packing density of Binder5-QS1-QS2

corresponded to  $QS2/(QS1+QS2)$  ratio of 40.14 vol.%. The final experimental results show the optimum UHPC-2.5mm-Paste5 has the highest spread-flow of 309 mm and the 28 days compressive strength of 172.2 MPa when  $QS3/(QS3 + \text{blend of } 40\% \text{ QS2 and } 60\% \text{ QS1})$  ratio was 10 vol.% (i.e.  $QS1/QS2/QS3 = 54/36/10$  vol.%) (notated UHPC-2.5mm-Paste5-54QS1-36QS2-10QS3). The calculated optimum aggregate corresponding to the computed highest packing density was good agreement with the experiment, expressed by  $QS1/QS2/QS3$  ratios of 52.81/35.41/11.78 vol.%.

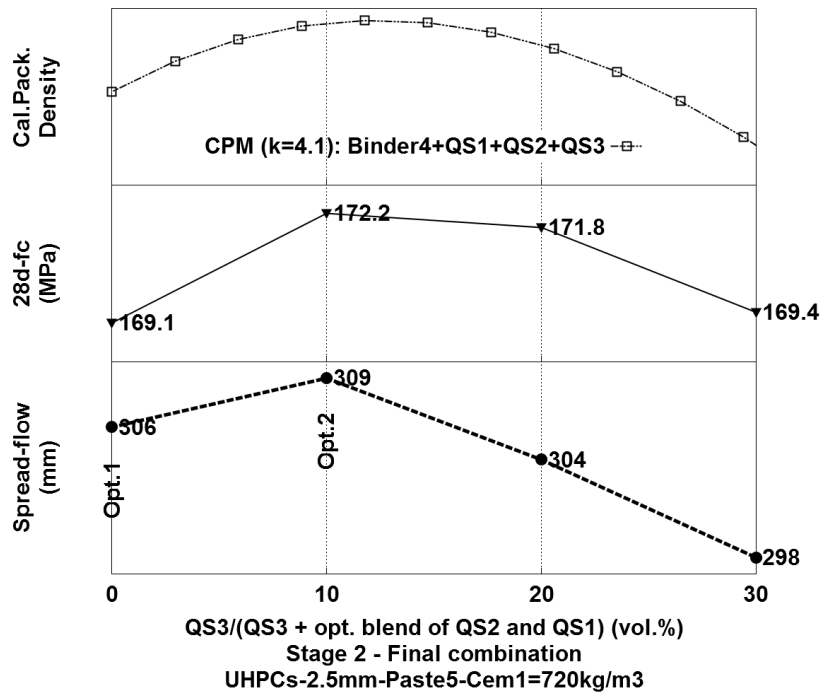


FIGURE 5.34.: STAGE2 - Stepwise optimization for UHPCs-2.5mm using Paste5 and QS1-QS2-QS3 aggregate. Two diagrams from bottom: the experimental results of the spread-flow and 28 days compressive strength of concretes with Paste5 containing 720 kg Cem1 when QS3 replaces the blend of 60 vol.% QS1 and 40 vol.% QS2 gradually. The optimum UHPC-2.5mm was determined at  $QS1/QS2/QS3 = 54/36/10$  vol.%. The top diagram: Estimation of the packing density of Binder5-QS1-QS3 mixtures, in which the volume mean diameter of Binder5 is 11.514  $\mu\text{m}$ ,  $\text{Binder5}/(\text{Binder5}+QS1+QS2+QS3)$  ratio is 43.2 vol.% and  $QS2/QS1$  ratio is 40.14/59.86 vol.%, using Compressible Packing Model with K-value of 4.1.

The self-flowability of UHPC-2.5mm-Paste5-54QS1-36QS2-10QS3 was much higher than that of the optimum UHPC-2.5mm-Paste3-54QS1-36QS2-10QS3, although they have the same paste content and the packing density of Paste5 was lower than that of Paste3. This can be attribute to the highly efficient filler effect of limestone powder due to its low Hamaker constant in water as introduced in section 2.2.1. However, similar to UHPC-2.5mm-Paste4-51QS1-34QS2-15QS3, the 28 days compressive strength of UHPC-2.5mm-Paste5-54QS1-36QS2-10QS3 was much lower than that of UHPC-2.5mm-Paste3-54QS1-36QS2-10QS3 due to low activity and low rate of reaction of ground granulated blast furnace slag compared to silica fume.

## 5. Mix proportioning of UHPC

UHPC-2.5mm-Paste5-54QS1-36QS2-10QS3 was not used for further investigation into steel fibre reinforced UHPC. However, its strength development was still examined and shown in Figure 5.35.

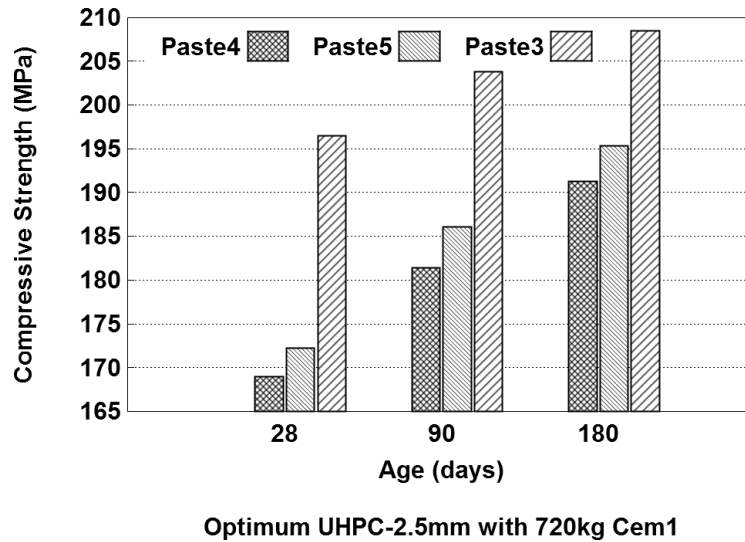


FIGURE 5.35.: Strength development of the optimum UHPC-2.5mm-Paste3, UHPC-2.5 Paste4 and UHPC-2.5 Paste5. The compressive strength developed quickly in the first 28 day, especially Paste3 containing SF2. Then, the strength developed slowly, the lowest rate for UHPC-2.5mm-Paste3 and the highest rate for concrete with Paste5 containing GGBFS.

## 5.5. Concluding remarks

### For mix proportioning of paste:

- Taking into account the cost and performance efficiencies of reactive and inert powders three different binder types were developed, representing some possible cases of the use of reactive and inert powders for high performance blended binder. Binder type 1 contained Cem1, quartz powder and ultra-fine silica fume SF2, in which a small amount of SF2 was used. Binder type 2 consisted of Cem1 and high amount of ultra-fine fly ash FA due to the high filler effect and low cost of ultra-fine fly ash FA. Binder type 3 included Cem1, ground granulated blast furnace slag (GGBFS) and ultra-fine limestone powder, in which a high amount of reactive GGBFS was used. However, GGBFS had a very low filler effect, the addition of the inert ultra-fine limestone powder was necessary to improve the packing density of binder type 3.
- The physical-chemical interaction of fines is very complicated. Therefore, the proportion of blended binder could not be calculated exactly by using the existing particle packing models. However, based on Fennis's idea described in 2.3.2.4 the modification of the loosening effect and wall effect coefficients of the Compaction - Interaction Packing Model (CIPM) taking into account the effect of surface forces of fines is expected for a good estimation of binder mix proportion.

- The addition of ultra-fine particles increases the packing density of blended binder but it also leads to a significant increase of total surface area of particles resulting in the decrease of the efficient water film thickness, which govern the flowability of paste. Therefore, concerning the workability improving the optimum mix proportion of blended binder having ultra-fine particle represents a compromise between improvement of the packing density of granular mixture and satisfaction of a sufficient fluidity.
- In this study the proportion of blended binders had to be determined experimentally. Based on the rule of stepwise combination for granular materials and by mean of the superplasticizer-water solution demand test method, the optimum proportions of blended binders were established regarding the improvement of packing density and fluidity.
- The saturated amounts of superplasticizer SP1 for the optimum binders at a given W/Cem1 ratio of 25 wt.% were determined by assessment of the paste viscosity and the concrete self-flowability when SP1 content varied. The viscosity of paste was measured by using a rotational rheometer. The results of paste viscosity were good agreement with the results of concrete spread-flow. Therefore, determination of the saturated superplasticizer amount based on assessment of the concrete spread-flow was recommended taking an extra useless consumption of superplasticizer in the liquid film around aggregate particles into account.
- The developed optimum pastes can be modified easily by varying the cement content to satisfy the concrete's requirements of self-flowing properties and 28 days compressive strength up to 190 MPa.

### **For mix proportioning of concrete:**

- Based on the rule of stepwise combination for granular materials and by assessment of the rheological of the whole concrete having a constant paste (content, mix proportion) the optimum proportions of blended aggregate were established taking into account the influence of the modification of aggregate (grading, packing density, shape) on the improvement of packing density and fluidity of the whole concrete.
- The experimental results indicate that the spread-flow of concrete is good agreement with its plastic viscosity. Concrete with the lowest viscosity also has the highest spread-flow. The increase of particle packing density of concrete resulted in a significant improvement of the plastic viscosity and the self-flowability. The compressive strength of concretes tend to increase as the packing density increased (smaller than 10%). However, the concrete with the highest packing density (recognized by the highest self-flowability and the lowest viscosity) is not insured to possess the highest strength.
- The experimental results pointed out that the use of the modified Andreasen and Andersen equation-based ideal curve cannot guarantee to achieve an optimum UHPC having a given and high paste volume because the materials characteristics such as shape, packing density, the surface forces of fines are not taken into account. In addition, the use of the highest packing density aggregate, which can be estimated by the existing particle packing models (the Compaction - Interaction Packing Model, the Compressible Packing Model) or determined experimentally, cannot insure to obtain the highest performances of self-flowability and viscosity for UHPC with a

## 5. Mix proportioning of UHPC

given and high paste volume. The interaction between fine particles of the given paste and coarse particles of aggregate have to be taken into account in the particle packing calculation of the whole concrete. The experiments based on the proposed approach of stepwise optimization of particle packing density have to be carried out to obtain the optimum concrete, and to verify the estimated result of mix proportion from the existing particle packing models.

- The Compressible Packing Model could be used to determine the optimum proportion of round granular aggregate mixture when it was assumed that binder had only one size of volume mean diameter. For aggregate mixture including angular particles the result of mix proportion computed by the Compressible Packing Model was much different with the result of experiment.
- The optimum UHPC-2.5mm-Paste4 and UHPC-2.5mm-Paste5 showed an excellent flowability but their strength development were slow, resulting in a low 28 days compressive strength of about 170 MPa in comparison to 28 days compressive strength of 196 MPa of the optimum UHPC-2.5mm-Paste3. Therefore, the optimum UHPC-2.5mm-Paste4 and UHPC-2.5mm-Paste5 were not used for further investigation on steel fibre reinforced UHPC. However, the use of the optimum UHPC-2.5mm-Paste4 and UHPC-2.5mm-Paste5 could be more attractive concerning their long-term strength (180 days compressive strength of about 190 MPa).
- The particle shape has a significant effect on the fluidity of concrete.
- Four developed concrete UHPC-1mm-Paste3, UHPC-2.5mm-Paste3, UHPC-4mm-Paste3, UHPC-8mm-Paste3 (see Table 5.2), were the standard mixtures for further development.

## 6. Steel fibre reinforced UHPC

### 6.1. Introduction

UHPC is very brittle when loaded. Thus, UHPC can absorb very little deformational energy before failure. Adding discrete short fibres to UHPC enhances the toughness, ductility and energy absorption capacity of the composite because a fibre in the path of a propagating crack bridges the crack opening and resists further crack growth by dissipating energy during pull-out. According to Naaman [2003a], in order to be effective in brittle UHPC matrix, fibres must have the following properties: (i) a tensile strength significantly higher than that of concrete; (ii) a bond strength with the concrete matrix preferably of the same order as or higher than the tensile of matrix; (iii) an elastic modulus in tension significantly higher than that of the concrete matrix; (iv) the Poisson's ratio and the coefficient of thermal expansion preferably of the same order as the matrix. That is why steel fibre is the most suitable fibre for UHPFRC.

The tensile stress in the composite at the first cracking of matrix ( $\sigma_{cc}$ ), and the ultimate tensile stress ( $\sigma_{pc}$ ) can be calculated by Equations (6.1) and (6.2) respectively (Naaman [1972, 2003b], Bentur and Mindess [2007]). In addition, the critical volume fraction of fibres for obtaining strain-hardening with 3-D random fibres distribution can be estimated by Equation (6.3). In order to use Equation (6.2) in the post-cracking zone, it is assumed that: (i) a critical crack exists across the entire section of the tensile member, (ii) the crack is normal to the tensile stress field, and (iii) the contribution of the matrix is negligible. Figure 6.1 shows the stress-strain response of high performance fibre reinforced concrete (HPFRC) in comparison to conventional fibre reinforced concrete.

$$\sigma_{cc} = \sigma_{mu}(1 - V_f) + \alpha_1 \alpha_2 \tau_f V_f \frac{L_f}{D_f} \leq \sigma_{mu} \left[ 1 + \left( \frac{E_f}{E_m} - 1 \right) V_f \right] \quad (6.1)$$

where:  $V_f$ , volume fraction of fibres;  $L_f$ , fibre length;  $D_f$ , fibre diameter;  $L_f/d_f$ , fibre aspect ratio;  $\sigma_{mu}$ , tensile strength of the matrix;  $\tau_f$ , average fibre-matrix bond strength, constant along the entire fiber length;  $\alpha_1$ , coefficient representing the fraction of of bond mobilized at first matrix cracking;  $\alpha_2$ , efficiency factor of fibre orientation in the uncracked state of the composite;  $E_f/E_m$ , the ratio of the elastic moduli of fibre and matrix.

$$\sigma_{pc} = \lambda_1 \lambda_2 \tau_f V_f \frac{L_f}{d_f} \quad (6.2)$$

where:  $\lambda_1$  and  $\lambda_2$  are the orientation and efficiency factors of fibres.

$$(V_f)_{critical} = \frac{2\sigma_{mu}}{\tau_f} \frac{1}{\frac{L_f}{D_f}} \quad (6.3)$$

6. Steel fibre reinforced UHPC

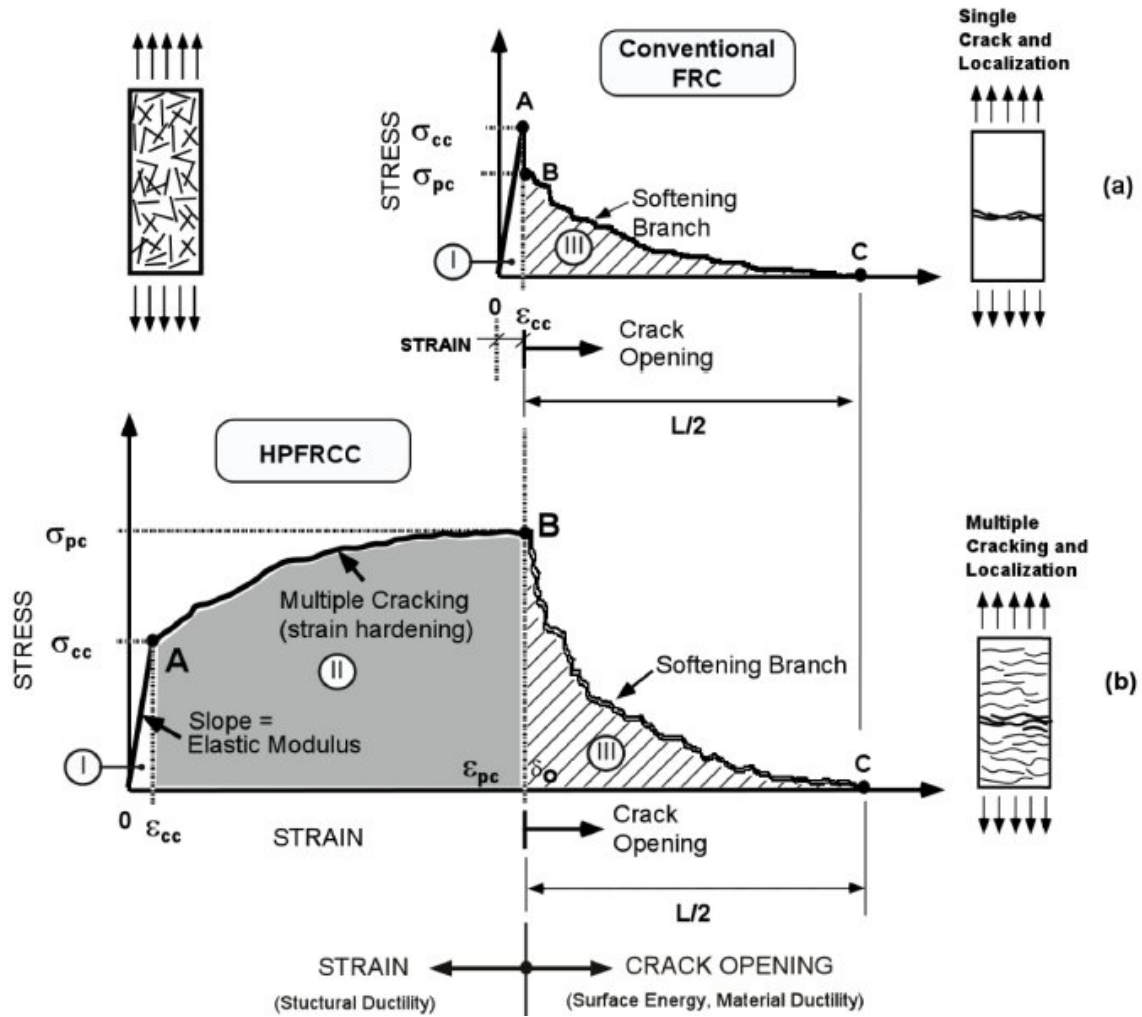


FIGURE 6.1.: Stress-strain (or elongation) curve in tension of fibre reinforced concretes: (a) strain-softening conventional fibre reinforced concrete; (b) strain-hardening high performance fibre reinforced concrete (Naaman [2003a]).

Equation (6.1) indicates that the first cracking tensile stress  $\sigma_{cc}$  of UHPFRC and the tensile strength of matrix  $\sigma_{mu}$  are nearly same if steel fibre content is low.

Improvement of the post-cracking strength is an important aim of UHPFRC mix design. Based on the working mechanism of the cementitious composite described by Equation (6.2), various approaches have been proposed.

- It is clear to realize that if the volume fraction of fibres ( $V_f$ ), the fibre length ( $L_f$ ) and the average bond strength at the fibre matrix interface ( $\tau_f$ ) are kept constant, the reduction of fibre diameter ( $D_f$ ) increases the density of fibre crossing ( $\lambda_3$ ) as well as the fibre aspect ratio, resulting in increase of the ultimate tensile stress ( $\sigma_{pc}$ ). However, the smaller the fibre diameter is, the larger the total surface area of fibres have, the interaction between fibres and granular concrete mixture is stronger. Therefore, the workability of fibre concrete is affected considerably, a high paste volume is needed. This is suitable to explain for the reason of using fine steel fibre in

reinforcing UHPC, which have high paste volume and fine aggregate in comparison with other kind of concrete.

- The densification of the transition zone between fibre and matrix by ultra-fine particles with high chemical - filler effect and the improvement of the mechanical bond between fiber and matrix by modification of the fibre geometry are feasible to increase the post-cracking strength of the composite with a given fibre volume content and fibre aspect ratio.
- Using high fibre content and long fibre allow to increase the ultimate tensile stress ( $\sigma_{pc}$ ) but the cost of UHPFRC increases, the mixing and casting of fiber UHPC are very difficult.

Basically, the average fibre-matrix bond strength ( $\tau_f$ ) is governed by adhesion, friction and mechanical anchorage by deformations on the fibre surface or by overall complex geometry (Bentur and Mindess [2007]). Many studies (Bathia and Trottier [1994]; Robins et al. [2002]; Cunha et al. [2010]; Zile and Zile [2013]) pointed out that mechanically deformed fibers are more effective than straight fibers in improving the fibre-matrix interactions, resulting in a better pullout resistance as well as flexural and tensile behaviours, for examples in case of UHPFRC:

- For straight smooth fibre with embedded length of  $L_f/2$ : Orange et al. [2000] and Wuest [2007] measured  $\tau_f$  of 10 MPa and 6.9 MPa for fibre sizes of  $L_f/D_f = 5\text{mm}/0.2\text{mm}$  and  $L_f/D_f = 10\text{mm}/0.2\text{mm}$  respectively. Chan and Chu [2004] reported that  $\tau_f$  slightly increases from 4.82 MPa to 5.48 MPa when silica fume content of Reactive Powder Concrete increases up to 30 wt.% of cement for a fibre size of  $L_f/D_f = 13\text{mm}/0.16\text{mm}$ .
- Naaman [2000] invented twisted polygonal fibre. An intensive investigation was carried out by Naaman and coworker (Chandransu and Naaman [2003], Sujivorakul and Naaman [2003], Kim et al. [2008], Wille and Naaman [2012]) at the University of Michigan to compare the effectiveness of smooth, hooked, and twisted polygonal fibre in reinforcing cement composites. The results demonstrated that twisted polygonal fibre is the best fibre, the fibres achieve the most effective mechanical bond and provide a slip-hardening bond stress. Wille [2012] reported that the equivalent bond strength of deformed fibres embedded in UHPC was five times the equivalent bond strength of straight fibers embedded in the same matrix. The equivalent bond strength of straight steel fibres could be improved by optimizing the UHPC matrix through composition and particle size distribution, reported  $\tau_f$  of 8.7 MPa for a fibre size of  $L_f/D_f = 13\text{mm}/0.2\text{mm}$ .
- Wille et al. [2011, 2012] investigated the tensile and bending behaviour of UHPFRC using straight smooth steel fibre ( $L_f/d_f = 13\text{mm}/0.2\text{mm}$ ), hooked steel fibre ( $L_f/D_f = 30\text{mm}/0.38\text{mm}$ ) and tailoring twisted polygonal fibre ( $L_f/D_f = 30\text{mm}/0.3\text{mm}$ ), and reported that the ratio of equivalent bending strength to direct tensile strength ranged between 2.4 and 2.65. Using an UHPC matrix with a compressive strength of 200 MPa the ultimate tensile stress  $\sigma_{pc}$  were 14.2 MPa, 14 MPa, 14.9 MPa corresponding with 2.5 vol.% straight smooth steel fibre ( $V_f \cdot L_f/D_f = 1.625$ ), 2 vol.% hooked steel fibre ( $V_f \cdot L_f/D_f = 1.579$ ) and 2 vol.% twisted polygonal fibre ( $V_f \cdot L_f/D_f = 2.0$ ) respectively.

## 6. Steel fibre reinforced UHPC

Actually, UHPFRC with a strain-hardening behaviour is expected for structural application. It is, however, not a simple way of adding high volume fibre which can be computed by Eq. (6.3). The UHPC matrix and fibre content, geometry have to be tailored to achieve the optimum rheological behaviour in the fresh state as well as the highest mechanical performance in the hardened state of fibre concrete.

Grünewald and Walraven [2001, 2004], Dhonde et al [2007], Ferrara et al [2007] and Martinie et al. [2010] demonstrated that the workability of fibre self-compacting concrete decreases corresponding the increase of the yield stress when the product  $V_f^*L_f/D_f$ , defined as the fiber factor, increases. In addition, Swamy and Mangat [1974] and Grünewald and Walraven [2001, 2004] emphasized that it is important to determine the critical concentration of fibres to prevent forming of fibre clumps or balls in concrete mixture and to ensure a uniform fibre distribution, the critical concentration of fibres is depended on concrete matrix composition and fibre characteristics.

Martinie et al. [2010] proposed Equation (6.4) to estimate the maximum amount of fibers in fine UHPC, above that fibers tend to form clumps or balls and entrap air in the mixture.

$$(V_f)_{max-concentration} = \frac{400}{\frac{L_f}{D_f}} \left(1 - \frac{V_S}{\beta_S}\right) \quad (6.4)$$

where:  $L_f$ , fibre length;  $D_f$ , fibre diameter;  $V_S$ , volume fraction of sand in the mixture;  $\beta_S$ , packing density of the sand. Martinie suggested a  $\beta_S$  value of 0.65 for fine UHPFRC with rounded sand.

In the priority program SPP 1182 of the German Research Foundation, an intensive investigation was performed by Fröhlich and Schmidt [2014] to evaluate the test methods for assessment of UHPFRC performance in fresh and hardened states. Two types of straight smooth steel fibre were used, short fibre with  $L_f/D_f$  ratio of 9mm/0.22mm and long fibre with  $L_f/D_f$  ratio of 17mm/0.22mm. The results showed that the slump flow of fibre concretes were decreased significantly when fibre contents increased up to 2.5 vol.%, UHPC with 8 mm coarse aggregate was strongly affected by fibre content in comparison to fine grain UHPC (M2Q, M3Q and B5Q mixtures as shown in Table 1.1 in Chapter 1). In addition, the increase of fibre length, volume led to a significant increase of post-cracking flexural tensile strength and toughness.

In summary, the optimum fibre content of UHPFRC represents a good compromise between mechanical properties in the hardened state and workability in the fresh state.

## 6.2. Investigation objective and methodology

### 6.2.1. Investigation objective

In the previous work four optimum self-compacting UHPCs were developed, these mixtures had different maximum grain size of 1 mm, 2.5 mm, 4 mm, 8 mm and compressive strength of about 190 MPa as described in Table 5.2 in section 5.4.4.1. In this investigation

six different high strength steel fibres were employed to improve the ductility of these UHPCs. Four micro steel fibres were two types of smooth straight fibres (F1:  $L_{f1}/D_{f1} = 13\text{mm}/0.2\text{mm}$ ; F2:  $L_{f2}/D_{f2} = 20\text{mm}/0.2\text{mm}$ ) and two types of crimped fibres (F3:  $L_{f3}/D_{f3} = 9\text{mm}/0.12\text{mm}$ ; F4:  $L_{f4}/D_{f4} = 12\text{mm}/0.18\text{mm}$ ) while two indented macro steel fibres were hooked ends fibre (F5:  $L_{f5}/D_{f5} = 30\text{mm}/0.55\text{mm}$ ) and straight fibre (F6:  $L_{f6}/D_{f6} = 25\text{mm}/0.3\text{mm}$ ), as represented in Figure 6.2. Fibre F1 was OL 13/0.20 steel fibre type from Bekaert, its tensile strength was  $2600\text{ N/mm}^2$ . Fibres F2, F5, F6 with tensile strength of  $2200\text{ N/mm}^2$  were supplied by Stratec Abrasive and Fibre Technology GmbH having trade names of FM 20/0.2, FE 30/0.55 and FG 25/0.3. Fibres F3 and F4 having tensile strength of  $3300\text{ N/mm}^2$  were produced by Voestalpine Special Wire GmbH.

The objective of this investigation was to determine the most effective fibre for producing self-compacting UHPFRC considering the improvement of tensile performance and material saving.

First, the pullout tests were carried out to assess the influence of fibre geometries on the pullout resistance. Because fibre F1 ( $L_{f1}/D_{f1} = 13\text{mm}/0.2\text{mm}$ ) and fibre F2 ( $L_{f2}/D_{f2} = 20\text{mm}/0.2\text{mm}$ ) were the smooth and straight fibres and their fibre-matrix bonds were similar, fibres F1 and F2 were then selected for the investigation into the influence of the fibre types, volume and the matrices composition on the self-flowing ability and the mechanical behaviour of UHPFRCs. In a further investigation, the fine UHPC with maximum grains of 1 mm was modified by increasing the cement content for a more fibre addition to guarantee a higher 7 MPa ultimate tensile strength of UHPFRC. A comparative investigation into the mechanical behaviour of the UHPFRCs with six different fibre types was conducted employing bending and direct tensile tests. Furthermore, the tensile constitutive properties of UHPFRCs were estimated by an inverse analysis based on the four-point bending test results. The most effective steel fibre for reinforcing UHPCs could be selected convincingly.

### 6.2.2. Testing methods

**Mixing procedure:** A concrete batch of 30-60 liters for producing specimens of compressive, flexural, tensile tests was produced using an ELBA Laboratory Compulsory Mixer, see Figure 6.3. The speed of the spiral mixing tool of the mixer is controlled by changing the frequency of current using an inverter. The mixing procedure was as follows: (i) dry cementitious mixture including cement, quartz powder, silica fume (and other powders if any) were added to the mixer, then mixed for 60 seconds at the speed I of 25 round per minute; (ii) 80 wt.% water was added for 60 seconds while the mixing tool was working at the speed I, the premixed remaining water with superplasticizer was then added for 30 seconds; (iii) the paste was homogenized for 240 seconds at the mixing tool speed II of 50 round per minute; (iv) the aggregate was added to the paste at the mixing tool speed I for 120 seconds and concrete was homogenized for 120 seconds at the mixing tool speed II; (v) for fibre adding, the micro steel fibre had to be gone through a mesh with 15 mm mesh opening to against the forming of fibre ball, as shown in Figure 6.3, the further mixing time at this stage was 180 seconds.

**Casting and curing:** all specimens were casted without any compaction. After

## 6. Steel fibre reinforced UHPC

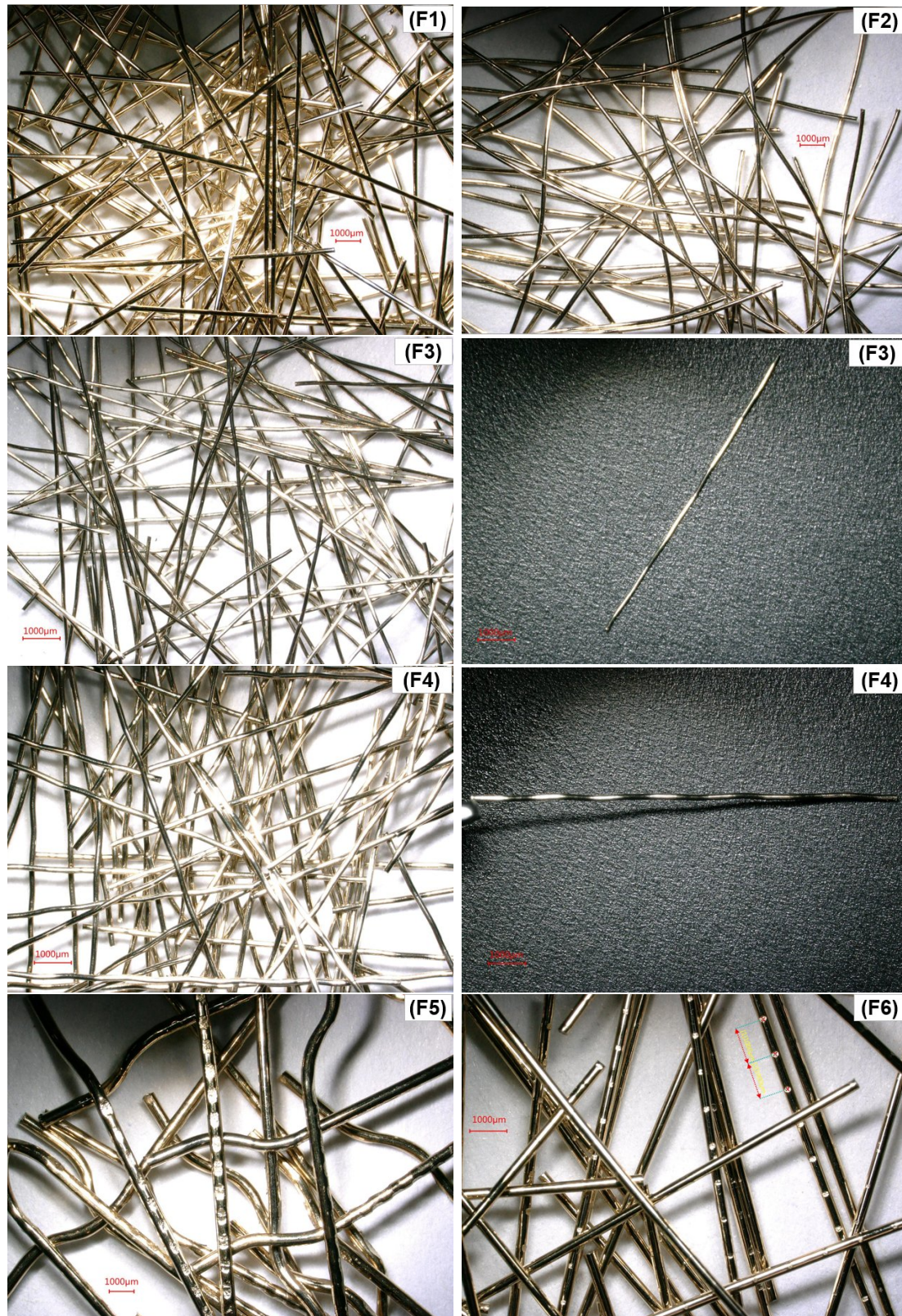


FIGURE 6.2.: The used fibres in the research project: smooth straight fibres: F1 -  $L_1/D_1 = 13\text{mm}/0.2\text{mm}$ , F2 -  $L_2/D_2 = 20\text{mm}/0.2\text{mm}$ ; crimped fibres: F3 -  $L_3/D_3 = 9\text{mm}/0.12\text{mm}$ , F4 -  $L_4/D_4 = 12\text{mm}/0.18\text{mm}$ ; indented and hooked ends fibre: F5 -  $L_5/D_5 = 30\text{mm}/0.55\text{mm}$ ; indented straight fibre: F6 -  $L_6/D_6 = 25\text{mm}/0.3\text{mm}$ .



FIGURE 6.3.: Compulsory Mixer for preparation of UHPFRC.

casting, the specimens were covered with plastic sheet and stored at room temperature for 24 hours. The specimens were then removed from their moulds and stored at ambient laboratory conditions for additional 27 days. All mechanical tests were carried out at 28 days of age of concrete.

**Slump-flow test:** according to DIN EN 12350-8 [2010] was applied to assess the self-flowability of UHPCs with and without fibres. Two minutes after cone lifting, from the spread-flow of the concrete, two diameters perpendicular to each other were determined and their mean was reported, the T500-time was also recorded in the test.

**Specimens preparation and compression test:** The compression test was carried out according to DIN EN 12390-3 [2009]. For each UHPFRC mixture, six cube specimens of 100 mm were produced to determine the compressive strength. Both loading faces of all specimens were ground before testing. The loading rate was 0.6 MPa/s. The mean values were reported.

**Specimens preparation and pullout test:** The pullout test can be carried out using single-sided specimens (Grünwald [2004]; Markovic [2006]; Cunha [2010]) or double-sided specimens (Bathia and Trottier [1994]; Robins et al. [2002]; Chan and Chu [2004]) with a single fibre or an array of fibres. The advantages and disadvantages of these pullout test configuration were analyzed in detail by Cunha [2010]. In this research project, single-sided specimens were applied for pullout test, as shown in Figure 6.4. For each kind of fibre fifteen separated fibres were stuck vertically into three bases made of Styropor<sup>®</sup>, each base with size of 20x40x160 mm<sup>3</sup> included five fibres. The styropor bases with fibres were put into a three-gang mould 40x40x160 mm<sup>3</sup>. The fresh UHPC with maximum grains of 1 mm was then filled into the mould. Thus, the protruding part of the fibre from the styropor base was the embedded length of the fibre in UHPC matrix and equals a half fibre length. A servo-controlled universal testing machine with a capacity of 1000 kN was used. In order to obtain a high precise of the load values, a HBM<sup>®</sup> load cell with a capacity of 2 kN was attached to the machine test frame. The styropor was removed at 28 days of age of concrete for fibre pullout test. The concrete block with five free part of fibres (that get out of concrete block) was kept tightly on the bedplate of the machine. The free part of the single fibre was held securely by a grip, as described in Figure 6.5. The rate of displacement of the loading head was constant 0.05 mm/min during testing. Linear

## 6. Steel fibre reinforced UHPC

Variable Differential Transformer (LVDT) could not be fixed to measure the fibre pullout slip due to the very short length of the fibre as also of the protruding end. Therefore, only the data of pullout force and crosshead displacement were recorded. The average fibre-matrix bond strength  $\tau_f$  is computed by Equation 6.5

$$\tau_f = \frac{F_{max}}{\pi D_f L_{f,embedded}} \quad (6.5)$$

where:  $F_{max}$ , maximum pull-out load;  $D_f$ , fibre diameter;  $L_{f,embedded}$ , fibre embedded length.



FIGURE 6.4.: Specimens preparation for pullout test.



FIGURE 6.5.: Configuration of the single fibre pullout test. The embedded length equals a half length of fibre.

**Specimens preparation and bending test:** For each UHPFRC mixture, six beams of  $140 \times 140 \times 560 \text{ mm}^3$  (which allows a 3-D orientation of fibres) were produced to investigate the effectiveness of fibres in improving the ductility and toughness of UHPC. Self-compacting UHPFRC was poured, without vibration, at one end of the mould and left to spread into place. Four-point bending test on unnotched specimen was carried out according to the ASTM C1609/C1609M [2012], standard test method for flexural

## 6.2. Investigation objective and methodology

performance of fiber reinforced concrete. The parameter calculations when Peak Load (Modulus of Rupture) is greater than First-Peak Load in accordance with this standard is shown in Figure 6.6. The First-Peak point is defined as a point where the slope is zero. However, in all case of this investigation, the UHPFRCs showed a stable deflection-hardening, the First-Peak Load could not be determined clearly. ASTM C1609/C1609M defines that the total area under the load - deflection curve up to a net deflection of  $L/m$  is the toughness  $T_m^D$ , in which  $L$  is the span length and  $m$  is a positive number. In this investigation, toughness value at a certain deflection is an important information to evaluate the effect of fiber type, volume on the energy absorption capacity of concrete. For this purpose, besides the point of the Peak Load, three points corresponding to the deflections of  $L/1000 = 0.42$  mm,  $L/600 = 0.7$  mm,  $L/150 = 2.8$  mm were considered for the comparative calculation regarding toughness and residual strength. A servo-controlled bending machine was used, the rate of displacement of the loading head was constant 0.2 mm/min during testing. The test setup is illustrated in Figures 6.7.

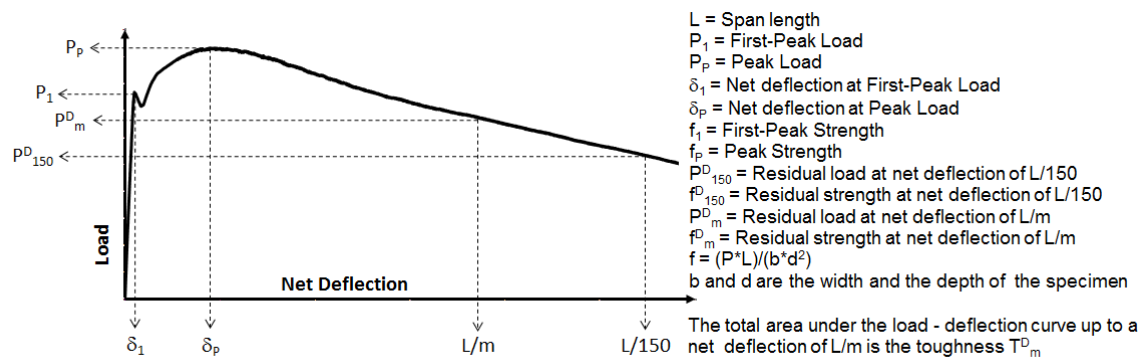


FIGURE 6.6.: Example of parameter calculations when Peak Load greater than First-Peak Load according to the ASTM C1609/C1609M.

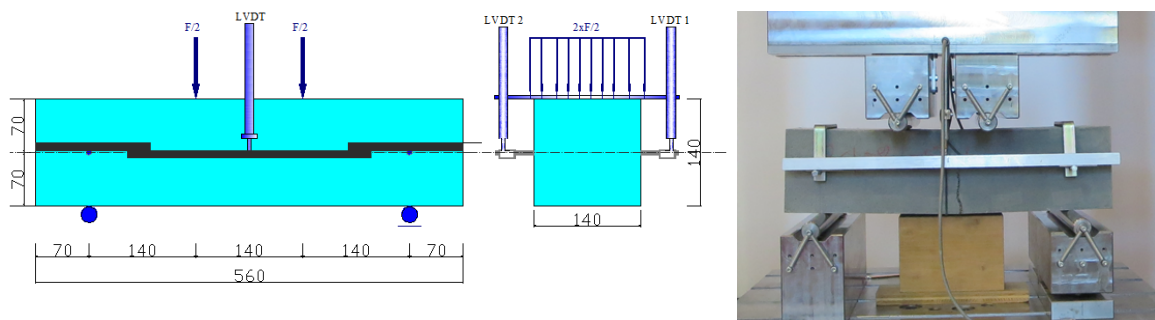


FIGURE 6.7.: Four-point bending test on unnotched beam of  $140 \times 140 \times 560$  mm<sup>3</sup> according to the ASTM C1609/C1609M

**Specimens preparation and direct tensile test:** A standard test method for determination of the direct tensile behaviour of UHPFRC is not available currently. However, various configurations of direct tensile test were introduced in literature, as summarized by Wille [2014]. Figure 6.8 shows some kind of end shapes of uniaxial tension

## 6. Steel fibre reinforced UHPC

test specimens (Kasai and Ikeda [1993], from Kanakubo [2006]), including three boundary conditions of pin-pin, pin-fix and fix-fix. Kanakubo [2006] indicated that failure often occurs at the end of specimen or grip portion in the specimens with a uniform cross section. Furthermore, the effect of bending moment on the direct tensile behaviour is significant in a direct tensile test. The bending moment effect can be reduced when the pin-pin condition is used. Figure 6.9 shows a direct tensile test setup developed by Graybeal and Baby [2013] for both cast and extracted UHPFRC specimens.

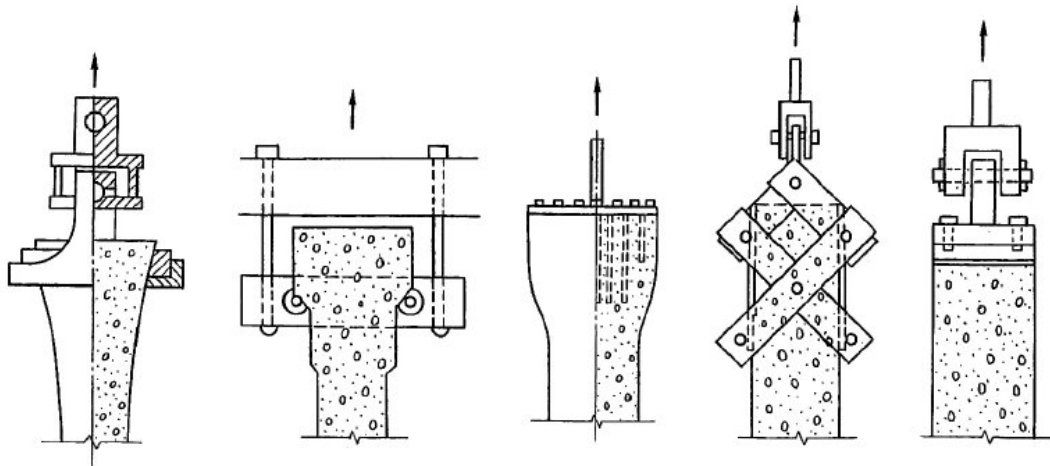


FIGURE 6.8.: Example of end shapes for direct tensile test (Kasai and Ikeda [1993], from Kanakubo [2006]).

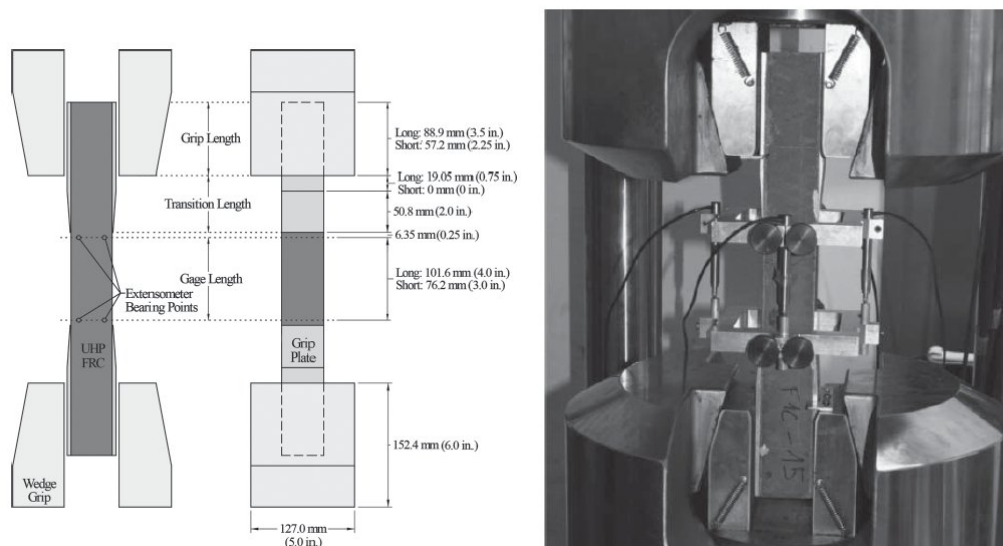


FIGURE 6.9.: Direct tensile test setup developed by Graybeal and Baby [2013]

In this research project, dog-bone shape specimens with a circular bays, which reduces stress concentration and allows the failure occur at the weakest spot in the material (Vliet and Mier [2000]), were used, as illustrated in Figure 6.10. The cross section area in the

## 6.2. Investigation objective and methodology

middle (50mm x 150mm) of the specimen is 40% smaller than that of the specimen ends. Self-compacting UHPFRC was poured, without vibration, at one end of the mould and left to spread into place. After casting, the specimens were covered with plastic sheet and stored at room temperature for 24 hours. Then, the specimens were removed from their moulds and stored at ambient laboratory conditions for additional 27 days. The tension test was carried out at 28 days age of the specimen. The bottom end of the specimen was fixed on the bedplate of test machine and the top end of the specimen was connected to an adapter having a pin to create rotating boundary condition. The strain was captured with a parallel ring extensometer containing four linear variable differential transformers (LVDTs), the gage length was 320 mm. Tests were performed under displacement control with a constant displacement rate of 0.0025 mm/s. There specimens were tested for a fibre content of each kind of fibres.

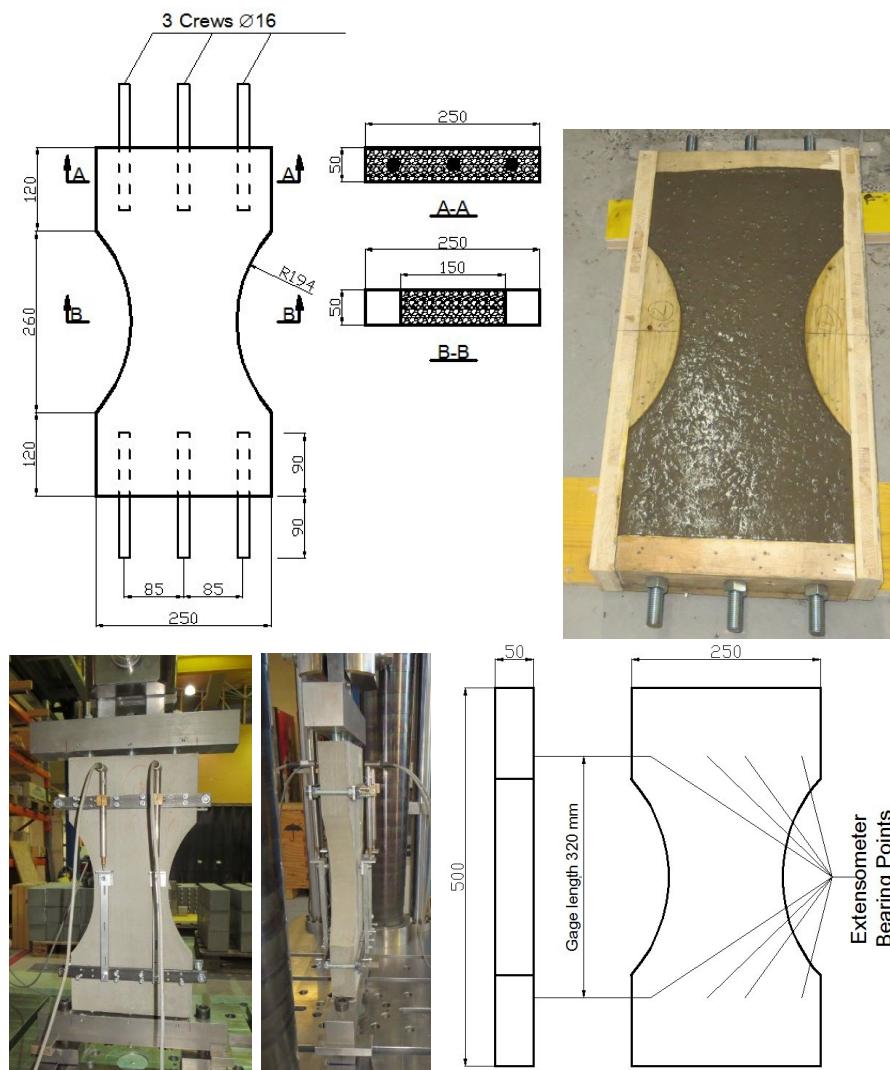


FIGURE 6.10.: Specimen preparation and direct tension test setup.

### 6.2.3. Inverse analysis based on four-point bending test for estimation of the tensile constitutive properties of UHPFRC

Kanakubo [2006] indicated that specimen geometry, size and boundary conditions have a significant influence on results of the direct tensile tests. In this research project in order to obtain a good analysis and interpretation of the experimental results a back calculation based on four-point bending test for estimation of the tensile properties was performed.

Several back-calculation methods were proposed to estimate the tensile behaviour of UHPFRC based on four-point bending test (AFGC [2013]; Baby et al. [2013]; Lopez et al. [2015]). In this research project the inverse analysis approach developed by Lopez et al. [2015] was used. Lopez's method is described as an iterative method based on a complete experimental law using load-deflection. In the method Lopez proposed an equation that relates the experimental mid-span deflection ( $\delta$ ) and curvature ( $\chi$ ), and an analytical moment ( $M$ ) - curvature ( $\chi$ ) close-form formulation. In the method a constitutive law in both compression and tension is assumed. These parameters are then modified during the iterative process to minimize the error between the experimental moment ( $M_{exp}$ ) - curvature curve ( $\chi$ ) and the analytical moment ( $M$ ) - curvature curve ( $\chi$ ). The inverse analysis procedure is illustrated in Figure 6.11.

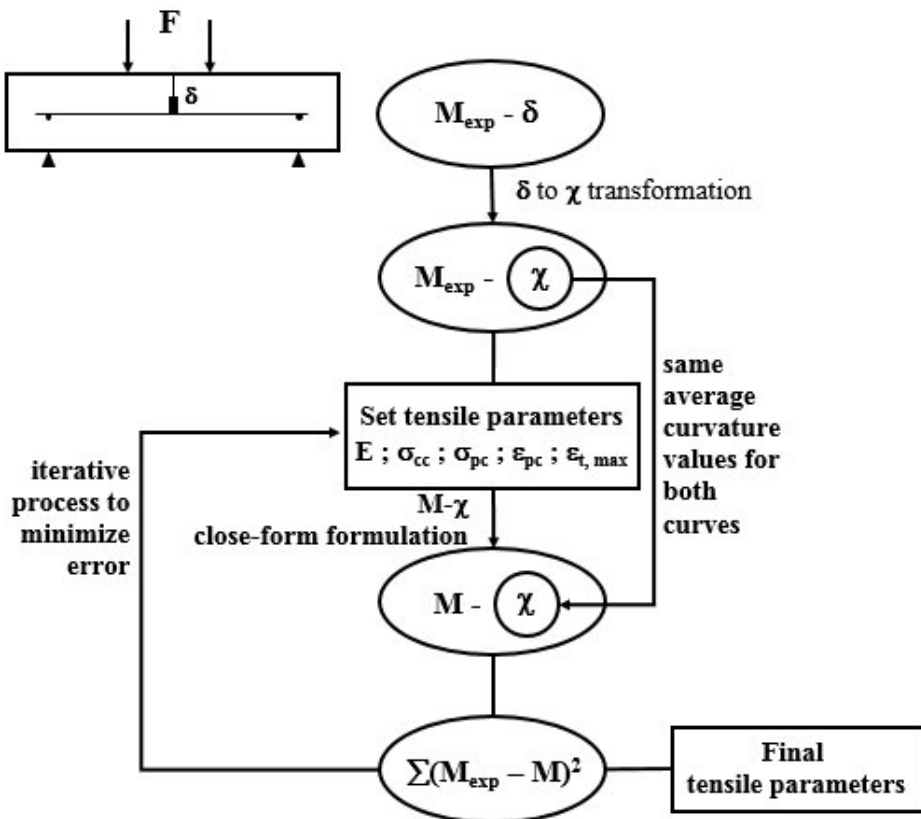


FIGURE 6.11.: Scheme for the inverse analysis procedure acc. to Lopez et al. [2015].

### 6.3. Experimental results

#### 6.3.1. The effect of fibre types on fibre pullout resistances

The optimum UHPC-1mm having 193.5 MPa compressive strength ( $f_{c,cube}$ ) was used for fibre pullout tests. The pullout test results of each kind of fibre are represented in Figures 6.12, 6.13, 6.14. Obviously, the mechanical anchorage play an important role in improving fibre pullout resistances when the average fibre-matrix bond strength  $\tau_f$  of the deformed fibres F3, F4, F5 in UHPC-1mm matrix were much higher than that of smooth straight fibres F2 and F2 and indented straight fibre F6. However, a high risk of fibre failure have to be considered in case of high bond strength fibre-matrix together with long embedded length of fibre.

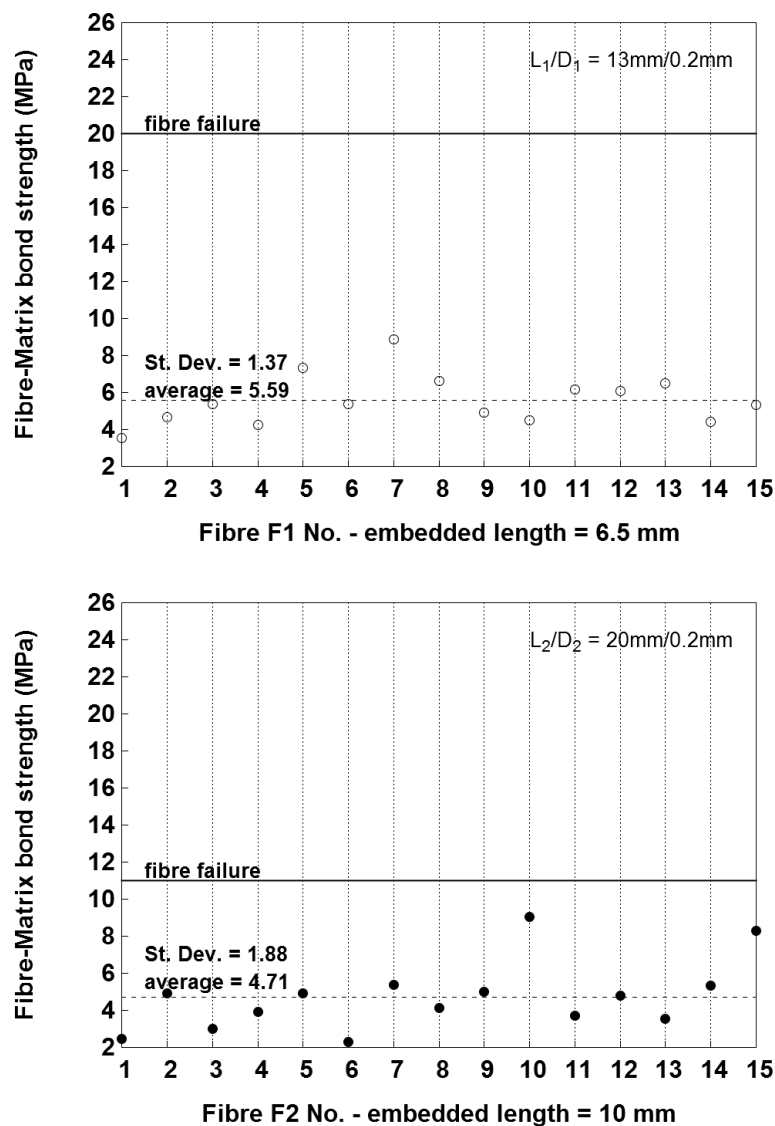


FIGURE 6.12.: The pullout resistances of smooth straight fibres F1 and F2 in the matrix of UHPC-1mm. The fibre-matrix interaction is governed by chemical bond and friction.

## 6. Steel fibre reinforced UHPC

It should be noted that the average fibre-matrix bond strengths of fibres F1 and F2 were relative low in comparison with the reported values of literature mentioned in section 6.1.

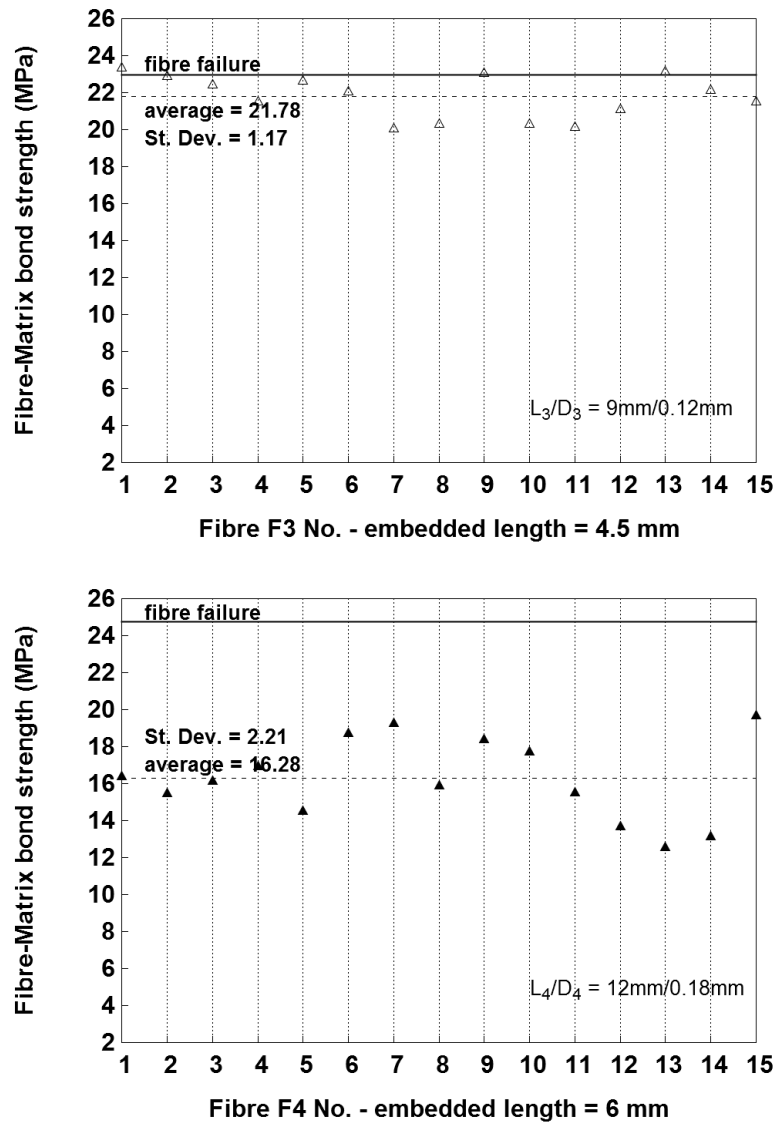


FIGURE 6.13.: The pullout resistances of crimped fibres F3 and F4 in the matrix of UHPC-1mm.

A very high bond between crimped fibre F3 and the matrix UHPC-1mm led to a very high uniaxial tensile stress in the fibre, which were equal to or very closed to the fibre ultimate tensile stress, due to its small diameter. The failure of a half of number of tested fibres implied the disadvantage of fibre F3 in UHPC matrix having 190 MPa compressive strength at 28 days and higher with time. A shorter fibre length is required to against the fibre failure but the efficiency in strengthening is reduced. A longer wavelength or a decrease of the wave height could be a suitable solution for fibre F3. Fibre modification, however, is not discussed in this research project. The geometry of fibre F4 was quite good, fibre-matrix bond was high but was safe to use regarding the strength development

of UHPC matrix. Clearly, fibres F3 and F4 are very appropriate for a conventional UHPC matrix with 150 MPa at 28 days age because of their good mechanical anchorage.

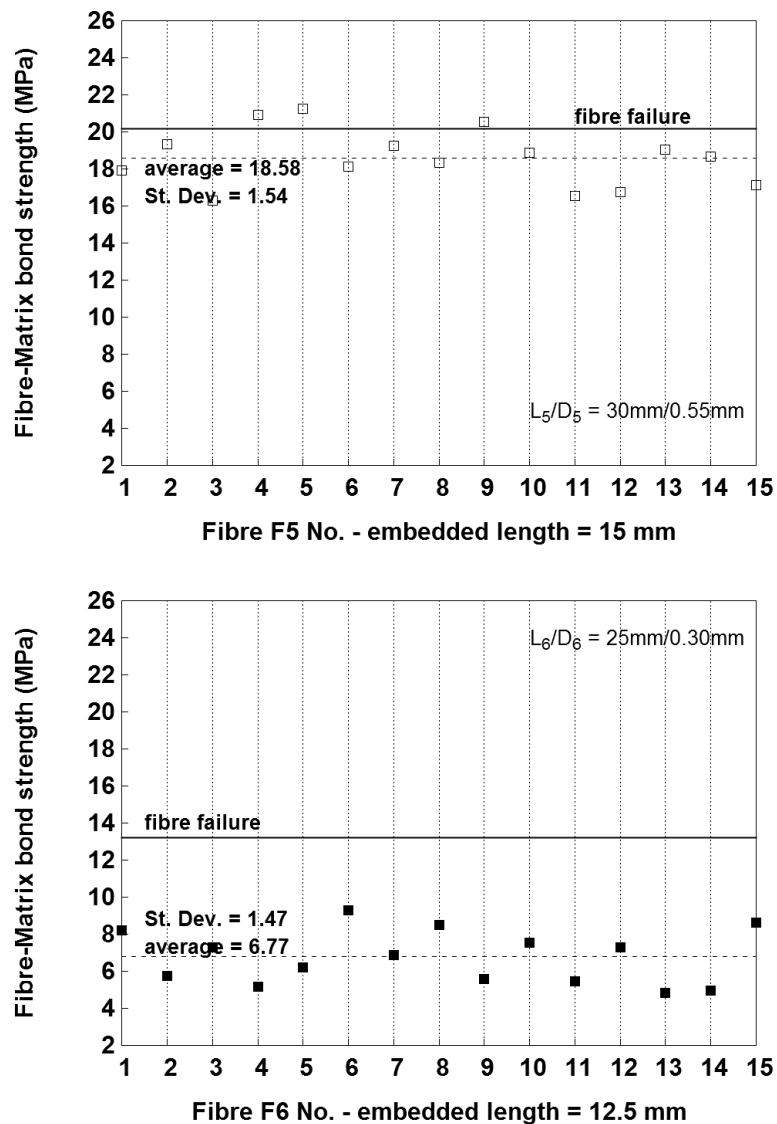


FIGURE 6.14.: The pullout resistances of indented hooked ends fibre F5 and indented straight fibre F6 in the matrix of UHPC-1mm.

The experimental results of fibres F5 and F6 indicated that the effect of the hooked ends on improving pullout resistance was much higher than that of the indented surface. However, a high risk of fibre failure was recognized for fibre F5. A shorter fibre length or no indented surface could be a good solution for fibre F5 in a matrix with higher 190 MPa compressive strength at 28 days age. The fibre F6 with indented surface shows a better bond with matrix in comparison to the smooth straight fibres F1 and F2.

Normally, it is expected that the higher the fibre-matrix bond is, the better mechanical behaviour the composite shows. However, the working mechanism of the cementitious

## 6. Steel fibre reinforced UHPC

composite described by Equation (6.2) points out that it is impossible to predict the mechanical properties of composite only based on the single fibre pullout test results.

### 6.3.2. The effect of fibre types, content and matrix compositions on the properties of UHPFRC in fresh and hardened states

For the application of the four developed optimum UHPC matrices (UHPC-1mm, UHPC-2mm, UHPC-4mm and UHPC-8mm) it was necessary to investigate the influence of fibre types, content and matrix compositions on the self-flowability in fresh state as well as on the compressive, flexural, direct tensile behaviours in hardened state of UHPFRC.

Fibre F1 and fibre F2 were smooth and straight fibres, they had the same diameter, their pullout resistances in UHPC-1mm matrix were similar. Therefore, fibres F1 and F2 were selected for the investigation.

First, the maximum fibre concentration for obtaining self-flowing properties of UHPFRC was determined experimentally. The flexural and tensile behaviours of UHPFRCs with the maximum fibre concentration were then examined.

#### 6.3.2.1. Effect of fibres F1, F2 contents and matrix compositions on the flowability of UHPFRCs

Table 6.1 shows the experimental results of the maximum concentration of fibres F1 and F2 for self-compacting UHPFRC using the four developed optimum UHPC matrices. Figure 6.15 shows the experimental results of slump-flow and T500-time of these UHPFRCs with a fibre volume of no higher than the maximum fibre concentration for achieving a slump-flow of more than 650 mm. It is interesting to recognize that in case of UHPC-1mm-720kgCem1 the estimated maximum fibre concentrations of fibre F1 ( $L_{f1}/D_{f1} = 13\text{mm}/0.2\text{mm}$ ) (1.8 vol.%) and Fibre F2 ( $L_{f2}/D_{f2} = 20\text{mm}/0.2\text{mm}$ ) (1.16 vol.%) applying Eq. (6.4) were relatively close to the experimental results (1.75 vol.% for F1 and 1 vol.% for F2).

TABLE 6.1.: The experimental results of the maximum concentration of fibres F1 and F2 and the equivalent fibre factors for self-compacting UHPFRCs with maximum grain sizes of 1 mm, 2 mm, 4 mm and 8 mm.

Fibre type		UHPC-1mm	UHPC-2.5mm	UHPC-4mm	UHPC-8mm
F1 13mm/0.2mm	Max. Concentration [vol.%]	1.75	1.5	1.5	1
	Fibre factor ( $L_{f1}/D_{f1}$ )* $V_{f1}$	1.138	0.975	0.975	0.65
F2 20mm/0.2mm	Max. Concentration [vol.%]	1	0.75	0.75	0.5
	Fibre factor ( $L_{f2}/D_{f2}$ )* $V_{f2}$	1	0.75	0.75	0.5

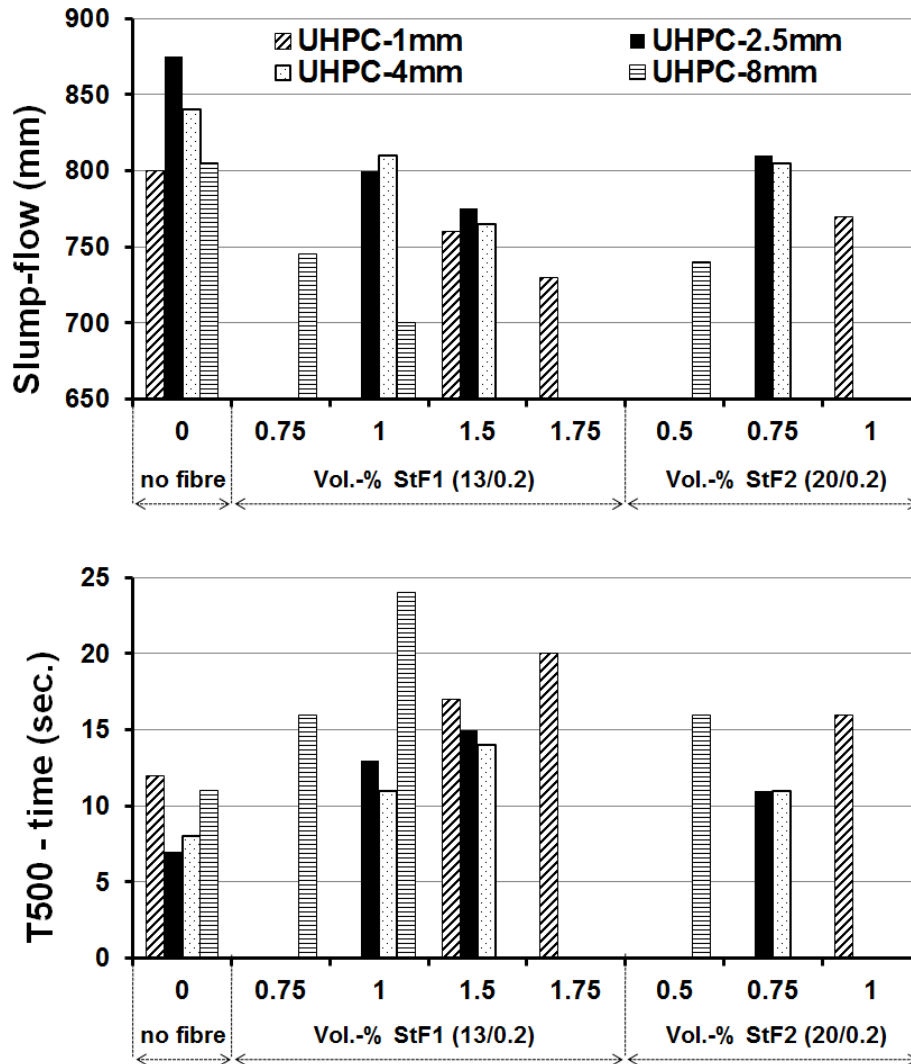


FIGURE 6.15.: The slump-flow (top) and T500 time (bottom) of UHPCs with and without fibres F1, F2. The fibre contents were no higher than the maximum fibre concentration.

A homogenous fibre distribution and a good self-flowability of UHPFRCs were observed as the fibre contents were less than or equal to the maximum fibre concentration. The slump-flow test results indicated that the maximum fibre concentration increased at increasing the paste volume and the content of the smaller 1 mm aggregate. Indeed, the three UHPCs with maximum grain size of 1 mm, 2.5 mm and 4 mm had the same paste (characteristics and volume fraction) but the maximum fibre concentration of both fibres for UHPC-1mm was the highest. Further, compared with other matrices, the maximum fibre concentration of UHPC-8mm with a higher aggregate volume fraction and a high content of the larger 1 mm aggregate was the lowest. The higher the fibre factor  $(L_f/d_f) \cdot V_f$  was, the more the slump flow decreased. However, there was a strong interaction between long fibres and aggregates, leading to a lower flowability of long fibre concrete compared with short fibre concrete showing the same fibre factor. In addition, the larger the maximum

## 6. Steel fibre reinforced UHPC

aggregate size was, the lower flowability the fibre concrete possess.

It should be noted that the further investigation into the flexural and tensile behaviours of UHPFRCs using the same maxtrix and the maximum concentration of fibres F1 and F2 is meaningful to evaluate the materials efficiency of fibres F1 and F2 because the self-flowability of these UHPFRCs were nearly similar (the difference of less than 50 mm slump-flow).

Figure 6.16 shows UHPFRCs with fibre clumps when the maximum fibre concentrations were exceeded. Exactly, the flowability of fibre concrete lost quickly and fibre clumps appeared thickly when long fibre content increased slightly more the maximum fibre concentration.

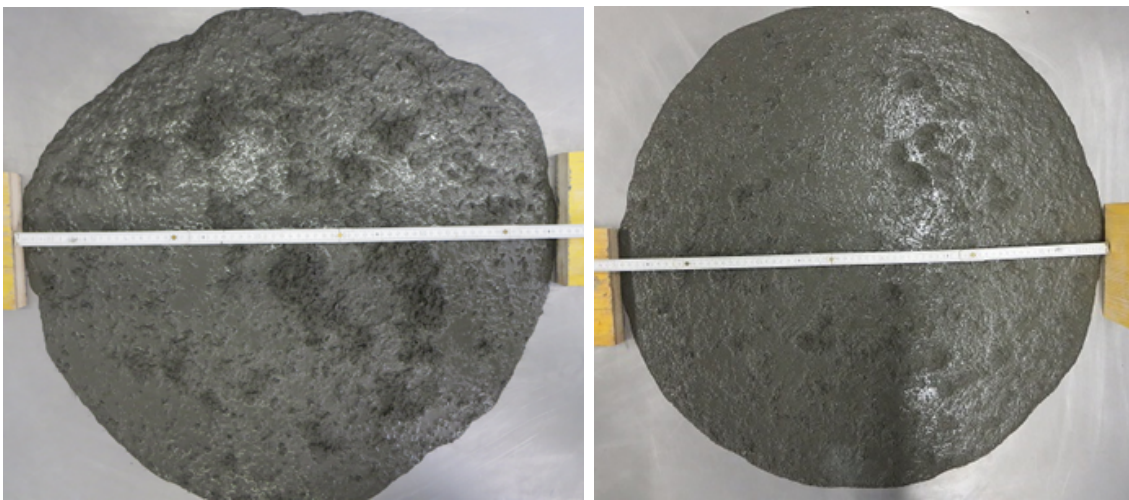


FIGURE 6.16.: Fibre clumps in the UHPC-8mm - 0.75 vol.% F2 (left side) and in the UHPC-2.5mm - 1.75 vol.% F1 (right side). Although these fibre concretes have the slump-flow of 650 mm and 700 mm, respectively, they cannot be used in practice.

### 6.3.2.2. Effect of fibres F1, F2 contents and matrix compositions on the mechanical behaviour of UHPFRC

The experimental results of the UHPFRCs compressive strength are shown in Table 6.2. Figure 6.17 depict both the envelope and average flexural stress - deflection response from the bending tests of the UHPFRCs having the critical fibre content (for the self-flow properties). The measurements of the peak strength ( $f_p$ ), the residual strength ( $f_m^D$ ) and the toughness ( $T_m^D$ ) at the specified points of the load-deflection curve are also presented in Table 6.2.

The compression test results showed that the addition of steel fibres up to the maximum fibre concentrations for self-flow properties influenced negligibly on the compressive strength of UHPFRCs (less than 2% increasing).

The experimental results of bending tests indicated that the flexural behaviours of UHPFRCs using the same maxtrix and the maximum concentration of fibres F1 and

F2 were nearly same but fibre F2 content was equal to a half fibre F1 content. These concretes also had the same flowability as mentioned in the previous investigation of fibre concentration. Therefore, it can be concluded that the material efficiency of long fibre F2 is better than that of short fibre F1.

During the beam casting, the fibres tended to orient in the direction of flow, which is also the direction of applied stress, resulting in a good improvement in bending behaviour, but this effect decreased as the grain size of aggregate increased. Indeed, the bending test results show that using the same volume of 1% F1, the flexural strength and the toughness at the peak points decrease with increase of aggregate size in cases of UHPC-2.5mm, UHPC-4mm and UHPC-8mm. Also, a similar phenomenon can be observed for the comparison of UHPC-1mm, UHPC-2.5mm and UHPC-4mm at 1.5 vol.% F1.

In order to guarantee about the advantage of fibre F2 compared to fibre F1, direct tensile tests were performed for UHPFRC-1mm containing 1.75 vol.% F1 and UHPFRC-1mm containing 1 vol.% F2. Furthermore, a back-calculation was conducted to estimate the tensile constitutive properties of these fibre concrete. The experimental and estimated results are shown in Figures 6.18, 6.19 and Table 6.3.

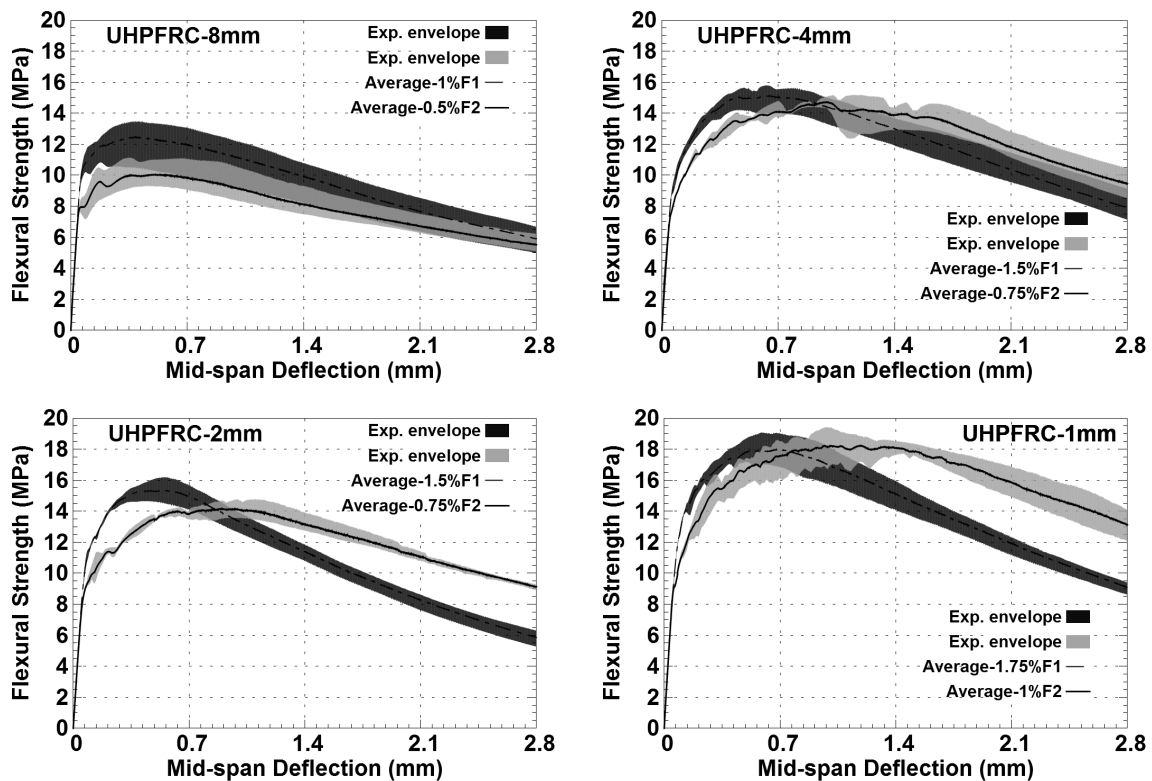


FIGURE 6.17.: The effect of fibres F1 and F2 on the flexural behaviours of UHPFRC-8mm, 4mm, 2mm, 1mm.

## 6. Steel fibre reinforced UHPC

TABLE 6.2.: The compressive strength and the average flexural properties of UHPFRCs.

Matrix	Fibre	$f_{c,cube}$	Flexural strength [MPa] and toughness [Nm] (values in parentheses)				
			Peak ( $\delta_P; f_P$ )		Specified deflections [mm]		
			$\delta_P$ [mm]	$f_P$	0.42	0.7	2.8
UHPC-8mm	0.5- F2	193.8	0.511	10.04 (29.95)	9.93 (24.01)	9.81 (42.24)	5.52 (145.1)
	0.75- F1	194.2	0.358	9.6 (20.10)	9.54 (23.97)	9.07 (41.02)	4.58 (133.4)
	1-F1	193.3	0.388	12.47 (27.41)	12.40 (30.00)	11.95 (52.34)	5.90 (173.5)
UHPC-4mm	0.75- F2	200.8	0.992	14.72 (81.01)	13.04 (28.49)	14.09 (53.59)	9.45 (227.2)
	1-F1	199.7	0.561	12.65 (39.80)	12.43 (28.22)	12.51 (51.24)	6.04 (177.7)
	1.5- F1	199.2	0.646	15.11 (50.95)	14.88 (32.33)	15.01 (59.78)	7.92 (219.6)
UHPC-2mm	0.75- F2	199.1	0.899	14.16 (71.77)	13.08 (28.48)	13.82 (53.53)	9.13 (218.4)
	1-F1	199.8	0.459	13.17 (33.64)	13.16 (30.29)	12.72 (54.02)	7.06 (189.8)
	1.5- F1	198.3	0.551	15.33 (47.33)	15.32 (34.23)	14.93 (62.11)	5.85 (198.8)
UHPC-1mm	1-F2	196.1	1.181	18.23 (121.88)	16.02 (34.32)	17.56 (65.32)	13.12 (292)
	1.5- F1	195.6	0.615	18.23 (61.22)	17.82 (38.43)	18.22 (71.34)	9.54 (262.2)
	1.75- F1	195.9	0.679	17.98 (68.55)	17.36 (38.46)	17.96 (71.01)	9.11 (256.8)

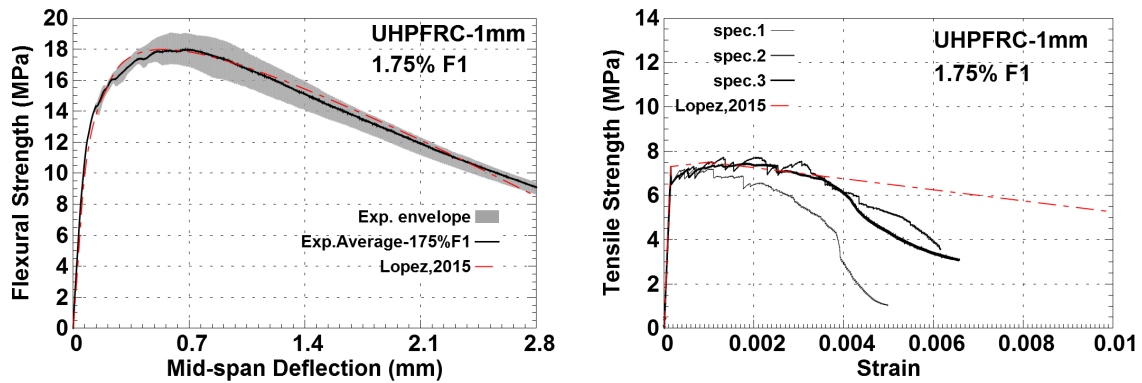


FIGURE 6.18.: Deflection-hardening and Strain-hardening behaviours of UHPFRCs-1mm having 1.75 vol.% F1, experimental and estimated results.

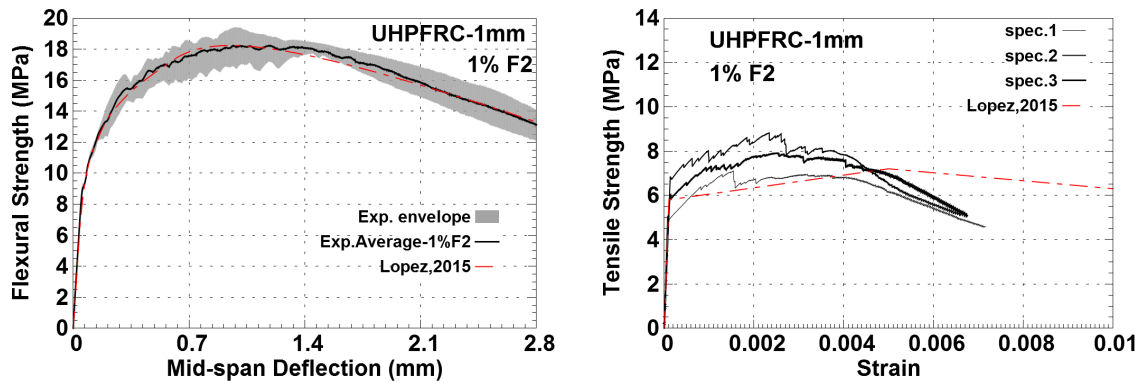


FIGURE 6.19.: Deflection-hardening and Strain-hardening behaviours of UHPFRCs-1mm having 1 vol.% F1, experimental results and estimated result by Lopez's method.

TABLE 6.3.: Experimental and estimated tensile results of UHPFRC-1mm containing 1.75 vol.% F1 and 1 vol.% F2.

Matrix	Fibre [vol.%]	Specimen No.	Tensile strength [MPa] and Strain[%]				
			$\sigma_{cc}$	$\epsilon_{cc}$	$\sigma_{pc}$	$\epsilon_{pc}$	$\epsilon_{t,max}$
UHPC-1mm	1.75-F1	Exp-1	7.33	0.156	6.76	0.157	–
		Exp-2	6.59	0.153	7.72	1.322	–
		Exp-3	6.30	0.126	7.43	1.825	–
		Exp-Average	6.74	0.145	7.30	1.101	–
		Estimation	7.3	0.140	7.5	1.000	31
UHPC-1mm	1-F2	Exp-1	5.06	0.069	7.11	1.543	–
		Exp-2	6.83	0.136	8.82	2.340	–
		Exp-3	5.89	0.123	7.90	2.511	–
		Exp-Average	5.93	0.109	7.94	2.131	–
		Estimation	5.8	0.105	7.2	5.000	45

The stress - strain-hardening behaviour was observed for both UHPFRC-1mm using 1.75 vol.% F1 and 1 vol.% F2. The ultimate tensile strength of 7 MPa was sure of success. The use of 1 vol.% fibre F2 (having a high fibre aspect ratio of  $L_{f2}/D_{f2}=20\text{mm}/0.2\text{mm}=100$ ) improved significantly the ultimate tensile strength and the strain capacity of UHPFRC in comparison to the use of 1.75 vol.% fibre F1 (with a lower fibre aspect ratio  $L_{f1}/D_{f1}=13\text{mm}/0.2\text{mm}=65$ ).

### 6.3.3. Experimental assessment of the effectiveness of six different fibres in reinforcing UHPC

The above investigation focusing the effect of fibres F1, F2 and matrices composition on UHPFRC properties indicate that the fine grain UHPC-1mm is the most suitable matrix for production of ductile UHPFRC with high steel fibre volume. Only UHPC-1mm was used for further investigation. However, in order to achieve a better self-flowability

## 6. Steel fibre reinforced UHPC

and a good fibre distribution of concrete with a high steel fibre volume the paste volume of UHPC-1mm was increased by increasing of Cem1 content from 720 kg/m<sup>3</sup> up to 750 kg/m<sup>3</sup>, notated UHPC-1mm-750kgCem1, corresponding to paste volume of 561.6 lit/m<sup>3</sup>.

Table 6.4 shows the content of each kind of fibre for direct tensile test and four-point bending test to evaluate the effectiveness of these fibres in reinforcing UHPC-1mm-750kgCem1. All fibre concretes showed a good self-flowing properties with the slump-flow of no less than 750 mm and no fibre clumps.

TABLE 6.4.: Fibre contents for bending and tension test.

	Fibre content (vol.%)					
	F1	F2	F3	F4	F5	F6
Bending test	2	1.5	1.5	1.5	2	1.75
Tension test	2	1.5	1.5	1.5	2	1.75

Figures 6.20, 6.21, Tables 6.5, 6.6 show the influence of fibre types, contents on the flexural and tensile behaviours UHPFRC, including the experimental and estimated results.

The experimental results of bending and direct tensile tests are in good agreement. Surprisingly, UHPFRC-1mm-750kgCem with 2 vol.% F5 possessed the weakest flexural and tensile behaviours in comparison to others although the single fibre pull-out resistance of fibre F5 was much higher than that of fibres F1 and F2. This may be attributed to the lowest density of fibre crossing, the lowest fibre aspect ratio of fibre F5 and the low fibre factor of UHPFRC-1mm-750kgCem-2vol.%F5. In addition, the real fibre-matrix bond strength of fibres F1 and F2 in the specimens of flexural and tensile tests, that formed by a homogeneous mixing process of UHPC matrix and fibres, may be much higher than the results of single fibre pull-out test, it could be a suitable reason for the observed phenomenon.

The estimation of the tensile properties based on four-point bending test showed that the first cracking tensile stress  $\sigma_{cc}$  of fibre concrete (which approximate to the matrix tensile strength as mentioned at the beginning of this chapter) was in range of 6-8 MPa. However, a high scattering of the experimental  $\sigma_{cc}$  of 5.7 MPa up to 10.3 MPa was observed and has not explained yet.

Comparing the experimental and estimated tensile strengths of a UHPFRC group pointed out that fibres in the thin dog-bone specimen might have a 2-D distribution and tended to orient in the direction of applied stress leading to higher results of the experiment. Furthermore, the experimental  $\sigma_{pc}$  was computed using a constant area of the middle cross-section of the dog-bone specimen resulting to an overestimate.

The experimental results showed that the flexural deflection-hardening response, the modulus of rupture of UHPFRC-1mm-750kg-2vol.%F1 were better than that of UHPFRC-1mm-750kg-1.5vol.%F3. However, the experimental  $\sigma_{pc}$  of UHPFRC-1mm-

750kg-1.5vol.%F3 was higher than that of UHPFRC-1mm-750kg-2vol.%F1. The higher density of fibre crossing, the greater fibre pull-out resistance of fibre F3 in comparison with fibre F1 and the good fibre orientation in the thin dog-bone specimen of fibre F3 could be the reason.

TABLE 6.5.: The average flexural properties of UHPFRCs-1mm-750kgCem1 with different fibres types, contents.

Matrix	Fibre [vol.%]	Flexural strength [MPa]				
		Peak ( $\delta_P; f_P$ )		Specified deflections [mm]		
		$\delta_P$ [mm]	$f_P$	0.42	0.7	2.8
UHPC-1mm-750kgCem1	2-F1	0.819	19.48	18.60	19.40	9.15
	1.5-F2	1.364	26.40	21.40	22.70	16.40
	1.5-F3	0.734	17.20	16.40	17.20	3.89
	1.5-F4	0.988	21.22	20.92	20.57	6.55
	2-F5	0.460	14.20	14.17	13.83	4.86
	1.75-F6	1.160	22.09	18.36	20.70	12.33

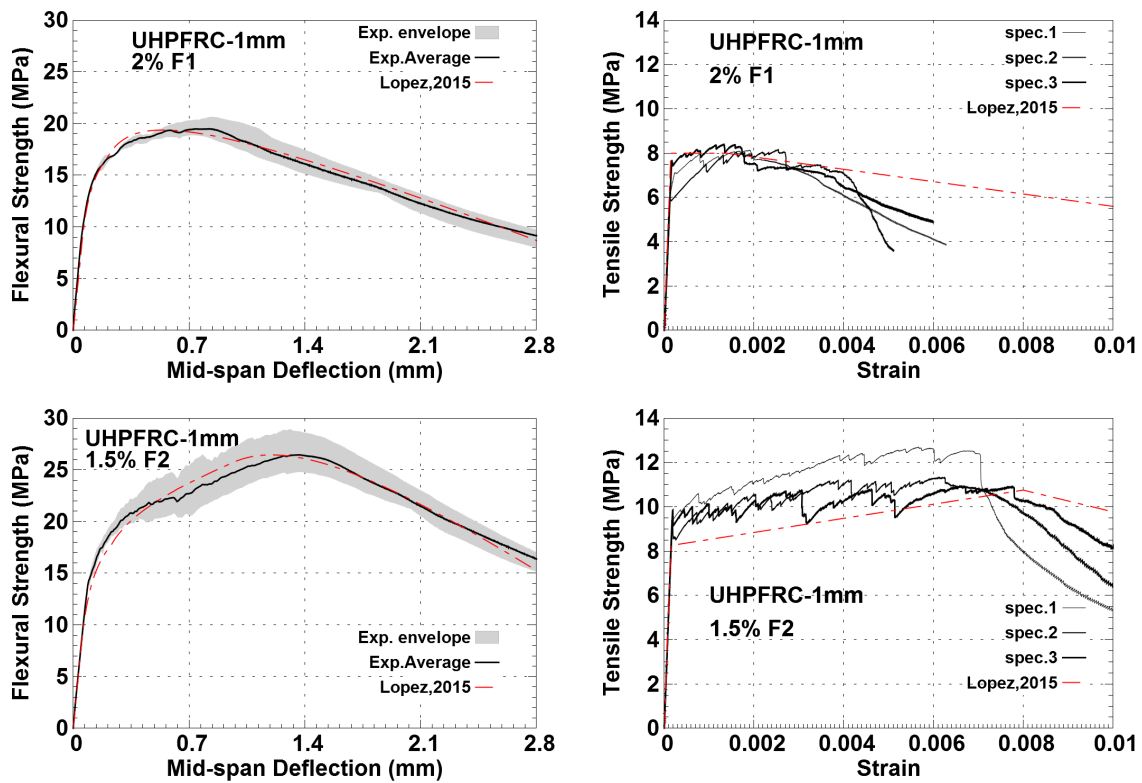


FIGURE 6.20.: Influence of fibres F1, F2 on the flexural and tensile behaviours of UHPFRCs-1mm-750kgCem1, experimental results and estimation.

6. Steel fibre reinforced UHPC

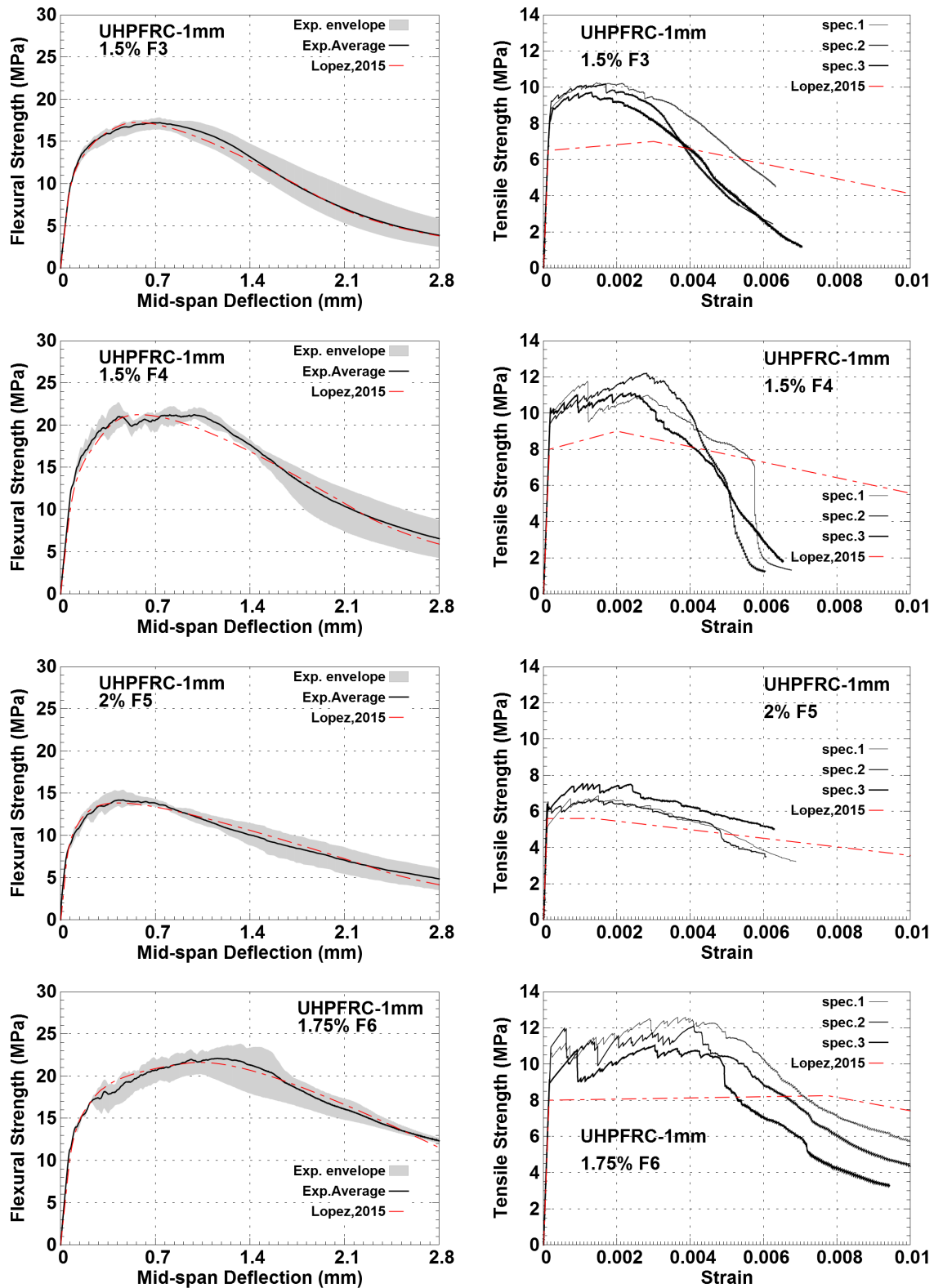


FIGURE 6.21.: Influence of fibres F3, F4, F5, F6 on the flexural and tensile behaviours of UHPFRCs-1mm-750kgCem1, experimental results and estimation.

TABLE 6.6.: Tension test results of UHPFRCs-1mm-750kgCem1 with six different fibre types and contents.

Matrix	Fibre [vol.%]	Specimen No.	Tensile strength [MPa] and Strain[%o]				
			$\sigma_{cc}$	$\epsilon_{cc}$	$\sigma_{pc}$	$\epsilon_{pc}$	$\epsilon_{t,max}$
UHPC-1mm-750kgCem1	2-F1	Exp-1	5.09	0.094	8.13	1.906	–
		Exp-2	5.78	0.111	8.16	2.544	–
		Exp-3	6.33	0.135	8.39	1.33	–
		Exp-Average	5.73	0.113	8.23	1.927	–
		Estimation	8.0	0.145	8.0	1.4	30
UHPC-1mm-750kgCem1	1.5-F2	Exp-1	9.53	0.197	12.68	5.663	–
		Exp-2	9.48	0.186	11.31	6.238	–
		Exp-3	9.82	0.187	10.92	6.624	–
		Exp-Average	9.61	0.190	11.64	6.175	–
		Estimation	8.25	0.15	10.75	8	30
UHPC-1mm-750kgCem1	1.5-F3	Exp-1	8.63	0.190	10.26	1.454	–
		Exp-2	8.59	0.180	10.19	1.684	–
		Exp-3	8.13	0.179	9.71	1.299	–
		Exp-Average	8.45	0.183	10.05	1.479	–
		Estimation	6.5	0.13	7.0	3	20
UHPC-1mm-750kgCem1	1.5-F4	Exp-1	9.54	0.172	11.76	1.200	–
		Exp-2	9.58	0.172	12.21	2.813	–
		Exp-3	10.27	0.189	11.11	2.374	–
		Exp-Average	9.80	0.178	11.69	2.129	–
		Estimation	8.0	0.16	9	2	23
UHPC-1mm-750kgCem1	2-F5	Exp-1	5.27	0.094	6.85	1.494	–
		Exp-2	6.55	0.123	6.67	1.446	–
		Exp-3	6.36	0.114	7.53	1.067	–
		Exp-Average	6.06	0.110	7.02	1.336	–
		Estimation	5.6	0.102	5.6	1.4	25
UHPC-1mm-750kgCem1	1.75-F6	Exp-1	10.87	0.193	12.58	3.656	–
		Exp-2	10.93	0.199	12.09	4.090	–
		Exp-3	9.14	0.162	11.03	3.037	–
		Exp-Average	10.31	0.185	11.90	3.594	–
		Estimation	8.0	0.151	8.25	7.75	30

The results pointed out that fibre F4 was more effective than fibre F3 in improving ductility of concrete using the same fibre volume due to the higher fibre aspect ratio of fibre F4. In addition, fibre F4 was much more advantage than fibre F1 because such fibres have nearly same length, fibre aspect ratios, density of fibre crossing but the flexural deflection-hardening response and tensile strain-hardening response of UHPFRC-1mm-750kg-1.5vol.%F4 was better than that of UHPFRC-1mm-750kgCem-2 vol.% F1.

The longer length of fibre F6 in comparison to the length of fibre F2 led to a better fibre orientation in the direction of applied stress in the thin dog-bone specimen and resulted in the same ultimate tensile strength of UHPFRC-1mm-750kg-1.75vol.%F6 and UHPFRC-1mm-750kg-1.5vol.%F2. However, in 3-D fibres distribution of the bending specimens the experimental flexural results and the estimated tensile properties showed

## 6. Steel fibre reinforced UHPC

that the ductility and toughness of UHPFRC-1mm-750kg-1.5vol.%F2 was better than that of UHPFRC-1mm-750kg-1.75vol.%F6.

The highest effectiveness of fibre F2 in improving ductility and toughness of UHPFRC-1mm was, once again, demonstrated convincingly. Using only 1.5 vol.% F2 the flexural strength deflection-hardening response and tensile strength strain-hardening response of UHPFRC-1mm-750kg-1.5%F2 was much better than that of others UHPFRCs-1mm-750kg having an equal or a higher fibre volume. In addition, the results implies that the single fibre F2 pullout resistance was much lower than the real fibre F2-matrix bond strength in the specimens of flexural and tensile tests.

### 6.4. Concluding remarks

Six different high strength steel fibres including smooth-straight fibres, crimped fibres, indented-hooked ends fibre and indented-straight fibre were employed to improve the ductility of the developed UHPC matrix.

The results of the pullout tests of single fibre in UHPC-1mm show that the deformed fibres possess a very high pullout resistance implying a high bond strength between the deformed fibres and matrix in contrast with the smooth-straight fibres. However, the fibre-matrix bond strength of fibres F1 and F2 in specimens of bending and tension tests that formed by a homogeneous mixing process of UHPC matrix and fibres may be much higher than the results of single fibre pull-out test.

An experimental study in the influence of fibre types, content and matrices composition was performed using all the developed optimum UHPC matrices and the smooth-straight fibres F1 and F2 to obtain insight into the fibre-matrix interactions that influence the self-compacting properties and the mechanical properties of UHPFRCs. It verifies convincingly that the determination and utilization of the maximum fibre concentration for a given UHPC matrix are significant to achieve the highest mechanical performance for self-compacting fibre concrete.

Within the developed optimum UHPC matrices, for UHPFRCs with maximum grain size up to 4 mm, the long fibre F2 was much more effective than the short fibre F1 in terms of cost saving and toughness improving, the concretes using the long fibres had a similar modulus of rupture and a better toughness in comparison to the concretes having twice higher short fibre volume fraction. Fibre factors of long fibre F2 were 1, 0.75, 0.75 for UHPCs-1, 2.5, 4 mm, respectively. Short fibre F1 with fibre factor of 1 was the best for UHPC-8mm. The tensile strain-hardening behaviour with a maximum post-cracking stress of no less than 7 MPa was achieved for both UHPFRC-1mm-1.75vol.% F1 and UHPFRC-1mm-1vol.%F2, and the higher effective of F2 was recognized.

The effectiveness of six different fibres in improving ductility and toughness of UHPC were evaluated through a comparative investigation into the flexural and tensile behaviours of UHPFRCs including experiment and estimation. Evidently, UHPFRCs-1mm with Cem1 content of no less than 720 kg/m<sup>3</sup> was the most suitable concrete matrix for high volume steel fibre reinforcing. Fibre F2 was the best fibre for achieving the highest quality of

ductile UHPFRC. The use of 1.5 vol.% fibre F2 guaranteed to achieve a strain-hardening UHPFRC with an ultimate tensile strength of higher than 10 MPa.

The modification of direct tensile test using a specimen with a sufficiently large size for a 3-D fibre distribution and a universal joint for reducing bending effect is needed for a good description of UHPFRC tensile behaviour.



## 7. Application of the developed UHPFRC

The developed UHPC-1mm-Paste3, UHPC-2.5mm-Paste3, UHPC-4mm-Paste3 and UHPC-8mm-Paste3 have been applied as standard mixtures for some UHPFRC projects of Institute of Structural Concrete such as Project No. 846023 “Substitution of Steel with UHPFRC” and Project No. 840397 “Structural design for the Quickway System”. The proposed mix design approach allows to modify these UHPC standard mixtures to satisfy the special requirement of designs. The modified UHPFRC can vary from stiff concrete to highly flowable concrete, in which the fibre content is sufficient for achieving stress strain-hardening behaviour. The success of the large scale tests demonstrated convincingly the feasibility of applying the developed UHPFRC and the effectiveness of the proposed mix design approach.

### 7.1. The project Substitution of Steel with UHPFRC

Substitution of Steel with UHPFRC is a federal funded joint research project under the auspices of the Austrian Research Promotion Agency (FFG): 846023. The joint research is carried out in cooperation with Graz University of Technology represented by the Institute of Structural Concrete, the Institute of Materials Testing and Building Materials, University of Applied Sciences Kärnten, and the Kirchdorfer and Voestalpine companies.

The detail information of the project was described by Hadl et al. [2016].

The aim of the project Substitution of steel by UHPFRC is to use the high capacity of UHPFRC effectively. This includes the development of specific elements that are usually made of steel. The project focuses on the development and feasibility of a hollow box girder, a UHPFRC composite column and a UHPFRC-steel-composite girder with a web made of steel and flanges made of UHPFRC.

#### 7.1.1. UHPFRC hollow box girder

The hollow box girder of UHPFRC, which can span up to 30 m, is produced in a factory of precast concrete element. It is a prestressed concrete element using pre-tensioning technique. Several girders are connected by a layer of normal strength concrete on the construction site, as described in Figure 7.1. This method enables short construction times and a long service life.

The box girder consists of a deck plate and thin webs of 0.06 m, and a bottom slab. Its thickness depends on the span of the girder, but is not more than 0.14 m. In the

## 7. Application of the developed UHPFRC

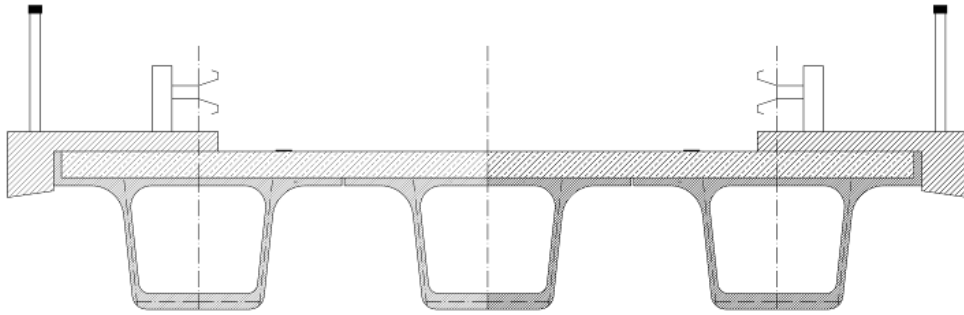


FIGURE 7.1.: Bridge cross section with UHPFRC box girders and a layer of normal strength concrete.

bottom slab, pretension strands are arranged in order to achieve the required bearing capacity. In order to prevent cracking during the pre-stressing work, strands are needed in the deck plate. The inclination of the thin webs is chosen according to construction demands and the casting process. Besides the prime load bearing function, the thin deck plate is used as formwork for casting the normal strength concrete layer.

Figure 7.2 illustrates the cross section of a girder with a span of 30 m. The total height of the bridge construction is 1.2 m, whereas the UHPC box girder has a height of 1 m, and a 0.2 m normal-strength concrete layer is included. 36 strands ( $A_P = 150 \text{ mm}^2$ ) in the bottom slab and 6 strands in the deck plate are required to ensure the bearing capacity. The girder should be made without conventional reinforcement. In order to avoid the formation of splitting cracks due to the transfer of prestressing forces, a high amount of micro steel fibre is required.

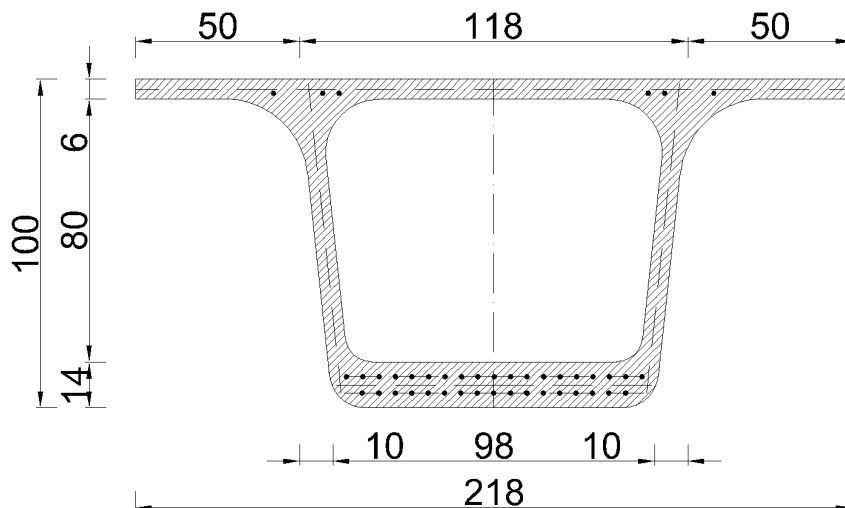


FIGURE 7.2.: Cross section of the UHPFRC girder including the prestressing strands.

The fibres F3 and F4 were used for reinforcing the concrete matrix of UHPC-1mm-750kgCem1. Pull-out tests according to RILEM TC RC 6 [1994] were carried out to



## 7. Application of the developed UHPFRC

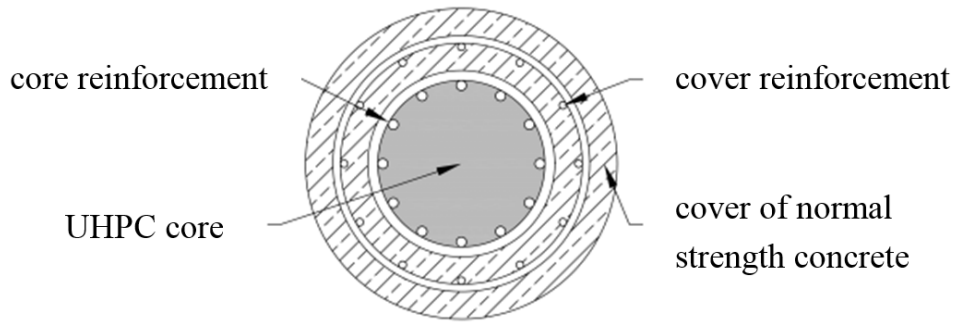


FIGURE 7.4.: Schematic cross section of the UHPC composite column.

The UHPC-8mm was modified by reducing Cem1 content from  $640 \text{ kg/m}^3$  down to  $600 \text{ kg/m}^3$  with the aim of reducing concrete shrinkage. In addition, the fibre F4 was used at low content of 0.5 and 0.75 vol.% when the UHPFRC core was surrounded by spiral reinforcement and normal strength concrete.

The influence of the spiral reinforcement on the confinement and load bearing capacity of the UHPFRC core was investigated. The UHPFRC core was tested without cover layer of normal strength concrete. UHPFRC columns with a height of 1 m and a diameter of 0.20 m were produced. All columns have a small amount of longitudinal reinforcement (8 rebars  $\phi 8\text{mm}$ ). Three types of specimens were examined: type A without spiral reinforcement, used as reference for determination of load bearing capacity; type B includes spiral reinforcement ( $\phi 8\text{mm}$ ) with spacing of 40 mm; type C includes spiral reinforcement ( $\phi 8\text{mm}$ ) with spacing of 25 mm. Furthermore, different amounts of steel fibres were investigated (0.5 and 0.75 vol.%). Figure 7.5 depicts the test setup.



FIGURE 7.5.: Different amount of spiral reinforcement (Types A and C) and test setups for the UHPC columns.

The columns without spiral reinforcement showed brittle characteristics, which was

expected. The fracture behaviour became more ductile as the amount of spiral reinforcement was increased. The maximum load bearing capacity and the structural behaviour are strongly influenced by spiral reinforcement until the failure occurs. The column behaves linear elastic up to about 80% of its load bearing capacity. The maximum load of all test series (3 specimens each) is approximately 5000 kN, which corresponded to a compressive strength of 160 MPa. Hence, the element strength was approx. 85% of the cylindrical compressive strength (185 MPa). The results also indicated that the steel fibre content has no significant impact on the structural behaviour.

The project is ongoing.

## 7.2. The project Structural Design for The Quickway System

Structural design for the Quickway System is a federal funded joint research project under the auspices of the Austrian Research Promotion Agency (FFG): 840397. The joint research is carried out in cooperation with S+W Wrlle Sparowitz Ingenieure ZT GmbH, Hans Lechner ZT GmbH and Graz University of Technology represented by the Institute of Construction Management and Economics, the Laboratory for Structural Engineering as well as the Institute of Structural Concrete.

The detail information of the project was described by Oppeneder et al. [2016].

Main principle of Quickway is to implement a slender but robust roadway network over existing road networks. The single elements are pre-fabricated and assembled on site by external tendons pre-stressing dry joints without any further measures of joint connection. For efficient and fast construction, Quickway is to be based on a modular construction kit.

The major girder elements are determined to be produced with UHPC to enable slender cross sections and lightweight elements. For simplification of the production ordinary reinforcement should generally be avoided by using fibers (UHPFRC). Exceptions are parts with high loads, e.g. anchoring of tendons, support areas or regions with high torsional forces.

Modular construction kit

- All girders consist of standard or curved middle elements between two end elements. The cross section is in all cases a hollow box with a monolithic connected parapet (in total  $h = 1.80$  m). The max. section thickness is 14 cm, however the webs of the box girder are arranged with haunches taking into account the vehicle wheel positions. In case of the curved element with  $R = 30$  m, the carriageway has a width of 2.75 m yielding a cross-sectional area of 1.14m, as shown in Figure 7.6.
- In longitudinal direction the girder is assembled by the external tendons prestressing a dry joint without any further measures, as illustrated in Figure 7.7. The shear resistance of the joint will be provided by friction in the cross section area. The requirements on the accuracy of such joints will be complied by the formwork, further details on related studies are given by Theiler et al [2015].

## 7. Application of the developed UHPFRC

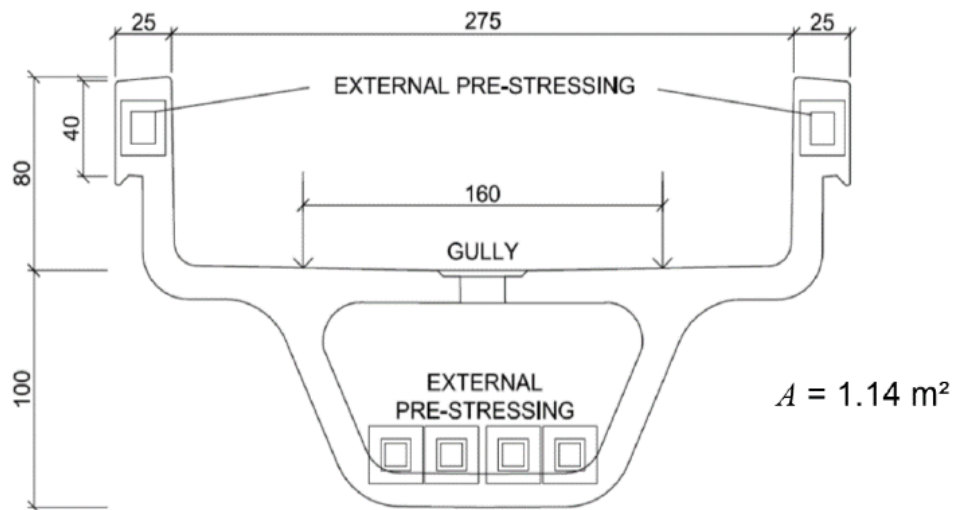


FIGURE 7.6.: Curved cross section.

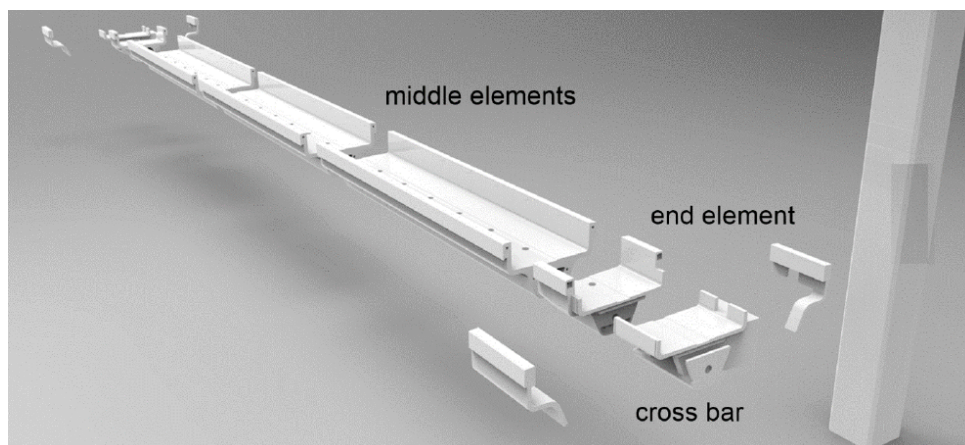


FIGURE 7.7.: Overview of the precast beam elements.

The UHPFRC-1mm-750kgCem1-1.5%F2 was applied for this project. The detail properties of UHPFRC-1mm-750kgCem1-1.5%F2 was examined and described in section 6.3.3.

A short beam segment of 0.5 m with full scale curved cross section was cast to evaluate the flowability of UHPFRC. Self-compacting UHPFRC was poured, without vibration, at one side of the formwork and left to spread into place, as illustrated in Figure 7.8. Concluding that the self-flowing properties of UHPFRC-1mm-750kgCem1-1.5%F2 was very good.

## 7.2. The project Structural Design for The Quickway System

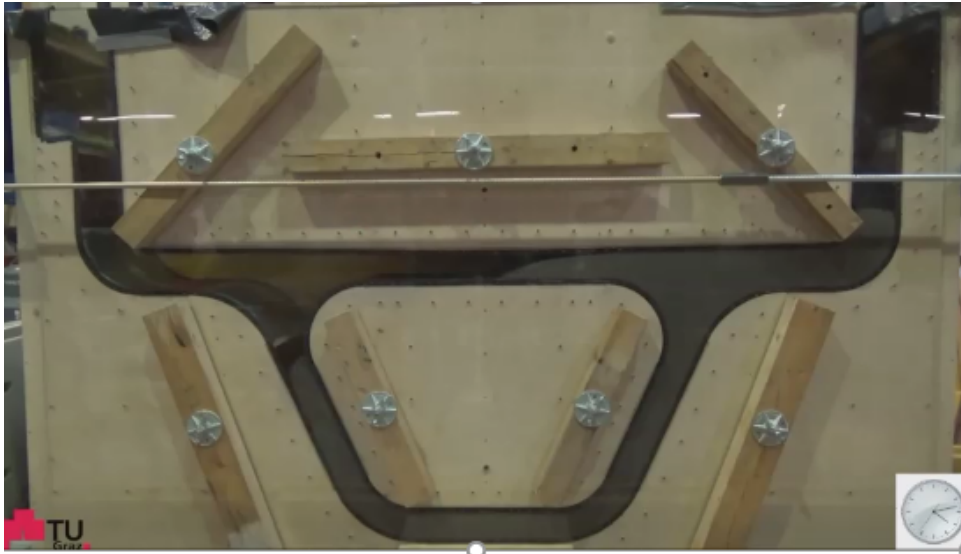


FIGURE 7.8.: Casting for beam segment of 0.5 m with full scale curved cross section, using self-compacting UHPFRC-1mm-Paste3 with 750 kg Cem1 and 1.5 vol.% StF 20mm/0.2mm.

The decisive girders of the Quicknet are the 40m long single spanned straight girder in bending and the 30m long single spanned curved girder in bending with torsion. The load bearing behaviour during closed and opened joints were analysed. Through the missing of consistent guidelines, and to verify the FEM calculations, a large-scale test was conducted. Hereby three straight elements in scale 1:2 with the designed UHPFRC was produced. They were connected with external straight tendons and dry joints to a cantilever beam. The loads from the straight and curved girder were applied on this girder. Special focus was hereby on the joint behaviour (friction coefficient and inaccuracy of the surface) and the behaviour of the UHPFRC in the area of the joint during bending combined with torsion. A special focus was also the fibre orientation and fibre distribution in the cross section of the girder.



FIGURE 7.9.: Evaluation of the structural performance of assembled system for Quickway.

## *7. Application of the developed UHPFRC*

Concluding, the test worked as expected and the ultimate load could be applied on the different girder types. The addition of fibres, achieve a ductile failure behaviour of the girders. With UHPFRC-1mm-750kgCem1-1.5%F2 the requirements for the static design was achieved. UHPFRC-1mm-750kgCem1-1.5%F2 is a suitable material for an application like Quickway. Complicated cross sections can be achieved with the self-compacting material as it was shown in the large scale-casting test. The high durability as well as the high bearing behaviour of the girders under compression in combination with external tendons and dry joint makes the developed UHPFRC to the optimal material for a precast pre-stressed modular construction.

## 8. Conclusions and recommendations

Selection of cements and superplasticizers concerning their compatibility in terms of packing density and strength improving is crucial to achieve the highest performance for UHPC/UHPFRC.

Ultra-fine highly reactive powder is indispensable for improving the microstructure of the bulk cementitious paste and the interfacial transition zone between hardened cementitious paste and aggregate as well as fibres in the production of UHPFRC. However, the extra amount of reactive powder which only play a role of filler can be replaced by an effective inert filler to reduce material cost.

The method of superplasticizer-water solution demand measurement by determining mixing energy, which was developed in this research project, is highly effective for assessment of the compatibilities of superplasticizers and powders of cements, silica fumes, ground granulated blast furnace slag, fly ash, quartz powders, limestone powder as also for determination of the optimum mix proportion of blended binder regarding particle packing density improvement.

Due to a very complex physical-chemical interaction of fines the proportion of blended binder have to be determined experimentally for achieving multi-objective optimization of flowability, packing density, compressive strength of blended binder.

The rule of stepwise combination for granular materials in combination with effective test methods for packing density measurement (i.e. the superplasticizer-water solution demand test, viscosity measurement using a rotational rheometer, spread-flow test) were applied successfully for mix proportioning of blended binder as well as of the whole concrete regarding the improvement of packing density, self-flowability and strength of concrete.

The modification of the loosening effect and wall effect coefficients of the Compaction - Interaction Packing Model (CIPM) taking into account the effect of surface forces of fines is necessary for each kind of reactive powder to apply the model for mix proportioning of blended binder.

The use of the highest packing density aggregate, which can be estimated by the Compaction - Interaction Packing Model or the Compressible Packing Model or determined experimentally, cannot insure to obtain the highest performances of self-flowability and viscosity for UHPC with a given and high paste volume. The interaction between fine particles of the given paste and coarse particles of aggregate have to be taken into account in the particle packing calculation of the whole concrete.

The modified Andreasen and Andersen equation-based ideal curve cannot guarantee

## 8. Conclusions and recommendations

to achieve an optimum UHPC having a given and high paste volume because the materials characteristics such as shape, packing density, the surface forces of fines are not taken into account.

Taking into account the interaction between fine particles of the given paste and coarse particles of a blended aggregate the Compressible Packing Model can be used to determine the optimum proportion of round granular aggregate mixture when it is assumed that binder has only one size of volume mean diameter. For aggregate mixture including angular particles the modification of the loosening effect and wall effect coefficients of the model is necessary to obtain a good agreement with experiment. The estimation using the model has to be verified by experiments based on the proposed approach of stepwise optimization of packing density.

A systematic and highly effective approach of stepwise optimization of particle packing density was proposed to design UHPFRC. The advantage of the proposed approach was convincingly verified by the success of the comprehensive investigations from the materials selection to the optimization of cementitious paste and the whole UHPC matrix and finishing by determination of the most effective fibre for improving the ductility and toughness of UHPFRC. Four self-compacting UHPFRCs with different maximum grain sizes of 1 mm, 2.5 mm, 4 mm, 8 mm and compressive strength of higher than 190 MPa at 28days age, were developed and applied successfully. These developed UHPFRCs can be modified easily to satisfy the special requirement of designs. UHPFRCs-1mm with Cem1 content of equal or higher than 720 kg/m<sup>3</sup> is the most suitable concrete matrix for high volume steel fibre reinforcing to achieve a ultimate tensile strength of higher than 7 MPa. Within the six different steel fibre types used in this research project, Fibre F2 ( $L_{f2}/D_{f2}=20\text{mm}/0.2\text{mm}=100$ ) is the best fibre for obtaining the highest quality of ductility UHPFRC, F2 content of no less than 1.5 vol.% guarantee achieving strain-hardening UHPFRCs-1mm with higher 10 MPa ultimate tensile strength and 26 MPa flexural strength.

## Bibliography

- ACI (2006). Guide for the use of silica fume in concrete. Reports, Guides, and Commentaries 234R-06, American Concrete Institute.
- AFGC (2002). *Ultra high performance fibre-reinforced concrete, Revised Edition*. Association Francaise de Gnie Civil (AFGC).
- AFGC (2013). *Ultra high performance fibre-reinforced concrete, Revised Edition*. Association Francaise de Gnie Civil (AFGC).
- AFGC/fib, editor (2009). *Proceedings of the International Workshop on Ultra High Performance Fibre Reinforced Concrete - Designing and Building with UHPFRC: State of the Art and Development, 17-18 November 2009, Marseille, France*.
- AFNOR (2016a). *National Addition To Eurocode 2 - Design Of Concrete Structures: Specifique Rules For Ultra-High Performance Fibre-Reinforced Concrete (UHPFRC)*. Association Francaise de Normalisation.
- AFNOR (2016b). *Ultra-High Performance Fibre-Reinforced Concrete - Specifications, Performance, Production And Conformity*. Association Francaise de Normalisation.
- Aïtcin, P. C. (2004). *High-Performance Concrete*, chapter Materials selection, pages 162–214. Taylor & Francis, p. c. aïtcin edition.
- Aïtcin, P. C. and Flatt, R. J. (2016). *Science and Technology of Concrete Admixtures*, chapter Portland cement, pages 27–51. Woodhead Publishing, p. c. aïtcin and r. j. flatt edition.
- Andreasen, A. H. M. and Andersen, J. (1930). Über die beziehung zwischen kornabstufungen und zwischenraum in produkten aus losen körnern (mit einigen experimenten) (in german). *Kolloid-Zeitschrift*, (50):217–228.
- ASTM (2008). *ASTM-C618-08: Standard Specification for Coal Fly Ash and Raw or Calcined Natural Pozzolan for Use in Concrete*. ASTM.
- ASTM (2012). *ASTM C1609/C1609M-12: Standard Specification for Flexural Performance of Fiber-Reinforced Concrete*. ASTM.
- Baby, F., Graybeal, B., Marchand, P., and Toutlemonde, F. (2013). Uhpfrc tensile behavior characterization: inverse analysis of four-point bending test results. *Materials and Structures*, 46:13371354.

## Bibliography

- Bache, H. H. (1981). Densified cement / ultra-fine particle-based materials. In *Proc. of the second International Conference on Superplasticizer in Concrete, Ottawa, Ontario, Canada*.
- Banthia, N. and Trottier, J. F. (1994). Concrete reinforced with deformed steel fibers, part i: Bond-slip mechanisms. *ACI Materials Journal*, 91:435–446.
- Bentur, A. and Mindess, S. (2007). *Fibre Reinforced Cementitious Composites*, chapter Fibrecement interactions: Stress transfer, bond and pull-out, pages 31–104. Taylor & Francis.
- Brouwers, H. J. H. (2006). Particle-size distribution and packing fraction of geometric random packings. *Physical Review E*, 74:031309– 1–14.
- Brouwers, H. J. H. and Radix, H. J. (2005). Self-compacting concrete: Theoretical and experimental study. *Cement and Concrete Research*, 35:2116–2136.
- Chan, Y.-W. and Chu, S.-H. (2004). Effect of silica fume on steel fiber bond characteristics in reactive powder concrete. *Cement and Concrete Research*, 34:1167–1172.
- Chandrangsu, K. and Naaman, A. E. (2003). Comparison of tensile and bending response of three high performance fiber reinforced cement composites. In *International Workshop High Performance Fiber Reinforced Cement Composites*.
- Coussot, P. (2005). *Rheometry of pastes, suspensions, and granular materials : applications in industry and environment*. John Wiley Sons, Inc., Hoboken, New Jersey, John Wiley Sons, Inc., 111 River Street, Hoboken, USA.
- Cunha, V. M. C. F. (2010). *Steel Fibre Reinforced Self-Compacting Concrete from Micro-Mechanics to Composite Behaviour*. PhD thesis, University of Minho, University of Minho, Portugal.
- Cunha, V. M. C. F., Barros, J. A. O., and Sena-Cruz, J. M. (2010). Pullout behavior of steel fibers in self compacting concrete. *Journal of Materials in Civil Engineering*, 22:1–9.
- de Larrard, F. (1999). *Concrete Mixture Proportioning: A scientific approach*. E & FN SPON.
- Dhonde, H. B., Mo, Y. L., Hsu, T. T. C., and Vogel, J. (2007). Fresh and hardened properties of self-consolidating fiber-reinforced concrete. *ACI Materials Journal*, 104:491–500.
- Diamond, S. (1997). Alkali silica reactions - some paradoxes. *Cement and Concrete Composites*, 19:391–401.
- Diamond, S., Sahu, S., and Thaulow, N. (2004). Reaction products of densified silica fume agglomerates in concrete. *Cement and Concrete Research*, 34:1625–1632.
- DIN-EN (2009). *DIN EN 12390-3: 2009-07, Testing hardened concrete Part 3: Compressive strength of test specimens*. DIN-EN.

- DIN-EN (2010). *DIN EN 12350-8: 2010-12, Testing fresh concrete Part 8: Self-compacting Concrete Slump-flow test*. DIN-EN.
- EuropeanStandard (1998). *EN-1097-3:1998: Test for mechanical and physical properties of aggregates - Part 3: Determination of loose density and voids*. European Standard.
- EuropeanStandard (2000). *EN-206-1:2000: Concrete - Part 1: Specification, performance, production and conformity*. European Standard.
- EuropeanStandard (2005a). *EN 13263-1:2005: Silica fume for concrete - Part 1: Definitions, requirements and conformity criteria*. European Standard.
- EuropeanStandard (2005b). *EN 450-1:2005: Fly ash for concrete - Part 1: Definitions, requirements and conformity criteria*. European Standard.
- EuropeanStandard (2006). *EN 15167-1:2006: Ground granulated blast furnace slag for use in concrete, mortar and grout - Part 1: Definitions, requirements and conformity criteria*. European Standard.
- EuropeanStandard (2013). *EN-1097-6:2013: Test for mechanical and physical properties of aggregates - Part 6: Determination of particle density and water absorption*. European Standard.
- Fehling, E., Middendorf, B., and Thiemicke, J., editors (2016). *Proceedings of the Fourth International Symposium on Ultra-High Performance Concrete and High Performance Materials, 9-11 March 2016, Kassel, Germany*. Kassel University Press GmbH.
- Fehling, E., Schmidt, M., and Geisenhanslüke, C., editors (2004). *Proceedings of the International Symposium on Ultra-High Performance Concrete, 13-15 September 2004, Kassel, Germany*. Kassel University Press GmbH.
- Fehling, E., Schmidt, M., and Stürwald, S., editors (2008). *Proceedings of the Second International Symposium on Ultra-High Performance Concrete, 5-7 March 2008, Kassel, Germany*. Kassel University Press GmbH.
- Fehling, E., Schmidt, M., Walraven, J., Leutbecher, T., and Fröhlich, S. (2013). *Be-ton Kalender 2013 Ultra High Performance Concrete UHPC: Fundamentals, Design, Examples*. Ernst & Sohn.
- FennisHuijben, S. A. A. M. (2010). *Design of Ecological Concrete by Particle Packing Optimization*. PhD thesis, Delft University of Technology, Delft University of Technology, The Netherlands.
- Ferrara, L., Park, Y.-D., and Shah, S. P. (2007). A method for mix-design of fiber-reinforced self-compacting concrete. *Cement and Concrete Research*, 37:957971.
- Ferraris, C. F. and de Larrard, F. (1998). Testing and modelling of fresh concrete rheology. Internal report 6094, Building and Fire Research Laboratory, National Institute of Standard and Technology, USA.

## Bibliography

- FIB (2009). *Textbook on behaviour, design and performance for structural concrete - Volume 1*. the International Federation for Structural Concrete, Federal Institute of Technology Lausanne - EPFL, Section Gnie Civil.
- fib AFGC, R., editor (2013). *Proceedings of the RILEM-fib-AFGC International Symposium on Ultra-High Performance Fibre-Reinforced Concrete, 1-3 October 2013, Marseille, France*.
- Flatt, R. J. and Houst, Y. F. (2001). A simplified view on chemical effects perturbing the action of superplasticizers. *Cement and Concrete Research*, 31:1169–1176.
- Franks, G. V. (2008). *Introduction to Particle Technology*, chapter Chapter 5: Colloids and Fine Particles, pages 118–152. John Wiley & Sons Ltd, m. rhodes edition.
- Fröhlich, S. and Schmidt, M. (2014). *Sustainable Building with Ultra-High Performance Concrete: Results of the German Priority Programme 1182 funded by Deutsch Forschungsgemeinschaft (DFG)*, chapter Testing of Ultra High Performance Concrete, pages 129–176. Kassel University Press GmbH, michael schmidt and ekkehard fehling and susanne fröhlich and jenny thiemicke edition.
- Fuller, W. B. and Thompson, S. E. (1907). The laws of proportioning concrete. *Transactions of the American Society of Civil Engineers*, Paper No. 1053:67–172.
- Funk, J. E. and Dinger, D. R. (1994). *Predictive process control of crowded particulate suspensions : applied to ceramic manufacturing*. Kluwer Academic Publishers, New York.
- Furnas, C. C. (1929). Flow of gasses through beds of broken solids. *Bureau of Mines Bulletin*, (307):168 pages.
- Furnas, C. C. (1931). Grading aggregates - mathematical relations for beds of broken solids of maximum density. *Industrial and Engineering Chemistry*, 23(9):1052–1058.
- Geisenhanslüke, C. (2009). *Influence of the granulometry of fine particles on the rheology of pastes*. PhD thesis, Kassel University, Department of Building Materials and Building Chemistry, University of Kassel - Germany.
- Gelardi, G. and Flatt, R. J. (2016). *Science and Technology of Concrete Admixtures*, chapter Working mechanisms of water reducers and superplasticizers, pages 257–278. Woodhead Publishing, p. c. aïtcin and r. j. flatt edition.
- Gelardi, G., Mantellato, S., Marchon, D., Palacios, M., Eberhardt, A. B., and Flatt, R. J. (2016). *Science and Technology of Concrete Admixtures*, chapter Chemistry of chemical admixtures, pages 149–218. Woodhead Publishing, p. c. aïtcin and r. j. flatt edition.
- Glotzbach, C., Stephan, D., and Schmidt, M. (2014). Interparticular interaction between fine particle in uhpc and their manipulation. In *Sustainable Building with Ultra-High Performance Concrete: Results of the German Priority Programme 1182 funded by Deutsch Forschungsgemeinschaft (DFG)*, pages 45–60.

- Graybeal, B. A. and Baby, F. (2013). Development of direct tension test method for ultra-high performance fiber-reinforced concrete. *ACI Materials Journal*, 110:177–186.
- Grünewald, S. (2004). *Performance-based design of self-compacting fiber reinforced concrete*. PhD thesis, Delf University of Technology, Delf University of Technology, Netherlands.
- Grünewald, S. and Walraven, J. C. (2001). Parameter-study on the influence of steel fibers and coarse aggregate content on the fresh properties of self-compacting concrete. *Cement and Concrete Research*, 31:1793–1798.
- Gutteridge, W. A. and Dalziel, J. A. (1990a). Filler cement: The effect of the secondary component on the hydration of portland cement: Part 2: Fine hydraulic binders. *Cement and Concrete Research*, 20(6):853–861.
- Gutteridge, W. A. and Dalziel, J. A. (1990b). Filler cement: The effect of the secondary component on the hydration of portland cement: Part i. a fine non-hydraulic filler. *Cement and Concrete Research*, 20(5):778–782.
- Ha, L. T., Müller, M., Siewert, K., and Ludwig, H. M. (2015). The mix design for self-compacting high performance concrete containing various mineral admixtures. *Materials and Design*, 72:51–62.
- Hadl, P., della Pietra, R., Hoang, K. H., Pilch, E., and Tue, N. V. (2015). Application of uhpc as road bridge topping within the adaptation of an existing conventional bridge to an integral abutment bridge in austria. *Beton- und Stahlbetonbau*, 110(2):162–170.
- Hadl, P., Vojvodic, G., Hoang, K. H., and Tue, N. V. (2016). Substitution of steel components by uhpc. In *The Sixth International Conference on Structural Engineering, Mechanics and Computation, Cape Town, South Africa*.
- Hansen, T. C. (1986). Physical structure of hardened cement paste: A classical approach. *Materials and Structures*, 19(6):423–436.
- HeidelbergCement (2014). *Betontechnische Daten 2014*. Heidelberg Cement.
- Heinz, D., Gerlicher, T., and Urbonas, L. (2014). Properties of ultra-high performance concrete with low cement clinker binder systems. In *Sustainable Building with Ultra-High Performance Concrete: Results of the German Priority Programme 1182 funded by Deutsch Forschungsgemeinschaft (DFG)*, pages 61–92.
- Hunger, M. (2010). *An integral design concept for ecological Self-Compacting Concrete*. PhD thesis, Eindhoven University of Technology, Eindhoven University of Technology, The Netherlands.
- Hüsken, G. (2010). *A Multifunctional Design Approach for Sustainable Concrete - With Application to Concrete Mass Products*. PhD thesis, Eindhoven University of Technology, Eindhoven University of Technology, The Netherlands.
- Hüsken, G. and Brouwers, H. J. H. (2008). A new mix design concept for earth-moist concrete: A theoretical and experimental study. *Cement and Concrete Research*, 38:1246–1259.

## Bibliography

- ISO (2014). *ISO 9276-2: Representation of results of particle size analysis Part 2: Calculation of average particle sizes/diameters and moments from particle size distributions*. ISO.
- Jawed, I. and Skalny, J. (1978). Alkalies in cement: A review: Ii. effects of alkalies on hydration and performance of portland cement. *Cement and Concrete Research*, 8(1):37–51.
- Kanakubo, T. (2006). Tensile characteristics evaluation method for ductile fibre-reinforced cementitious composites. *Journal of Advanced Concrete Technology*, 4:3–17.
- Kim, D. J., Naaman, A. E., and El-Tawil, S. (2008). Comparative flexural behavior of four fiber reinforced cementitious composites. *Cement and Concrete Composites*, 30:917–928.
- Kwan, A. K. H., Chan, K. W., and Wong, V. (2013). A 3-parameter particle packing model incorporating the wedging effect. *Powder Technology*, 237:172–179.
- Kwan, A. K. H., Li, L. G., and Fung, W. W. S. (2012). Wet packing of blended fine and coarse aggregate. *Materials and Structures*, 45:817–828.
- Lam, L., Wong, Y. L., and Poon, C. S. (2000). Degree of hydration and gel-space ratio of high volume fly ash cement systems. *Cement and Concrete Research*, 30:747–756.
- Lombay, G., Sundararajan, S., Wang, K., and Subramaniam, S. (2011). A test method for determining adhesion forces and hamaker constants of cementitious materials using atomic force microscopy. *Cement and Concrete Research*, 41:11571166.
- Lopez, J. A., Serna, P., Navarro-Gregori, J., and Camacho, E. (2015). An inverse analysis method based on deflection to curvature transformation to determine the tensile properties of uhpfc. *Materials and Structures*, 48:37033718.
- Lothenbach, B., Scrivener, K., and Hooton, R. D. (2011). Supplementary cementitious materials. *Cement and Concrete Research*, 41:1244–1256.
- Ma, J., Orgass, M., and Tue, N. V. (2008). Influence of addition method of superplasticizer on the properties of fresh uhpc. *Proceeding of the second international symposium on UHPC*, pages 93–100.
- Markovic, I. (2006). *High-Performance Hybrid-Fibre Concrete - Development and Utilization*. PhD thesis, Delft University of Technology, Delft University of Technology, The Netherlands.
- Marquardt, I. (2002). Determination of the composition of self-compacting concretes on the basis of the water requirements of the constituent materials presentation of a new mix concept. *Betonwerk + Fertigteiltechnik BFT*, 11:22–30.
- Martinie, L., Rossi, P., and Roussel, N. (2010). Rheology of fiber reinforced cementitious materials: classification and prediction. *Cement and Concrete Research*, 40:226–234.
- Mehta, P. K. and Monteiro, P. J. M. (2006). *Concrete: Microstructure, Properties, and Materials - 3rd Edition*, chapter Strength, pages 49–84. The McGraw-Hill Companies, Inc., p.k. mehta, p.j.m. monteiro edition.

- Miettinen, K. and Mäkelä, M. M. (2000). Interactive multiobjective optimization system www-nimbus on the internet. *Computer Operations Research*, 27:709–723.
- Miettinen, K. and Mäkelä, M. M. (2006). Synchronous approach in interactive multiobjective optimization. *European Journal of Operational Research*, 170:909–922.
- Miller, K. T., Melant, R. M., and Zukoski, C. F. (1996). Comparison of the compressive yield response of aggregate suspensions: Pressure filtration, centrifugation, and osmotic consolidation. *Journal of the American Ceramic Society*, 79(10):2545–2556.
- Mills, R. H. (1966). Factors influencing cessation of hydration in water cured cement pastes. In *Special Report No. 90, Proceedings of the Symposium on the Structure of Portland Cement Paste and Concrete, Highway Research Board, Washington DC, USA*, pages 406–424.
- Mindess, S., Young, J. F., and Darwin, D. (2003a). *Concrete - 2nd Edition*, chapter Mineral admixtures and blended cement, pages 93–114. Pearson Education, Inc.
- Mindess, S., Young, J. F., and Darwin, D. (2003b). *Concrete - 2nd Edition*, chapter Hydration of portland cement, pages 57–91. Pearson Education, Inc.
- Müller, H. S. and Reinhardt, H. W. (2010). *BetonKerlender 2010: Brücken Betonbau im Wasser*, chapter Beton, pages 291–436. Ernst and Sohn, Berlin, k. bergmeister; f. fingerloos; j.d. wörner edition.
- Naaman, A. E. (1972). *A Statistical Theory of Strength for Fibre Reinforced Concrete*. PhD thesis, Massachusetts Institute of Technology, Massachusetts Institute of Technology.
- Naaman, A. E. (2000). Optimized geometries of fiber reinforcement of cement, ceramic and polymeric based composites - patent number 6060163. *United States Patent*, US006060163A:Patent Number 6060163.
- Naaman, A. E. (2003a). Engineered steel fibre with optimal properties for reinforcement of cement composites. *Journal of Advanced Concrete Technology*, 1:241–252.
- Naaman, A. E. (2003b). Strain hardening and deflection hardening fibre reinforced cement composites. In *Proceedings of the Fourth International RILEM Workshop on High Performance Fibre Reinforced Cement Composites, 1518 June 2003, Ann Arbor, USA*.
- Nachbaur, L., Nkinamubanzi, P. C., Nonat, A., and Mutin, J. C. (1998). Electrokinetic properties which control the coagulation of silicate cement suspensions during early age hydration. *Journal of Colloid and Interface Science*, 202:261–268.
- Neville, A. M. (1996). *Properties of concrete - Fourth and Final Edition*. Longman.
- Odler, I. and Wonnemann, R. (1983). Effect of alkalis on portland cement hydration: I. alkali oxides incorporated into the crystalline lattice of clinker minerals. *Cement and Concrete Research*, 13(4):477–482.
- Okamura, H. and Ozawa, K. (1995). Mix design for selfcompacting concrete. *Concrete library of the JSCE*, 25:107–120.

## Bibliography

- Oppeneder, J., Sparowitz, L., and Tue, N. V. (2016). Structural design for the quickway system. In *Proceedings of the 4th International Symposium on UHPC and Nanotechnology for High Performance Construction Materials, Kassel, Germany*.
- Orange, G., Dugat, J., and Acker, P. (2000). Ductal: new ultra high performance concretes. damage resistance and micromechanical analysis. In *Fibre Reinforced Concrete BEFIB 2000: Proceeding of the Fifth International RILEM Symposium, Lyon, France.*, pages 781–790.
- Papadakis, V. G. (1999a). Effect of fly ash on portland cement systems: Part i. low-calcium fly ash. *Cement and Concrete Research*, 29:1727–1736.
- Papadakis, V. G. (1999b). Experimental investigation and theoretical modeling of silica fume activity in concrete. *Cement and Concrete Research*, 29:79–86.
- Papadakis, V. G. (2000). Effect of fly ash on portland cement systems: Part ii. high-calcium fly ash. *Cement and Concrete Research*, 30:1647–1654.
- Pietsch, W. (2005). *Agglomeration in Industry: Occurrence and Applications*, chapter Chapter 3: Agglomeration Fundamentals - Chapter 4: Undesired Agglomeration: Methods of Avoiding or Lessening its Effect, pages 7–31. WILEY-VCH Verlag GmbH & Co, w. pietsch edition.
- Plank, J. and Hirsch, C. (2007). Impact of zeta potential of early cement hydration phases on superplasticizer adsorption. *Cement and Concrete Research*, 37:537–542.
- Plank, J. and Sachsenhauser, B. (2009). Experimental determination of the effective anionic charge density of polycarboxylate superplasticizers in cement pore solution. *Cement and Concrete Research*, 39:1–5.
- Plank, J., Schröfl, C., Gruber, M., Lesti, M., and Sieber, R. (2009). The effectiveness of polycarboxylate superplasticizer in ultra-high strength concrete: The importance of pce compatibility with silica fume. *Journal of Advanced Concrete Technology*, 7(1):5–12.
- Powers, T. C. and Brownyard, T. L. (1947). Studies of the physical properties of hardened portland cement. *Journal of The American Concrete Institute*, 43.
- Puntke, W. (2002). Wasseranspruch von feinen kornhaufwerken. *Beton*, 52:252–248.
- Ramge, P. and Lohaus, L. (2010). Robustness by mix design a new approach for mixture proportioning of scc. In *Proceedings of SCC 2010: Design, Production and Placement of Self-Consolidating Concrete, 2629 September 2010, Montreal, Canada*.
- Regourd, M. (1978). Cristallisation et ractivit de l'aluminate tricalcique dans les ciments portland. *Il Cemento*, 75(3):323–336.
- Reichel, M., Sparowitz, L., and Freytag, B. (2011a). Bridge wild völkermarkt prestressed arched structure made of precast uhpc-segments. part 1 design and detailing. *Beton- und Stahlbetonbau*, 106(12):827–835.

- Reichel, M., Sparowitz, L., and Freytag, B. (2011b). Bridge wild völkermarkt prestressed arched structure made of precast uhpc-segments. part 2 erection, accompanying research, quality control. *Beton- und Stahlbetonbau*, 106(12):827–835.
- Resplendino, J. and Toutlemonde, F. (2011). *Designing and Building with Ultra High Performance Fiber Reinforced Concrete State of the Art and Development*. ISTE Ltd and John Wiley & Sons Inc.
- Richard, P. and Cheyrezy, M. (1995). Composition of reactive powder concretes. *Cement and Concrete Research*, 25(7):1501–1511.
- RILEM-TC (1994). *RILEM Recommendations for the Testing and Use of Constructions Materials*, chapter RC 6 Bond test for reinforcement steel. 2. Pull-out test, 1983, pages 218 – 220. E FN SPON, rilem-tc edition.
- Robins, P., Austin, S., and Jones, P. (2002). Pull-out behaviour of hooked steel fibres. *Materials and Structures*, 35:434–442.
- Sakai, E., Yamada, K., and Ohta, A. (2003). Molecular structure and dispersion-adsorption mechanisms of comb-type superplasticizers used in japan. *Journal of Advanced Concrete Technology*, 1(1):16–25.
- Sakai, Y. and Ikeda, N. (1993). *Testing Method of Concrete in Japanese*. Tokyo: Gijutsu Shoin.
- Schmidt, M. and Fehling, E. (2005). Ultra-high performance concrete - research development and application in europe. In *Proc. of the 7th International Symposium on the Utilization of High-Strength / High-Performance Concrete*, pages 51–78.
- Schmidt, M., Fehling, E., Fröhlich, S., and Thiemicke, J. (2014). *Sustainable Building with Ultra-High Performance Concrete: Results of the German Priority Programme 1182 funded by Deutsch Forschungsgemeinschaft (DFG)*. Kassel University Press GmbH.
- Schmidt, M., Fehling, E., Glotzbach, C., Fröhlich, S., and Piotrowski, S., editors (2012). *Proceedings of the Third International Symposium on Ultra-High Performance Concrete and Nanotechnology for High Performance Construction Materials, 7-9 March 2012, Kassel, Germany*. Kassel University Press GmbH.
- Schröfl, C., Gruber, M., and Plank, J. (2012). Preferential adsorption of polycarboxylate superplasticizers on cement and silica fume in ultra-high performance concrete (uhpc). *Cement and Concrete Research*, 42:1401–1408.
- Somasundaran, P., Mehta, S. C., Yu, X., and Krishnakumar, S. (2009). *Handbook of surface and colloid chemistry - Third Edition*, chapter Colloid Systems and Interfaces Stability of Dispersions through Polymer and Surfactant Adsorption, pages 155–196. Taylor & Francis Group, k.s. birdi edition.
- Soroka, I. and Setter, N. (1977). The effect of fillers on strength of cement mortar. *Cement and Concrete Research*, 7(4):449–456.

## Bibliography

- Sritharan, S., Wille, K., and Graybeal, B., editors (2016). *Proceedings of the First International Interactive Symposium on Ultra-High Performance Concrete, 18-20 July 2016, Des Moines, Iowa, USA*. Iowa State University.
- Stovall, T., de Larrard, F., and Buil, M. (1986). Linear packing density model of grain mixtures. *Powder Technology*, 48:1–12.
- Sujivorakul, C. and Naaman, A. E. (2003). Tensile response of hpfrc composites using twisted polygonal steel fibers. In *Proceedings of Fiber Reinforced Concrete: Innovation of Value, ACI Convention, Toronto, ACI Special Publication Vol.216 pp.161-180*.
- Swamy, R. N. and Mangat, P. S. (1974). Influence of fiber-aggregate interaction on some properties of steel fiber reinforced concrete. *Materials and Structures*, 7:307314.
- Taylor, H. F. W. (1997a). *Cement Chemistry - 2nd edition*, chapter Hydration of Portland Cement, pages 187–224. Thomas Telford, h. f. w. taylor edition.
- Taylor, H. F. W. (1997b). *Cement Chemistry - 2nd edition*, chapter Composite cements, pages 261–293. Thomas Telford.
- Teichmann, T. (2008). *Influence of the granulometrie and the water content on the strength and density of cement stone*. PhD thesis, Kassel University, Department of Building Materials and Building Chemistry, University of Kassel - Germany.
- Theiler, W., Reicht, O., and Tue, N. V. (2015). Effect of the inaccuracy on the stress distribution in dry connections of modular constructions. In *Proceedings of the fibs 2015 Symposium: Concrete Innovation and Design, Copenhagen, Denmark*.
- Uchikawa, H., Hanehara, S., and Sawaki, D. (1997). The role of steric repulsive force in the dispersion of cement particles in fresh paste prepared with organic admixture. *Cement and Concrete Research*, 27(1):37–50.
- U.S.DOT-FHWA (2007-2015). *UHPC Projects*. U.S.Department of Transportation - Federal Highway Administration <http://www.fhwa.dot.gov/research/resources/uhpc/>.
- Ushiro, M., Atarashi, D., Kawakami, H., and Sakai, E. (2013). The effect of superplasticizer present in pore solution on flowability of low water-to-powder cement paste. *Cement Science and Concrete Technology*, 1:102–107.
- van Vliet, M. R. A. and van Mier, J. G. M. (2000). Size effect of concrete and sandstone. *HERON*, 45:91–108.
- Vogt, C. (2010). *Ultrafine particles in concrete - Influence of ultrafine particles on concrete properties and application to concrete mix design*. PhD thesis, Royal Institute of Technology, School of Architecture and the Built Environment, Division of Concrete Structures, Stockholm, Sweden.
- Wall, S. (2002). *Handbook of applied surface and colloid chemistry - Volume 2*, chapter Solid Dispersions, pages 3–21. Thomas Telford, krister holmberg edition.

- Westman, A. E. R. and Hugill, H. R. (1930). The packing of particles. *Journal of the American Ceramic Society*, 13:767–779.
- White, H. E. and Walton, S. F. (1936). Particle packing and particle shape. *Journal of the American Ceramic Society*, 20:155–166.
- Wille, K., El-Tawil, S., and Naaman, A. E. (2014). Properties of strain hardening ultra high performance fiber reinforced concrete (uhp-frc) under direct tensile loading. *Cement and Concrete Composites*, 48:53–66.
- Wille, K., Kim, D. J., and Naaman, A. E. (2011). Strain-hardening uhpfrc with low fiber contents. *Materials and Structures*, 44:583–598.
- Wille, K. and Naaman, A. E. (2012). Pullout behavior of high-strength steel fibers embedded in ultra-high-performance concrete. *ACI Materials Journal*, 109:479–488.
- Wille, K., Naaman, A. E., El-Tawil, S., and Parra-Montesinos, G. J. (2012). Ultra-high performance concrete and fiber reinforced concrete: achieving strength and ductility without heat curing. *Materials and Structures*, 45:309324.
- Winnefeld, F., Becker, S., Pakusch, J., and Götz, T. (2007). Effects of the molecular architecture of comb-shaped superplasticizers on their performance in cementitious systems. *Cement and Concrete Composites*, 29:251–262.
- Wong, H. H. C. and Kwan, A. K. H. (2008). Packing density of cementitious materials: part 1 measurement using a wet packing method. *Materials and Structures*, 41:689–701.
- Wuest, J. (2007). *Comportement structural des bétons de fibres ultra performants en traction dans des éléments composés*. PhD thesis, Ecole Polytechnique Fédérale de Lausanne - EPFL, Lausanne, Switzerland.
- Yajun, J. and Cahyadi, J. H. (2003). Effects of densified silica fume on microstructure and compressive strength of blended cement pastes. *Cement and Concrete Research*, 33:1543–1548.
- Yamada, K., Takahashi, T., Hanehara, S., and Matsuhisa, M. (2000). Effects of the chemical structure on the properties of polycarboxylate-type superplasticizer. *Cement and Concrete Research*, 5:197–207.
- Yang, M., Neubauer, C. M., and Jennings, H. M. (1997). Interparticle potential and sedimentation behavior of cement suspensions: Review and results from paste. *Advn Cem Bas Mat*, 5:1–7.
- Yoshioka, K., Sakai, E., Daimon, M., and Kitahara, A. (1997). Role of steric hindrance in the performance of superplasticizers for concrete. *Journal of the American Ceramic Society*, 80(10):2667–2671.
- Yoshioka, K., Tazawa, E., Kawai, K., and Enohata, T. (2002). Role of steric hindrance in the performance of superplasticizers for concrete. *Cement and Concrete Research*, 32:1507–1513.

## Bibliography

- Yu, R., Spiesz, P., and Brouwers, H. J. H. (2014). Mix design and properties assessment of ultra-high performance fibre reinforced concrete. *Cement and Concrete Research*, 56:29–39.
- Yu, R., Spiesz, P., and Brouwers, H. J. H. (2015). Development of an eco-friendly ultra-high performance concrete with efficient cement and mineral admixtures uses. *Cement and Concrete Composites*, 55:383–394.
- Zile, E. and Zile, O. (2013). Effect of the fiber geometry on the pullout response of mechanically deformed steel fibers. *Cement and Concrete Research*, 44:18–24.
- Zingg, A., Winnefeld, F., Holzer, L., Pakusch, J., Becker, S., Figi, R., and Gauckler, L. (2009). Interaction of polycarboxylate-based superplasticizers with cements containing different c3a amounts. *Cement and Concrete Composites*, 31:153–162.

## A. Appendix A: Materials properties

TABLE A.1.: Passing volume - Particle size distribution of the used cements and reactive fillers.

Size ( $\mu\text{m}$ )	Powders							
	Cem1	Cem2	Cem3	Cem4	FA	GGBFS	SF1	SF2
0.042	0.00	0.00	0.00	0.00	0.00	0.00	0.00	0.00
0.046	0.00	0.00	0.00	0.00	0.00	0.00	0.02	0.01
0.050	0.00	0.00	0.00	0.00	0.00	0.00	0.06	0.03
0.055	0.00	0.00	0.00	0.00	0.00	0.00	0.11	0.06
0.061	0.00	0.00	0.00	0.00	0.00	0.00	0.21	0.12
0.067	0.00	0.00	0.00	0.00	0.00	0.00	0.43	0.24
0.073	0.00	0.00	0.00	0.00	0.00	0.00	0.83	0.47
0.080	0.00	0.00	0.00	0.00	0.00	0.00	1.45	0.84
0.088	0.00	0.00	0.00	0.00	0.00	0.00	2.27	1.36
0.097	0.00	0.00	0.00	0.00	0.00	0.00	3.25	2.04
0.100	0.00	0.00	0.00	0.00	0.00	0.00	4.40	2.89
0.117	0.21	0.11	0.23	0.20	0.42	0.17	5.74	3.95
0.128	0.35	0.19	0.38	0.33	0.70	0.29	7.29	5.26
0.141	0.51	0.28	0.55	0.47	1.01	0.42	9.07	6.86
0.155	0.68	0.37	0.74	0.63	1.35	0.56	11.09	8.78
0.170	0.87	0.47	0.94	0.81	1.72	0.72	13.41	11.07
0.186	1.08	0.59	1.16	1.00	2.13	0.89	16.11	13.81
0.205	1.31	0.71	1.41	1.21	2.58	1.07	19.30	17.07
0.225	1.56	0.85	1.68	1.44	3.08	1.28	23.11	20.96
0.247	1.83	1.00	1.97	1.69	3.62	1.50	27.68	25.56
0.271	2.13	1.16	2.30	1.97	4.21	1.75	33.10	30.90
0.297	2.46	1.34	2.65	2.28	4.87	2.02	39.33	36.90
0.326	2.82	1.54	3.04	2.62	5.58	2.32	46.22	43.35
0.358	3.22	1.75	3.47	2.98	6.37	2.65	53.47	49.96
0.393	3.66	1.99	3.94	3.39	7.23	3.01	60.71	56.41
0.431	4.14	2.25	4.46	3.83	8.18	3.40	67.55	62.37
0.45	4.37	2.38	4.71	4.05	8.64	3.59	70.22	64.65
0.55	6.01	3.06	6.40	5.29	10.86	4.89	81.15	73.82
0.65	7.49	3.74	7.90	6.38	12.83	6.06	86.73	78.37
0.75	8.84	4.42	9.23	7.58	15.43	7.11	89.47	80.55
0.90	10.66	5.44	10.98	9.56	18.42	8.52	90.44	81.28
1.10	12.82	7.54	12.97	11.59	21.05	10.17	90.49	81.32
1.30	14.76	9.36	14.68	13.02	24.04	11.65	90.51	81.36
1.55	16.99	10.94	16.56	14.75	27.41	13.35	90.60	81.61
1.85	19.49	12.98	18.59	16.80	30.70	15.27	90.76	82.15

A. Appendix A: Materials properties

2.15	21.85	15.23	20.45	18.90	34.50	17.14	90.87	82.67
2.50	24.48	17.08	22.49	21.41	39.83	19.26	90.93	83.09
3.00	27.98	19.05	25.19	24.84	54.54	22.21	90.94	83.41
3.75	32.66	21.15	28.84	29.27	61.02	26.36	90.96	83.70
4.50	36.65	23.15	32.02	32.81	68.74	30.17	91.21	83.99
5.25	40.20	25.49	34.92	35.88	76.73	33.74	91.86	84.40
6.25	44.46	28.92	38.51	39.46	84.00	38.23	92.78	85.10
7.50	49.32	34.16	42.70	43.67	89.09	43.52	93.38	85.92
9.00	54.60	39.37	47.27	48.37	93.47	49.35	93.66	86.40
10.50	59.36	44.37	51.35	52.68	96.62	54.58	94.01	86.61
12.50	65.11	50.57	56.28	57.72	98.60	60.77	94.85	87.27
15.00	71.46	57.46	61.83	63.47	99.58	67.40	95.97	88.84
18.00	77.97	64.61	67.81	70.01	99.97	73.94	96.80	90.55
21.50	84.11	70.63	73.97	77.25	100	79.87	97.38	91.44
25.50	89.35	77.23	79.88	84.62	100	84.72	98.08	91.82
30.50	93.78	83.61	85.69	91.18	100	88.70	98.89	92.37
36.50	96.82	89.07	90.65	96.52	100	91.45	99.44	93.93
43.50	98.52	93.22	94.39	99.00	100	93.17	99.72	96.43
51.50	99.31	96.04	96.90	99.74	100	94.27	99.92	98.67
61.50	99.66	97.96	98.56	100	100	95.15	100	99.81
73.50	99.83	99.14	99.41	100	100	95.93	100	100
87.50	99.91	99.79	99.77	100	100	96.63	100	100
105	100	100	100	100	100	97.34	100	100
125	100	100	100	100	100	97.99	100	100
150	100	100	100	100	100	98.64	100	100
180	100	100	100	100	100	99.21	100	100
215	100	100	100	100	100	100	100	100

TABLE A.2.: Passing volume - Particle size distribution of the used inert fillers.

Size ( $\mu\text{m}$ )	Powders				
	LSP	QP110	QP16900	QP10000	QP2500
0.10	0.00	0.00	0.00	0.00	0.00
0.45	2.91	5.33	3.70	2.47	0.64
0.55	4.95	7.68	5.08	3.39	0.96
0.65	7.32	9.53	6.32	4.23	1.27
0.75	9.95	12.08	7.43	4.98	1.59
0.90	14.23	15.14	8.92	6.00	2.05
1.10	20.28	18.93	10.64	7.17	2.67
1.30	26.44	22.46	12.15	8.20	3.28
1.55	33.94	26.54	13.81	9.33	4.03
1.85	42.23	31.05	15.58	10.54	4.90
2.15	49.52	35.23	17.19	11.64	5.73
2.50	56.71	39.78	18.93	12.81	6.65
3.00	67.87	45.77	21.20	14.35	7.86

3.75	73.74	53.71	24.23	16.42	9.52
4.50	79.99	60.42	26.90	18.25	11.01
5.25	84.73	66.21	29.34	19.96	12.44
6.25	89.53	72.74	32.40	22.13	14.29
7.50	93.82	79.35	36.04	24.75	16.53
9.00	97.10	85.38	40.13	27.76	19.1
10.50	98.84	89.7	43.93	30.59	21.52
12.50	99.73	93.77	48.63	34.13	24.57
15.00	99.98	96.92	54.04	38.28	28.16
18.00	100	98.89	60.02	42.97	32.21
21.50	100	99.72	66.40	48.14	36.64
25.50	100	99.97	72.87	53.67	41.35
30.50	100	100	79.71	60.06	46.77
36.50	100	100	86.06	67.01	52.68
43.50	100	100	91.20	74.10	58.84
51.50	100	100	94.75	80.71	64.99
61.50	100	100	97.14	86.82	71.46
73.50	100	100	98.47	91.51	77.67
87.50	100	100	99.19	94.57	83.23
105	100	100	99.64	96.62	88.42
125	100	100	99.88	97.90	92.61
150	100	100	99.99	98.89	96.09
180	100	100	100	99.57	98.39
215	100	100	100	99.94	99.66
255	100	100	100	100	99.98
305	100	100	100	100	100

TABLE A.3.: Computing the residual packing densities of monosized classes of polydisperse quartz sand QS1 based on its experimentally actual packing density.

Quartz sand QS1		K-value	$\beta_{\text{exp}}$	monosized classes			$\beta$	$\beta_i$
Size ( $\mu\text{m}$ )	Passing (vol.%)			Class i	Size ( $\mu\text{m}$ )	$y_i$ (vol.%)		
2580.23	100			1	2341.24	7.08	0.66633	
2124.39	92.92			2	1927.62	35.84	0.66774	
1749.08	57.08			3	1587.07	41.07	0.66891	
1440.07	16.01			4	1306.68	13.06	0.66987	
1185.65	2.95			5	1075.83	1.59	0.67067	
976.19	1.36	9	0.6360	6	885.77	0.65	0.6744	
803.73	0.71			7	729.28	0.30	0.67187	
661.73	0.41			8	600.44	0.16	0.67232	
544.83	0.25			9	494.36	0.08	0.67269	
448.57	0.17			10	407.02	0.04	0.67299	
369.32	0.13			11	335.11	0.13	0.67324	
304.08	0							

A. Appendix A: Materials properties

TABLE A.4.: Computing the residual packing densities of monosized classes of polydisperse quartz sand QS2 based on its experimentally actual packing density.

Quartz sand QS2		K-value	$\beta_{\text{exp}}$	monosized classes			$\beta$	$\beta_i$
Size ( $\mu\text{m}$ )	Passing (vol.%)			Class i	Size ( $\mu\text{m}$ )	$y_i$ (vol.%)		
1185.65	100			1	1075.83	1.98		0.67217
976.19	98.02			2	885.77	18.52		0.67283
803.73	79.5			3	729.28	34.73		0.67338
661.73	44.77			4	600.44	31.34		0.67383
544.83	13.43			5	494.36	11.37		0.67420
448.57	2.06	9	0.6420	6	407.02	1.35	0.6759	0.67451
369.32	0.71			7	335.11	0.34		0.67476
304.08	0.37			8	275.91	0.16		0.67497
250.36	0.21			9	227.17	0.08		0.67514
206.13	0.13			10	187.03	0.13		0.67528
169.71	0							

TABLE A.5.: Computing the residual packing densities of monosized classes of polydisperse quartz sand QS3 based on its experimentally actual packing density.

Quartz sand QS3		K-value	$\beta_{\text{exp}}$	monosized classes			$\beta$	$\beta_i$
Size ( $\mu\text{m}$ )	Passing (vol.%)			Class i	Size ( $\mu\text{m}$ )	$y_i$ (vol.%)		
304.08	100			1	275.91	2.07		0.66872
250.36	97.93			2	227.17	7.10		0.66889
206.13	90.83			3	187.03	18.75		0.66903
169.71	72.08			4	153.99	31.26		0.66914
139.73	40.82			5	126.78	24.66		0.66924
115.04	16.16			6	104.38	10.68		0.66932
94.72	5.48	9	0.6470	7	85.94	3.29	0.66968	0.66938
77.98	2.19			8	70.76	1.21		0.66943
64.21	0.98			9	58.25	0.53		0.66948
52.86	0.45			10	47.96	0.23		0.66951
43.52	0.22			11	39.49	0.11		0.66954
35.84	0.11			12	32.51	0.11		0.66957
29.50	0							

TABLE A.6.: Computing the residual packing densities of monosized classes of polydisperse crushed basalt CrB1 based on its experimentally actual packing density.

crushed basalt CrB1		K-value	$\beta_{\text{exp}}$	monosized classes			$\beta$	$\beta_i$
Size ( $\mu\text{m}$ )	Passing (vol.%)			Class i	Size ( $\mu\text{m}$ )	$y_i$ (vol.%)		
9000	100			1	8485.28	4.3		0.60570
8000	95.70			2	6693.28	51.40		0.61114
5600	44.30	9	0.6080	3	4732.86	38.70	0.6326	0.61724
4000	5.60			4	2828.42	4.70		0.62333
2000	0.90			5	1414.21	0.90		0.62795
1000	0							

TABLE A.7.: Computing the residual packing densities of monosized classes of polydisperse crushed basalt CrB2 based on its experimentally actual packing density.

crushed basalt CrB2		K-value	$\beta_{\text{exp}}$	monosized classes			$\beta$	$\beta_i$
Size ( $\mu\text{m}$ )	Passing (vol.%)			Class i	Size ( $\mu\text{m}$ )	$y_i$ (vol.%)		
5600	100	9	0.5960	1	4732.86	2.55	0.6280	0.61282
4000	97.45			2	2828.42	83.20		0.61882
2000	14.25			3	1414.21	10.95		0.62338
1000	3.30			4	894.42	3.30		0.62508
800	0							

TABLE A.8.: Packing densities, water demand, superplasticizers demand of the used cements examined by the method of superplasticizer-water solution demand test.

	<b>Cem1</b>	<b>Cem2</b>	<b>Cem3</b>	<b>Cem4</b>
			Using water only	
Packing density (%)	56.04	56.10	56.50	55.80
Water demand ( $W^*/C$ wt.%)	25.30	25.66	25.24	25.55
SP demand ( $SP^*/C$ wt.%)	0	0	0	0
		Using SP1-water solution with SP1/W = 10 wt.%		
Packing density (%)	63.70	63.48	61.78	61.08
Water demand ( $W^*/C$ wt.%)	16.78	17.22	18.52	18.77
SP demand ( $SP^*/C$ wt.%)	1.678	1.722	1.852	1.877
		Using SP2-water solution with SP2/W = 10 wt.%		
Packing density (%)	62.30	61.23	60.16	60.69
Water demand ( $W^*/C$ wt.%)	17.82	18.96	19.83	19.08
SP demand ( $SP^*/C$ wt.%)	1.782	1.895	1.982	1.908
		Using SP3-water solution with SP3/W = 10 wt.%		
Packing density (%)	62.10	60.34	59.71	60.27
Water demand ( $W^*/C$ wt.%)	17.96	19.68	20.20	19.42
SP demand ( $SP^*/C$ wt.%)	1.796	1.968	2.020	1.942

TABLE A.9.: The influence of SP1 concentration in SP1-Water solution on the packing density of Cem1.

	<b>SP1/W (wt.%) in SP1-water solution</b>				
	0	10	12.5	15	17.5
Packing density (%)	56.04	63.70	64.42	64.86	64.80
Water demand ( $W^*/C$ wt.%)	25.30	16.78	15.92	15.29	15.02
SP demand ( $SP^*/C$ wt.%)	0	1.678	1.990	2.294	2.628

A. Appendix A: Materials properties

TABLE A.10.: The influence of three superplasticizers SP1, SP2, SP3 on the 28 days compressive strength of Cem1, 2, 3 and 4 with W/C = 25 wt.% and SP/C = 2 wt.%, normalized with respect to 28 days compressive strength of Cem1-SP1

	<b>SP1</b>	<b>SP2</b>	<b>SP3</b>
<b>Cem1</b>	100.0	99.2	90.3
<b>Cem2</b>	94.7	83.1	82.7
<b>Cem3</b>	92.3	82.1	83.2
<b>Cem4</b>	94.1	82.8	81.8

TABLE A.11.: Packing densities, water demands, SP1 demands of silica fumes (SF1, SF2), fly ash (FA), ground granulated blast furnace slag (GGBFS or BFS), quartz powders (QP1, QP2, QP3, QP4) and lime stone powder (LSP) examined by the method of superplasticizer-water solution demand test.

	<b>SF1</b>	<b>SF2</b>	<b>FA</b>	<b>BFS</b>	<b>QP1</b>	<b>QP2</b>	<b>QP3</b>	<b>QP4</b>	<b>LSP</b>
	Using water only								
Packing density (%)	59.43	60.43	57.41	56.02	61.28	57.44	54.89	54.50	69.18
Wa. demand (W*/C wt.%)	31.03	29.76	29.56	27.84	24.02	28.17	31.25	31.74	16.50
SP demand (SP*/C wt.%)	0	0	0	0	0	0	0	0	0
	Using SP1-water solution with SP1/W = 10 wt.%								
Packing density (%)	52.55	57.40	66.88	58.03	61.65	58.01	56.10	55.30	69.54
Wa. demand (W*/C wt.%)	37.15	30.54	17.86	23.21	21.41	24.91	26.93	27.82	14.68
SP demand (SP*/C wt.%)	3.715	3.054	1.786	2.321	2.141	2.491	2.693	2.782	1.468

TABLE A.12.: The influence of types and content of reactive powders on the 28 days compressive strength of binders containing Cem1 and reactive powders with W/Cem1 = 25wt.% and SP1/Cem1 = 2wt.%

	<b>Reactive Powder / Cem1 ratios (wt.%)</b>						
	0	10	15	20	30	40	50
<b>Cem1</b>	100	–	–	–	–	–	–
<b>SF2</b>	–	114.5	116.0	116.0	–	–	–
<b>SF1</b>	–	112.4	113.1	113.8	–	–	–
<b>GGBFS</b>	–	104.5	–	111.5	113.8	114.3	112.3
<b>FA</b>	–	–	–	105.1	110.4	112	108

## B. Appendix B: Experimental data of pastes and concretes

TABLE B.1.: The variation in the packing density of QP<sub>i</sub>-Cem1 blends, FA-Cem1 blends and GGBFS-Cem1 blends when Cem1 was replaced progressively by QP<sub>i</sub> (i=1,2,3,4), or FA, or GGBFS, applying the method of SP1-Water solution demand test with SP1/W of 10 wt.%.

Addition/Cem1 (wt.%)	Packing density (%) of blends of					
	QP1-Cem1	QP2-Cem1	QP3-Cem1	QP4-Cem1	FA-Cem1	BFS-Cem1
0	63.7	63.7	63.7	63.7	63.7	63.7
10	65.3	65.0	64.7	64.1	64.8	64.2
20	65.9	65.7	65.7	64.1	65.8	64.9
30	67.0	66.6	66.7	64.2	66.7	65.3
35	–	66.7	–	–	–	–
40	67.4	66.6	66.3	–	67.3	65.1
50	66.5	66.1	66.1	–	66.9	–
60	66.1	65.3	65.3	–	–	–

TABLE B.2.: The variation in the packing density of mixtures containing SF2 and the optimum blends (QP<sub>i</sub>+Cem1) when the optimum blends (QP<sub>i</sub>+Cem1) were replaced progressively by SF2, applying the method of SP1-Water solution demand test with SP1/W of 10 wt.%.

QP1/Cem1 (wt.%)	QP2/Cem1 (wt.%)	QP3/Cem1 (wt.%)	SF2/(QP(i)+Cem1) (wt.%)	Packing density (%) of blends of		
				SF2-QP1-Cem1	SF2-QP2-Cem1	SF2-QP3-Cem1
40	35	30	0	67.4	66.70	66.7
40	35	30	2.5	68.8	67.6	67.4
40	35	30	5.0	70.6	68.9	68.4
40	35	30	7.5	72.1	70.4	69.7
40	35	30	10.0	73.0	71.3	70.7
40	35	30	12.5	74.0	72.2	72.1
40	35	30	15.0	74.9	72.8	72.4
40	35	30	17.5	75.2	73.3	72.8
40	35	30	20.0	75.1	73.4	73.4
40	35	30	22.5	75.4	73.8	73.8

B. Appendix B: Experimental data of pastes and concretes

TABLE B.3.: The computed water-powder volume ratios of mixtures containing SF2 and the optimum blends (QP<sub>i</sub>+Cem1), SF2 increased progressively and W/Cem1 of 25 wt.% was constant.

QP1/Cem1 (wt.%)	QP2/Cem1 (wt.%)	QP3/Cem1 (wt.%)	SF2/(QP(i)+Cem1) (wt.%)	Water-Powder vol. ratios of blend of		
				SF2-QP1- Cem1	SF2-QP2- Cem1	SF2-QP3- Cem1
40	35	30	0	0.52668	0.54865	0.57254
40	35	30	2.5	0.50960	0.53078	0.55381
40	35	30	5.0	0.49359	0.51404	0.53626
40	35	30	7.5	0.47856	0.49832	0.51979
40	35	30	10.0	0.46442	0.48354	0.50430
40	35	30	12.5	0.45109	0.46960	0.48970
40	35	30	15.0	0.43850	0.45645	0.47593
40	35	30	17.5	0.42660	0.44401	0.46291
40	35	30	20.0	0.41532	0.43224	0.45059
40	35	30	22.5	0.40463	0.42107	0.43890

TABLE B.4.: The variations in efficient-water to solid volume ratios and of the film thickness of the efficient water in ternary binders containing SF2 and the optimum blends (QP1+Cem1), SF2 increased progressively and W/Cem1 of 25 wt.% was constant.

QP1/Cem1 (wt.%)	SF2/(QP1+Cem1) (wt.%)	V <sub>eff.-water</sub> /V <sub>solid</sub>	t <sub>eff.-water</sub> (nm)
40	0	0.03926	17.5
40	2.5	0.061164	22.0
40	5.0	0.077604	23.6
40	7.5	0.089222	23.7
40	10.0	0.096500	22.9
40	12.5	0.099801	21.6
40	15.0	0.099379	19.8
40	17.5	0.095406	17.7
40	20.0	0.087975	15.3
40	22.5	0.077105	12.7

TABLE B.5.: The variations in efficient-water to solid volume ratios and of the film thickness of the efficient water in ternary binders containing SF2 and the optimum blends (QP2+Cem1), SF2 increased progressively and W/Cem1 of 25 wt.% was constant.

QP2/Cem1 (wt.%)	SF2/(QP2+Cem1) (wt.%)	$V_{\text{eff.-water}}/V_{\text{solid}}$	$t_{\text{eff.-water}}$ (nm)
35	0	0.043166	16.9
35	2.5	0.057372	18.6
35	5.0	0.068081	19.0
35	7.5	0.075627	18.7
35	10.0	0.080272	17.9
35	12.5	0.082220	16.8
35	15.0	0.081621	15.4
35	17.5	0.078582	13.9
35	20.0	0.073171	12.2
35	22.5	0.065420	10.3

TABLE B.6.: The variations in efficient-water to solid volume ratios and of the film thickness of the efficient water in ternary binders containing SF2 and the optimum blends (QP3+Cem1), SF2 increased progressively and W/Cem1 of 25 wt.% was constant.

QP3/Cem1 (wt.%)	SF2/(QP3+Cem1) (wt.%)	$V_{\text{eff.-water}}/V_{\text{solid}}$	$t_{\text{eff.-water}}$ (nm)
30	0	0.065453	23.5
30	2.5	0.074774	22.6
30	5.0	0.082011	21.5
30	7.5	0.087330	20.5
30	10.0	0.090865	19.3
30	12.5	0.092726	18.1
30	15.0	0.092997	16.9
30	17.5	0.091746	15.6
30	20.0	0.089020	14.3
30	22.5	0.084852	13.0

TABLE B.7.: Influence of SP1 on the plastic viscosity of the cementitious pastes having constant W/Cem1 of 25 wt.%. The optimum Binders 1, 2, 3 are the cementitious powders of Pastes1, 2, 3 respectively.

W/Cem1 (wt.%)	SP1/Cem1 (wt.%)	Relative Plastic Viscosity (N-mm/rpm)		
		Binder 1	Binder 2	Binder 3
25	1.854	0.3964	–	–
25	1.922	–	0.3765	–
25	1.881	–	–	0.2876
25	2	–	–	0.2526
25	2.5	0.3231	0.2770	0.2084
25	3	0.2869	0.2671	0.2102
25	3.25	–	–	0.2265
25	3.5	0.2855	0.309	–
25	4.0	0.3117	–	–

B. Appendix B: Experimental data of pastes and concretes

TABLE B.8.: The variation in the packing density of mixtures containing LSP and the optimum blends (GGBFS+Cem1) when the optimum blends (GGBFS+Cem1) were replaced progressively by LSP, applying the method of SP1-Water solution demand test with SP1/W of 10 wt.%.

GGBFS/Cem1 (wt.%)	LSP/(GGBFS+Cem1) (wt.%)	Packing density (%)
30	0	65.3
30	5	66.1
30	10	66.8
30	15	67.8
30	20	68.3
30	25	68.8
30	30	69.1

TABLE B.9.: The computed water-powder volume ratios of mixtures containing LSP and the optimum blends (GGBFS+Cem1), LSP increased progressively and W/Cem1 of 25 wt.% was constant.

GGBFS/Cem1 (wt.%)	LSP/(GGBFS+Cem1) (wt.%)	Water-Powder vol. ratios
30	0	0.5828
30	5	0.5518
30	10	0.5240
30	15	0.4988
30	20	0.4760
30	25	0.4551
30	30	0.4360

TABLE B.10.: Influence of SP1 content on the self-flowability of fine grain concretes containing the developed optimum binders, 720 kg/m<sup>3</sup> of Cem1, W/C ratio of 25 wt.%, quartz sand QS2 (0.3-0.8 mm)

SP1/Cem1 (wt.%)	Spread-flow of concrete containing				
	Binder 1	Binder 2	Binder 3	Binder 4	Binder 5
2.5	236	239	228	234	246
3.0	240	245	235	247	252
3.5	242	243	232	245	254
4.0	239	238	226	240	250

TABLE B.11.: The 28 days compressive strength of concrete formed by the modified Andreasen and Andersen equation-based ideal curve

Mix 1	Mix 4	Mix 5	Mix 6	Mix 9	Mix 10
187.3	181.1	169.4	183.7	173.0	168.6

## Curriculum Vitae



Name	Kim Huy Hoang
Date of birth	10th November 1981
Place of birth	Ho Chi Minh City, Vietnam.
1999 - 2004	Civil Engineering, Ho Chi Minh City University of Technology, Vietnam.
2004 - 2006	Master of science thesis at Department of Building Material, Ho Chi Minh City University of Technology, Vietnam. Thesis on the influence of autoclave curing on the physical-mechanical properties of high performance concrete containing various supplementary cementitious materials.
2006 - 2011	Research assistant on construction materials at Department of Building Materials, Ho Chi Minh City University of Technology, Vietnam.
2011 - 2017	Research assistant, PhD-study on ultra high performance concrete under the supervision of Prof. Dr.-Ing. habil. Nguyen Viet Tue at Institute of Structural Concrete, Graz University of Technology, Austria.



## Publications related to this research project

Hoang, K. H., Hadl, P., and Tue, N. V. (2016). A new mix design method for ultra-high performance concrete based on stepwise optimization of particle packing density. In: Proceedings of HiPerMat 2016: the 4th International Symposium on Ultra-High Performance Concrete and High Performance Materials, Kassel, Germany, March 9-11, 2016.

Hoang, K. H., Hadl, P., and Tue, N. V. (2016). A new mix design method for ultra-high performance concrete based on stepwise optimization of particle packing density. In: Proceedings of the First International Interactive Symposium on Ultra-High Performance Concrete, Des Moines, Iowa, USA, July 18-20, 2016.

Hoang, K. H., Hadl, P., and Tue, N. V. (2016). Influence of steel fibres and matrix composition on the properties of ultra-high performance fibre reinforced concrete. In: Proceedings of the First International Interactive Symposium on Ultra-High Performance Concrete, Des Moines, Iowa, USA, July 18-20, 2016.

Hoang, K. H., Tue, N. V. (2017). Comparative flexural and tensile behaviours of UHPFRC with different steel fibres. In: Proceedings of the 4th international conference on Strain-Hardening Cement-Based Composites (SHCC4), Dresden, Germany, September 18-20, 2017.